CLINICALLY RELEVANT MRE11 VARIANTS IN BLADDER CANCER

Sarah J Jevons

St Edmund Hall

Trinity Term 2015

University of Oxford

Supervisor

Dr Anne E Kiltie MA DM MRCP FRCR

Co-Supervisor

Dr Eva M^{C}Growder PhD

Assessment Committee

Dr Ester Hammond PhD

Professor Mark Meuth PhD

Thesis submitted to the University of Oxford

in accordance with the requirements for the degree of

Doctor of Philosophy

CANCER RESEARCH UK

MRC Medical Research Council

OXFORD INSTITUTE FOR RADIATION ONCOLOGY

The study presented in this thesis was performed at the Cancer Research UK/ Medical Research Council Oxford Institute for Radiation Oncology, University of Oxford. This work was supported by a scholarship from the Medical Research Council, and grants from Cancer Research UK.

Abstract

Personalised medicine aims to empower patients and clinicians to make informed choices in order to enhance treatment outcomes. Currently, muscle-invasive bladder cancer (MIBC) is treated with cystectomy or radiotherapy/chemoradiation with no clear survival advantage for either option. Identification of predictive biomarkers could facilitate choice between treatments and potentially improve overall survival rates. MRE11 is a damage signaling protein whose function is crucial for in the DNA damage response. Intriguingly, expression of MRE11 by immunohistochemistry (IHC) is a promising predictive biomarker of radiotherapy response in MIBC patients. Paradoxically in terms of DNA repair, patients with low expression of MRE11, have a significantly worse survival rate following radiotherapy than those expressing high levels of MRE11 (Choudhury *et al*. 2010; Laurberg *et al*. 2012). The aim of the project was to investigate the underlying mechanisms of MRE11 expression in bladder cancer.

A novel C-terminally truncated MRE11 variant was detected in bladder cancer cell lines and patient samples. The variant was the result of a post-translational cleavage of wild type MRE11 by caspase activity. Although caspases were responsible for the cleavage of MRE11, expression of the variant did not increase following the induction of apoptosis, implying that non-apoptotic caspases were involved. The variant was found to be less stable than wild type MRE11 and degraded by the proteasome.

Functional aspects of the variant were investigated and it was found that the variant was located in the nucleus, can complex with NBS1 and RAD50 and co-

localised with yH2AX at double-strand break sites. However, expression of the truncated variant led to a reduction in the efficiency of homologous recombination. The truncated variant is therefore likely to have a functional impact on DNA repair, potentially in a dominant negative manner.

This might explain why high MRE11 expression was associated with increased survival following radiotherapy in bladder cancer patients. The high expression of MRE11 could include detection of high levels of the variant, associated with defective DNA repair and hence increased radiosensitivity. An underlying mechanistic explanation further supports the use of MRE11 immunohistochemistry as a predictive biomarker. These findings could also contribute towards the development of novel treatment strategies for patients with bladder cancer.

Acknowledgments

I am extremely grateful to my supervisors Dr Anne Kiltie and Dr Eva M^{c}Growder. Thank you Anne for your time, advice and guidance, all of which are hugely appreciated. Also, for giving me the opportunity to be part of such an incredible lab. Thank you Eva for all of your positive encouragement throughout and especially during the thesis-writing phase, which was essential.

I'd like to express my profound thanks to all my friends and colleagues in the department; Chelsea, Jude, Helen, Alexa, Monica, Daniel, Selva, Christien, Katalin, Emma, Aswin and especially Giulia. A special thanks to Martin for never being too busy to stop and listen/explain/make me laugh, and Blaz who was often the reason for the laughter. Blaz, I've never met someone more inquisitive, sometimes even about science!

There are many people that have contributed to the project and I would like to thank Dr Anderson Ryan for providing the panel of lung cancer cell lysates and Dr Ester Hammond for the oesophageal cancer lysates. I am grateful to the Urological team at the Churchill Hospital, Oxford University Hospitals NHS Foundation Trust: the surgical team Professor Freddie Jeremy Hamdy, Mr J Crew and other consultant urologists, and the research nurses and biobanking staff for their help with tumour sample collections. I am also grateful to Professor Benedikt Kessler and his group at the TDI, Oxford, for their help with the mass spectrometry analysis and guidance on interpreting the analysis.

I am thankful to Professor Simon Morley from the University of Sussex for his encouragement towards me pursuing a research career.

I would like to thank my family for their support, belief and encouragement over the years. My parents have done so much for me and I would not have reached this stage without them. Thank you to my dad Kenneth Jevons and to my mum Christine M^{c}Killop and to my stepfather Jeremy Heaton, there is not enough space to express my gratitude, especially to you mum! My sisters Rachael and Alex, thank you so much!

A huge thanks to all of the members past and present of “Iffley Heights”. My time living in Oxford would not have been the same without you guys or the house and the support you’ve all given me is immense- Alex, Ellie, Jamie, Allie, Simon, Rob, Helena, Sally, Will, Mike, Ranya, Rhi, Mel, Dan and Anna.

Table of Contents

Abstract **3**

Acknowledgments **5**

List of Tables **14**

List of Figures **15**

Abbreviations **17**

CHAPTER 1 Introduction **20**

1.1 Bladder cancer **20**

1.1.1 Epidemiology 20

1.1.2 Histopathology of bladder cancer 22

1.1.3 Diagnosis of bladder cancer 25

1.1.4 Treatment of superficial bladder cancer 26

1.1.5 Treatment of muscle-invasive bladder cancer 31

1.1.6 Chemotherapy 32

1.1.7 Radical cystectomy 32

1.1.8 Radical radiotherapy 33

1.1.9 Multimodality treatment 33

1.1.10 Comparison of RC and RT 35

1.1.11 Genetic variants in bladder cancer 36

1.2 DNA damage and DNA repair mechanisms **39**

1.2.1 Ionising radiation and DNA damage 39

1.2.2 DNA damage response 42

1.2.3 Double strand break DNA repair pathways 43

1.2.4 Pathway choice 51

1.2.5 Cell cycle and the DNA damage response 52

1.2.6 IR-induced apoptosis 53

1.3 The MRN complex 54

1.3.1 MRE11 58

1.3.2 Clinical relevance of MRE11 61

1.4 MRE11 in bladder cancer 62

1.5 Aims 64

CHAPTER 2 Materials and Methods 65

2.1 Solutions and buffers 65

2.2 Tissue culture 69

2.2.1 Cell lines 69

2.2.2 Culture conditions 70

2.2.3 Cell culture 71

2.2.4 Cell cryopreservation 71

2.2.5 Cytotoxic treatments 72

2.3 Patient samples 72

2.3.1 Ethical approval 72

2.3.2 Bladder tumour extract preparation 72

2.4 Protein expression assay 73

2.4.1 Lysate preparation 73

2.4.2 Protein concentration quantification 73

2.4.3 Western blot analysis 74

2.5 Immunoprecipitation of MRE11 for mass spectrometry analysis .. 75

2.6 Co-immunoprecipitation of endogenous proteins 76

2.7 Immunoprecipitation of HA-tagged proteins 77

2.8 Mass spectrometry..... 77

2.8.1 Digestion 78

2.8.2 Mass spectrometry data analysis 78

2.9 Cloning of MRE11 78

2.9.1 RNA extraction 78

2.9.2 Complementary DNA preparation 79

2.9.3 Primer design 80

2.9.4 Polymerase chain reaction (PCR) 80

2.9.5 TOPO cloning 82

2.9.6 Screening colonies 82

2.9.7 Diagnostic restriction enzyme digestion 83

2.9.8 Mini-prep 84

2.9.9 Sequencing 84

2.9.10 Maxi-prep 84

2.9.11 Site-directed mutagenesis 85

2.10 Plasmid transfection..... 87

2.10.1 FuGENE HD transfection reagent 87

2.10.2 X-tremeGENE transfection reagent 87

2.11 Quantitative PCR 88

2.11.1 qPCR data analysis 89

2.12 Rapid amplification of cDNA ends (RACE) 90

2.13 Immunofluorescence microscopy and analysis of foci..... 90

2.14 Transient MRE11 knockdown 91

2.15 Stable MRE11 knockdown 92

2.15.1 shRNA design 92

2.15.2 Annealing siRNA oligonucleotides 93
2.15.3 Ligation of annealed siRNA into pSilencer vectors 93
2.15.4 MRE11 or scrambled control shRNA transfection 94
2.15.5 Clone screening 94
2.16 Stable MRE11 re-expression 95
2.17 *I-SceI* HR assay 95
2.17.1 HR *I-SceI* construct and stable expression in the T24 cell line 95
2.17.2 HR assay transfections 96
2.17.3 HR assay sample preparation 97
2.17.4 GFP and DsRed detection 98
2.18 Clonogenic survival assay 98
2.19 Irradiation of cells 99
2.20 Statistics and data analysis 99
CHAPTER 3 Identification of a novel MRE11 variant in bladder cancer tumours and bladder cancer cell lines 100
3.1 Introduction 100
3.2 Results 102
3.2.1 MRE11 protein expression in bladder tumours 102
3.2.2 MRE11 protein expression in bladder cancer cell lines 106
3.2.3 MRE11 protein expression in other cancer cell lines 108
3.2.4 MRE11 expression in bladder cancer cell line lysates 110
3.2.5 MRE11 immunoprecipitation 111
3.2.6 Mass spectrometry sequencing of MRE11 112
3.2.7 Rapid amplification of MRE11 3'cDNA 115
3.2.8 Fractionated western blot analysis of RT112 cell lysate 117

3.2.9 Co-immunoprecipitation of endogenous MRE11 119

3.2.10 Cloning of MRE11 and site-directed mutagenesis to emulate truncation 121

3.2.11 Co-immunoprecipitation of HA-tagged truncated MRE11 and co-localisation of NBS1 and the truncated MRE11 protein 123

3.2.12 HA-tagged truncated MRE11 co-localises with yH2AX foci 126

3.3 Discussion 128

3.3.1 MRE11 variant detection in bladder tumours 128

3.3.2 Identification of the MRE11 variant 131

3.3.3 Nuclear location of truncated MRE11 protein 133

3.3.4 MRN complex formation 134

3.3.5 Recruitment of truncated MRE11 to IRIF 136

CHAPTER 4 Stability and cause of the truncated MRE11 variant..... 138

4.1 Introduction 138

4.2 Results 142

4.2.1 Stability of MRE11 142

4.2.2 Proteasomal degradation of MRE11 144

4.2.3 The effect of inhibiting caspase function on the truncated MRE11 protein 146

4.2.4 Effect of induction of apoptosis on MRE11 expression 149

4.2.5 Effect of panobinostat on MRE11 expression 151

4.2.6 Effect of panobinostat on MRE11 and caspase activity 153

4.2.7 Modulation of caspase transcription by panobinostat 157

4.2.8 Site-directed mutagenesis of caspase cleavage motif in MRE11 159

4.3 Discussion 161

4.3.1 MRE11 stability and degradation 161

4.3.2 MRE11 caspase and apoptotic response 162

4.3.3 The effect of panobinostat on the MRN complex 164

4.3.4 Caspase motif mutation 166

CHAPTER 5 MRE11 knockdown and functional impact of the MRE11 variant on DNA repair 167

5.1 Introduction 167

5.2 Results 169

5.2.1 Transient MRE11 knockdown 169

5.2.2 Stable MRE11 knockdown 171

5.2.3 MRE11 knockdown radiosensitivity 175

5.2.4 Nuclease inhibitors of MRE11 178

5.2.5 Reduced pATM recruitment in the RT112-derived MRE11 knockdown cell line 180

5.2.6 Re-expression of wild type or truncated MRE11 in the RT112 MRE11 knockdown cell line 183

5.2.7 Optimisation of transient re-expression of wild type or truncated MRE11 in the RT112 MRE11 knockdown cell line 186

5.2.8 Expression of truncated MRE11 in T24 bladder cancer cell line 189

5.2.9 yH2AX foci resolution 195

5.2.10 I-SceI homologous repair assay 198

5.3 Discussion 202

5.3.1 MRE11 knockdown 202

5.3.2 MRE11 knockdown radiosensitivity 203

5.3.3 Re-expression of MRE11 in RT112 205

5.3.4 Re-expression of MRE11 in the T24 cell line 207

5.3.5 yH2AX resolution after IR 207

5.3.6 I-SceI homologous repair assay 209

CHAPTER 6 General discussion and future plans 212

6.1 General discussion 212

6.2 Future plans 215

References 217

APPENDICES A-G 236

List of Tables

Table 1.1 Tumour Node Metastasis System for the classification of bladder tumours 23
Table 1.2 Recurrence and progression score for non-muscle-invasive bladder cancer. 28
Table 1.3 Probability of recurrence and progression in NMIBC. 29
Table 1.4 Treatment choice in muscle-invasive bladder cancer. 36
Table 1.5 Characteristics of the three molecular bladder subtypes. 39
Table 2.1 Antibodies used for western blot analysis 75
Table 2.2 cDNA preparation components per reaction 79
Table 2.3 Primer sequences for MRE11 cloning 80
Table 2.4 PCR components 81
Table 2.5 PCR conditions 81
Table 2.6 TOPO cloning reagents 82
Table 2.7 Restriction enzyme digest components 83
Table 2.8 Restriction enzymes and expected size of cut products 83
Table 2.9 Sanger sequencing primer sequences 84
Table 2.10 Site-directed mutagenesis primer sequences for early stop codon 85
Table 2.11 Site-directed mutagenesis primer sequences for caspase motif 86
Table 2.12 Site-directed mutagenesis reaction components 86
Table 2.13 Site-directed mutagenesis reaction conditions 87
Table 2.14 FuGENE HD transfection guideline volumes 87
Table 2.15 qPCR experiment components 88
Table 2.16 qPCR primer sequences 89
Table 2.17 HR assay *I-SceI* treatments 97
Table 2.18 HR assay *I-SceI* transfection volumes 97

List of Figures

Figure 1.1 Classification of the stages of bladder cancer according to the tumour node metastasis system. 24
Figure 1.2 Overview of the management of non-muscle-invasive bladder cancer. 30
Figure 1.3 Overview of the management of muscle-invasive bladder cancer. 31
Figure 1.4 Indirect of direct DNA damage caused by ionising radiation. 40
Figure 1.5 Double strand break (DSB) repair via homologous recombination. 45
Figure 1.6 Double strand break (DSB) repair via non-homologous end-joining pathway. 48
Figure 1.7 Double strand break (DSB) repair via microhomology-mediated end-joining. 50
Figure 1.8 The MRN complex. 55
Figure 1.9 The RAD50 component of the MRN complex. 57
Figure 1.10 The NBS1 component of the MRN complex. 58
Figure 1.11 The MRE11 protein. 60
Figure 3.1 Expression of the MRN complex proteins in bladder tumours. 103
Figure 3.2 Correlation of the expression of the MRN complex proteins in bladder tumours. 105
Figure 3.3 Expression of the MRN complex proteins in bladder cancer cell lines. 107
Figure 3.4 Expression of the MRN complex proteins in oesophageal and lung cancer cell lines. 109
Figure 3.5 Protein lysate generation. 110
Figure 3.6 Immunoprecipitation of MRE11. 111
Figure 3.7 Mass spectrometry sequencing of wild type MRE11 and the MRE11 variant. 114
Figure 3.8 Amplification of MRE11 3'cDNA ends. 116
Figure 3.9 Cellular localisation of the MRN complex proteins. 118
Figure 3.10 Immunoprecipitation of the endogenous MRN complex proteins. 120
Figure 3.11 Cloning of wild type and truncated MRE11. 122

Figure 3.12 The truncated MRE11 protein directly complexes with NBS1 and RAD50. 125
Figure 3.13 The truncated MRE11 protein is recruited to sites of DNA damage. 127
Figure 4.1 Stability of the MRN complex proteins. 143
Figure 4.2 Proteasomal degradation of MRE11. 145
Figure 4.3 Establishing the concentration of Z-VAD capable of inhibiting caspase activity. 147
Figure 4.4 The effect of caspase inhibition on MRE11 expression. 148
Figure 4.5 The effect of apoptotic stimulation on MRE11 expression. 150
Figure 4.6 The effect of panobinostat on MRE11 expression. 152
Figure 4.7 The effect of panobinostat on homologous repair (HR) protein expression. 156
Figure 4.8 Transcription of *CASP* genes after panobinostat treatment in RT112 bladder cancer cell line. 158
Figure 4.9 Site-directed mutagenesis of a potential caspase cleavage motif in MRE11. 160
Figure 5.1 Transient knockdown of MRE11. 170
Figure 5.2 Stable knockdown of MRE11. 174
Figure 5.3 Sensitivity of the RT112-derived MRE11 knockdown cell line to ionising radiation. 177
Figure 5.4 The effect of MRE11 nuclease inhibition on radiosensitivity. 179
Figure 5.5 Reduced pATM signalling in the RT112-derived MRE11 knockdown cell line. 182
Figure 5.6 Western blot analysis of MRE11 re-expression. 185
Figure 5.7 Transient expression of wild type (WT) MRE11 in the RT112-derived MRE11 knockdown cell line. 188
Figure 5.8 Stable expression of truncated MRE11 in the T24 cell line. 190
Figure 5.9 Expression of truncated MRE11 in the T24 cell line. 192
Figure 5.10 Expression of MRE11 in T24 cell line clones. 194
Figure 5.11 DNA repair kinetics following ionising radiation. 197
Figure 5.12 *I-SceI* HR repair assay. 200

Abbreviations

Alt-NHEJ: alternative NHEJ

AML: acute myeloid leukaemia

ATLD: Ataxia telangiectasia-like disorder

ATM: Ataxia telangiectasia mutated protein

ATP: adenosine triphosphate

BCG: Bacillus Calmette-Guerin

BCON: bladder carbogen nicotinamide

BSA: bovine serum albumin

BST: bladder-sparing treatment

BT: bladder tumour

BUG: British Uro-oncology Group

BAUS: British Association of Urological Surgeons

CDKN2A: cyclin-dependent kinase inhibitor 2A gene

CIS: *carcinoma in situ*

CSS: cause specific survival

CO_2: carbon dioxide

Ct: threshold cycle

CT: computed tomography

DAPI: 4',6-diamidino-2-phenylindole dihydrochloride

DDR: DNA damage response

dHJ: double Holliday junction

DMEM: Dulbecco's Modified Eagle Medium

DMSO: dimethylsulphoxide

DNA: deoxyribonucleic acid

cDNA: copy DNA

dsDNA: double strand DNA

DNA-PK: DNA protein kinase

dNTP: deoxyribonucleotide triphosphate

DRR: DNA damage response

DSB: double strand break

DSS: disease-specific survival

DTT: dithiothreitol

EBT: external beam therapy

EDTA: ethylene diamine tetra acetic acid

EORTC: European Organisation for Research and Treatment of Cancer

ERCC2: excision repair cross-complementation group 2

FANCA: Fanconi anaemia complementation group A

FBS: Fetal bovine serum

FGFR3: fibroblast growth factor receptor 3

FHA: forkhead associated

GC: gemcitabine cisplatin

HRAS: Harvey rat sarcoma viral oncogene

HCl: hydrochloric acid

HDAC: Histone deacetylase

HEPES: N-2-Hydroxyethylpiperazine-N'-2'-ethanesulfonic acid

HF: high fidelity

dH_2O: distilled water

ddH_2O: double distilled water

HG: high grade

HR: homologous recombination

IAP: inhibitor of apoptosis protein

IHC: immunohistochemistry

IR: ionising radiation

LG: low grade

MIBC: muscle-invasive bladder cancer

MMC: mitomycin C

MMEJ: microhomology-mediated end-joining

MRE11: meiotic recombination 11

MRN: MRE11-RAD50-NBS1 complex

M-VAC: methotrexate vinblastine Adriamycin cisplatin

NAT: N- acetyltransferase

NBS: Nijmegen breakage syndrome

NHEJ: non-homologous end-joining

NLS: nuclear localisation signal

NMIBC: non-muscle-invasive bladder cancer

PBS: phosphate buffered saline

PCR: polymerase chain reaction:

qPCR: quantitative polymerase chain reaction

PTEN: phosphatase and tensin homolog

RC: radical cystectomy

RNA: ribonucleic acid

ROS: reactive oxygen species

RPM: revolutions per minute

RT: radiotherapy

SCC: squamous cell carcinoma

SDS: sodium dodecyl sulfate

SDSA: synthesis-dependent strand annealing

shRNA: small hairpin RNA

siRNA: small interfering RNA

SPARE: Selective Bladder Preservation Against Radical Excision Trial

SqCC: squamous cell carcinoma

SSB: single-strand break

STAG2: stromal antigen 2

TBE: tris-borate EDTA

TCC: transitional cell carcinoma

TMT: trimodality therapy/treatment

TNM: Tumour Node Metastasis

TP53: tumour protein p53

TUR: transurethral resection (of the bladder tumour)

TURBT: transurethral resection of the bladder tumour

UC: urothelial carcinoma

Ub: ubiquitin

UPP: ubiquitin proteasome pathway

WCE: whole cell extract

CHAPTER 1 Introduction

1.1 Bladder cancer

1.1.1 Epidemiology

Bladder cancer is the 4th most common cancer in males and the 12th in females in Europe and is more prevalent in the western world than elsewhere. In the UK, bladder cancer is the 4th and 13th most common cancer in males and females, respectively, with 10,400 patients being diagnosed with bladder cancer each year (Cancer Research UK). In 2012 in the UK, approximately 5,200 people died from bladder cancer (Cancer Research UK).

Bladder cancer is more prevalent in men than women with a ratio of 3.8 to 1 (Witjes *et al*. 2014). However, women tend to present with more advanced disease and have a worse survival rate (Fajkovic *et al*. 2011). Although current trends show 5-year survival rates to be increasing for most cancer types, bladder cancer in women is an exception. The 5-year survival for women diagnosed between 2007–2011 is projected to be 49.1% and for those diagnosed between 2008–2012, 48% (Office for National Statistics 2014).

Bladder cancer is most common in the elderly population, with the average age at diagnosis being 68 years old, and over half of new patients diagnosed in the UK are over 75 years old (Gallagher & Milowsky 2009; Cancer Research UK)

Tobacco smoking is the most established risk factor for bladder cancer in both males and females and is thought to account for approximately 50% and 20% of cases, respectively (Babjuk *et al*. 2013; Freedman *et al*. 2011). Smokers are more genetically susceptible to bladder cancer development if they possess a

polymorphism in a gene from the N- acetyltransferase (NAT) family, NAT2. NAT2 is an enzyme that is important in the clearance of carcinogenic aromatic amines via acetylation. The *NAT2* genotype causes this acetylation process to be slower, leading to the build up of aromatic amines (Kiriluk *et al*. 2012; Burger *et al*. 2013). The second most prominent risk factor, accounting for approximately 10–20% of all cases of bladder cancer, is exposure to agents such as aromatic amines, polycyclic aromatic hydrocarbons and diesel engine exhaust (Burger *et al*. 2013). Exposure to these products often occurs in an occupational setting, for example in paint processing, dye manufacturing, leather production, rubber and textile industries and professions involving exposure to carbon emissions (Babjuk *et al*. 2013; Brown *et al*. 2012). Historically, these are male dominated industries, offering a possible explanation as to why bladder cancer is more prevalent in males and in more developed countries. However, differences in oestrogen and androgen levels between men and women have also been implicated in the difference in gender prevalences (McGrath *et al*. 2006).

Schistosomiasis (chronic cystitis or inflammation of the bladder caused by Schistosoma haematobium) is associated with an increased risk for the development of squamous cell carcinoma (SCC) and urothelial carcinoma (Zheng *et al*. 2012). It is particularly widespread in some parts of North Africa, where the waterborne parasitic trematode leads to the infection by travelling up the urethra from infested water. The fact that the pathogen is common in Egypt has contributed to a two-fold higher incidence of bladder cancer there than in some Western countries (Ploeg *et al*. 2009; Burger *et al*. 2013).

1.1.2 Histopathology of bladder cancer

Bladder cancer is usually of the transitional cell type (TCC) but may be squamous cell type (SqCC). Other rarer subtypes include adenocarcinoma and small cell carcinoma. SqCCs tend to present as solid bulky tumours that contain no identifiable transitional cells and are frequently associated with chronic irritation (Burger *et al*. 2013). Adenocarcinomas are derived from the urothelium and are neoplastic cells that form glandular structures and often produce mucin, sometimes causing the tumour to appear gelatinous and may be associated with primitive rests of mesenchymal tissue (Eble *et al*. 2004; Mazzucchelli *et al*. 2012; Dahm & Gschwend 2003). The typical TCC is derived from the transitional cells of the urothelium, hence it is now called urothelial carcinoma (UC). This thesis will primarily focus on UCs.

Approximately 90% of bladder cancers in North America and Europe are UCs presenting as either flat lesions or papillary lesions that grow into the bladder lumen. The distinction between the two is based on different morphologies such as: atypia, nuclear pleomorphism, nuclear polarity, cellular mitoses and gross appearance. These tumours can be classified using the Tumour Node Metastasis (TNM) system (Table 1.1), to assign a stage according to the extent of invasion into the bladder wall, the extension to local or distant lymph nodes and their metastasis beyond the bladder (International Union Against Cancer 2009).

Table 1.1 Tumour Node Metastasis System for the classification of bladder tumours

Adapted from (Bostrom *et al*. 2010).

T- Primary tumour
TX Primary tumour cannot be assessed
T0 No evidence of primary tumour
Ta Non-invasive papillary carcinoma
Tis Carcinoma in situ: 'flat tumour'
T1 Tumour invades subepithelial connective tissue
T2 Tumour invades muscle
T2a Tumour invades superficial muscle (inner half)
T2b Tumour invades deep muscle (outer half)
T3 Tumour invades perivesical tissue:
T3a microscopically
T3b macroscopically (extravesical mass)
T4 Tumour invades any of the following: prostate stroma, seminal vesicles, uterus, vagina, pelvic wall, abdominal wall
T4a Tumour invades prostate stroma, seminal vesicles, uterus, or vagina
T4b Tumour invades pelvic wall or abdominal wall
N – Regional Lymph Nodes
NX Regional lymph nodes cannot be assessed
N0 No regional lymph node metastasis
N1 Metastasis in a single lymph node in the true pelvis (hypogastric, obturator, external iliac, or presacral)
N2 Metastasis in multiple lymph nodes in the true pelvis (hypogastric, obturator, external iliac, or presacral)
N3 Metastasis in a common iliac lymph node(s)
M – Distant Metastasis
M0 No distant metastasis
M1 Distant metastasis

At presentation, 75% of patients are diagnosed with non-muscle-invasive bladder cancer (NMIBC), meaning that the cancer is either confined to the mucosa (stage Ta, *carcinoma in situ* [CIS]) or to the submucosa, (lamina propria, stage T1; Babjuk *et al*. 2013; Figure 1.1). The remaining 25% of patients present with muscle-invasive bladder cancer (MIBC), meaning that the cancer has invaded into (T2) and through (T3) the muscle wall of the bladder. Further invasion by the tumour into the pelvic side wall or surrounding organs, such as the prostate or vagina, is classified as T4.

Previously, bladder tumours were also graded histologically according to a three grade system, generally becoming more dysmorphic with invasive characteristics.

1. Grade 1, well differentiated: tumours have the least degree of anaplasia
2. Grade 2, moderately differentiated: tumours have a degree of anaplasia
3. Grade 3, poorly differentiated: tumours have the most severe degree of anaplasia (Bostrom *et al*. 2010).

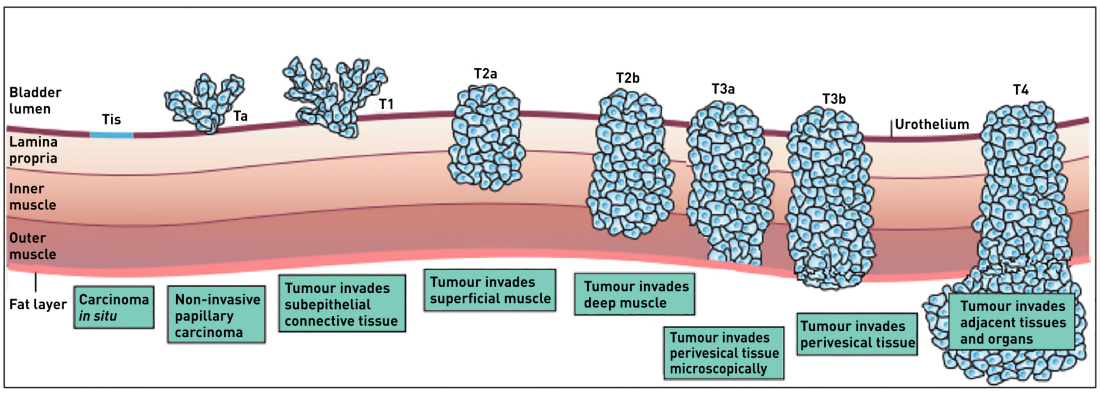

Figure 1.1 Classification of the stages of bladder cancer according to the tumour node metastasis system.
CIS and Ta remain in the urothelial layer of the bladder, whereas T1 invades the lamina propria. Stages T2a and b invade the muscle layer of the bladder to varying degrees. T3a microscopically invades the perivesical fat, whereas T3b macroscopically invades the perivesical tissue. T4 invades nearby tissues and organs. Adapted from Knowles & Hurst (2015).

Currently, bladder tumours are graded according to a two grade classification, namely low grade (LG) and high grade (HG) (Bostrom *et al*. 2010). Defining tumour stage and grade is important for determining prognosis and treatment options for individual patients. MIBC can further be categorised by lymph node and metastatic status, as outlined in Table 1.1.

Patients with superficial NMIBC have a good prognosis, with 5-year survival rates between 80 and 90%, whereas patients with MIBC have 5-year survival rates of 50% (Cancer Research UK). Due to the high frequency of recurrence, the need for continuous monitoring and the success of management, bladder cancer is one of the costliest malignancies to treat throughout the life of a patient (Sievert *et al*. 2009).

1.1.3 Diagnosis of bladder cancer

Approximately 85% of patients with bladder cancer may experience painless gross haematuria – visible blood in the urine (Babjuk *et al*. 2013; Cancer research UK). Others present with microscopic haematuria on testing for unrelated conditions. However, this is also seen in bladder or kidney infections or other inflammation of the urinary tract. Therefore, further testing is required to establish the importance of a finding of microscopic haematuria. Other presenting symptoms depend on the location and characteristics of the tumour and may include: urgency, frequency and pain when urinating. Patients with more advance tumours can also experience obstruction of the urinary tract and pelvic, back and abdominal pain (Cancer Research UK).

Testing the urine to rule out the presence of infection or to examine the cellular morphology (urine cytology), is a first line method of assessment. Flexible cystoscopy is then performed in which the urothelial lining of the bladder is visually inspected to identify potential bladder causes of the bleeding (Babjuk *et al*. 2013). The urinary tract will also be visualised using a computed tomography (CT) urogram (Babjuk *et al*. 2013).

After being diagnosed with bladder cancer, suitable patients will undergo a transurethral resection of bladder tumour (TURBT or TUR) in which all visible lesions are removed (Babjuk *et al*. 2013). This allows the cellular type and pathological stage of the tumour to be determined and is also an important therapeutic and sometimes curative step.

1.1.4 Treatment of superficial bladder cancer

As stated above, TUR is the first treatment performed after diagnosis of NMIBC. The aim is to identify and completely remove all papillary tumours, including a biopsy of the muscle wall (Mariappan *et al*. 2010), as well as to identify CIS lesions and ensure correct staging of the tumour(s) (Babjuk *et al*. 2013; Mostafid & Brausi 2012).

The recurrence rate of bladder tumours is high and is experienced by up to 70% of patients. Multiple factors influence tumour recurrence such as: tumour aggressiveness (related to grade), incomplete resection (related to stage) and implantation of tumour cells after TUR. Therefore, surgical expertise is required to ensure complete removal of the tumour(s), with recurrence rates varying from 3.5% to 20.6% depending on the institute (Brausi *et al*. 2002). Tumour recurrence

can be reduced by the administration of a single instillation of intravesical chemotherapy, usually mitomycin C, after TUR in order to abolish any circulating or residual tumour cells (Sylvester *et al*. 2004; Gudjónsson *et al*. 2009).

The risk of recurrence and progression of NMIBC can be determined using the European Organisation for Research and Treatment of Cancer (EORTC) guidelines (Sylvester *et al*. 2006) with the most important risk factors for recurrence being the number of tumours, their size and prior recurrences (Table 1.2). The aim of the score is to group patients with low, intermediate, and high risk of recurrence in order to direct further treatment choice (Sylvester *et al*. 2006; Table 1.3). Patients with NMIBC who have intermediate or high recurrence risk are treated with adjuvant intravesical bacillus Calmette-Guerin (BCG) immunotherapy, which is more effective in reducing recurrence and progression than chemotherapy when maintained for 1 to 3 years (Bohle & Bock 2003; Shelley *et al*. 2004; Malmström *et al*. 2009).

Following the initial TUR, a second TUR is performed in all patients with T1 staging and in those at high risk of recurrence. Figure 1.2 provides an overview of the treatment strategy for patients with NMIBC.

Table 1.2 Recurrence and progression score for non-muscle-invasive bladder cancer.

Factors contributing to the recurrence and progression risk score in NMIBC. Adapted from: (Sylvester *et al*. 2006).

Factor	Recurrence	Progression
Number of tumours		
Single	0	0
2 to 7	3	3
≥8	6	3
Tumour size		
<3 cm	0	0
≥3 cm	3	3
Prior recurrence rate		
Primary	0	0
≤1 recurrence/year	2	2
>1 recurrence/year	4	2
T category		
Ta	0	0
T1	1	4
CIS		
No	0	0
Yes	1	6
Grade		
G1	0	0
G2	1	0
G3	2	5
Total score	**0–17**	**0–23**

Table 1.3 Probability of recurrence and progression in NMIBC.

Risk categorised according to total score calculated from Table 1.2. Patients are grouped according to those at low, intermediate and high risk. Adapted from: (Sylvester *et al*. 2006).

Recurrence score	Probability of recurrence at 1 year (95% CI)		Probability of recurrence at 5 years (95% CI)	
0	15%	(10–19%)	31%	(24–37%)
1–4	24%	(21–26%)	46%	(42–49%)
5–9	38%	(35–41%)	62%	(58–65%)
10–17	61%	(55–67%)	78%	(73–84%)
Progression score	**Probability of progression at 1 year (95% CI)**		**Probability of progression at 5 years (95% CI)**	
0	0.2%	(0–0.7%)	0.8%	(0–1.7%)
2–6	1.0%	(0.4–1.6%)	6%	(5–8%)
7–13	5%	(4–7%)	17%	(14–20%)
14–23	17%	(10–24%)	45%	(35–55%)

CI = confidence interval | Low risk | Intermediate risk | High risk

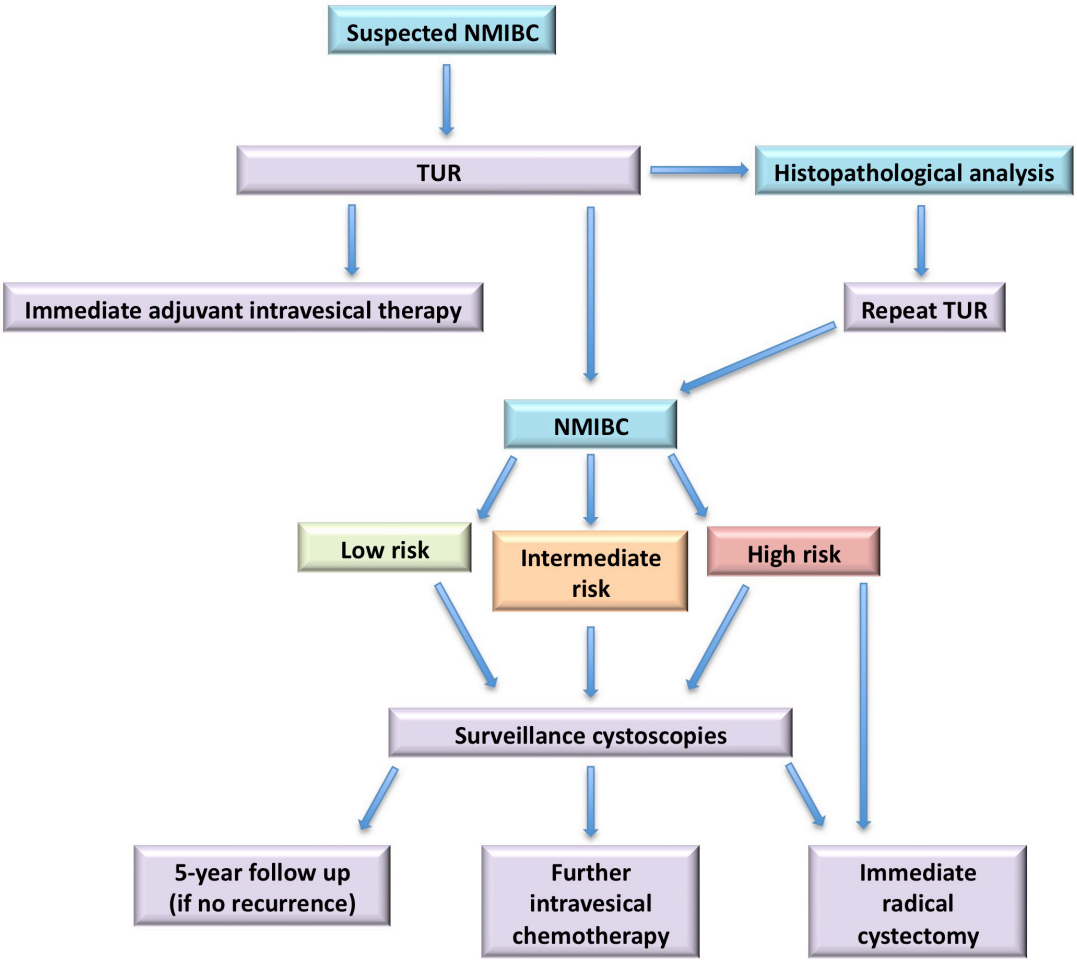

Figure 1.2 Overview of the management of non-muscle-invasive bladder cancer. TUR = transurethral resection. Adapted from: British Uro-oncology Group (2013).

1.1.5 Treatment of muscle-invasive bladder cancer

Approximately 50% of NMIBC are likely to progress into MIBC, with CIS lesions more frequently advancing to MIBC compared with papillary lesions (Sylvester *et al*. 2006). Treatment of CIS and MIBC involves either radical cystectomy (RC) or radiotherapy (RT) -based bladder preserving treatments, often in combination with neoadjuvant chemotherapy prior to definitive treatment to reduce the risk of micrometastatic disease (Witjes *et al*. 2014; Griffiths 2013). An overview of the management of MIBC is outlined in Figure 1.3.

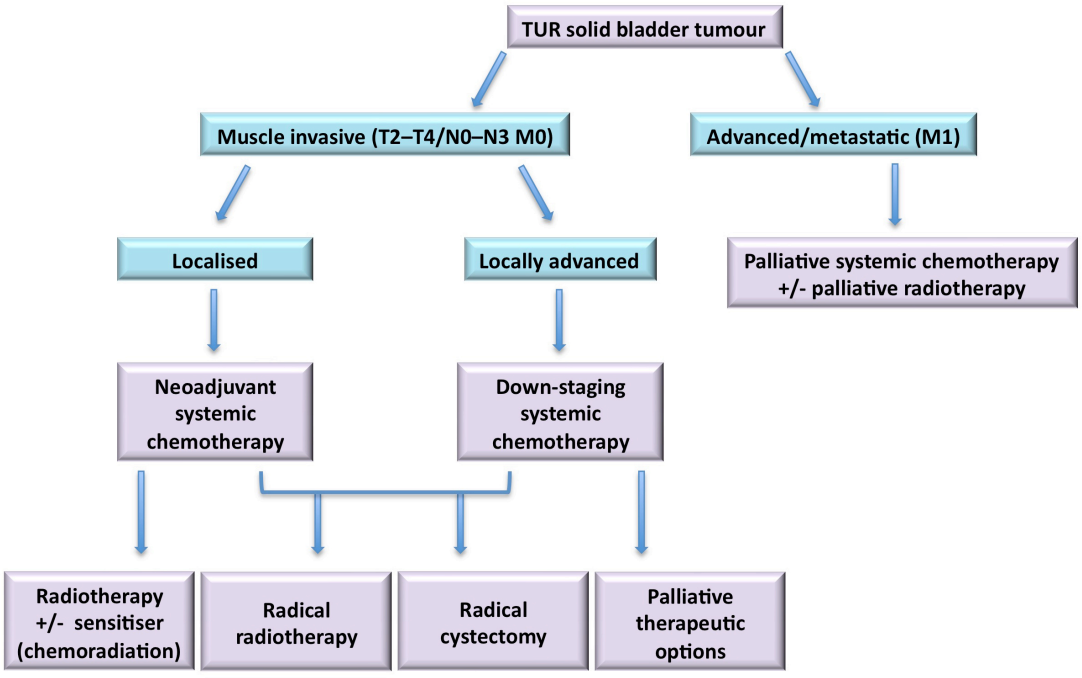

Figure 1.3 Overview of the management of muscle-invasive bladder cancer.
TUR = transurethral resection. Adapted from: Griffiths (2013) and British Uro-oncology Group (2013).

1.1.6 Chemotherapy

Chemotherapy has been shown to improve overall survival in bladder cancer patients when used in combination with radical therapies. The current guidelines on the management of bladder cancer developed by the British Uro-oncology Group (BUG) and the British Association of Urological Surgeons (BAUS) recommend three chemotherapy strategies:

1. Neoadjuvant chemotherapy given prior to RT or RC, involving three cycles of cisplatin-based chemotherapy, often in combination with other agents, e.g. gemcitabine-cisplatin (GC) or methotrexate-vinblastine-adriamycin-cisplatin (M-VAC);
2. Down-staging for patients with locally advanced or node-positive, non-metastatic disease involving 3−6 cycles of chemotherapy to optimise response to RT and RC;
3. Synchronous chemoradiation involving chemotherapy given concurrently with RT (British Uro-oncology Group 2013).

1.1.7 Radical cystectomy

RC is the surgical removal of the entire bladder, which is often performed with bilateral lymph node dissection in MIBC, and includes urinary diversion through conventional urostomy or generation of a neobladder (Hautmann *et al*. 2007). Acute complications associated with cystectomy include bleeding, infection and stomal problems. More severe complications experienced in up to 28% of patients relate to cardiac, respiratory and gastrointestinal problems, as well as a 3% mortality rate (Nieuwenhuijzen *et al*. 2008; Konety *et al*. 2006). The risk of

complications is increased by existing comorbidities and patient age. Major late complications of RC include possible incontinence, impotence, pouchitis (inflammation of the reservoir) and kidney infections, which will impact on patient quality of life (Nieuwenhuijzen *et al*. 2008). Therefore, it is important to give the patient the option of bladder preservation treatments.

1.1.8 Radical radiotherapy

Standard RT for the treatment of MIBC involves CT-planned external beam radiotherapy using fractionation schedules of 64 Gy in 32 fractions over 6.5 weeks, or 55 Gy in 20 fractions over 4 weeks (British Uro-oncology Group 2013). Acute side effects associated with RT include diarrhoea, tenesmus, proctitis, cystitis and lethargy. Patients can also experience late side effects such as bladder fibrosis, bladder atrophy, haematuria and erectile dysfunction (in men) and vaginal stenosis (in women, British Uro-oncology Group 2013). After RT, patients may also have to undergo a salvage cystectomy due to tumour recurrence or rarely due to severe bladder dysfunction. Occasionally, they may require surgery for bowel obstruction. Gastrointestinal complications are the biggest contributor to mortality after a salvage cystectomy (Chahal *et al*. 2003).

1.1.9 Multimodality treatment

Improvement of RT techniques, optimisation of chemotherapy and use of concurrent radiosensitisers in several recent clinical trials mean that bladder-preserving treatment is emerging as a standard of care for MIBC. Evidence suggests that a trimodality therapy (TMT) approach is optimal and involves an initial maximal TUR, followed by neoadjuvant chemotherapy and then RT

combined with various methods of concurrent chemotherapy delivery. Subsequent monitoring with regular cystoscopies should ensure prompt salvage RC for patients who do not respond or those with invasive recurrence (British Uro-oncology Group 2013).

A recent evaluation of multiple studies assessing TMT, where 80% of patients retained an intact bladder after 5 years, demonstrated low rates of invasive tumour recurrence and high disease specific survival (DSS) of 71% and 65% over 5 and 10 years, respectively (Mak *et al*. 2014). Of the 20% of patients who did require a salvage cystectomy, DSS rates were still 60% and 47% at 5 and 10 years, respectively. This is comparable to the DSS reported following an immediate RC (Ploussard *et al*. 2014). The Phase III BC2001 trial demonstrated that combining concurrent 5-fluorouracil and mitomycin C (MMC) chemotherapy with RT improved 2-year locoregional recurrence free survival across all tumour stages (T2–T4) by 13% compared with RT alone (67% vs. 54%) (James *et al*. 2012). In a further Phase II study of patients receiving chemoradiotherapy with concurrent weekly gemcitabine, DSS at 3 years was 82%, with 89% of patients retaining their bladder (Choudhury *et al*. 2011).

As failure of RT is associated with tumour hypoxia, the BCON (bladder carbogen nicotinamide) trial aimed to improve radiosensitivity by increasing oxygenation of the tumour. This was achieved using a carbogen breathing apparatus (2% CO_2 and 98% O_2), administered 5 minutes before and during RT plus an oral dose of nicotinamide 1.5 to 2 hours before each fraction. This resulted in a 13% (48% vs. 35%) improvement in overall survival compared with RT alone; 83% of patients retained an intact bladder (Hoskin *et al*. 2010).

1.1.10 Comparison of RC and RT

Despite multiple clinical trials (reviewed by Ploussard *et al*. 2014) and several retrospective analyses (Kotwal *et al*. 2008; Arcangeli *et al*. 2015) indicating similar or even increased survival outcomes for RT compared with RC, the implementation in the clinic of organ-preserving TMT for bladder cancer has been limited. No randomised trials have directly compared RC and TMT and the recent SPARE (Selective Bladder Preservation Against Radical Excision) phase III trial unfortunately failed due to multiple factors, such as lack of patient recruitment (Huddart *et al*. 2010).

The main disadvantage of RC is the removal of the bladder and despite improvement in urinary diversion strategies, these techniques still have a significant impact on patient quality of life and are high risk in certain patient groups, such as the elderly. It is therefore vital to identify patient characteristics (Table 1.4) as well as tumour markers that will direct treatment choice in order to maximise survival outcome in the patient population overall.

Table 1.4 Treatment choice in muscle-invasive bladder cancer.
Factors to consider when making treatment choice for muscle-invasive bladder cancer between surgery and radiotherapy. British Uro-oncology Group (2013).

Preference for surgery	Preference for radiotherapy
• Poor bladder function, especially small capacity • Widespread CIS or CIS remote from muscle-invasive tumour • Large volume tumours • Multifocal disease • Pre-existing hydronephrosis (unless treated stenting or nephrostomy) • Active inflammatory bowel disease • Severe lower urinary tract symptoms	• Unifocal disease • Maximum TUR • Good bladder capacity • Minimal or moderate lower urinary tract symptoms • No CIS distant to primary tumour • Unfit for surgery due to comorbidities • Patient preference

1.1.11 Genetic variants in bladder cancer

A great deal of research has been conducted in identifying the molecular subtypes of bladder cancer, and defining their origin in order to understand the vast variation in disease presentation and treatment response. The bladder layers are comprised of the mucosa (urothelium, lamina propria, muscularis mucosa), the muscle layer (muscularis propria), adventitia and serosa/peritoneum at the dome. The urothelium of the bladder comprises of a layer of basal cells (closer to the smooth muscle wall), several layers of intermediate cells and a single layer superficial cells (closer to bladder lumen, Apodaca 2004). It has been reported that these different populations of urothelial cells contribute to the development of bladder cancer subtypes, with papillary lesions arising from intermediate cells whereas CIS and MIBC arise from basal cells (Goebell & Knowles 2010).

NMIBC and MIBC have also shown distinct differences in genetic makeup, leading to the hypothesis that there are multiple pathways leading to carcinogenesis, rather than just the progression of NMIBC to MIBC (Goebell & Knowles 2010). Papillary lesions often have gain of function mutations in the fibroblast growth factor receptor 3 gene (*FGFR3*) and Harvey rat sarcoma viral oncogene (*HRAS*) causing these mutations to be associated with low tumour grade and stage and better prognosis (Knowles & Hurst 2015). Mutations in *FGFR3* occur in over 80% of Ta-1 tumours compared with approximately 40% of T2–3 tumours. Many of the MIBC tumours with a mutation in *FGFR3* also have deletion of the cyclin-dependent kinase inhibitor 2A gene (*CDKN2A*) located in chromosome 9, which is lost in 50% of all bladder carcinomas (Knowles & Hurst 2015). Efforts are being made to exploit these traits as urinary biomarkers in order to detect recurrence in voided urine and reduce the frequency of surveillance cystoscopies (Zuiverloon *et al*. 2013).

CIS and MIBC lesions often contain loss of function mutations in tumour suppressor genes, such as tumour protein p53 (*TP53*), retinoblastoma (*RB*) and phosphatase and tensin homolog (*PTEN*), leading to inactivation of the p53 and RB pathways. The inactivation of *TP53* occurs in over 40% of T2 tumours but rarely in NMIBC (Knowles & Hurst 2015).

NMIBC more frequently have mutations in stromal antigen 2 (*STAG2*) than MIBC, whereas, MIBC have been shown to have inactivating mutations in DNA repair and DNA damage checkpoint genes, including excision repair cross-complementation group 2 (*ERCC2*), ataxia-telangiectasia mutated (*ATM*) and Fanconi anaemia complementation group A (*FANCA*) (Knowles & Hurst 2015).

Another common feature of MIBC is a high level of genomic rearrangements and chromothripsis, which is less frequently seen in NMIBC (Morrison *et al*. 2014).

Sjödahl *et al* (Sjödahl *et al*. 2012) identified intrinsic molecular subtypes of bladder cancer across all grades and disease stages. From this work, three groups identified subtypes of MIBC at the molecular level using gene expression profiling, classifying MIBC into three major subtypes: 'basal-like', 'p53-like' and 'luminal', although classification varied slightly between the groups (The Cancer Genome Atlas Research Network 2014; Choi *et al*. 2014; Damrauer *et al*. 2014). The categorisation of MIBC by this means identified differential prognosis and response to chemotherapy between the subtypes which has the potential to be exploited in the clinic. For example the p53-like subtype exhibits resistance to neoadjuvant chemotherapy. Further characteristics are defined in Table 1.5 (Choi *et al*. 2014; Knowles & Hurst 2015).

Table 1.5 Characteristics of the three molecular bladder subtypes.
Molecular subtypes of bladder cancer defined by Choi *et al*. (2014). Adapted from (Knowles & Hurst 2015).

	Luminal	p53- like	Basal
Prognosis	Better OS and DSS than basal subtype	Better OS and DSS than basal subtype	Poor OS and DSS
Response to neoadjuvant chemotherapy	Responsive	Resistant	60% of tumours resistant
Additional features	Mutation in FGFR3	Active p53-associated gene expression signature	More common in women Squamous features

1.2 DNA damage and DNA repair mechanisms

1.2.1 Ionising radiation and DNA damage

Patients treated with conventional radiotherapy are exposed to ionising radiation (IR) in the form of photons. These particles are able to ionise or eject electrons from molecules within the cell. The high-energy electrons subsequently collide with additional molecules causing further ionisations, losing energy as they travel (Joiner & van der Kogel 2009). Radiation can induce DNA lesions directly through the deposition of energy on DNA molecules or indirectly through free radicals generated near to the DNA, the latter being responsible for the majority of DNA lesions caused by IR at 30–40% and 60–70%, respectively (Lomax *et al*. 2013) (Figure 1.4).

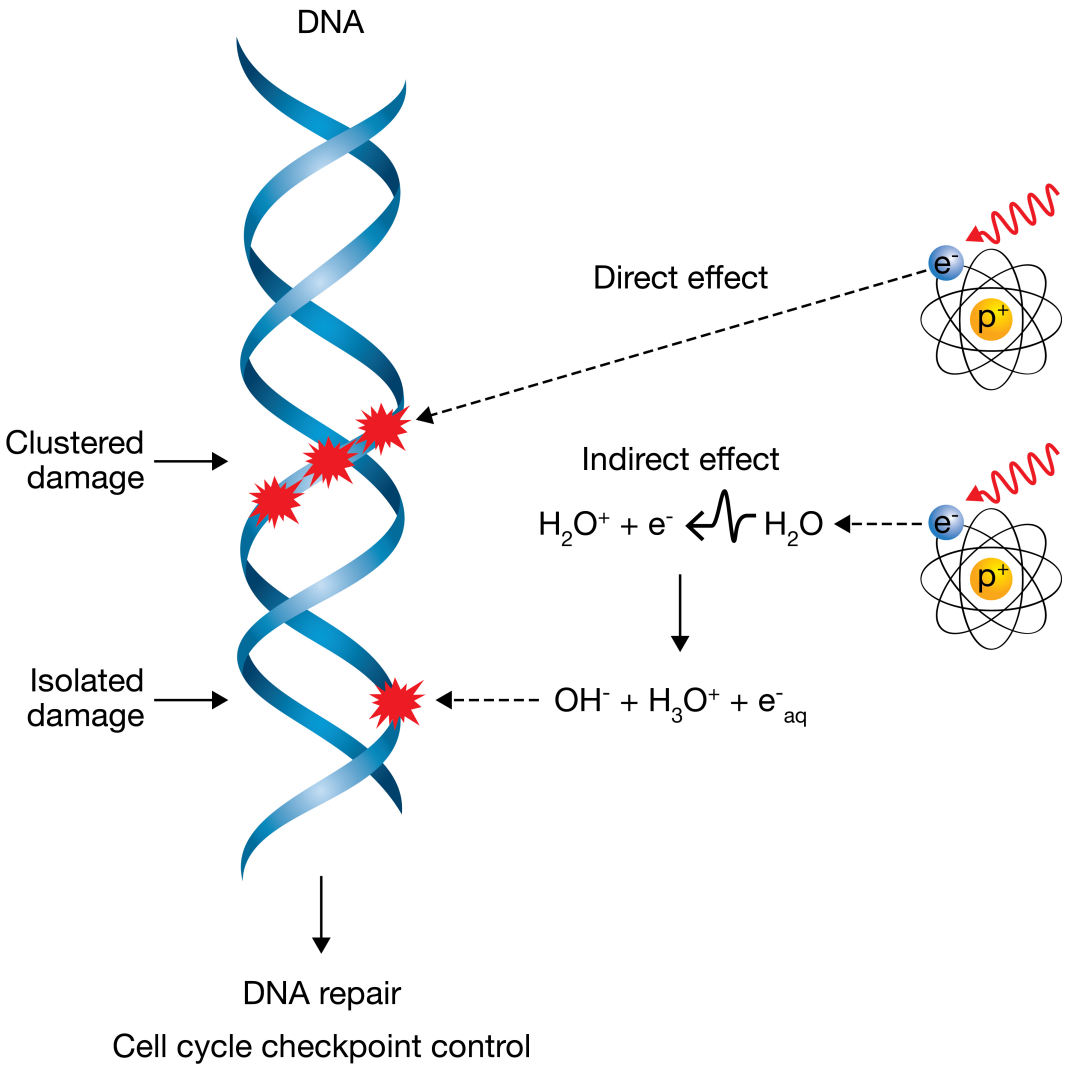

Figure 1.4 Indirect of direct DNA damage caused by ionising radiation.
Photons (red wave) cause ionisations, ejecting electrons from atoms in the cells. These can harm DNA directly. Alternatively, ejected electrons can cause radiolysis of water, and free radicals can harm the DNA molecule indirectly. Adapted from (Morgan & Sowa 2005).

IR from linear accelerators is used to treat patients with MIBC and is known as external beam therapy (EBT). Various types of DNA lesions are produced by radiation. A 2 Gy fraction of IR, a typical therapeutic dose, will result in approximately 3000 DNA lesions per cell, which is much lower than the number of endogenous DNA lesions encountered by the cells daily (Lomax *et al*. 2013; Swenberg *et al*. 2011).

However, endogenous and IR induced lesions vary in their distribution across the DNA, with IR typically causing ionisations to occur within a confined region, leading to the formation of damage clusters compared with the isolated lesions resulting from endogenous damage (Lomax *et al*. 2013).

The complexity of DNA lesions created by IR is also much greater including double-strand breaks (DSBs), which arise less frequently endogenously. DSB are the most cytotoxic lesions caused by IR and are not only generated immediately following radiation exposure but can also occur later due to stalled replication forks and collapse at single-strand breaks (SSBs) (Harper *et al*. 2010; Groth *et al*. 2012; Bennett *et al*. 1993). The complexity of DSB also varies depending on the chromatin structure surrounding the break and the break characteristics. Complex DSBs, which include those with oxidised bases, large single-stranded DNA overhangs or damage on the 3' phosphate, lead to a greater burden on DNA repair mechanisms (Yajima *et al*. 2013). This results in genomic instability and cell death, especially in cancer cells with compromised DNA repair pathways.

The "5Rs" of radiobiology refer to the main contributing factors that control the response of cancerous cells to fractionated radiotherapy. These are: *repair* of DNA damage following IR, *repopulation* of cells (cell division) and *redistribution* of

cell cycle phases, tumour *reoxygenation*, with low tissue oxygen resulting in reduced radiosensitivity, and intrinsic cellular *radiosensitivity.* These factors differ between cancer and non-cancerous cells and present possible therapeutic targets and have also limitations in the use RT for cancer therapy (Good & Harrington 2013; Schaue & McBride 2015).

1.2.2 DNA damage response

Endogenous sources of DNA damage, such as reactive oxygen species (ROS) resulting from aerobic respiration, can lead to as many as 50,000 DNA modifications per day (Swenberg *et al*. 2011). In most cells these simple DNA lesions can be repaired rapidly and efficiently in order to maintain genome integrity. However, if left unrepaired these lesions can lead to aberrant cellular behaviour resulting in the development of cancer.

To overcome DNA damage and avoid potentially lethal genetic alterations, cells have developed a complex network of signalling pathways, collectively known as the DNA damage response (DDR). These pathways orchestrate the detection and subsequent repair of DNA damage, transiently arresting cell cycle progression to ensure the maintenance of genomic stability (Jackson & Bartek 2009).

Ataxia telangiectasia mutated (ATM) and the MRE11-RAD50-NBS1 (MRN) protein complex are the earliest to respond to DNA DSBs (Rupnik *et al*. 2010). The C-terminus of NBS1 is required to recruit ATM to DSBs, after which ATM is autophosphorylated on serine-1981 (Bakkenist & Kastan 2003; Falck *et al*. 2005). ATM then goes on to phosphorylate many downstream targets, including the MRN complex, CHK2 kinase and H2AX on serine 139 (yH2AX), amplifying the DDR

signal (Kijas *et al*. 2015; Matsuoka *et al*. 1998; Burma *et al*. 2001). Once detected there are three main DNA DSB repair pathways: homologous recombination (HR) non-homologous end joining (NHEJ) and microhomology-mediated end-joining (MMEJ).

1.2.3 Double strand break DNA repair pathways

Homologous recombination

Homologous recombination (HR) is a complex process and is therefore a slower repair pathway than NHEJ. However, unlike NHEJ it is accurate and allows all genetic information to be retained at the DSB site (Beucher *et al*. 2009). The initiation of HR involves DNA end resection in a 5'-3' direction, creating 3' -ssDNA overhangs. The MRN complex, in collaboration with CtIP and BRCA1, plays a crucial role in this resection step via both the endo- and exo- nuclease activity of MRE11, committing cells to HR (Sartori *et al*. 2007; Shibata *et al*. 2014; Buis *et al*. 2012). As MRE11 only possesses 3'-5' exonuclease activity, other nucleases are involved, including BLM and Exo1 (Garcia *et al*. 2011). Replication protein A (RPA) rapidly binds and stabilises the resulting ssDNA and, in a process involving BRCA2 and PALB2, is subsequently displaced for RAD51 to be loaded. Preferably a homologous DNA sequence from a sister chromatid will then invade the strand, generating a displacement loop (D-loop) (Buisson *et al*. 2010). However, homologous sequences from across the genome can be utilised but this is more likely to result in incorrect pairing and mutagenesis. Therefore, HR is mainly used in S/G2, where a sister chromatid is available, and not in G1 phases of the cell cycle (Kass & Jasin 2010). The intermediate DNA formation is then resolved by

either a double Holliday junction (dHJ) pathway, resulting in crossover or non-crossover products, or by synthesis-dependent strand annealing (SDSA), resulting in non-crossover DNA (Figure 1.5; Buisson *et al*. 2010).

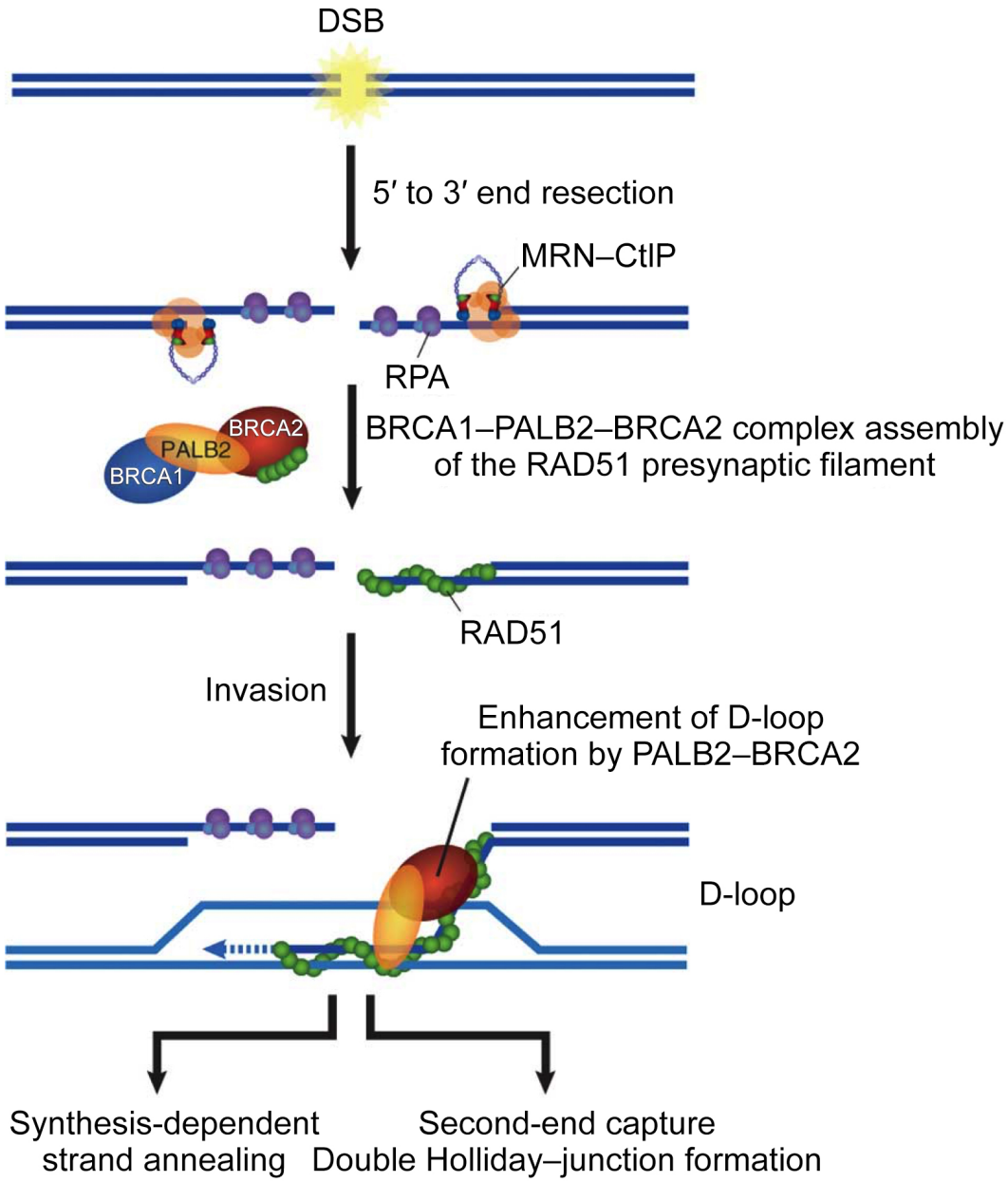

Figure 1.5 Double strand break (DSB) repair via homologous recombination. Model showing the synergistic activity of PALB2 and BRCA2 resulting in the stimulation of homologous recombination. Following damage to the DNA, resection by MRN and CtIP occurs. RAD51 is activated by PALB2-BRCA2 resulting in the invasion of an undamaged template. This leads to synthesis-dependent strand annealing or second-end capture and double–Holliday junction formation, so allowing DSB repair. Adapted from Buisson *et al*. (2010).

HR is not only important for IR-induced DSB repair but is also required during VDJ recombination and stalled replication fork rescue. Therefore mutations in genes encoding HR proteins, namely BRCA1 and 2, have been strongly associated with the development of cancers such as breast and ovarian cancer (Levy-Lahad & Friedman 2007; Pal *et al*. 2005). However, this also leaves tumours that are reliant on NHEJ to repair DSBs vulnerable to therapies that are able to exploit synthetic lethality, an important concept in current cancer therapies. This includes use of the PARP inhibitor olaparib for the treatment of BRCA1- and BRCA2-deficient tumours, which acts by inhibiting SSB repair leading to replication fork collapse, hence the formation of DSBs which require HR for repair (Fong *et al*. 2009; Tutt *et al*. 2010). In cells with a compromised HR pathway, this leads to greater cell death.

Non-homologous end-joining

As well as ATM and MRN, the highly abundant Ku protein is another DNA damage-sensing protein. Ku exists as a heterodimer of two structurally related proteins, Ku70 and Ku80, which rapidly bind to either side of a DSB, bridging the gap between the DNA ends (Lieber 2010). This stabilises the break and initiates DNA repair via the non-homologous end-joining (NHEJ) pathway. This includes the recruitment of DNA-dependent protein kinase catalytic subunit (DNA-PK) to facilitate the DNA end ligation by XRCC4, DNA ligase IV and XLF proteins (Figure 1.6; (Lieber 2010; Chan *et al*. 2002). Limited end processing can occur by the nuclease Artemis to generate ligatable ends, a process that is more likely to be required at IR-induced DSBs. Unlike HR, NHEJ is error-prone as there is no

sequence homology to use as a template (Bétermier *et al*. 2014). This can result in sequence alteration and either loss or gain of bases at the DSB site. However, due to the speed at which ends can be re-joined, NHEJ is the most prominent repair pathway utilised by the cells, particularly in the G1 phase of the cell cycle.

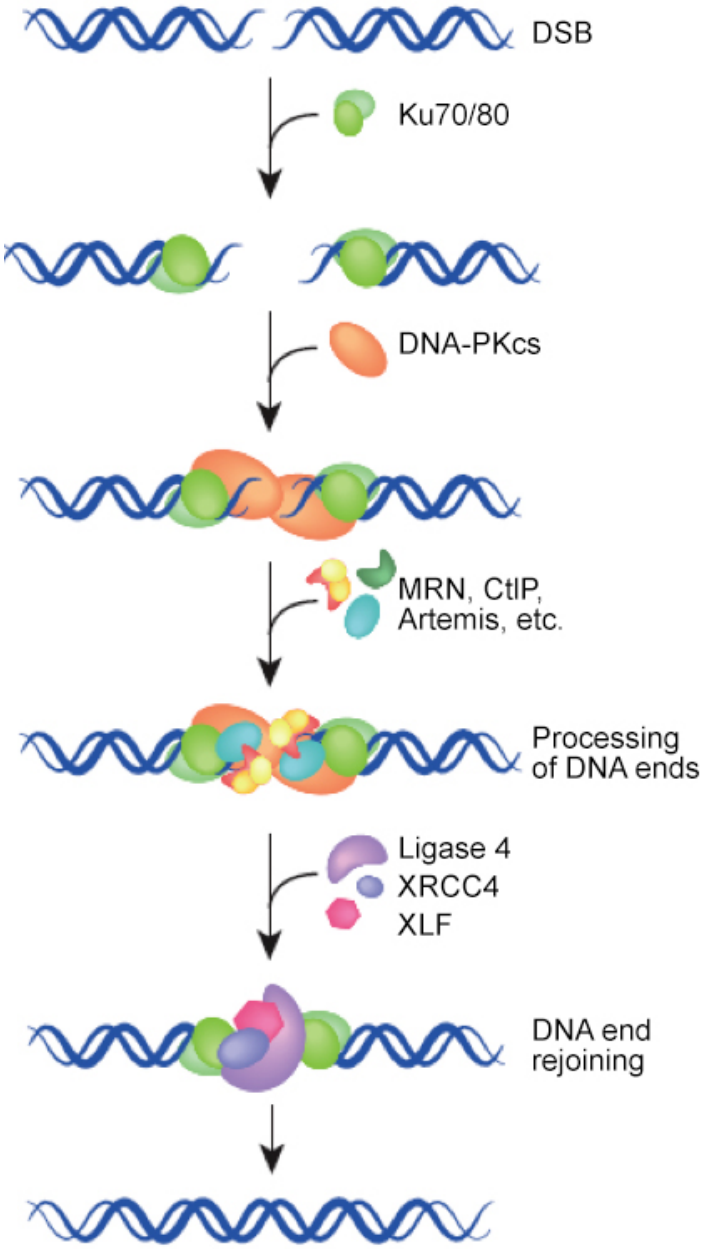

Figure 1.6 Double strand break (DSB) repair via non-homologous end-joining pathway.

The Ku heterodimer (Ku70/80) and the DNA-PK catalytic subunit (DNA-PKcs) combine to form the DNA-PK holoenzyme. Additional enzymes (e.g. MRN, CtIP, Artemis) process the DNA ends, which are then rejoined by the ligase 4 (LIG4)/XRCC4/XLF complex. Adapted from Dueva & Iliakis (2013).

Microhomology-mediated end-joining

Although HR and NHEJ are considered the two main DNA repair pathways, there is evidence of other pathways that repair DSBs, microhomology-mediated end-joining (MMEJ) being one of these. Originally thought of as a 'back-up' pathway if NHEJ or HR are unable to repair, there is now evidence to suggest that MMEJ is used throughout the cell cycle, independent of whether NHEJ and HR are functioning or not (Truong *et al*. 2013). For example, the frequent use of MMEJ during immunoglobulin gene class-switch recombination (McVey & Lee 2008). The exact mechanism of MMEJ has not been defined, and it is often grouped with alternative NHEJ (alt-NHEJ). However, the defining feature of MMEJ is re-joining at regions of microhomology, typically 5–30 nucleotides in length, after resection at the DSB site. Similarly to HR, this involves MRN and CtIP and is independent of Ku and DNA-PK (Truong *et al*. 2013), although unlike HR, no template sequence is utilised. The regions of microhomology can be up to 1 Kb from the DSB site and therefore this pathway is error-prone and can result in the loss of large amounts of genetic information at the break (Figure 1.7; Dueva & Iliakis 2013). Bentley *et al* demonstrated that MMEJ is a preferential DSB repair pathway in some bladder tumours, offering a potential therapeutic target for these tumours, such as the use of PARP inhibitors in BRCA-deficient tumours (Bentley *et al*. 2004; Fong *et al*. 2009; Tutt *et al*. 2010).

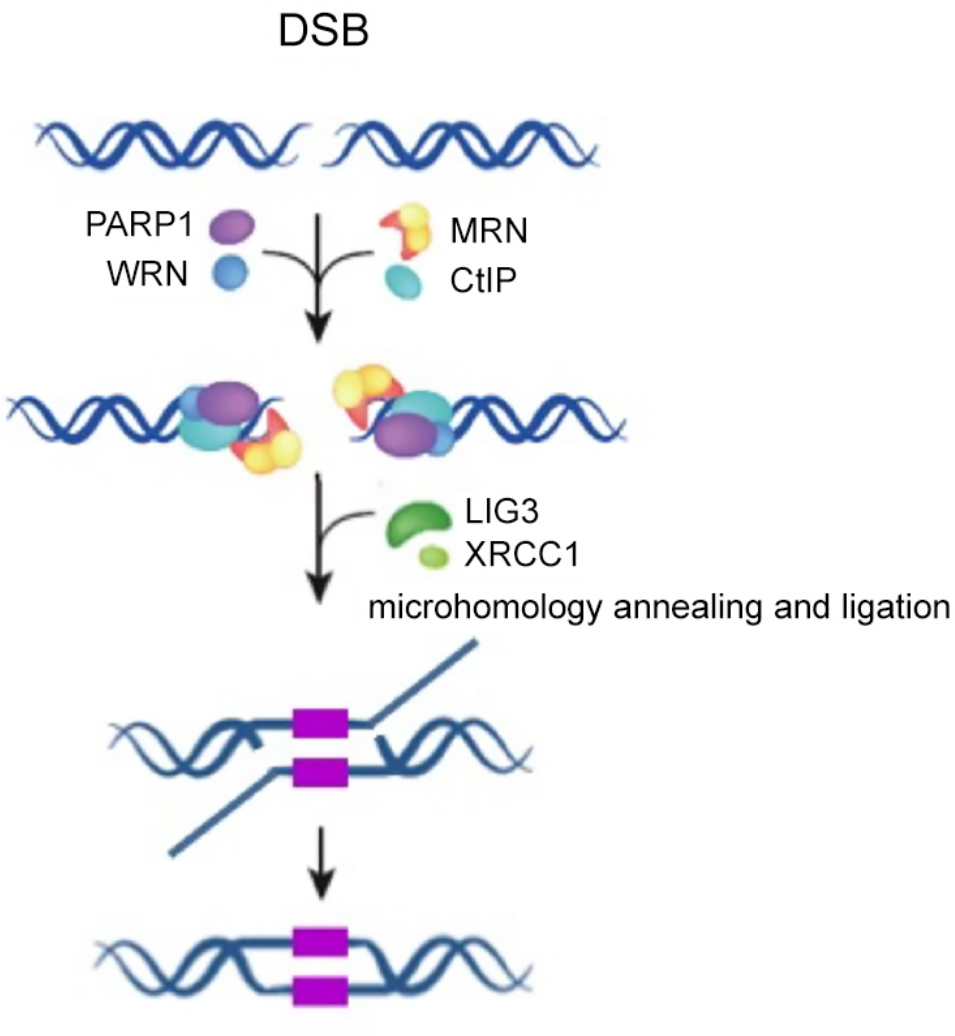

Figure 1.7 Double strand break (DSB) repair via microhomology-mediated end-joining.

PARP-1 and the MRN complex initiate resection of DNA ends. DNA annealing is mediated by XRCC1 and DNA Ligase III enzymes to join DNA at regions of microhomology. Purple boxes represent areas of microhomology. Adapted from Dueva & Iliakis (2013).

1.2.4 Pathway choice

Evidence suggests that the choice of pathway is utilised is a tightly regulated and finely tuned mechanism. However, the decision process is not yet fully understood. The complexity of the break, chromatin structure and cell cycle phase can all influence pathway choice (Yajima *et al*. 2013; Kass & Jasin 2010). Another influencing factor could be the timing of recruitment of either NHEJ proteins (Ku) or HR proteins (MRE11), with the two proteins competing for initiation of their respective pathways (Rupnik *et al*. 2010; Shibata *et al*. 2014). The amount of resection at the break site directs repair towards HR and MMEJ rather than NHEJ. However, for this resection to occur it has been suggested that Ku needs to be displaced (Shao *et al*. 2012).

The complexity of the break, such as clustered damage, influences the cell to utilise HR, in preference to NHEJ, which has reduced efficiency at repairing these breaks due to limited resection capacity (Lomax *et al*. 2013). HR predominates in repairing DSB that occur in regions of heterochromatin (HC), as ATM is involved in the phosphorylation of KAP-1, a process that relaxes the HC to allow repair to occur (Goodarzi *et al*. 2008).

Cell cycle phase is the most critical factor in DSB repair choice, as HR is mostly restricted to late S and G2 phases of the cell cycle, where a sister chromatid is available to act as a template. NHEJ and MMEJ do not carry this restriction and so operate throughout the cell cycle (Kass & Jasin 2010). The levels of HR proteins such as RAD51 and BRCA1 increase as cells progress from S to G2 phase and CDKs play a critical role in the control of phosphorylation and activation of HR proteins, such as CtIP (Buis *et al*. 2012; Yu & Chen 2004; Shrivastav *et al*. 2008).

Additional cell cycle influences on pathway choice include the phosphorylation of RIF1 by 53BP1 in the G1 cell cycle phase suppressing BRCA1 recruitment, therefore promoting NHEJ (Escribano-Diaz *et al*. 2013). In the S and G2 phases, however, BRCA1-CtIP limit RIF1 accumulation and HR proceeds. Furthermore BLM, the affected protein in patients with Bloom's syndrome, promotes MMEJ or NHEJ depending on a variety of interacting factors. In the presence of 53BP1 and RIF1, BLM promotes NHEJ by blocking extensive resection by the MRN complex and CtIP. In contrast, when 53BP1 and RIF1 are absent, BLM encourages resection resulting in MMEJ (Grabarz *et al*. 2013).

1.2.5 Cell cycle and the DNA damage response

In addition to repairing the DNA damage, the DDR is responsible for halting cell cycle progression, firstly for the repair to take place and secondly to ensure no damaged cells replicate, thereby maintaining genome stability.

Checkpoint arrest occurs through the activation of the downstream targets of ATM and ATR, CHK2 and CHK1, respectively (Matsuoka *et al*. 1998). ATR and its downstream target CHK1, respond to DNA damage through the intra-S phase cell cycle checkpoint. This occurs through CHK1-mediated degradation of Cdc25A, inhibiting firing of replication origins therefore halting DNA replication (Bartek *et al*. 2004; Xiao *et al*. 2003; Sørensen *et al*. 2003). To limit the cells entry into mitosis whilst DNA damage is present, ATR also mediates the G2/M cell cycle checkpoint, this time via the phosphorylation and subsequent degradation of Cdc25C (Donzelli & Draetta 2003).

ATM and its downstream target CHK2 prevent cells entering S phase via

activation of the G1/S cell cycle checkpoint. This occurs via the phosphorylation of p53, a target of both ATM and CHK2 (Banin *et al*. 1998). Once phosphorylated p53 is no longer degraded via MDM2, in addition ATM directly phosphorylates MDM2, further preventing p53 degradation (Khosravi *et al*. 1999). This stabilisation results in increased transcription of genes involved in cell cycle checkpoint activation, for example p21, as well as apoptotic genes (discussed below) (Sullivan *et al*. 2012).

Additionally, the intra-S phase checkpoint is activated by MDC1 binding to yH2AX (Lou *et al*. 2006). MDC1 subsequently recruits MRN and ATM via interactions with NBS1, further amplifying and sustaining checkpoint signals until damage is resolved (Chapman & Jackson 2008). Cancerous cells frequently develop mechanisms to over-come IR induced cell cycle arrest. However, the abrogation of checkpoints can also be exploited as a cancer therapy.

1.2.6 IR-induced apoptosis

When DNA lesions are too great and exceed the repair capacity of the cells, programmed cell death occurs via apoptosis, mitotic catastrophe or necrosis (Surova & Zhivotovsky 2013). Again, the DDR plays a role in this response via p53, a downstream target of ATM via CHK2 (Banin *et al*. 1998). Phosphorylation and activation of p53, a critical transcription factor, regulates the expression of an array of genes involved in the apoptotic response.

Apoptosis involves a cascade of cellular response, subsequently leading to activation of a family of cysteine proteases called caspases. Firstly, 'initiator' caspases (caspase-2, -8, -9, or -10) are activated, subsequently leading to the

cleavage and activation of 'executioner' caspases (caspase-3 or -7). These events result in the proteolytic cleavage of specific cellular substrates and, ultimately, cell death (Shalini *et al*. 2015).

1.3 The MRN complex

As discussed, the MRN complex is vital for the detection and repair of DNA DSBs and has many key roles in repair pathway choice, cell cycle control and downstream signalling, as well as the repair process. Furthermore, MRN is present at replication forks and telomeres and prevents DSBs from forming at these locations, thus avoiding genomic instability. This thesis will focus on the role of the MRN complex in DSB repair. The MRN complex is highly conserved and consists of meiotic recombination 11 (MRE11), RAD50 and Nijmegen breakage syndrome 1 (NBS1) proteins. Loss of expression of any of the three proteins leads to embryonic lethality in mice (Zhu *et al*. 2001; Wu *et al*. 2008; Theunissen *et al*. 2003).

In vivo, the complex exists as a heterohexamer with a central globular DNA-binding head, consisting of an MRE11 dimer, which binds to two NBS1 proteins and two RAD50 proteins (Lamarche *et al*. 2010; Williams *et al*. 2010; Figure 1.8).

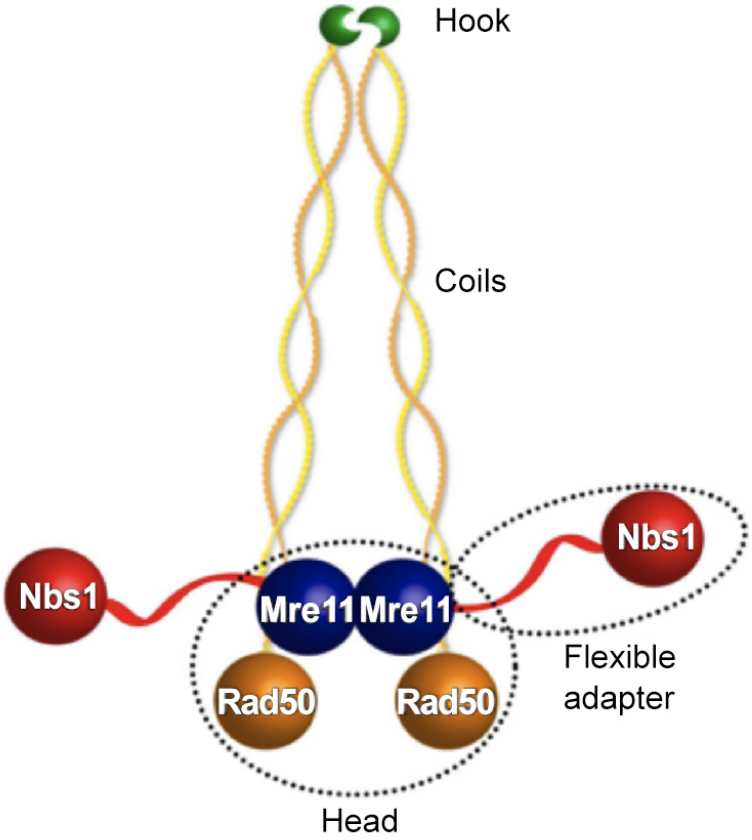

Figure 1.8 The MRN complex.

MRN assembles as a heterohexamer comprising four key regions. The processing 'head' is made up of the MRE11 dimer and two RAD50 ABC ATPase domains. The 'coils' and 'hook' are encoded by RAD50. Lastly, there is the NBS1 'flexible adapter' that affords the principle link to signalling functions. Adapted from: Williams *et al*. (2010).

RAD50

RAD50 binds to MRE11 via Walker A and B domains located at opposing ends of the protein. In between the Walker domain is a coiled domain that folds at a central CXXC motif to create a coiled-coil domain (Figure 1.9). This extends distally from the globular head of the MRN complex and links the two RAD50 proteins by a zinc hook (Figure 1.8; Hopfner *et al*. 2002).

The coiled coil domains of RAD50 are long and flexible regions allowing the MRN complex to hold a range of DNA molecules structures together (De Jager *et al*. 2001). This contributes to DSB repair in several ways. Firstly, the coiled domains can extend to tether either side of the break and keep the ends in close proximity for repair, it has been suggested that this the proximity of ends could stimulate DNA ligases, such as the DNA ligase IV ortholog in yeast (Chen *et al*. 2001). Secondly, as the MRE11 dimer is located at one end of the coiled region, the length of the fully extended coiled-coil domains could act to limit the resection distance. Finally, the zinc hook allows interaction with a second MRN dimer complex, potentially as a way of linking two sister chromatids during HR (Hopfner *et al*. 2002). RAD50 also possesses ATP-binding cassettes that are crucial for the binding and unwinding of DNA at DSB sites (Hopfner *et al*. 2001).

Mutations in *RAD50* result in Nijmegen breakage syndrome-like disorder (NBSLD). Patients with NBSLD are short in stature, have bird-like faces and mental retardation. The MRN complex does not form foci at DSB sites in these patients, resulting in an increased radiosensitivity (Waltes *et al*. 2009).

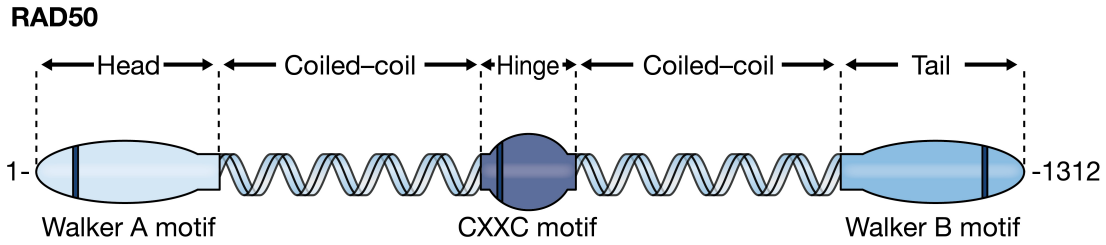

Figure 1.9 The RAD50 component of the MRN complex.
The functional domains are indicated above the figure. Reproduced from: (D'Amours & Jackson 2002)

NBS1

NBS1 flexibly extends from the globular core of the MRN complex and, although no enzymatic functions have been uncovered, it is important for the recruitment of key DDR proteins, such as ATM and CtIP (Lee & Paull 2004; Wang *et al*. 2013). CtIP recruitment occurs via 'forkhead-associated' (FHA) and BRCA1 C-terminus (BRCT) domains at the amino terminus of NBS1 (Figure 1.10). The interaction between CtIP and NBS1 requires CDK-dependent phosphorylation of CtIP at specific sites and subsequently orchestrates further phosphorylation of CtIP by ATM, therefore promoting HR (Wang *et al*. 2013; Buis *et al*. 2012). This recruitment encourages further interactions between ATM and CtIP with the MRE11-RAD50 core (Williams *et al*. 2009). NBS1 also acts downstream of ATM in regulating the intra-S-phase checkpoint, a process that requires interaction of NBS1 with MDC1, again via the FHA and BRCT domains of NBS1 (Wu *et al*. 2008; Chapman & Jackson 2008).

Patients with mutations in *NBN,* the gene that encodes NBS1, develop Nijmegen breakage syndrome (NBS), characterised by microcephaly, immunodeficiency and increased risk of cancer development (Carney *et al*. 1998; Hiel *et al*. 1996). After

exposure to IR, NBS1 is crucial for the re-localisation of MRE11-RAD50 complexes to the nucleus, in NBS cells lacking NBS1, MRE11 and RAD50 still interact but are unable to enter the nucleus and remain in the cytoplasm. Therefore cells cannot repair DSBs and are more sensitive to radiation (Desai-mehta *et al*. 2001; Carney *et al*. 1998).

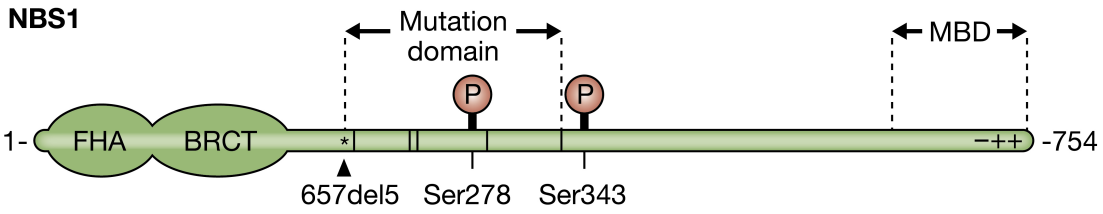

Figure 1.10 The NBS1 component of the MRN complex.
The functional domains are indicated above the figure. The positions of residues affected by mutations that occur in NBS patients are represented by vertical lines. The residue that is affected by the most common mutation (657del5) is noted with a star. Ser278 and Ser343, two important phosphorylation sites, are also shown. MBD = MRE11-binding motif; BRCT = BRCA1 carboxy-terminal; FHA = forkhead-associated.

1.3.1 MRE11

MRE11 is the core of the MRN complex and influences DNA repair in multiple ways. MRE11 possesses both 3'-5' dsDNA exonuclease activity and ssDNA endonuclease activity, controlled by four highly-conserved phosphoesterase motifs at the amino terminal (Figure 1.11; Paull & Gellert 1998). Evidence suggests that the nuclease functions of MRE11 influence DNA pathway choice. Shibata *et al* demonstrated that inhibition the endonuclease function of MRE11 allows cells to repair by NHEJ. However, once a nick has been created

downstream of the break site by MRE11 endonuclease function, the cells are committed to using HR to repair the break (Shibata *et al*. 2014). Therefore, inhibiting the exonuclease function of MRE11 could offer an important therapeutic target, as the cells are committed to HR but cannot proceed. The generation of ssDNA by MRE11 is an important step in HR and MMEJ and is enhanced by but not dependent on RAD50, NBS1 and CtIP binding (Zhuang *et al*. 2009; Williams *et al*. 2007).

The C-terminus of MRE11 contains a glycine–arginine-rich domain (GAR) domain, the methylation of which also contributes to MRE11 exonuclease activity (Dery *et al*. 2008).

DNA binding of the MRN complex occurs through the C-terminus of MRE11, and the protein is able to interact with both single and double stranded DNA (de Jager *et al*. 2001).

More recently, the C-terminus of MRE11 has been shown to possess a cyclin-dependent kinase 2 (CDK2) binding region which facilitates the CDK2-dependent phosphorylation of CtIP and subsequent interaction with BRCA1 to promote HR (Buis *et al*. 2012). As well as aiding the phosphorylation of CtIP, the direct interaction between MRE11 and CDK2 promotes the endonuclease activity of MRE11 (Yuan & Chen 2009; Sartori *et al*. 2007). Furthermore, a recent study also identified phosphorylation sites at the C-terminus of MRE11, which upon phosphorylation by ATM, lead to the control and restricted resection of DNA ends by Exo1 (Kijas *et al*. 2015).

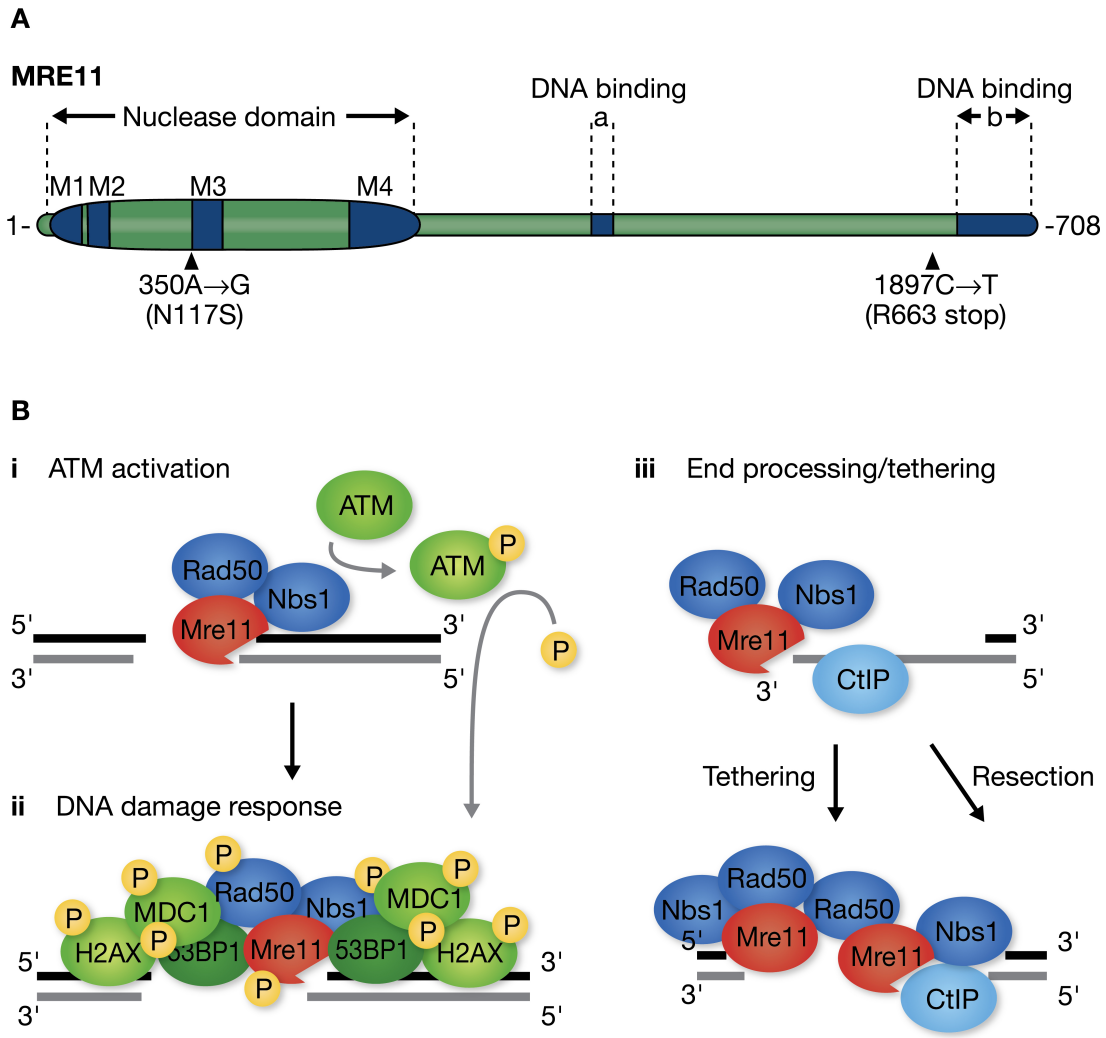

Figure 1.11 The MRE11 protein.

(A) Structure of MRE11. M1 to M4 represent the relative position of the four conserved phosphoesterase motifs. The residues affected by mutations in patients with ataxia-telangiectasia-like disease (ATLD) are marked by triangles below the figure. (B) Functionality of MRE11. (i) MRE11 interacts with NBS1 and RAD50 to form the MRN complex, which in turn activates ATM kinase; (ii) together with other ATM substrates, ATM kinase participates in the DNA damage response; (iii) the MRN complex can also act to tether broken ends, and participates with CtIP and other factors to resect the broken ends. Adapted from: D'Amours & Jackson (2002) and Zha *et al*. (2009).

1.3.2 Clinical relevance of MRE11

Patients with germ line mutations of *MRE11* present with clinical feature similar to patients with ataxia telangiectasia (AT), caused by mutations of *ATM,* and patients with NBS. This gave the first insight into the relationship between these proteins and subsequently patients with *MRE11* mutations were diagnosed with ataxia telangiectasia-like disorder (ATLD) (Stewart *et al*. 1999). There are several mutations that give rise to ATLD, often translating into complete loss of MRE11 protein expression or expression of a C-terminally truncated protein, due to the introduction of an early stop codon at the 633 amino acid position (Stewart *et al*. 1999). Similar to patients with AT and NBS, patients with ATLD have chromosomal instability, increased sensitivity to ionising radiation and an increased risk of cancer development (Stewart *et al*. 1999; Uchisaka *et al*. 2009). As a result of reduced MRE11 expression the expression of NBS1 and RAD50 are also low, suggesting the stability of the three proteins is related (Regal *et al*. 2013; Stewart *et al*. 1999). The truncated form of MRE11 described in patients with ALTD-1 is still able to interact with NBS1 and RAD50, however formation of IR-induced damage foci does not occur (Theunissen *et al*. 2003).

As well as patients with ATLD, an *MRE11* splice variant has been described in the colorectal HCT116 cell line. Here, a frameshift mutation results in an MRE11 protein lacking the $5{-}7^{th}$ exons, a region that partially encodes the nuclease motifs. Due to defective exonuclease activity and impaired MRN complex formation this results in an increased sensitivity to replication stress (Wen *et al*. 2008; Rodriguez *et al*. 2008).

Furthermore, both germline and somatic mutations in the *MRE11A* gene have shown predisposition to breast cancer (Bartkova *et al*. 2008), lymphomas (Fukuda *et al*. 2001), and colorectal cancer (Giannini *et al*. 2002).

1.4 MRE11 in bladder cancer

Our group has been interested in MRE11 in MIBC for some years now. Most recently, in an effort to identify radiosensitisers for patients with MIBC, we demonstrated that the HDAC inhibitor panobinostat is able to radiosensitise bladder cancer cell lines. This occurs through the down-regulation of MRN complex proteins, although the underlying mechanism remains unclear (Groselj *et al*. 2013).

A study performed by Teo *et al* identified a novel *MRE11A* germline variant associated with poor outcome following RT. Furthermore, a second variant was identified that influences MRE11 isoform expression, leading to greater expression of *MRE11* isoform 2 (lacking exon 16), potentially having a clinical impact (Teo *et al*. 2014).

Two independent studies have positively correlated the expression of MRE11 with DSS in patients treated with RT. However, no correlation with DSS was seen in cystectomy patients (Choudhury *et al*. 2010; Laurberg *et al*. 2012). Our Choudhury *et al* study showed that patients whose tumours had high expression levels of MRE11, as detected by immunohistochemistry, had a significantly better 3-year DSS rate when receiving radiotherapy compared with cystectomy (70% vs. 54%) (Choudhury *et al*. 2010) Therefore, paradoxically, patients with high MRE11 expression in their tumours are more likely to benefit from radical RT than from

cystectomy.

In order to improve survival for patients with MIBC, there is a need to develop biomarkers able to identify patients for whom RC or bladder-preserving therapies are more beneficial, by exploiting tumour characteristics. MRE11 is a potential biomarker for these patients. Although further investigation is required.

1.5 Aims

The central hypothesis explored in this thesis was the existence of MRE11 variants in bladder tumours and the implications this might have on DNA repair mechanisms. The overall aim of this research was to investigate the expression of MRE11 in bladder cancer patient samples and bladder tumour cell lines in order to elucidate the underlying mechanisms of the paradoxical immunohistochemistry result observed previously in our laboratory.

An MRE11 variant was discovered in patient tumour samples obtained from the Urological Department of the Churchill Hospital, which led to the following specific aims:

1. To identify the variant and elucidate how the protein differed from wild type MRE11.

2. To evaluate the likely impact of the MRE11 variant on MRE11 function, particularly in terms of DSB repair.

The following objectives were set to achieve these aims:

- To use mass spectrometry to elucidate the peptide sequence of wild type and variant MRE11, thus identifying peptides that were not present in the variant.
- To assess the stability of the variant and to examine previously reported MRE11 functions, such as complex formation and recruitment to DSBs.
- To generate a cell line with stable expression of the variant from which further functional studies could be performed, such as evaluation of the impact of the variant on radiosensitivity and HR repair.

CHAPTER 2 Materials and Methods

2.1 Solutions and buffers

Freezing solution

100 µl DMSO (Sigma-Aldrich, Irvine, UK)

400 µl appropriate serum free medium

500 µl FBS

Hypotonic lysis buffer

10 mM Tris-HCl pH 8.0 (Sigma-Aldrich, St. Louis, MO)

1 mM EDTA (Sigma-Aldrich, St. Louis, MO)

5 mM DTT (Sigma-Aldrich, St. Louis, MO)

Stored at room temperature, except DTT, which was stored at -20^{o}C and added fresh before use.

High salt buffer

50 mM Tris-HCl pH 7.5 (Sigma-Aldrich, St. Louis, MO)

1 M KCl (Sigma-Aldrich, St. Louis, MO)

2 mM EDTA (Sigma-Aldrich, St. Louis, MO)

2 mM DTT (Sigma-Aldrich, St. Louis, MO)

Stored at room temperature, except DTT, which was stored at -20^{o}C and added fresh before use.

Dialysis buffer

20 mM Tris-HCl pH 8.0 (Sigma-Aldrich, St. Louis, MO)

0.1 M KOAc (Sigma-Aldrich, St. Louis, MO)

20% (vol/vol) glycerol (Sigma-Aldrich, St. Louis, MO)

0.5 mM EDTA (Sigma-Aldrich, St. Louis, MO)

1 mM DTT (Sigma-Aldrich, St. Louis, MO)

Made fresh on the day of use.

SDS lysis buffer (Dr Anne Kiltie)

50 mM HEPES (Sigma-Aldrich, St. Louis, MO)

100 mM NaCl (Fisher Scientific, Loughborough, UK)

10 mM EDTA (Sigma-Aldrich, St. Louis, MO)

1% w/v Triton X-100 (Sigma-Aldrich, Dorset, UK)

4 mM sodium pyrophosphate (AppliChem, Darmstadt, Germany)

2 mM sodium orthovanadate (Sigma-Aldrich, St. Louis, MO)

10 mM sodium fluoride (Sigma-Aldrich, St. Louis, MO)

50 mM β-glycerophosphate (Sigma-Aldrich, St. Louis, MO)

1% SDS (Fisher Scientific, Loughborough, UK)

Final pH 7.5 with 10 M NaOH (Sigma-Aldrich, St. Louis, MO)

1 X complete, Mini, EDTA-free protease inhibitor cocktail (Roche, Indianapolis, IN) was added immediately prior to use (1 tablet per 10 ml).

Lysis buffer (Dr Anderson Ryan)

50 mM Tris-HCl, pH 7.6 (Sigma-Aldrich, St. Louis, MO)

137 mM sodium chloride (Sigma-Aldrich, St. Louis, MO)

10% glycerol (Sigma-Aldrich, St. Louis, MO)

0.1% Igepal (Sigma-Aldrich, St. Louis, MO)

0.1% SDS (Fisher Scientific, Loughborough, UK)

50 mM sodium fluoride (Sigma-Aldrich, St. Louis, MO)

1mM sodium orthovanadate (Sigma-Aldrich, St. Louis, MO)

1 X complete, Mini, EDTA-free protease inhibitor cocktail (Roche, Indianapolis, IN) was added immediately prior to use (1 tablet per 10 ml).

Lysis buffer (Dr Ester Hammond)

9 M Urea (Sigma-Aldrich, St. Louis, MO)

75 mM Tris-HCl, pH7.5 (Sigma-Aldrich, St. Louis, MO)

0.15 M β-mercaptoethanol (Sigma-Aldrich, St. Louis, MO)

Non-SDS lysis buffer

50 mM HEPES (Sigma-Aldrich, St. Louis, MO)

100 mM NaCl (Fisher Scientific, Loughborough, UK)

10 mM EDTA (Sigma-Aldrich, St. Louis, MO)

1% w/v Triton X-100 (Sigma-Aldrich, Dorset, UK)

4 mM sodium pyrophosphate (Sigma-Aldrich, St. Louis, MO)

2 mM sodium orthovanadate (Sigma-Aldrich, St. Louis, MO)

10 mM sodium fluoride (Sigma-Aldrich, St. Louis, MO)

50 mM β-glycerophosphate (Sigma-Aldrich, St. Louis, MO)

Final pH 7.5 with 10 M NaOH (Sigma-Aldrich, St. Louis, MO)

1 X complete, Mini, EDTA-free protease inhibitor cocktail (Roche, Indianapolis, IN) was added immediately prior to use (1 tablet per 10 ml).

Laemmli sample buffer

Obtained premade from Sigma-Aldrich (St. Louis, MO)

4% SDS

20% glycerol

10% 2-mercaptoethanol

0.004% bromphenol blue

0.125 M Tris HCl

Final pH 6.8

10 X Running buffer

1 M Tris base (Fisher Scientific, Rockford, IL)

1 M HEPES (Sigma-Aldrich, St. Louis, MO)

1% SDS (Fisher Scientific, Loughborough, UK)

Stored at room temperature. To generate 1 X running buffer 100 ml of 10 X Running buffer was added to 900 ml of dH_2O.

10 X Transfer buffer

25 mM Tris base (Fisher Scientific, Rockford, IL)

2 M glycine (Fisher Scientific, Rockford, IL)

To generate 1 X transfer buffer, 100 ml of 10 X Transfer buffer and 200 ml of 100% Methanol (Fisher Scientific, Rockford, IL) were added to 700 ml dH_2O. 10 X transfer buffer was stored at room temperature. 1 X transfer buffer was cooled to -20^{o}C prior to use.

PBS

To make up a 1 X solution, one PBS tablet (Gibco, Paisley, UK) was added to 500 ml of dH_2O. The solution was then autoclaved.

0.05% PBS-Tween

Two hundred and fifty microliters of Tween-20 (Promega, Madison, WI) was added to 500 ml of PBS.

Blocking buffer

PBS-Tween (0.05%) was mixed with Li-Cor buffer (Li-Cor Biosciences UK Ltd, Cambridge, UK) at a 1:1 v/v ratio.

Wash buffer for immunoprecipitation

10 mM Tris-HCL pH 7.4 (Sigma-Aldrich, St. Louis, MO)

2 mM EDTA (Sigma-Aldrich, St. Louis, MO)

150 mM Triton X-100 (Sigma-Aldrich, Dorset, UK)

2 mM sodium orthovanadate (Sigma-Aldrich, St. Louis, MO)

1 X complete, Mini, EDTA-free protease inhibitor cocktail (Roche, Indianapolis, IN) was added immediately prior to use (1 tablet per 10 ml).

Brilliant Blue R Concentrate

Obtained pre-made from Sigma-Aldrich (St. Louis, MO)

0.25% Brilliant blue R

40% methanol

7% acetic acid

Prior to use Brilliant blue R Concentrate was diluted 1:1 with dH_2O

De-stain solution

10% acetic acid (Sigma-Aldrich, St. Louis, MO)

40% dH_2O

50% methanol (Fisher Scientific, Rockford, IL)

10 X Tris-borate EDTA buffer

Tris-borate EDTA (TBE) buffer was purchased as 10 X from Bio-Rad (Bio-Rad Laboratories, Hempstead, UK).

To generate 1 X TBE buffer, 100 ml of 10 X TBE buffer was added to 900 ml dH_2O.

1% agarose gel

2 g agarose (Sigma-Aldrich, St. Louis, MO)

200 ml 1 X TBE buffer

2.2 Tissue culture

2.2.1 Cell lines

The bladder cancer cell lines RT112, 253J and the normal human urothelial (NHU) cell line 1754 were kindly provided by Prof MA Knowles (Leeds Institute of Molecular Medicine, UK). T24, CAL29, RT4, HT1376, VMCUB and 5637 cell lines were purchased from the DSMZ (Braunschweig, Germany). Stable CAL29-dervived gemcitabine resistant cells (CALgem) were generated in-house by Dr

Martin Kerr (CRUK/MRC Oxford Institute for Radiation Oncology), as previously described (Kerr *et al*. 2014).

All bladder cancer cell lines have been authenticated recently by extensive genomic analysis (microsatellite typing and array-based copy number analysis) by the DNA Diagnostics Centre (London, UK).

Dr Andy Ryan kindly provided a panel of lung cancer cell line lysates. Dr Ester Hammond kindly provided a panel of oesophageal cancer cell line lysates. Both Dr Andy Ryan and Dr Ester Hammond kindly provided RT112 and T24 bladder cancer cell line lysates generated using the protocols from their laboratories.

2.2.2 Culture conditions

All cell lines were maintained at 37°C, 5% CO_2 in a humidified incubator. RT112, T24 and 5637 cells were cultured in RPMI-1640 medium, 1 mM L-glutamine (Sigma-Aldrich, Irvine, UK). CAL29 and CALgem cells were cultured in Dulbecco's Modified Eagle Medium (DMEM) and GlutaMAX (Gibco, Paisley, UK). RT4 cells were cultured in McCoys medium, 1 mM L-glutamine (Gibco, Paisley, UK). All culture medium was supplemented with 10% foetal bovine serum (FBS). CALgem medium was further supplemented with 10 μM gemcitabine.

All RT112- and T24- derived cell lines were cultured in RPMI-1640 medium supplemented with 1 mM L-glutamine. Stable puromycin-selected MRE11 knockdown cell lines were maintained in medium further supplemented with 1 mg/ml puromycin (Fisher Scientific, Rockford, IL). *I-SceI* cell lines (containing HR Pem1-GFP reporter construct; Seluanov *et al*. 2010) were supplemented with 1.2 mg/ml G-418 solution (Roche, Indianapolis, IN). *I-SceI* MRE11 knockdown cell

lines were supplemented with 1.2 mg/ml G-418 solution (Roche, Indianapolis, IN) and 1 mg/ml puromycin (Fisher Scientific, Rockford, IL).

Trypsin was purchased as ready to use solution, gamma-irradiated 0.12% w/v trypsin-EDTA (SAFC global). All reagents were stored at 4^{o}C, except puromycin which was stored at -20^{o}C and thawed just before use.

2.2.3 Cell culture

For culturing cell lines, medium was first pre-warmed in a water bath to 37^{o}C. Trypsin was warmed to room temperature. Growth medium was removed from flasks through aspiration and an appropriate volume of trypsin was added to cover cell monolayer (10 ml for T175 cm^2 flask). This was incubated at 37^{o}C, in 5% CO_2 until cells had detached (approximately 3-6 minutes). Trypsin was neutralised with 1.5 X volume of growth medium before transferring to a centrifuge tube. Cells were pelleted by centrifugation in a Heraeus Labofuge 400 centrifuge (Fisher Scientific, Rockford, IL) at 1,300 rpm (328 g) for 3 minutes. Supernatant was removed by aspiration and cells were resuspended in an appropriate amount of growth medium, based on the pellet size (approximately 10 ml) by pipetting up and down. For the maintenance of cells, 2 x 10^6 cells for RT112 and derivative cell lines or 3 x 10^6 cells for CAL29 and CALgem cells were seeded in T175 tissue flasks in a final volume of 25 ml growth medium.

2.2.4 Cell cryopreservation

For freezing, log-phase cells were pelleted as described in section 2.2.3. After pelleting, the supernatant was removed and the pellet was resuspended in 1 ml freezing solution (see Buffers/Solutions).

2.2.5 Cytotoxic treatments

Z-VAD-FMK, cyclohexamide and MG-132 were purchased from Sigma-Aldrich, (Irvine, UK) and dissolved in DMSO (Sigma-Aldrich, Irvine, UK) to a 1 mM stock concentration. Gemcitabine was purchased from Sigma-Aldrich, (Irvine, UK) and dissolved in ddH_2O to a 1 mM stock concentration Single-use aliquots were stored at -20°C. Mirin, PFM39 and PFM01 were kindly provided by Davide Moiani (The Scripps Research Institute, La Jolla). Panobinostat (LBH-589) was purchased from Selleck Chemicals (Houston, TX) and dissolved in DMSO (Sigma-Aldrich, Irvine, UK) to a 1 mM stock concentration. Single use aliquots were stored at -80 ^{o}C.

2.3 Patient samples

2.3.1 Ethical approval

Ethical approval for patient samples was obtained from South Central Oxford – C 09/H0606/5.

2.3.2 Bladder tumour extract preparation

Bladder tumour tissue biopsies were dissected to remove diathermic tissue then washed three times in 40 ml ice cold PBS and once in 20 ml hypotonic lysis buffer (see Buffers/Solutions). Tumours were re-suspended in an equal volume of hypotonic lysis buffer to their weight. After 20 minutes on ice, cells were lysed by homogenisation using a loose-fitting glass dounce homogenizer, followed by a tight-fitting glass dounce homogenizer, and the following protease inhibitors were added: aprotinin, pepstatin, leupeptin at 1 μg/ml. After 20 minutes on ice, 0.5 vol of high salt buffer was added and cells were centrifuged at 55,000 rpm (163,700 g) for 56 minutes. The supernatant was dialyzed for 1 hour in 1 L dialysis

buffer (see Buffers/Solutions) and a further 2 hours in fresh dialysis buffer. The final extract was snap frozen in liquid nitrogen and stored at -80°C until use.

2.4 Protein expression assay

2.4.1 Lysate preparation

Cell lysates were prepared by removal of growth medium and washing with ice cold PBS. Cells were scraped in ice-cold PBS and pelleted by centrifuging at 14,000 rpm (20,817 g), 4°C for 3 minutes. Cell pellets were lysed in 30–100 µl SDS lysis buffer (see Buffers/Solutions), depending on pellet size. Lysates were sonicated for 10 seconds twice and cooled on ice between each round. Sonicated lysates were centrifuged at 14,000 rpm (20,817 g) for 15 minutes at 4°C. Supernatant was collected into clean Eppendorf tubes.

2.4.2 Protein concentration quantification

Protein concentration was determined by a bicinchoninic acid assay (BCA), using the Pierce BCA protein assay kit (Fisher Scientific, Rockford, IL). A range of bovine serum albumin standards, diluted from 0.1 to 2 mg/ml, and 1 µl of lysed protein samples were loaded in duplicate onto a 96-well plate (Corning Inc., Corning, NY). A 200 µl mix of Reagent A and B at a ratio of 1:10 from the assay kit was incubated with each sample for 30-60 minutes at 37°C. Following incubation, absorbance was measured at 562 nm on a POLARstar Omega plate reader. The protein concentration of each sample was then calculated by plotting absorbance against the standard curve of a dilution series of bovine serum albumin.

2.4.3 Western blot analysis

Twenty to forty micrograms of protein lysate was diluted to a 20 µl volume in lysis buffer. Laemmli buffer (2X) (Sigma-Aldrich, St. Louis, MO) was added at a 1:1 ratio to give a final volume of 40 µl. Samples were heated to 100°C on an Accublock Digital Dry Bath for 5 minutes and resolved on a 4–20% (w/v) polyacrylamide Tris/glycine gel at 100 V for 70 minutes. Each gel contained at least one Amersham Full Range Rainbow Marker lane (GE Healthcare Life Sciences, Little Chalfont, UK). Transfer of proteins to a nitrocellulose membrane with 0.45 µm pores using Tris/glycine transfer buffer was performed at 40 V for 2 hours. Protein-bound membranes were subsequently maintained under constant gentle rotation during all blocking, washing and antibody incubations, at the specified temperatures. Membranes were blocked in Odyssey blocking buffer (Li-cor Biosciences, Cambridge, UK) for 1 hour and then incubated overnight at 4°C in 1:1 v/v Odyssey blocking buffer:PBS-Tween containing primary antibody. The next day, primary antibody was removed and the blots were washed four times in PBS-Tween, 5 minutes per wash, followed by incubation with secondary antibody for 1 hour at room temperature. Following removal of the secondary antibody, the membranes were washed three times as above, with a final wash in PBS. Labelled proteins were detected and quantified using an Odyssey IR Imaging System (Li-cor Biosciences, Cambridge, UK).

2.1 Antibodies used for western blot analysis

Antibody	Source	Primary	Secondary
CtIP	Abcam	1:1,000	Mouse
CtIP	Abcam	1:1,000	Rabbit
PARP1	Cell Signaling	1:1,000	Rabbit
MRE11	Abcam	1:1,000	Rabbit
MRE11	Abcam	1:1,000	Mouse
Total H2AX	Millipore	1:1,000	Rabbit
γH2AX	Abcam	1:2,000	Rabbit
Rad50	Abcam	1:1,000	Mouse
NBS1	Novus Biologicals	1:1,000	Rabbit
IgG	Cell Signaling	1:1,000	Rabbit
β-actin	Abcam	1:2,000	Mouse
Ku80	NeoMarkers	1:1,000	Mouse
Ku70	Abcam	1:1,000	Mouse
HA	Abcam	1:1,000	Mouse
p21	Abcam	1:1,000	Rabbit
RAD51	Santa Cruz Biotechnology	1:1,000	Rabbit
H3K18	Cell Signaling	1:1,000	Rabbit
pATMs1981	Cell Signaling	1:2,000	Rabbit

2.5 Immunoprecipitation of MRE11 for mass spectrometry analysis

Immunoprecipitation experiments were carried out using at least 5 x 150 mm^2 tissue culture dishes of cells at 80% confluence. Cells were washed, scrapped in ice cold PBS and pelleted at 14,000 rpm (20,817 g), 4^oC for 3 minutes. Cell pellets were lysed in 1 ml lysis buffer without SDS (see Buffers/Solutions). Lysates were incubated on ice for 15 minutes, and then passed through a 21-gauge needle 40 times to shear the chromatin. Lysates were centrifuged at 14,000 rpm (20,817 g) for 15 minutes at 4°C and the supernatant removed into a clean Eppendorf. Protein lysate was pre-cleared for unspecific protein bindingby incubating with 30 µl magnetic Protein A/G Dynabeads (Novex by Life Technologies) for 1 hour at 4°C with continuous rotation. Samples were placed in a DynaMag-Spin magnetic holder and the supernatant transferred into a clean Eppendorf. Ten microliters of

MRE11 mouse primary antibody (Abcam 214) was incubated with supernatant overnight at 4°C, with rotation. The next day, 40 µl of magnetic Protein A/G Dynabeads were added followed by a further 2 hour incubation, as above. Samples were placed in the DynaMag-Spin magnetic holder and the supernatant removed. Beads were washed six times in wash buffer. Forty microliters of 2X Laemmli sample buffer was added to the beads, which were subsequently incubated at 100°C for 5 minutes to elute protein bound to beads. Samples were placed in the DynaMag-Spin magnetic holder and the supernatant removed to a clean Eppendorf.

Supernatant was resolved on a 4–20% (w/v) polyacrylamide Tris/glycine gel and incubated with Coomassie Brilliant Blue stain (Bio-Rad Laboratories, Hemel Hempstead, UK) for 1 hour at room temperature, with rotation. De-stain solution was used to remove excess stain in order to aid visualisation of the protein bands. Visible bands were cut out using a sterile scalpel and submitted for mass spectrometry analysis.

2.6 Co-immunoprecipitation of endogenous proteins

Cell pellets were lysed in 30–100 µl non-SDS lysis buffer (see Buffers/Solutions), depending on pellet size. Lysates were incubated on ice for 15 minutes and passed through a 21-gauge needle 40 times to the shear chromatin. Lysates were centrifuged at 14,000 rpm for 15 minutes at 4°C and supernatant removed to a clean Eppendorf. Protein lysate was pre-cleared for unspecific protein binding by incubating with 10 µl magnetic Protein A/G Dynabeads (Novex by Life Technologies) for 1 hour at 4°C, with rotation. Samples were placed in a

DynaMag-Spin magnetic holder and the supernatant transferred into a clean Eppendorf. Lysate was divided equally and incubated overnight at 4°C whilst continuously rotating with either no primary antibody or 5 µl of the following primary antibodies; MRE11 mouse, NBS1 rabbit, RAD50 mouse, IgG rabbit, IgG mouse, HA mouse. Forty micrograms of protein lysate was separated to act as a whole cell extract (WCE) control. The following day 20 µl of magnetic Protein A/G Dynabeads were added and incubated for 2 hours, as above. Samples were placed in the DynaMag-Spin magnetic holder and the supernatant removed. Beads were washed six times in SDS free lysis buffer. Forty microliters of 2X Laemmli sample buffer was added to the beads, which were subsequently incubated at 100°C for 5 minutes to elute protein bound to beads. Samples were placed in the DynaMag-Spin magnetic holder to remove the beads and the lysates were analysed by western blot as previous described in section 2.4.3.

2.7 Immunoprecipitation of HA-tagged proteins

Immunoprecipitation of HA-tagged proteins was carried out as described in section 2.6. However, the primary antibody incubation was omitted. Instead lysates were incubated with Anti-HA-conjugated magnetic beads (Fisher Scientific, Rockford, IL) overnight.

2.8 Mass spectrometry

Bands of interest were excised from the gel and submitted for mass spectrometry analysis (Kessler Group, Target Discovery institute (TDI), Oxford, UK), using the following protocol, which is standard for the Kessler group.

2.8.1 Digestion

Gel slices were reduced in 10 mM DTT buffer for 10 minutes at room temperature and alkylated with 50 mM iodoacetamide buffer at room temperature for 30 minutes. Digestion was carried out with either trypsin (final concentration 20 ng/µl) or elastase at 37^{o}C overnight. Gel slices were incubated with 50% and then 85% acetonitrile extraction buffer for 10 minutes each. Samples were dried down using vacuum centrifuge and re-suspended in 2% acetonitrile buffer with 0.1% formic acid.

2.8.2 Mass spectrometry data analysis

Samples were analysed on an Orbitrap QExactive mass spectrometer coupled to an Ultimate 3000 LC (Thermo Scientific, Wilmington, DE). Peaklists were generated using Sequest and searched using the Target Discovery Institute in-house MASCOT server against the SwissProt database (version 20131208) for human proteins (20,353 sequences). The following parameters were used: trypsin or elastase enzymatic cleavages allowing for up to two missed cleavages, peptide tolerance of 10 parts per million, fragment mass tolerance 0.5 Da, fixed modification as a result of carbamidomethylation of cysteine, and variable modifications of oxidation of methionine and deamidation of asparagine or glutamine. The MASCOT cut off score applied was 20.

2.9 Cloning of MRE11

2.9.1 RNA extraction

Cloning of the *MRE11A* gene was performed using the bladder cancer cell line, 5637, at a seeding density of 1 x 10^{7} cells. The following day, the cells were

trypsinised, pelleted and the RNA was extracted following the RNeasy MinElute kit, according to the manufacturer's protocol (Qiagen, Hilden, Germany). The concentration of RNA was determined using a Nanodrop (Thermo Scientific, Wilmington, DE).

2.9.2 Complementary DNA preparation

Complementary DNA (cDNA) was generated from 5 µg RNA, using a high capacity cDNA reverse transcription kit (Applied Biosystems, Foster City, CA) as per manufacturer's instructions. Table 2.2 details the component of each reaction. The RNA was made up to a total volume of 10 µl with RNase-free dH_2O (Qiagen, Hilden, Germany). The final reaction volume was 20 µl.

Table 2.2 cDNA preparation components per reaction

Component	Volume
10X RT buffer	2 µl
25X dNTP (25 µM)	0.8 µl
Oligo random primers	2 µl
RT enzyme (MultiScribe™ reverse transcriptase, 50 U/µl)	1 µl
5 µg RNA	10 µl
RNase-free dH_2O	4.2 µl

2.9.3 Primer design

Primers were designed using IDT PrimerQuest software (available from www.idtdna.com/primerquest/Home/Index) to amplify the coding region of human MRE11 (CCDS ID: CCDS8299. Accessed Jan 2013).

The addition of an HA tag to the N-terminus of the MRE11 coding region was achieved by including the HA sequence on the 5' end of the forward primer. Five additional nucleotides were added at the 5' end of the HA tag, including an ATG start codon and a Kozak sequence to allow expression. Primer sequences are listed in Table 2.3.

Table 2.3 Primer sequences for MRE11 cloning

MRE11 plasmid	Forward 5'-3'	Reverse 5'-3'	Product size
Full length pcDNA™3.3	ccagaggagcttgactgacc	gctctttccctcaactttgg	2469 bp
N-terminus HA-tagged full length pcDNA™3.3	agcatgtacccatacgatgttcc agattacgctaccataaaaatg agtactgcagatgc	gcatgtttctcagtgccatt aaa	2196 bp

2.9.4 Polymerase chain reaction (PCR)

PCR was performed using Platinum *Taq* DNA Polymerase High Fidelity (Life Technologies, Carlsbad, CA). The components in Table 2.4 were combined in a final volume of 20 µl and run on a 2720 thermal cycler (Applied Biosystems, Warrington, UK) under the conditions outlined in Table 2.5**.**

Table 2.4 PCR components

Component	Final concentration	Volume per reaction
10X HF PCR Buffer	1X	2 µl
10 mM dNTP mixture	0.2 mM each	0.4 µl
50 mM $MgSO_4$	2 mM	0.8 µl
20 µM forward primer	0.4 µM	0.4 µl
20 µM reverse primer	0.4 µM	0.4 µl
Template DNA	50-200 ng	1 µl
Platinum *Taq* HF 5 U/µl	0.4 units	0.08 µl
Millipore, dH_2O	to 20 µl	14.92 µl

Table 2.5 PCR conditions

Temperature	Time	Cycles
94°C	30 seconds	1X
94°C	15 seconds	
55°C	15 seconds	35X
68°C	3 minutes	
68°C	7 minutes	1X
4°C	5 minutes	1X

PCR products were separated by gel electrophoresis on a 1% agarose gel, supplemented with GelRed Nucleic Acid Stain (Bioutium, Hayward, CA). HyperLadder™ 1 Kb was loaded as the DNA size reference. The samples were run at 100 V until adequate separation was achieved (45–90 minutes) and DNA was visualised using a Molecular Imager FX ProPlus (Bio-Rad Laboratories, Hemel Hempstead, UK.)

By using the marker as a reference, DNA bands of the correct size were excised and gel purified using a QIAquick Gel Extraction Kit (Qiagen, Hilden, Germany), as per the manufacturer's protocol. DNA sample were eluted in 30 µl of EB buffer.

2.9.5 TOPO cloning

TOPO cloning kit pcDNA™3.3-TOPO (Life Technologies, Carlsbad, CA) vectors were used to insert purified MRE11 cDNA into expression plasmids. Each TOPO cloning reaction was prepared using the reagents outlined in Table 2.6, followed by incubation for 30 minutes at room temperature.

Table 2.6 TOPO cloning reagents

Reagent	Volume
PCR product	2 µl
dH_2O	1 µl
Salt solution	0.5 µl
pCR-TOPO vector	0.5 µl

At the end of the incubation period 2 µl of each reaction was added to separate 50 µl vials of One Shot Top10 *Escherichia coli* competent cells (Fisher Scientific, Rockford, IL), followed by incubation on ice for 30 minutes. The cells were heat-shocked at 42^{o}C for 30 seconds, in a temperature controlled water bath. After this, the cells were placed on ice for at least 1 minute prior to the addition of 250 µl of room temperature SOC medium (Sigma-Aldrich, St. Louis, MO), which was added under aseptic conditions. The vials were sealed and incubated at 37^{o}C for 1 hour, with constant horizontal shaking at 200 rpm. A total of of 10–100 µl of each transformation was spread onto pre-warmed LB agar plates containing ampicillin selection antibiotic. Plates were incubated at 37^{o}C overnight.

2.9.6 Screening colonies

Single colonies were selected using individual pipette tips. A copy of each colony was maintained by streaking part of the colony onto a master plate containing

ampicillin and the remaining part of the colony was then inoculated directly into PCR master mix containing primers to amplify the *MRE11* gene. PCR reactions were performed with Platinum Taq under conditions described in section 2.9.4. PCR products were separated by gel electrophoresis on a 1% agarose gel. DNA bands of the expected size for *MRE11* were excised and gel purified.

2.9.7 Diagnostic restriction enzyme digestion

In order to ensure that the *MRE11* sequence was cloned into the vector in the correct orientation, the PCR products excised in section 2.9.6 were digested with restriction enzymes as outlined in Table 2.7 in a final volume of 20 µl. For all reactions the restriction enzyme was added last. Reactions were incubated at 37^{O}C for 1 hour. Loading dye was added and digests were separated on a 1% agarose gel at 100 V. The expected sizes of the restriction enzyme digested products are outlined in Table 2.8.

Table 2.7 Restriction enzyme digest components

Component	Volume
10X NEBuffer	2 µl
PCR product	2 µl
Restriction enzyme	1 µl
dH_2O	15 µl

Table 2.8 Restriction enzymes and expected size of cut products

Restriction enzyme	Size of products
None	7455
BamHI	1626, 5829
BglII	298, 2489, 4668
EcoRI	439, 7162

2.9.8 Mini-prep

Colonies showing correct restriction enzyme patterns were picked from the master plate and inoculated into 5 ml LB broth containing ampicillin selection antibiotic. These were placed at 37^{o}C with constant shaking at 200 rpm overnight. The following day plasmid DNA was isolated from the culture using the QIAprep Spin Miniprep Kit (Qiagen, Hilden, Germany), as per the manufacturer's protocol.

2.9.9 Sequencing

To ensure no mutations had been generated during the cloning procedure plasmid DNA at 100 ng/µl was submitted for Sanger sequencing (Source BioScience, UK) with the primers outlined in Table 2.9. This allowed for the entire *MRE11* sequence to be analysed using CLC Sequence Viewer software (CLC bio, Aarhus, Denmark).

Table 2.9 Sanger sequencing primer sequences

Primer	Sequence 5'-3'
CMV	cgcaaatgggcggtaggcgtg
F2	tccagacatttttaacccaga
R1	gctctttccctcaactttgg

2.9.10 Maxi-prep

Isolation of large quantities of plasmid DNA was obtained by maxi prep using the Qiagen Maxi Prep Kit (Qiagen, Hilden, Germany), as per the manufacturer's protocol.

2.9.11 Site-directed mutagenesis

2.9.11.1 Early STOP codon

In order to allow expression of the truncated MRE11 protein, primers were designed to mutate the adenine at position 1702 into a thymine using the QuikChange Primer Design Program (available from: www.agilent.com/genomics/qcpd). Sequences are outlined in Table 2.10.

Table 2.10 Site-directed mutagenesis primer sequences for early stop codon

Primer	Sequence
MRE11_a1702tF	ctcggcctcttcctt**a**gttggttgctgctga
MRE11_a1702tR	tcagcagcaaccaac**t**aaggaagaggccgag

2.9.11.2 Caspase cleavage motif

Primers to mutate the first and fourth lysine residue of the potential caspase cleavage motif in MRE11 were designed using the QuikChange Primer Design Program (available from: www.agilent.com/genomics/qcpd). Sequences are outlined in Table 2.11.

Site-directed mutagenesis was performed as per the QuikChange II XL Site-Directed Mutagenesis Kit (Agilent Technology, Santa Clara, CA). Components in Table 2.12 were combined and mixed before the addition of *PfuUltra* HF DNA polymerase to a final volume of 50 µl. Reactions were run on a 2720 thermal cycler (Applied Biosystems, Foster City, CA) under the conditions outlined in Table 2.13.

Following this 1 µl of *Dpn*I restriction enzyme (10 U/µl) was incubated with the PCR reactions for 1 hour at 37^{o}C. Then, 2 µl of *Dpn*I digested DNA was transformed in 45 µl of XL10-Gold ultracompetent cells by incubating on ice for

30 minutes. Cells were heat-shocked at 42^{o}C for 30 seconds and incubated on ice for 1 minute before the addition of 500 µl of SOC medium. Transformations were incubated at 37^{o}C whilst shaking at 250 rpm for 1 hour. A total of 10–100 µl of cells were spread on LB-agar plates containing ampicillin and incubated at 37^{o}C overnight.

For confirmation of mutation, single colonies were picked plasmid DNA isolated (according to Materials and Methods 2.9.8) before submitting for sequencing (Materials and Methods 2.9.9) with an appropriate primer.

Table 2.11 Site-directed mutagenesis primer sequences for caspase motif

Primer	Sequence
CaspMotifF	ggttgctgctgagatgctggcatcagaggcattagccatctgttctg
CaspMotifR	cagaacagatggctaatgcctctgatgccagcatctcagcagcaacc

Table 2.12 Site-directed mutagenesis reaction components

Reagent	Volume
10X reaction buffer	5 µl
10 ng dsDNA MRE11 plasmid template	1 µl
Forward primer (20 µM)	0.4 µl
Reverse primer (20 µM)	0.4 µl
dNTP mix	1 µl
QuikSolution	3 µl
ddH_2O	38.2 µl
PfuUltra HF DNA polymerase	1 µl

Table 2.13 Site-directed mutagenesis reaction conditions

Temperature	Time	Cycles
95°C	1 minutes	1X
95°C	50 seconds	18X
60°C	50 seconds	
68°C	7 minutes	
68°C	10 minutes	1X
4°C	5 minutes	1X

2.10 Plasmid transfection

2.10.1 FuGENE HD transfection reagent

Prior to transfection, cells were seeded and incubated overnight to reach 60% confluency. The following day, plasmid DNA (1 µg/µl) was incubated with FuGENE HD transfection reagent (Promega, Madison, WI) at a 1:3, DNA: transfection reagent ratio in pre-warmed Opti-MEM medium containing reduced serum (Life Technologies, Carlsbad, CA) for 10 minutes. Table 2.14 outlines guideline volumes used depending on tissue culture plate size.

Table 2.14 FuGENE HD transfection guideline volumes

Size of plate	µl DNA (1 µg/µl)	µl FuGENE HD	µl Opti-MEM
6-well plate	4	12	200
5 cm plate	5	15	250
10 cm plate	10	30	500

2.10.2 X-tremeGENE transfection reagent

Transfections were carried out under the same conditions described above except a 1:4 plasmid DNA (1 µg/µl) to transfection reagent ratio was used. X-tremeGENE was purchased from Roche (Indianapolis, IN)

2.11 Quantitative PCR

For quantitative PCR (qPCR), cDNAs from DMSO or 50 nM panobinostat (24 hour)-treated cells were kindly provided by Dr Blaz Groselj.

For the qPCR experiments, a mastermix consisting of 2X SYBR Green PCR Mastermix (Applied Biosystems, Paisley, UK), cDNA (DMSO or panobinostat treated) and RNase-free dH_2O was made up (Table 2.15).

Table 2.15 qPCR experiment components

Component	Volume
2X SYBR Green	5 µl
cDNA	1 µl
RNase-free dH_2O	1.5 µl

Both forward and reverse primers were diluted to 0.5 µM. Then 7.5 µl of the mastermix was added to wells in a 96-well MicroAmp Reaction plate (Applied Biosystems, Warrington, UK) with 2.5 µl of the different primer stocks. The final volume of the reaction was 10 µl per well. The intron-spanning *caspase* primer sequences were designed using IDT PrimerQuest software (available from www.idtdna.com/primerquest/Home/Index). Forward and reverse primer sequences are outlined in Table 2.16.

Table 2.16 qPCR primer sequences

Primer	Forward primer	Reverse primer
ATP5B	ACCATCAAAGGATTCCAGCA	GCTTTTGCCACAGCTTCTTC
SHADA	TGGGAACAAGAGGGCATCTG	CCACCACTGCATCAAATTCATG
CASP 1	GACTCTCAAGGAGTACTTTCTTCC	CTTCTAGGGAGCAAAGCTTGA
CASP 2	TTCTGGAGAAGGACATCATCAC	GTTCCACATTCTGGCTGAAAC
CASP 3	GGGATCGTTGTAGAAGTCTAACTG	CAACACCACTGTCTGTCTCAA
CASP 4	TTGACATCACAGGGATGAAGG	GCTCTGGTCTGGTAGCAAAT
CASP 6	CACTTAACACTGCCAGAAAGG	GCAGTAGTTCTTCTGCTTTAAGAT
CASP 7	AGATTCAGTGGATGCTAAGCC	GTCTTGATGGATCGCATGGT
CASP 8	AGTGAGCAGATCAGAATTGAGG	GACCCTCTTCTCCATCTCTATGA
CASP 9	TCCAACATCGACTGTGAGAAG	GCAAAGCCAGCACCATTT
CASP 10	CTGTACCAAAGAGGAAGTGGAG	GCCTTCTGACAGTTCGTAGAG
CASP 14	GTTGTGCCTTCGTGGTACT	CACAATCTCATCTCCACCTACTG

2.11.1 qPCR data analysis

The qPCR data analysis was performed as described by Livak & Schmittgen (2001).

For the analyses of the genes of interest, the Ct (threshold cycle) values were subtracted from the Ct values of the *ATP* and *SHADA* housekeeping genes (normaliser and calibrator), according to the following formula:

$\Delta\Delta Ct = \Delta Ct_{calibrator}(Ct_{calibrator} - Ct_{normaliser}) - \Delta Ct_{sample}$ of interest$(Ct_{sample} - Ct_{normaliser})$

and the values calculated according the following formula:

Relative quantity to calibrator = $2^{-\Delta\Delta Ct}$

Furthermore, the relative comparison between the treated sample (panobinostat) was made and compared with the control treated sample (DMSO) (set as 1).

Samples were run on a 7500 Fast Real-time qPCR system (Applied Biosystems, Warrington, UK) under the following conditions: 20 seconds at 50°C, followed by

10 minutes at 95°C, then 40 cycles of 1 minute at 60°C, 15 seconds at 95°C, 1 minute at 60°C, 1 minute at 95°C.

2.12 Rapid amplification of cDNA ends (RACE)

Total RNA was extracted from T24 and RT112 cell lines as described in section 2.9.1. Synthesis of cDNA from 1.25 µg RNA was conducted using a 3'RACE kit (Invitrogen, Carlsbad, CA) as per the kit protocol. cDNA generated from control RNA (100 ng) provided with the kit was used as a positive control. PCR amplification of T24 and RT112 MRE11 3'-cDNA ends was conducted using a gene specific primer (GSP): 5'-TCCAGACATTTTTAACCCAGA-3'. A universal amplification primer (UAP) provided with the kit was used as the antisense primer. Control primers included with the kit were used to amplify control cDNA. DNA amplification and detection was conducted as described in section 2.9.4.

2.13 Immunofluorescence microscopy and analysis of foci

For immunofluorescence experiments, 2.5 x 10^5 cells were plated onto sterile coverslips in 5 cm^2 tissue culture dishes in 4 ml culture medium. The following day, cells were irradiated with 5 Gy. After irradiation the medium was aspirated, the dishes washed twice with PBS and fresh complete medium added. Cells were incubated for the indicated times at 37^{o}C prior to fixation. All subsequent incubations and washes were performed at room temperature with rotation on a mini gyro-rocker SSM3, unless otherwise stated. Cells were washed with PBS and fixed with 4% paraformaldehyde containing 0.1% Triton X-100 for 20 minutes. Cells were washed again with PBS before permeabilisation using 0.5% Triton X-100 for 15 minutes. Cells were washed with PBS and blocked in 5% bovine serum

albumin (BSA) for 1 hour. Samples were incubated with the appropriate primary antibody at a 1:1000 concentration in 5% BSA and incubated overnight at 4^{o}C with no rotation.

The following day, primary antibody was removed and the coverslips were washed three times in PBS for 5 minutes. Coverslips were incubated with secondary antibodies, namely, anti-mouse (Alexa Flour 488, Invitrogen, Carlsbad, CA), anti-rabbit (Alexa Flour 555, Invitrogen, Carlsbad, CA) or both, in 5% BSA at a 1:1000 concentration for 1 hour. The following washes were performed for 5 minutes with rotation on a mini gyro-rocker SSM3. Coverslips were washed three times in PBS and once in PBS containing 1:1,000 concentration of 1 mg/ml 4', 6-diamidino-2-phenylindole dihydrochloride (DAPI, Sigma-Aldrich) before a final wash in dH_2O. Coverslips were mounted onto slides with Flouromount G. The slides were left to fix in darkness overnight and scanned using the Zeiss LSM 780 confocal microscope. Slides were stored in dark conditions at 4^{o}C.

2.14 Transient MRE11 knockdown

RT112 cells were seeded at different densities depending on treatment time. For 24 and 48 hour treatments, 4 x 10^5 cells were seeded and for 72 and 96 hour treatments, 3 x 10^5 cells were seeded, onto 10 cm^2 tissue culture dishes. Cells were incubated for 24 hours to reach at least 60% confluence prior to siRNA transfection. The MRE11 siRNA sequence was: 5'-GAACCUGGUCCCAGAGGAGdTdT-3' (Zhuang *et al*. 2009). The target for MRE11 siRNA oligonucleotides is located in the 5'-untranslated region of *MRE11* mRNA, to allow for expression of the MRE11 expression vectors which do not contain

this sequence. The oligonucleotide was synthesized by Qiagen (Hilden, Germany). Transfection of the siRNA was carried out using Oligofectamine (Invitrogen, Carlsbad, CA). A non-silencing sequence AllStars RNAi control (Qiagen, Hilden, Germany), was used as a control.

siRNA was incubated with pre-warmed Opti-MEM medium for 10 minutes at room temperature. Oligofectamine and Opti-MEM were incubated in an Eppendorf for 10 minutes at room temperature before addition of the siRNA, followed by a further incubation for 25 minutes. Cells were washed twice in PBS before 10 ml fresh media added before addition of the siRNA complexes. The final concentration of siRNA treatments was 100 nM per plate. The cells were incubated at 37°C in 5% CO_2 for 4 hours and gently rocked every hour. Expression levels of MRE11 were measured at different time points after transfection by western blot analysis (section 2.4.3).

2.15 Stable MRE11 knockdown

2.15.1 shRNA design

The MRE11 shRNA was designed according to the p*Silencer* 2.1-U6 puro vector manufacturer's instructions (Life Technologies, Carlsbad, CA) using the same sequence as the siRNA previously described (section 2.14). The sequences were

MRE11 shRNA sense: 5'-

GATCCGAACCTGGTCCCAGAGGAGTTCAAGAGACTCCTCTGGGACCAGGTTCTTTTTTG

GAAA-3',

MRE11 shRNA antisense: 5'-

AGCTTTTCCAAAAAAGAACCTGGTCCCAGAGGAGTCTCTTGAACTCCTCTGGGACCAGG

TTCGC-3'. Scrambled sense controls were designed using the same bases, but in a random order which had no homology with the human genome according to BLAST (NCBI). The sequences were: MRE11 Scrambled shRNA sense 5'GATCCACGAAGTGCGAGTCGCAGCTTCAAGAGAGCTGCGACTCGCACTTCGTTTTTTT GGAAA-3',

MRE11 Scrambled shRNA antisense 5'-AGCTTTTCCAAAAAAACGAAGTGCGAGTCGCAGCTCTCTTGAAGCTGCGACTCGCACTT CGTG-3'. Oligonucleotides were synthesised by Qiagen (Hilden, Germany).

2.15.2 Annealing siRNA oligonucleotides

Hairpin siRNA template oligonucleotides were dissolved in 100 µl nuclease-free H_2O and diluted to 1 µg/µl in TE buffer. Two microliters of both sense and antisense siRNA oligonucleotide were mixed with 46 µl 1X DNA annealing solution (Life Technologies, Carlsbad, CA). The mix was heated to 94°C for 3 minutes before incubation at 37°C for 1 hour.

2.15.3 Ligation of annealed siRNA into pSilencer vectors

Annealed hairpin siRNA was diluted to 8 ng/µl with nuclease-free H_2O before annealing into p*Silencer* 2.1-U6 puro vectors (Life Technologies, Carlsbad, CA). One microliter of annealed hairpin siRNA was incubated at room temperature for 3 hours with 1 µl p*Silencer* vector, 1 µl T4 DNA ligase (New England BioLabs, Hitchin, UK), 1 µl 10X T4 ligase buffer and made to a final volume of 10 µl with nuclease-free H_2O. Three microliters of the ligation was transformed as previously described (section 2.9.5) using One Shot TOP10 Chemically Competent *E. coli* cells (Fisher Scientific, Rockford, IL). Individual colonies were picked and

plasmid DNA was isolated by mini-prep as previously described (section 2.9.8). Three microliters of isolated plasmid DNA was digested with 1 µl *BamHI* and 1 µl *HindIII* digestion enzymes (New England BioLabs, Hitchin, UK) in the presence of 2 µl 10X buffer (New England BioLabs, Hitchin, UK) in a final volume of 20 µl for 2 hours at 37°C. Digests were separated on a 1% agarose gel to detect positive clones with an insert of 65 bp. Promising clones were sent for Sanger sequencing using M13 forward primer: 5'-GTTTTCCCAGTCACGAC-3' to confirm positive insertion with no mutation of the shRNA sequence.

2.15.4 MRE11 or scrambled control shRNA transfection

RT112 cells were seeded at a density of 1 x 10^6 onto 10 cm^2 tissue culture dishes and incubated overnight at 37°C to reach 60% confluence. Cells were transfected with 10 µg of the shRNA plasmid DNA using FuGENE transfection reagent, as described in section 2.10.1. At least 24 hours following transfection, the medium was removed and fresh medium added containing the selection antibiotic 1 mg/ml puromycin (Fisher Scientific, Rockford, IL). Control dishes that did not undergo transfection, were also incubated with selection medium to permit determination of cell death in all non-transfected cells.

2.15.5 Clone screening

Fresh medium containing appropriate selection medium was added to the cells every few days until all cells on the control plates were dead. When transfected cells had formed colonies of approximately 50 cells, medium was removed and the cells were washed with PBS. Trypsin was added to the cells and subsequently incubated at 37^{o}C for 3 minutes. Before the cells had completely detached, they

were picked using a p200 pipette tip and individual colonies were transferred into single wells on a 24-well plate. Once confluent, colonies were transferred into 6-well plates and eventually into larger dishes. Clones were screened for MRE11 expression by western blot analysis. Clones with the lowest expression of MRE11 were expanded and frozen stocks generated.

2.16 Stable MRE11 re-expression

pcDNA 3.3 MRE11 expression plasmids were transfected with FuGENE or X-tremeGENE as outlines in section 2.10. At least 24 hours following transfection, the medium was removed and fresh medium added containing selection antibiotic, G-418 solution at 1.2 mg/ml (Roche, Indianapolis, IN). Clones were screened as described in section 2.15.5. For the co-transfection of pcDNA 3.3 MRE11 expression plasmids and shMRE11 pSilencer 2.1-U6 puro vectors (Life Technologies, Carlsbad, CA), the same protocol was used. However, both puromycin (1 mg/ml) and G-418 solution (1.2 mg/ml) were used during the selection procedure.

2.17 *I-SceI* HR assay

2.17.1 HR I-SceI construct and stable expression in the T24 cell line

Dr Martin Kerr created stable *I-SceI* expressing T24 cells as described as follows. The T24 cell line was transfected using FuGENE (section 2.10.1) with 10 µg of PvuI-digested HR Pem1-GFP reporter construct, kindly provided by Vera Gorbunova (Rochester, UK; Seluanov *et al*., 2010). The HR Pem1-GFP reporter construct contains a neomycin selection cassette and so clonal selection was achieved by growth in G-418 antibiotic. Further clonal selection was carried out

by examining GFP expression after transfection with a pCBASceI expression plasmid (#26477, Addgene, Cambridge, MA) and individual clones selected for low background GFP and *I-SceI*-induced GFP positivity, as decribed below.

The following work was carried out by myself in collaboration with Ms. Helen Scott. After stable integration of the HR Pem1-GFP reporter, MRE11 depletion was achieved using the same protocol described in section 2.15. Individual clones with the greatest MRE11 depletion, yet still with *I-SceI*-induced GFP positivity, were expanded for use in future experiments.

2.17.2 HR assay transfections

T24 HR MRE11 knockdown cells (described above) were seeded at a density of 1 x 10^4 cells in 5 cm^2 tissue culture plates. After 2 hours, cells were transfected with 1 µg pCAG-DsRed expression plasmid (# 11151 Addgene, Cambridge, MA) using FuGENE transfection reagent at a 1:3 DNA: transfection reagent ratio (section 2.10.1). Following a further 6 hour incubation the appropriate plates were transfected using FuGENE at a 1:3 ratio with 4 µg pCBASceI expression plasmid, or with a combination of 4 µg pCBASceI expression plasmid and 4 µg wild type MRE11 or truncated MRE11 pcDNA 3.3 expression plasmids. The transfections used in this thesis are outlined in Table 2.17. When a total concentration of 8 µg plasmid was transfected, the ratio of FuGENE remained consistent at 1:3, DNA: transfection reagent, therefore 24 µl of FuGENE was used. Volumes used for each transfection condition are described in Table 2.18. A master stock of pCBASceI expression plasmid transfection mix was made before subsequent addition of MRE11 pcDNA 3.3 expression plasmids to ensure equal transfection of the

pCBASceI expression plasmid in different treatments. Twenty-four hours following transfection the culture medium was removed and fresh medium added. Cells were incubated for a further 48 hours before GFP expression analysis.

Table 2.17 HR assay *I-SceI* treatments

Treatment	1st tranfection	2nd transfection
I-SceI	1 µg DsRED	4 µg *I-SceI*
I-SceI + wild type MRE11	1 µg DsRED	4 µg *I-SceI* + 4 µg wild type MRE11
I-SceI + truncated MRE11	1 µg DsRED	4 µg *I-SceI* + 4 µg truncated MRE11

Table 2.18 HR assay *I-SceI* transfection volumes

Plasmid	Total plasmid concentration	FuGENE volume	Opti-MEM volume
DsRED	1 µg	3 µl	100 µl
I-SceI	4 µg	12 µl	250 µl
I-SceI + wild type MRE11	8 µg	24 µl	500 µl
I-SceI + truncated MRE11	8 µg	24 µl	500 µl

2.17.3 HR assay sample preparation

Samples were prepared by removing the culture medium and washing the cell monolayers with PBS. Cells were then incubated with 1 ml trypsin at 37^{o}C until all cells had detached (approximately 5 minutes). Trypsin was neutralised using 4 ml growth medium before transferring into a 15 ml falcon tube and pelleting cells by centrifuging at 1,300 rpm (328 g) for 3 minutes. Supernatant was discarded and cells re-suspended in a suitable volume of PBS depending on cell pellet size (200–500 µl), by pipetting.

2.17.4 GFP and DsRed detection

Cells were analysed for GFP and DsRed positivity by flow cytometry on a FACSCalibur flow cytometer (Beckton Dickinson, Oxford, UK). For analysis the fraction of GFP positive cells detected was normalised to the number of DsRed positive cells as a measure of transfection efficiency for each individual treatment.

2.18 Clonogenic survival assay

The RT112, MRE11 knockdown or MRE11 scrambled control cell lines were seeded at 600 cells per 10 cm^2 dish in 10 ml normal growth medium. Indicated concentrations of cytotoxic agents were added to the medium in a 10 µl volume or 10 µl DMSO was used as a control. For radiosentivity clonogenic survival assays, cells were seeded and incubated for 2 hours prior to irradiation at indicated doses. Each treatment was performed in duplicate, three times. Cells were incubated at 37°C for 14 days, after which time the medium was discarded and the cells were fixed with methanol:acetic acid (3:1). This was discarded before incubating dishes with 5 ml of Brilliant Blue R Concentrate diluted 1:1 with dH_2O, for 1 hour. After staining was complete the dishes were washed with warm water, allowed to air dry and colonies (containing more than 50 cells) were counted using Oxford Optronix ColCount. The surviving fraction was determined by dividing the average number of colonies for each treatment by the average number of colonies in the control.

The sensitisation enhancement ratio (SER) was used to compare two cell survival fractions at 10% survival (SER_{10}). The graphs for the clonogenic survival assays

were drawn using GraphPad Prism 6.0 Software (La Jolla, CA), using the linear quadratic (LQ) model to plot the curves.

2.19 Irradiation of cells

In irradiation experiments, a Caesium-137 γ-ray source was used at a dose-rate of 1.7 Gy per minute.

2.20 Statistics and data analysis

All statistical analyses were performed using GraphPad Prism 6.0 Software (La Jolla, CA). The results were presented as the mean, with error bars representing the standard error of the mean (SEM). For the comparison of cell survival curves, a two-way ANOVA with Bonferroni's multiple comparison tests was used. For comparison of two samples, a Student's two-tailed, unpaired t-test was used. A p-value of <0.05 was regarded as statistically significant.

CHAPTER 3 Identification of a novel MRE11 variant in bladder cancer tumours and bladder cancer cell lines

3.1 Introduction

Treatment of muscle-invasive bladder cancer (MIBC) involves administration of cisplatin-based chemotherapy when patients are fit enough to receive this, followed by either radical cystectomy (surgical removal of the bladder), or trimodality treatment (TMT), based on the simultaneous delivery of chemotherapy and radiotherapy after a maximal transurethral resection of the bladder tumour (British Uro-oncology Group 2013; Witjes *et al*. 2014). TMT is considered an optimal bladder-sparing treatment. Although radical cystectomy has long been considered as the 'gold standard' treatment, particularly in North America and Europe, it is difficult to directly compare it with TMT as randomised clinical trials have not been undertaken (Arcangeli *et al*. 2015). The recent randomised SPARE trial was unsuccessful due to a number of factors, including physician and patient preferences (Huddart *et al*. 2010). However, retrospective studies suggest that there are no major differences in cause-specific survival (CSS) at 5 years between patients treated with radical cystectomy or radiotherapy (Kotwal *et al*. 2008). The aim of the research in our group is to improve our understanding of radiotherapy response in order to maximise patient survival following treatment, thus sparing some patients unnecessary surgical intervention, with the additional goal of organ preservation to improve patient quality of life.

The median age of bladder cancer patients at diagnosis is 68 years (Gallagher & Milowsky 2009). As bladder cancer is a disease of the elderly, patients often have impaired physical fitness meaning major surgical intervention with cystectomy is not always a viable option for MIBC. Patients often have poor renal function and so therapy with cisplatin or other nephrotoxic agents may also not be feasible (Rosenberg *et al*. 2005; Nicholson 2012).

There is a need to discover biomarkers capable of aiding treatment choice, so that patients can be directed to the treatment with the best predicted survival for them as an individual. Previous studies have shown that MRE11 could act as a potential biomarker for survival following radiotherapy in bladder cancer (Choudhury *et al*. 2010; Laurberg *et al*. 2012). These studies used immunohistochemistry (IHC) staining of patients' bladder tumour sections to determine MRE11 protein expression and correlated expression with 3-year CSS. Paradoxically, it was found that patients with tumours expressing high levels of MRE11 had improved 3-year CSS after radiotherapy treatment, but not after cystectomy. Similarly, in patients with early breast cancer, reduced expression of the MRN complex was found to correlate with reduced efficacy of radiotherapy (Söderlund *et al*. 2007). This was unexpected as it had been hypothesized that if a tumour were expressing high levels of MRE11 the tumour would be more proficient in double strand break repair following radiotherapy and therefore less sensitive to this treatment leading to reduced patient survival.

In light of these findings, we wanted to further investigate the expression of MRE11 in bladder cancer to determine how this might contribute to the unexplained results seen for survival following radiotherapy.

3.2 Results

3.2.1 MRE11 protein expression in bladder tumours

To examine MRN complex protein expression in bladder tumours, we obtained fresh biopsies of tumour tissue taken at transurethral resection of bladder tumour (TURBT) from patients with bladder tumours of varying stage and grade, treated in the Urology department of the Churchill Hospital, Oxford, UK. These were processed into cell-free protein extracts (Materials and Methods 2.3.2). This allowed the expression of the key DNA repair MRN complex proteins to be determined in the tumours by western blot analysis (Figure 3.1).

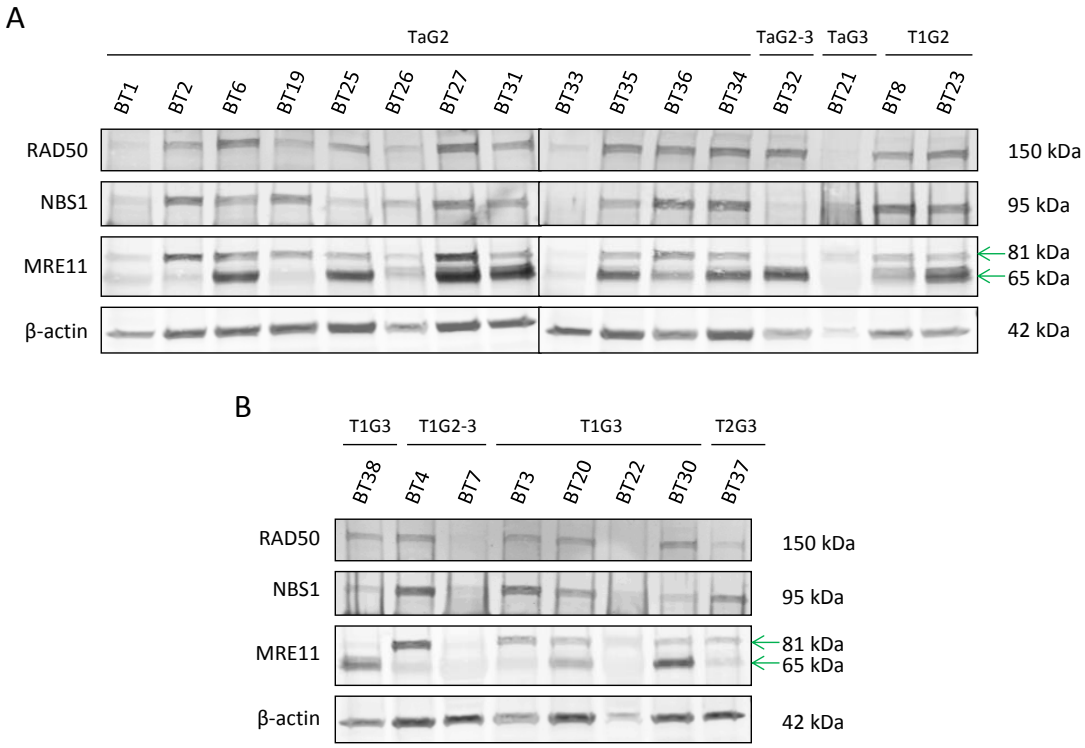

Figure 3.1 Expression of the MRN complex proteins in bladder tumours.
A and B) A panel of bladder tumours (BT) arranged in order of increasing grade and stage. Ta, T1 and T2 represent staging of bladder cancer, with Ta being less advanced and T2 being more advanced. G2 = grade 2 (less aggressive), G3 = grade 3 (more aggressive). Sizes of proteins are indicated on the right hand side. Note a green arrow highlighting the presence of a second MRE11 band of smaller molecular weight than that expected for wild type MRE11.

Protein expression was quantified in the tumour samples. Expression of the individual complex components did not correlate with stage or grade. However, there was great variability in expression of the complex in the tumours, from strong expression to barely detectable levels.

Of note, a secondary band was detected by western blot in some tumour samples when probing for MRE11. The band appeared at a lower molecular weight (approximately 65 kDa) than that expected for wild type (WT) MRE11 (81 kDa). The expression of this protein band did not correlate with tumour stage or grade

and varied widely between tumour samples. For example, BT2, BT19, BT4, BT3 and BT37 had strong expression of WT MRE11 with no detection of the smaller MRE11 protein band. In contrast, BT36, BT8, BT20 had a near equal ratio of WT MRE11 to the smaller product. Several of the tumours had stronger expression of the smaller MRE11 protein band, namely BT6, BT25, BT26, BT27, BT31, BT35, BT34, BT23, and BT30. Two tumours had very low expression of WT MRE11 and a strong expression of the smaller product; BT32 and BT38.

The expression of the secondary MRE11 band did not correlate with WT MRE11, NBS1 or RAD50 expression (Figure 3.2A-C). Indeed, no statistically significant linear relationship was found between expression of any of the MRN complex proteins, including the combined (total) expression of both MRE11 proteins (Figure 3.2). This might indicate that the relationship between the proteins is more complicated than a linear correlation.

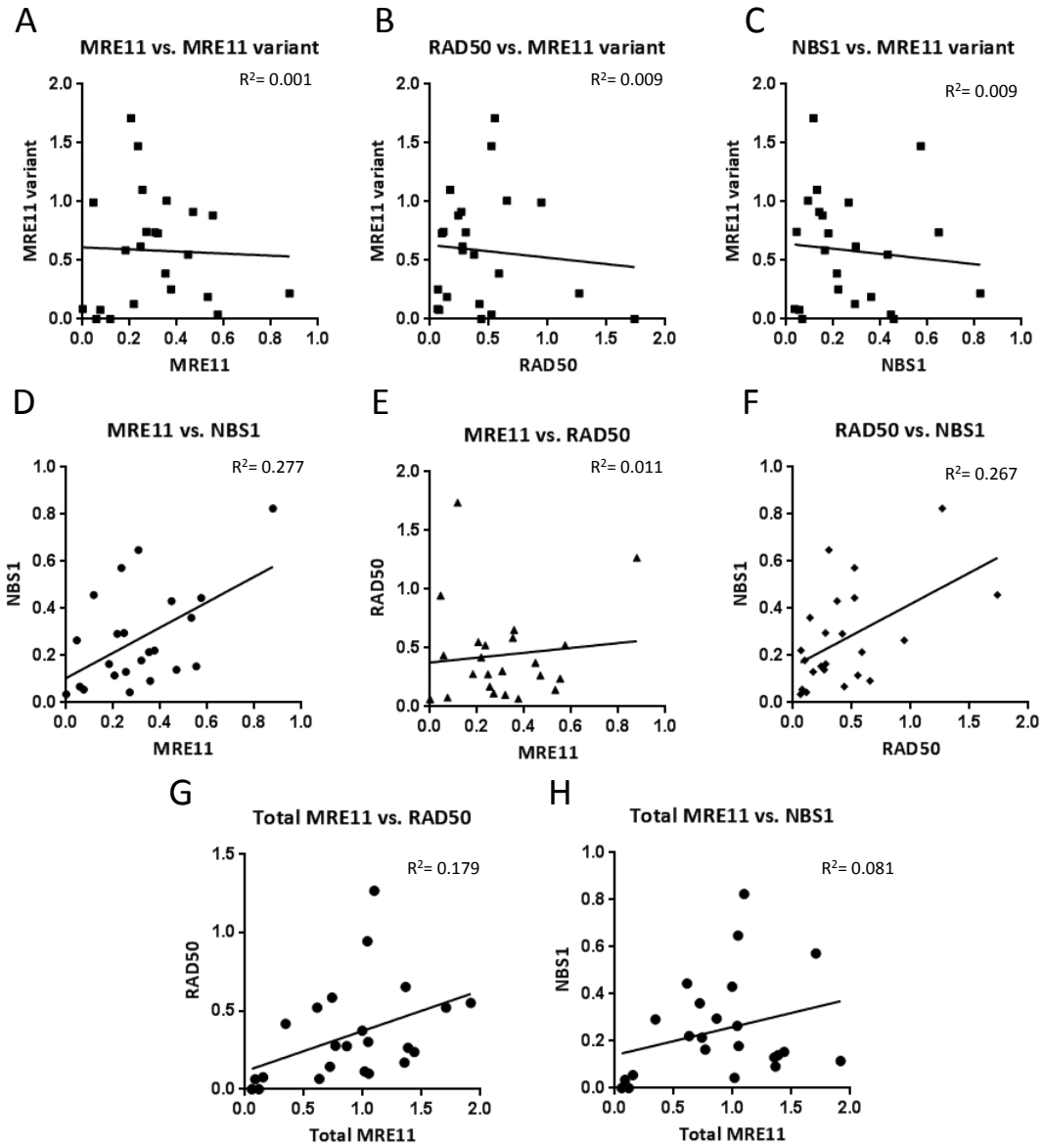

Figure 3.2 Correlation of the expression of the MRN complex proteins in bladder tumours.

A) Wild type MRE11 vs. MRE11 variant, B) RAD50 vs. MRE11 variant, C) NBS1 vs. MRE11 variant, D) Wild type MRE11 vs. NBS1, E) Wild type MRE11 vs. RAD50, F) RAD50 vs. NBS1, G) Total MRE11 vs. RAD50, H) Total MRE11 vs. NBS1. The coefficient of determination (R^2) value is shown for each analysis. A value of 0 indicates that the model explains none of the variability and therefore there is no correlation, values closer to 1 indicate that the model explains all of the variability and there is a greater correlation.

3.2.2 MRE11 protein expression in bladder cancer cell lines

As MRN complex levels were highly variable and having detected a smaller MRE11 protein band in patient bladder tumour extracts, the expression of the MRN proteins was further assessed in a panel of bladder cancer cell lines by western blot analysis (Figure 3.3). Bladder cell line extracts were generated according to Materials and Methods 2.4.1.

Expression of the MRN complex proteins was less variable in bladder cancer cell lines compared with bladder tumour extracts. However, certain cell lines were found to express an MRE11 protein band with a smaller molecular weight compared to WT MRE11, similar to that previously seen in the bladder tumour extracts. Expression of the smaller MRE11 protein band was most notable in the RT112 and CALgem bladder cancer cell lines. However, it was also faintly detectable in the CAL29 and VMCUB bladder cancer cell lines. Expression of the smaller MRE11 protein band was also detected in the normal human urothelial (NHU) cell line.

Furthermore, the MRE11 variant was only detected when using an antibody that binds to an internal domain of MRE11 and not detected when using an antibody that binds to the C-terminus of the protein. This indicated that the variant could be lacking the C-terminal domain.

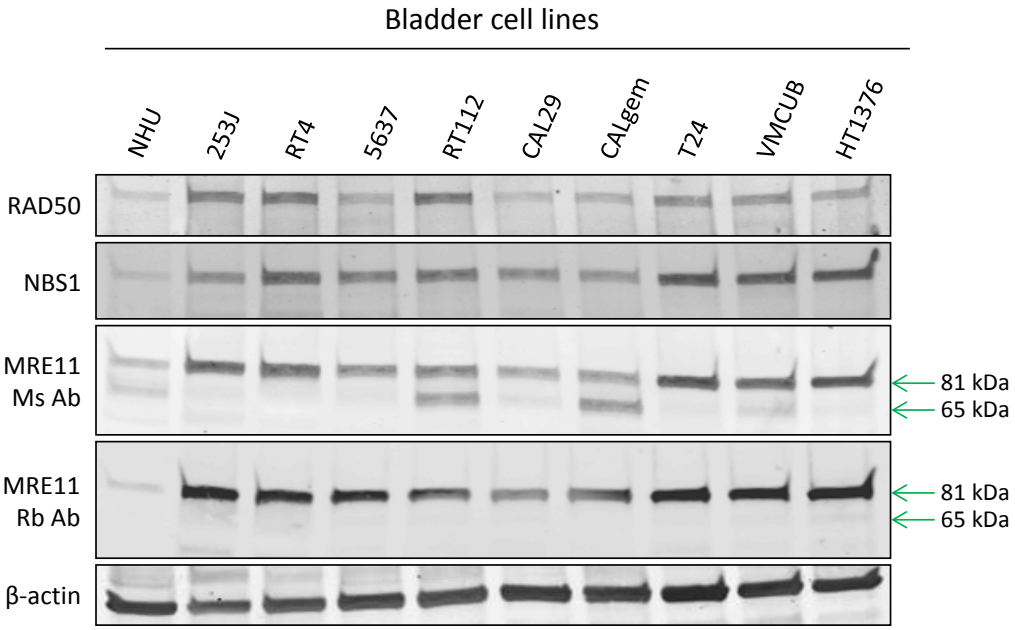

Figure 3.3 Expression of the MRN complex proteins in bladder cancer cell lines.
A) Western blot analysis showing expression of the MRN complex proteins in a panel of bladder cancer cell lines and a normal human urothelial cell line (NHU). Two MRE11 antibodies were used to detect expression of MRE11. A mouse antibody (Ms Ab) that binds to amino acids 182-582 (ab214) and a rabbit antibody that binds to the C-terminus (Rb Ab). β-actin was used as a loading control.

3.2.3 MRE11 protein expression in other cancer cell lines

In order to determine whether this variant is specific to bladder cancer or is detectable in other cancer types, a panel of oesophageal and lung cancer cell lines were also analysed for expression of the MRN complex proteins (Figure 3.4). In the panel of cell lines from both oesophageal and lung cancers an MRE11 protein band with a smaller molecular weight than WT MRE11 was not detected.

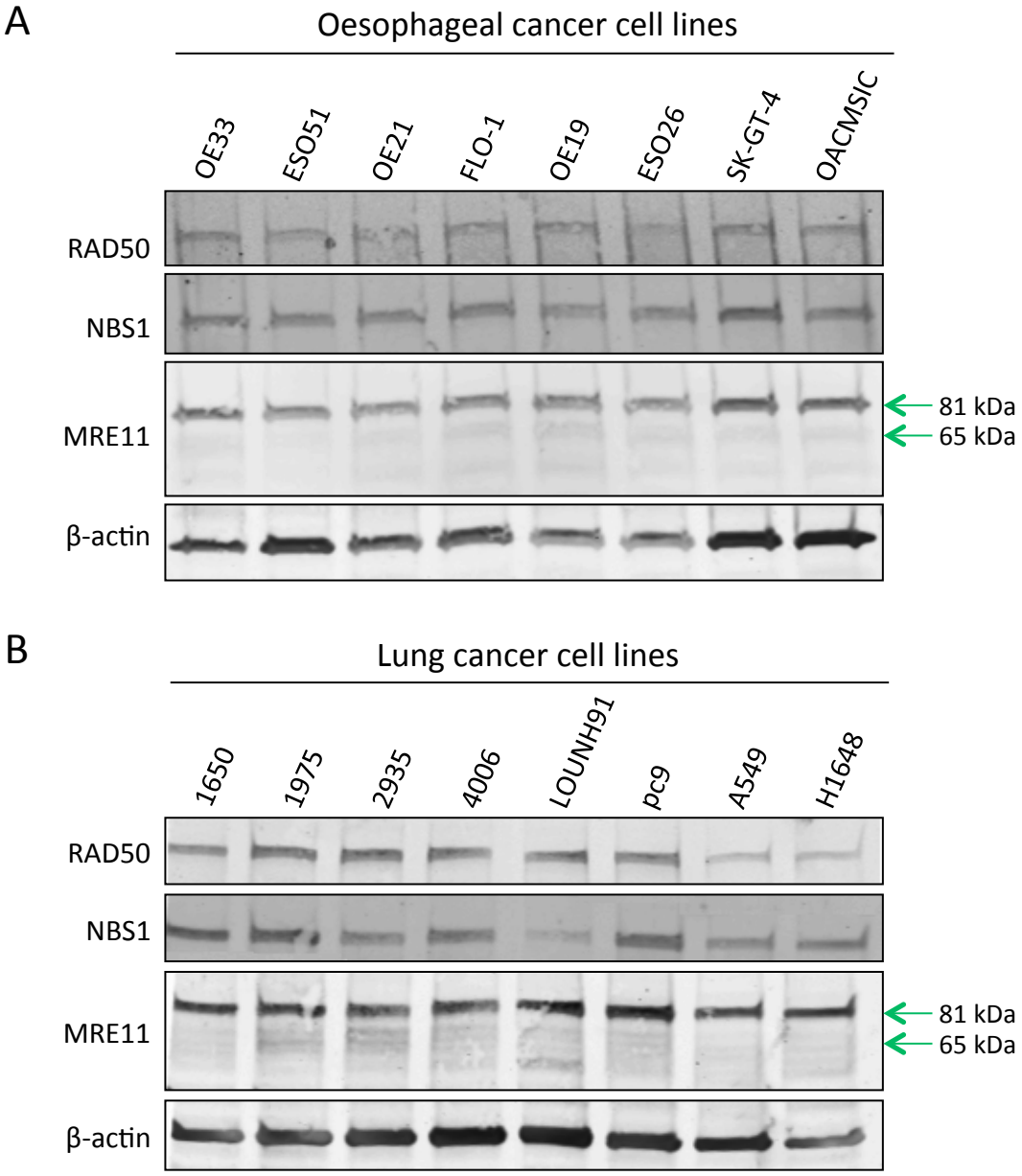

Figure 3.4 Expression of the MRN complex proteins in oesophageal and lung cancer cell lines.

Expression of the MRN complex in a panel of A) oesophageal and B) lung cancer cell lines. Extracts were kindly provided by Dr Ester Hammond and Dr Anderson Ryan (CRUK/MRC Oxford Institute for Radiation Oncology), respectively. β-actin was used as a loading control.

3.2.4 MRE11 expression in bladder cancer cell line lysates

It was intriguing to see that lysates generated using different techniques provided by Dr Ester Hammond and Dr Anderson Ryan (CRUK/MRC Oxford Institute for Radiation Oncology) did not show expression of a smaller MRE11 protein. In order to establish whether the smaller MRE11 protein was a result of lysate preparation, potentially as a result of protease activity, lysates where generated from the RT112 and T24 cell lines using different methods of protein extraction (Figure 3.5). The smaller MRE11 protein band was detected in lysates generated from the RT112 cell line using three different lysis methods. Each lysis method contained protease inhibitors (Materials and Methods 2.1) able to inhibit a wide range of proteases suggesting that the smaller band is unlikely to be a product of protease degradation during lysate preparation.

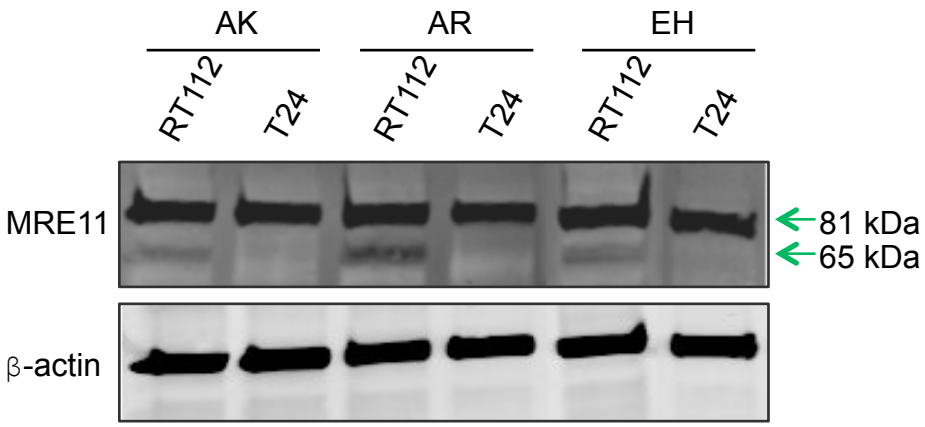

Figure 3.5 Protein lysate generation.
Western blot analysis of MRE11 expression in the RT112 and T24 bladder cancer cell lines, in lysates generated from protein extraction techniques used by Dr Anne Kiltie (AK), Dr Anderson Ryan (AR) and Dr Ester Hammond (EH). β-actin was used as a loading control.

3.2.5 MRE11 immunoprecipitation

To investigate the smaller MRE11 protein band, MRE11 was immunoprecipitated from the RT112 bladder cancer cell line using an MRE11 antibody that binds to amino acids 182-582, an internal region of MRE11. Both WT MRE11 and the smaller MRE11 protein band were precipitated as determined by western blot analysis (Figure 3.6A). A separate fraction of the MRE11 enriched extract was separated by gel electrophoresis and proteins visualised by Coomassie staining of the gel (Figure 3.6B).

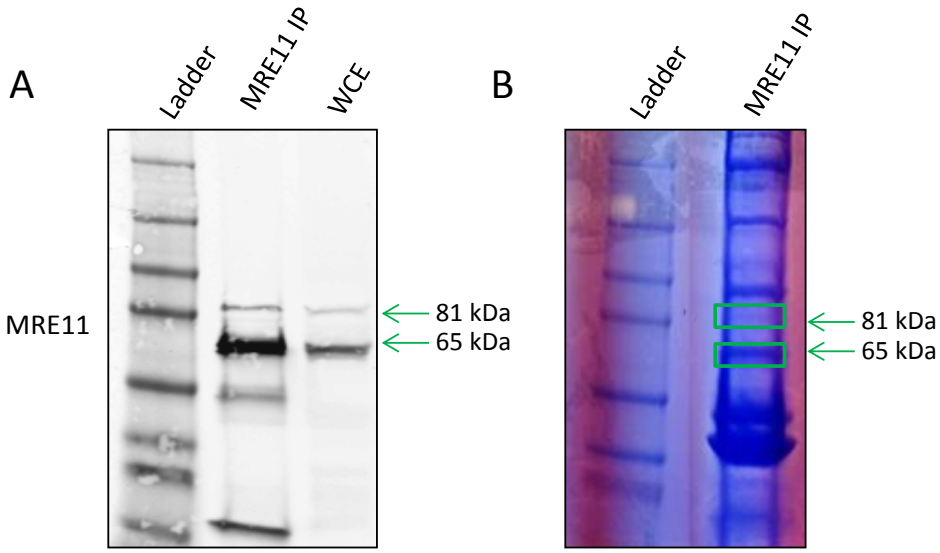

Figure 3.6 Immunoprecipitation of MRE11.
MRE11 was immunoprecipitated from the RT112 bladder cancer cell line. A) Western blot analysis of MRE11 expression in the MRE11- immunoprecipitated RT112 extract indicates two MRE11 bands at 81 kDa and 65 kDa. MRE11 expression in the whole cell extract (WCE) is indicated B) The corresponding Coomassie-stained gel of an MRE11 enriched lysate from the RT112 cell line. Green rectangles indicate where the gel was cut to excise bands for mass spectrometry analysis.

3.2.6 Mass spectrometry sequencing of MRE11

To identify the smaller protein band detected by the MRE11 antibody, bands corresponding to each protein were excised from the gel (Figure 3.7) and subsequently analysed by liquid chromatography-coupled tandem mass spectrometry (LC-MS/MS) by the Kessler group (Target Discovery Institute (TDI), Oxford). The proteins underwent digestion with either trypsin or elastase enzymes before mass spectrometry sequencing. This permitted the identification of peptides present in each sample and hence the elucidation of the difference between the WT MRE11 band and the smaller protein band, by determining which peptides are unique to the WT MRE11 protein.

The peptide sequence of MRE11 is shown in Figure 3.7. Peptides detected by the mass spectrometer were analysed by Mascot (Pappin *et al*. 1999) and are shown in red text. Mascot analysis showed MRE11 to be a top "hit" for both gel slices, suggesting that both the larger and smaller bands were indeed MRE11 (Appendix A). After tryptic digest, the protein coverage of the 81 kDa WT MRE11 protein band was 42%. After the same analysis, the peptide coverage of the 65 kDa MRE11 variant was 49%. Despite the coverage being greater for the variant, there were peptides detected at the C-terminus of the WT protein that were not detected in the variant. Green boxes highlight these peptides in Figures 3.7A and C.

Trypsin cleaves at the carboxyl side of the amino acids lysine (K) and arginine (R), except when followed by a proline (P) residue; this influences which peptides are detected depending on the distribution of these residues within the protein. Therefore, in order to map the peptides further, the samples were also digested

with elastase. Elastase is a serine protease that cleaves on the carboxyl side of small, hydrophobic residues, for example: valine (V), alanine (A) and glycine (G). In the elastase analysis, the peptide coverage of the variant was greater than the WT MRE11 analysis at 54% and 31%, respectively. Despite the lower percentage of sequence coverage again, there were C-terminal peptides detected in the WT MRE11 protein that were not detected in the MRE11 variant. Green boxes in Figure 3.7B and D highlight these peptides.

Peptides were detected at the C-terminus of MRE11 in the tryptic digest of the MRE11 variant that were not detected in the elastase digest, underlined in orange in Figure 3.7C and D. The validity of these peptides being present or absent is discussed later.

The MRE11 peptide coverage suggests that the secondary protein band detected at a lower molecular weight is an MRE11 variant. It also suggests that its lower molecular weight is due to the variant lacking C-terminal peptides, as these were not detected after mass spectrometry analysis following digestion with either trypsin or elastase enzymes.

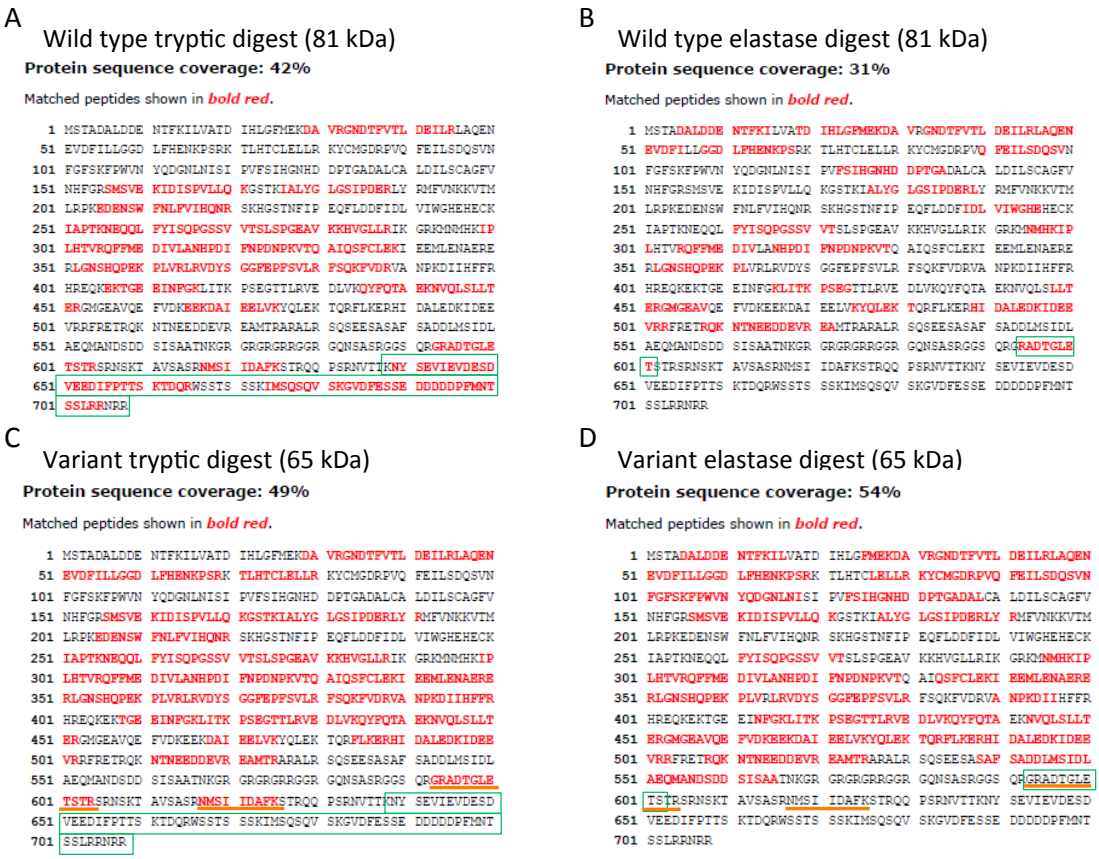

Figure 3.7 Mass spectrometry sequencing of wild type MRE11 and the MRE11 variant.

Mascot analysis (Pappin *et al*. 1999) of the peptide coverage of the 81 kDa protein band, representing wild type MRE11, digested with A) trypsin or B) elastase. Peptide coverage of the MRE11 variant digested with C) trypsin or D) elastase. Red peptides were identified by mass spectrometry with high confidence. Green boxes highlight peptides detected at the C-terminus of wild type MRE11, digested with either trypsin or elastase, that failed to be detected in the MRE11 variant. Orange lines highlight peptides that were detected in the tryptic digest of the MRE11 variant but not the elastase digest.

3.2.7 Rapid amplification of MRE11 3'cDNA

To decipher whether the C-terminal truncation of MRE11 was due to an alternate transcript being present in the RT112 cell line 3' rapid amplification of cDNA ends (RACE) of MRE11 was performed on cDNA generated from the RT112 and T24 cell lines. An oligo-dT adapter primer allowed the capture of mRNA transcripts containing a poly(A) tail region (Materials and methods 2.12). Amplification of the 3'cDNA end of MRE11 was performed using a gene specific primer (GSP) and a universal amplification primer (UAP) (Figure 3.8). Control cDNA was generated per kit protocol and amplified using control primers to generate a product of 720 bp (lane 1). Amplification of the 3'cDNA end of MRE11 from RT112 and T24 cell lines is shown in lanes 2 and 3, respectively. Isoforms 1 and 2 of MRE11 would be expected to generate PCR products of approximately 1,178 bp and 1120 bp, respectively. The size of these PCR products would be indistinguishable from each other on this percentage gel. As deduced from western blot analysis the molecular weight of the smaller MRE11 protein is approximately 65 kDa. Therefore, the 3'cDNA product generated from an alternative transcript would be approximately 752 bp. One band was present after the amplification of the 3'cDNA end of MRE11 in both RT112 and T24. This product was more than 1000 bp suggesting that expression of the smaller MRE11 protein is not due to an alternative transcript.

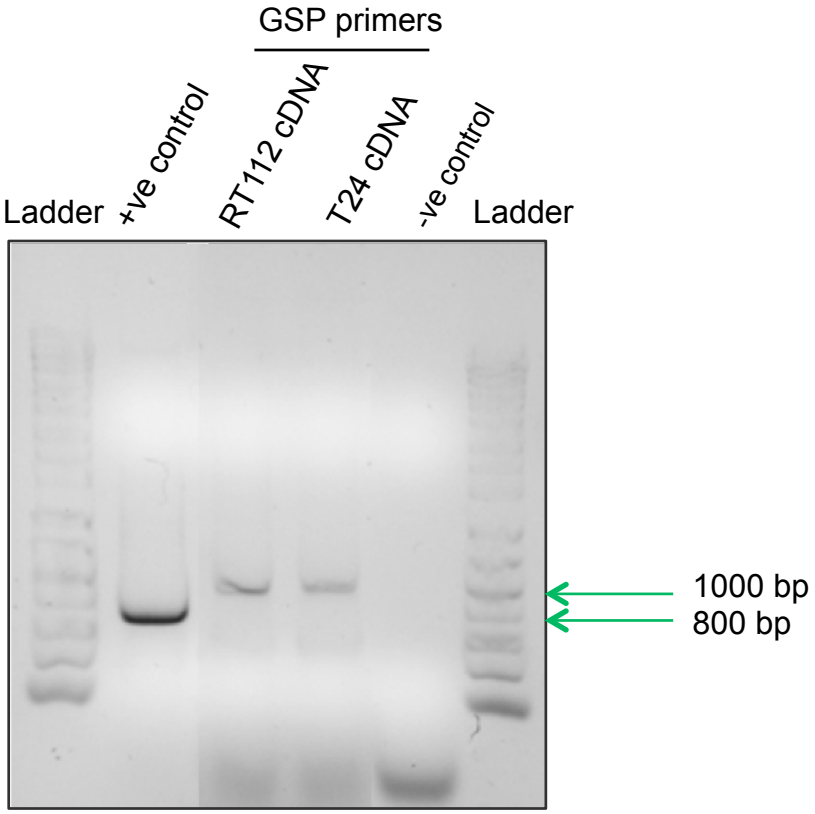

Figure 3.8 Amplification of *MRE11* 3'cDNA ends.

Amplification of *MRE11* 3'cDNA ends from RT112 and T24 cDNA using a gene specific primer (GSP) and universal amplification primer. Positive (+ve) and negative (-ve) controls are indicated. HyperLadder 1 kb was used as a marker for DNA product size.

3.2.8 Fractionated western blot analysis of RT112 cell lysate

DNA damage and repair occurs in the cell nucleus. After DNA damage the MRN complex proteins are localised in the nucleus, via the nuclear localisation signal (NLS) domain of NBS1 (Carney *et al*. 1998). For the truncated MRE11 protein to influence DSB repair, the protein would also need to be localised to the nucleus.

The localisation of the truncated protein was determined through fractionation of protein lysate from the RT112 cell line into cytosolic or nuclear fractions and subsequent western blot analysis (Figure 3.9).

Western blot analysis indicated that proteins of the MRN complex were predominantly located in the nuclear-enriched fraction of the cell lysate (Figure 3.9, Lane 2). Low MRN protein expression was also detected in the cytosolic fraction. The lack of cytosolic expression of total H2AX, a protein only present in the nucleus, confirmed that there was no contamination of the cytosolic fraction with nuclear proteins. The expression of β-actin verified that an adequate concentration of protein was loaded for representation of proteins located in the cytosolic fraction, confirming the low expression of the MRN proteins in this fraction and their predominant localisation in the nucleus. The truncated MRE11 protein was also found to be located largely in the nuclear-enriched fraction with other members of the complex, suggesting a potential influence on DSB repair. This implies that the truncated protein can interact with NBS1 to enter the nucleus.

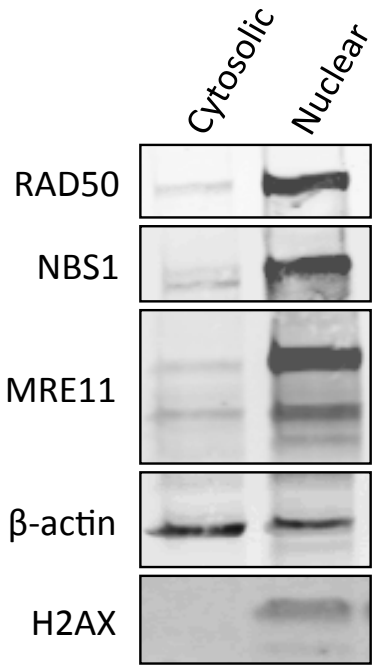

Figure 3.9 Cellular localisation of the MRN complex proteins.
Protein lysate from the RT112 cell line was enriched for either nuclear or cytosolic fractions. Western blot analysis shows expression of the MRN complex proteins in each fraction. Total H2AX was used as a marker of nuclear protein expression. β-actin was used as a protein loading control.

3.2.9 Co-immunoprecipitation of endogenous MRE11

After observing that the truncated MRE11 protein was present in the nuclear fraction of cells, which implies complex interaction with NBS1 and RAD50, this was next confirmed by co-immunoprecipitation of the MRN complex proteins. Endogenous proteins from an RT112 cell line protein lysate were immunoprecipitated, followed by western blot analysis to determine protein-protein interactions.

Immunoprecipitation with three antibodies targeting MRE11, RAD50 or NBS1 resulted in pull down of the reciprocal complex proteins. Truncated MRE11 was also immunoprecipitated with each of the antibodies (Figure 3.10). This suggests that the truncated protein was interacting with the complex. Control immunoprecipitates using IgG antibodies from both mouse and rabbit species confirmed that the pull downs were specific to the target proteins, as no expression of MRN complex proteins were seen in these pull downs. Furthermore, a bead only control indicated that there was antibody-protein specificity, as none of the MRN proteins were present in this precipitate. The protein expression in the whole cell extract (WCE) can be seen in the right hand lane.

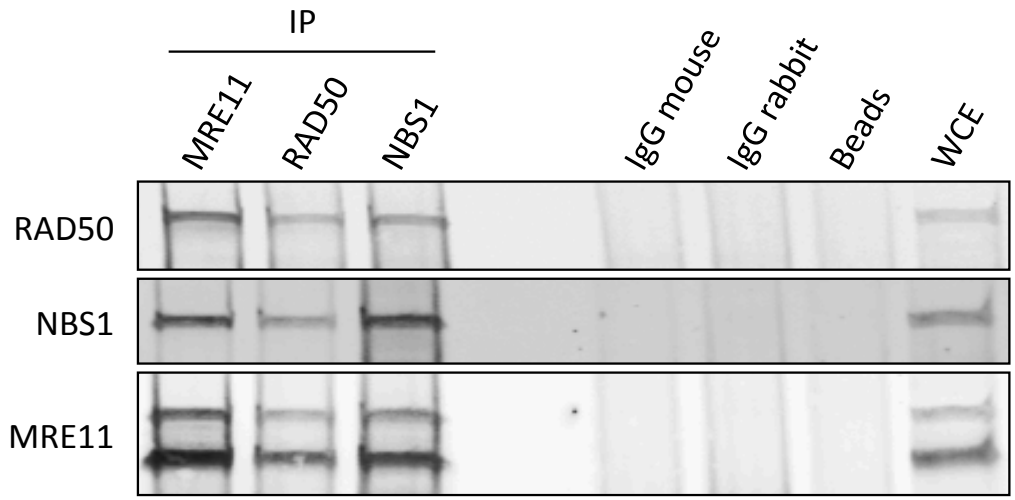

Figure 3.10 Immunoprecipitation of the endogenous MRN complex proteins.
Western blot analysis of endogenous protein pull down in the RT112 cell line using antibodies targeted to MRE11, RAD50 or NBS1. IgG mouse and rabbit antibodies are controls for non-specific pull down. Beads only control indicates that there was no unspecific protein binding to the beads. Expression of the MRN complex proteins in the whole cell extract (WCE) is represented in the right hand lane.

3.2.10 Cloning of MRE11 and site-directed mutagenesis to emulate truncation

To undertake functional studies of the MRE11 variant, both WT and truncated MRE11 were cloned into expression plasmid vector TOPO pcDNA3.3 (Materials and Methods 2.9)

Primers were designed to allow amplification of the coding region of MRE11. An HA epitope tag sequence was included at the 5' end of the forward primer: tacccatacgatgttccagattacgct, corresponding to the amino acid sequence YPYDVPDYA. PCR amplification was performed with a high fidelity Taq polymerase capable of adding A' overhangs to the PCR product to allow a TOPO cloning reaction to occur. Bacteria were transformed to replicate the plasmid and were plated onto ampicillin-containing agar to allow selection of individual colonies containing the plasmid. DNA was isolated from individual clones using a Qiagen mini prep kit and sequenced by Sanger sequencing to confirm accurate cloning of the MRE11 coding sequence in the correct orientation. An overview of the cloning strategy used is shown in Figure 3.11A.

In order to reproduce the MRE11 truncation, an early stop codon was introduced by site-directed mutagenesis, converting an adenine to a thymidine nucleotide and the corresponding codon from AAA to TAA, i.e. lysine to STOP. Lysine 568 residue was chosen as the point to terminate the protein as it would produce a protein of 65 kDa which would correspond with the predicted molecular weight of the endogenous truncated protein (determined by western blot).

The mutated amino acid is highlighted by a green circle in Figure 3.11B. The mutated sequence was confirmed using Sanger sequencing; the sequencing trace of WT vs. mutated is shown in Figure 3.11C.

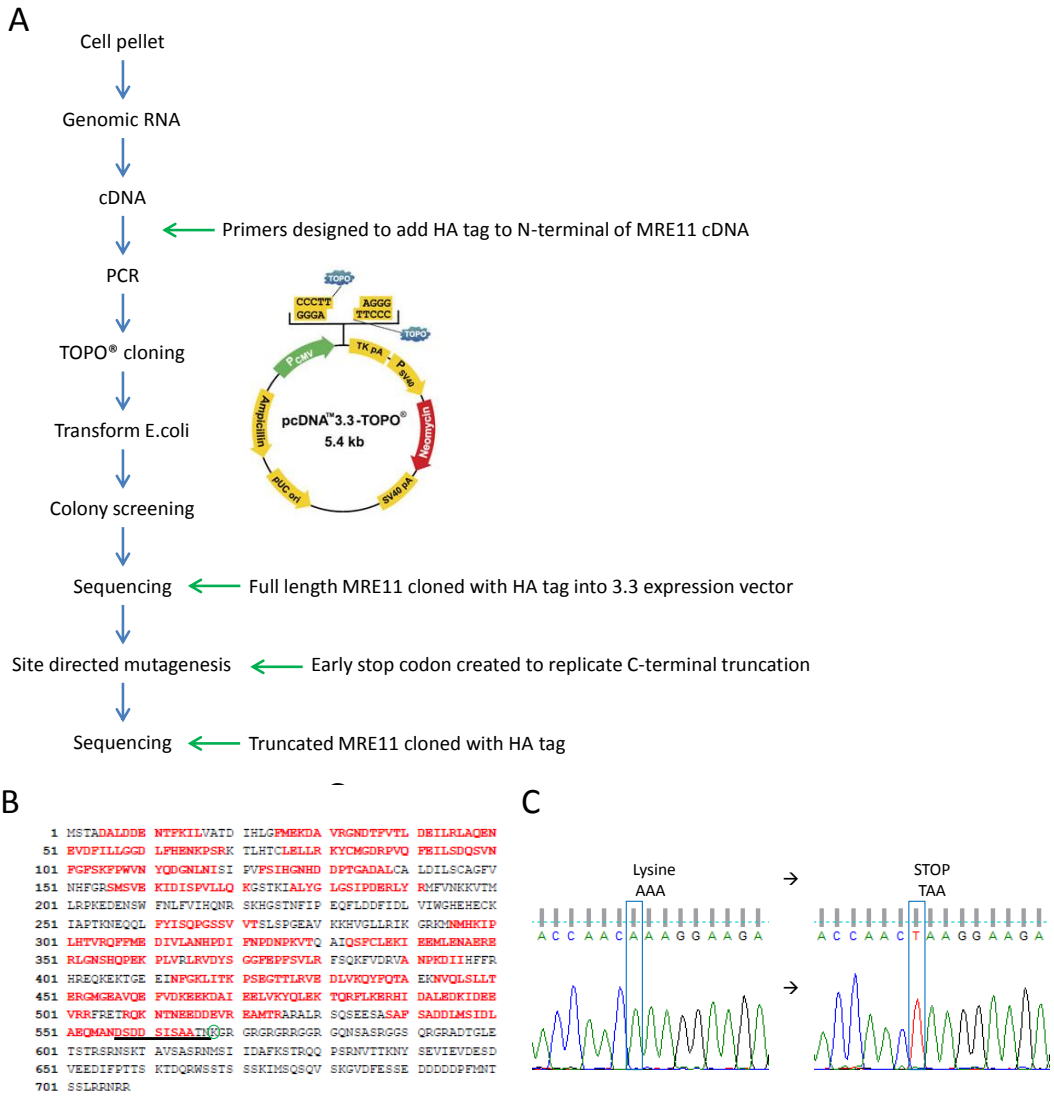

Figure 3.11 Cloning of wild type and truncated MRE11.

A) Overview of MRE11 cloning strategy. B) Mass spectrometry peptide sequence of truncated MRE11; the black line indicates likely area of truncation site. Green circle highlights the lysine residue mutated into a stop codon. C) Sequencing trace of site-directed mutagenesis to mutate A to T and introduce early stop codon. The mutated base is highlighted with a blue box.

3.2.11 Co-immunoprecipitation of HA-tagged truncated MRE11 and co-localisation of NBS1 and the truncated MRE11 protein

Endogenous immunoprecipitation of the MRN complex in the RT112 cell line suggested that the truncated MRE11 protein was able to interact with RAD50 and NBS1. However, as the MRN complex exists as a heterohexamer structure (van der Linden *et al*. 2009; Hopfner *et al*. 2001) this experiment did not fully determine whether the truncated MRE11 protein was interacting with monomeric WT MRE11 protein, thus leading to interaction with NBS1 and RAD50, or whether two truncated MRE11 proteins were capable of forming a homodimer and complexing with NBS1 and RAD50. To address this point, the expression vector described in Figure 3.11 coding for the truncated MRE11 protein with an HA tag was transfected into the T24 cell line, which does not express the truncation under control conditions (Figure 3.3). Immunoprecipitation of the truncated MRE11 protein was performed with anti-HA-Ab-conjugated Protein G beads targeting the HA tag. Subsequently, protein interactions were determined by western blot analysis (Figure 3.12A). The figure shows that a large proportion of MRE11 in the HA pull down was the truncated variant. Only a small amount of WT MRE11 was detected in the immunoprecipitated lysate when compared with the expression seen in the WCE (Figure 3.12A Lane 2). Substantial levels of NBS1 and RAD50 proteins were detected in the pull down. This suggests that the truncated MRE11 protein was able to homodimerise and thus interact with NBS1 and RAD50 directly, but also (to a lesser extent) that it could heterodimerise with WT MRE11.

Expression of the HA-tagged truncated MRE11 protein was not detected with an antibody targeted to HA in the WCE. This was thought to be due to weak antibody binding as, when comparing HA and MRE11 signal (marked with *) in the IP lane (Figure 3.12A, lane 1) the HA signal was weaker, despite these antibodies targeting the same protein. The truncated MRE11 protein was detected in the WCE on probing with an antibody targeting MRE11; this again suggests that the sensitivity of the HA antibody was less than that of MRE11. Therefore, despite the HA antibody not detecting the truncated protein in the WCE, it was considered to be present in the sample due to the detection by the MRE11 antibody.

To provide further evidence for an interaction between NBS1 and truncated MRE11, the localisation of HA-tagged truncated MRE11 protein and NBS1 was determined. The T24 cell line was transfected with the HA tagged truncated MRE11 expression vector. Localisation of HA tagged MRE11 and NBS1 was determined 2 hours following exposure to 5 Gy IR, using immunofluorescence microscopy (Figure 3.12B). DAPI staining indicates the nucleus of the cells through binding to A-T rich regions of DNA. An antibody specifically targeting the HA tag was used to determine which cells had undergone positive transfection. As can be seen in Figure 3.12B, despite DAPI and NBS1 staining showing the presence of multiple cells, not all cells were positive for HA staining, highlighting the specificity of the antibody and that positive cells had been successfully transfected. Areas of DNA damage can be seen through the increased intensity of the NBS1 antibody indicating ionising radiation-induced foci (IRIF). The merged image in the bottom right of the panel shows overlap between HA and NBS1

staining. Two yellow arrows highlight two repair foci with increased signal for both HA and NBS1. This can be seen more clearly enlarged in the yellow box, top right. This demonstrates co-localisation of the HA-tagged truncated MRE11 and NBS1 and therefore their likely interaction at IRIF.

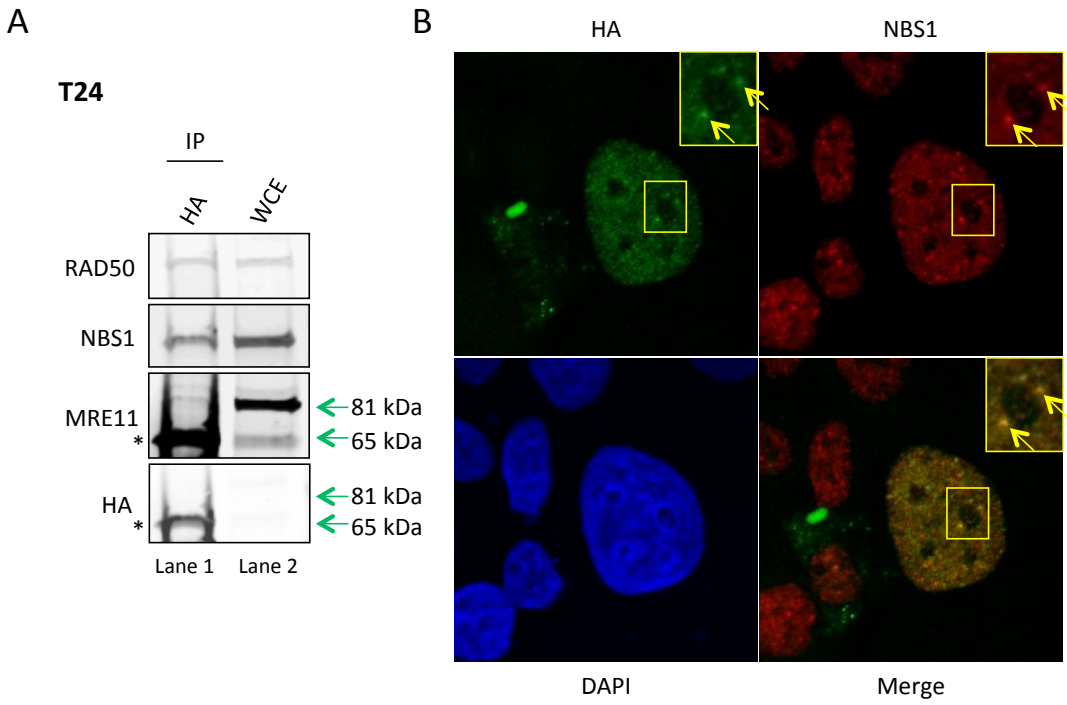

Figure 3.12 The truncated MRE11 protein directly complexes with NBS1 and RAD50.

A) Western blot analysis of immunoprecipitation in T24 cell line after transfection with the MRE11 truncated protein with an N-terminus HA tag. HA conjugated beads were used in the immunoprecipitation to bind the HA-tagged protein. Levels of MRE11, RAD50 and NBS1 bound to the truncated protein are shown in lane 1. Expression of the MRN complex in the whole cell lysate is shown in lane 2. B) Immunofluorescence microscopy of the T24 cell line after transfection with the MRE11 truncated protein expression vector with an N-terminus HA tag, 2 hours post exposure to 5 Gy ionising radiation. Top left panel shows HA antibody staining with the larger cell having undergone positive transfection. Top right panel shows NBS1 antibody staining, bottom left shows DAPI nuclear stain. Bottom right panel shows the merged image of HA and NBS1. Yellow boxes indicate areas that have been magnified. Examples of the co-localisation between HA and NBS1 foci highlighted by two yellow arrows.

3.2.12 HA-tagged truncated MRE11 co-localises with yH2AX foci

After showing that the truncated MRE11 protein co-localised with NBS1 and that this was likely to be at sites of DNA damage, further evidence of the ability of the truncated MRE11 protein to localise to sites of DNA damage was examined. This was determined by the co-localisation of the HA-tagged truncated MRE11 protein with DNA damage marker yH2AX, after exposure to IR. The T24 cell line was transfected with HA-tagged truncated MRE11 expression vector, and incubated for 48 hours to allow for expression of the protein to occur, after which time the cells were exposed to 5 Gy IR. Two hours following irradiation, the localisation of the HA-tagged MRE11 protein and yH2AX was determined by immunofluorescence microscopy Figure 3.13. DAPI fluorescent stain was used to indicate nuclei of individual cells, bottom left panel. As demonstrated in the top left panel of Figure 3.13, not all cells stained positively for the HA antibody, again confirming the specificity of the HA antibody and confirming that these cells had undergone positive transfection and were expressing the HA-tagged MRE11 protein, with high abundance in the nucleus. Several sites of DNA damage were seen due to the accumulation and increased intensity of signal emitted by the DNA damage marker protein yH2AX, top right panel. There was co-localisation of HA-tagged truncated MRE11 and yH2AX as seen by the overlap in red and green signal, thus forming yellow foci in the merged image, bottom right panel. Yellow arrows in the enlarged area indicated by a yellow box highlight three foci. This suggests recruitment of the truncated MRE11 protein occurs at sites of DNA damage following exposure to IR.

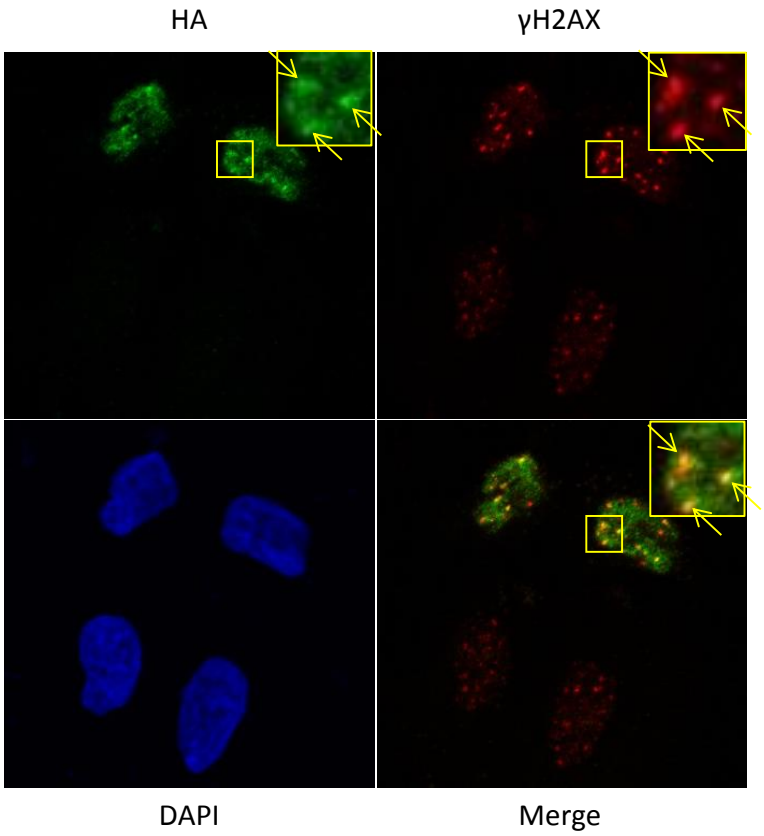

Figure 3.13 The truncated MRE11 protein is recruited to sites of DNA damage.
The T24 cell line was transfected with the truncated MRE11 expression vector with an N-terminus HA tag. Cells were exposed to 5 Gy IR and fixed 2 hours later. Immunofluorescence microscopy was used to determine localisation and signal emitted by HA and γH2AX, top left and right panels, respectively. DAPI stain indicates nuclei of cells, bottom left panel. Bottom right panel shows the merged signal of HA and γH2AX emission. Yellow boxes indicate areas that have been enlarged for clarity. Three examples of co-localisation of HA and γH2AX are highlighted by yellow arrows.

3.3 Discussion

3.3.1 MRE11 variant detection in bladder tumours

A novel MRE11 variant, which has not previously been described in the literature for bladder cancer or other cancer cell types, was detected in bladder tumour patient samples and in bladder cancer cell lines. Previously, MRE11 mutants have been examined in patients with ataxia-telangiectasia-like disorder (ATLD) and their presence leads to chromosomal instability, radiosensitivity, and DNA damage-dependent checkpoint defects (Stewart *et al*. 1999; Theunissen *et al*. 2003; Regal *et al*. 2013; Delia *et al*. 2004). It is therefore reasonable to hypothesise that a tumour expressing an MRE11 protein variant could potentially be more sensitive to DNA damaging agents. Carriage of MRE11 variants could therefore lead to improved patient survival following radiotherapy or treatment with other DNA damaging agents.

The presence of the MRE11 variant is also a possible explanation for the paradoxical results seen in two independent studies by Choudhury *et al* (2010) and Laurberg *et al* (2012) where patients with high MRE11 expression in tumours had a better 3-year CSS after radiotherapy. As these studies used IHC to quantify MRE11 expression with an antibody that binds to amino acids 182−582, an internal region of MRE11, it is not possible to determine whether WT MRE11 or MRE11 variants were being detected. The MRE11 variant in this thesis was found to have a C-terminus truncation, which prevented its detection by western blot analysis when using an antibody targeted to the C-terminus of MRE11.

The expression of the MRN complex proteins or the truncated MRE11 protein, determined by western blot, in bladder tumour patient samples did not correlate

with the stage or grade of tumours. This is in agreement with the lack of correlation of the MRN complex proteins seen when using IHC staining of tumours to determine expression (Choudhury *et al*. 2010).

The expression of the truncated MRE11 variant did not correlate with expression of the WT MRN complex proteins. Intriguingly, there was no inverse correlation between WT and truncated MRE11 expression. This was also observed in the RT112 cell line, under control conditions over the course of experiments undertaken. In the RT112 cell line, expression of truncated MRE11 variant was most often equal to that of WT MRE11. However, the truncation was also observed to be greater or less in a highly variable manner. A possible explanation for this is that it is passage dependent; as cells are passaged, their health decreases possibly leading to greater expression of the truncated variant although this requires further investigation.

Another noteworthy observation from examining expression of the MRN complex proteins in bladder cancer cell lines was the presence of the truncated MRE11 protein in the CALgem cell line and not CAL29 (Figure 3.3). The CALgem cell line is derived from the CAL29 cell line and by gradually increasing exposure to the cytidine analogue gemcitabine has become resistant, to the concentration of 10 μM (Kerr *et al*. 2014). Of note, the expression of the truncated MRE11 protein was only apparent in cells that were resistant to gemcitabine and not after incubation with gemcitabine for 48 hours (Appendix B). It is not known if the MRE11 truncation aided resistance to gemcitabine by overcoming cell cycle arrest after the generation of stalled replication forks. This is an interesting possibility, as $MRE11^{ATLD1/ATLD1}$ cells (lacking C-terminus) exhibit S and G2/M

checkpoint defects (Theunissen *et al*. 2003). It has been shown that low dCK levels are responsible for the resistance to gemcitabine in the CALgem cell line (Kerr *et al*. 2014) and so the MRE11 truncation may not have a role. However, the consistent expression of the truncation protein in this cell line warrants further investigation.

Although not statistically correlated, there did appear to be a relationship between expression of the MRN complex proteins in bladder tumours; this is in agreement with previous reports (Martin *et al*. 2014; Choudhury *et al*. 2010). However, it was not clear what influence the truncated variant had on complex expression. Expression of the MRN complex proteins in tumours was highly variable but the tumour extracts were generated from a whole tumour, and therefore heterogeneous cell populations would be present. It would be interesting to determine if certain areas of the tumour were more likely to express the truncated variant, such as more hypoxic areas, although this would likely need to be done via IHC staining and so optimisation of WT vs. variant MRE11 detection would need to be achieved.

Examining expression of the MRN complex in other cancer types, no expression of an MRE11 variant was seen, suggesting that this variant was possibly specific to bladder tumour tissue. This result not due to different lysate preparation methods as these techniques were used to generate protein extracts from the RT112 cell line and expression of the MRE11 variant was detected in these samples (Figure 3.5). This also suggests that the variant is unlikely to be a product of protease cleavage of MRE11 during lysate preparation as a broad range of protease inhibitors were used during protein extraction.

The detection of the truncated MRE11 protein in normal human urothelium (NHU) suggests that this variant was also not specific to cancerous tissue and could be observed in normal bladder tissue. However, this requires further investigation as immortalised cells growing in culture may not be the best model for normal bladder tissue. Determining MRE11 expression in biopsies from normal bladder tissue is a potential method of examining this.

3.3.2 Identification of the MRE11 variant

Mass spectrometry analysis confirmed that the smaller band detected was a truncated version of MRE11. The mass spectrometry analyses from both tryptic and elastase digest strongly suggest that C-terminus peptides were not present in the MRE11 variant.

Despite the stringent cut off score of the mass spectrometry analysis, 'spurious' peptides were detected at the C-terminus of the variant when digested with trypsin, underlined in orange (Figure 3.7C and D). From the mass spectrometry data the presence of these peptides remains inconclusive and could be explained by artefacts from the mass spectrometer, for example carry-over of peptides from previous runs. When the variant was digested with elastase the percentage of peptide coverage was 54%, greater than the coverage of either tryptic or WT elastase analyses. In this analysis, no peptides were detected at the C-terminus of MRE11, including a peptide which was detected in the wild-type elastase analysis despite the overall peptide coverage being much less at 31%. The elastase digest of the variant had the most convincing coverage and when taking into account the C-terminus peptides not being present, the coverage percentage can be

calculated as 68%. The lack of C-terminus peptides detected in this analysis was judged as significant. Therefore, following mass spectrometry analysis it was concluded that the MRE11 variant appears to have a C-terminus truncation. Based on this, and by assessing the molecular weight of the protein band, the truncation was deemed to be of approximately 143 amino acids. However, further work needs to be performed to address the precise cleavage site.

This was further supported by western blot analysis with an MRE11 antibody designed to bind to the C-terminus, which failed to detect the truncated variant.

The MRE11 variant detected in bladder cancer samples appeared to be distinctly different from the ATLD patient mutation. As determined by mass spectrometry analysis and determining the molecular weight of the smaller band, the bladder cancer variant appeared to lack a greater number of amino acids from the C-terminus. This was predicted to be approximately 140 amino acids, compared with the 75 amino acids that are not present in the ATLD mutated protein (Stewart *et al*. 1999). Furthermore, in the bladder extracts, the truncation does not appear to be caused by a germline mutation, as previous deep sequencing of germline DNA of *MRE11* in 186 bladder cancer patients has not identified any mutation corresponding to the 633 amino acid position of MRE11 (Teo *et al*. 2014) or other mutations which would cause a premature stop codon.

Although the same C-terminal domain of MRE11 was missing in ATLD patients compared with the bladder tumour extracts and cell lines, the impact on MRN function and HR repair could be substantially different due to the size of the deletion and the presence of the other MRN complex proteins, WT MRE11, RAD50 and NBS1.

An *MRE11* mutant allele has also been described in colorectal cancers (Wen *et al*. 2008). The mutant produces a splice variant of the *MRE11* cDNA, which eliminates exons 5–7. This results in a 593 amino acid protein that partially lacks a highly conserved nuclease motif of MRE11. The variant detected in bladder cancer again does not appear to be this mutant as the mass spectrometry detected peptides covering the 5^{th} to 7^{th} exons in both tryptic and elastase digests. The peptide coverage seen in all analyses at least partially covers all internal exons; therefore, there does not appear to be any internal portion of the MRE11 protein missing from the variant. Furthermore, screening of a panel of bladder cancer cell lines showed that none carry the mutation at the 4^{th} intron splice site leading to this deletion (Martin *et al.* 2014).

Amplification of the 3'cDNA region of *MRE11* (Figure 3.8) in the RT112 cell line indicated that there was no alternative transcript present that would translate into the smaller MRE11 protein. This leads us to believe that the MRE11 variant is potentially a result of a post-translational modification and not the result of a mutant transcript. Further work conducted in this thesis also substantiates this hypothesis.

3.3.3 Nuclear location of truncated MRE11 protein

For the truncated MRE11 protein to be exerting an effect on DSB repair, localisation of the protein to the nucleus would be essential. The abundance of truncated protein in a nuclear enriched fraction of the RT112 bladder cancer cell line (Figure 3.9) suggests that the protein was primarily located in the nucleus and therefore could be influencing DNA repair.

The nuclear location of truncated MRE11 suggests that the protein might compete with WT MRE11 in terms of binding to the NBS1 and RAD50 proteins. In NBS cells, which are deficient in NBS1, MRE11 and RAD50 are still capable of interaction but the complexes containing these two proteins are confined to the cytoplasm and cannot form nuclear foci (Carney *et al*. 1998). Therefore, the presence of truncation in the nuclear fraction suggests that it was still capable of interaction with NBS1. This was confirmed through co-immunoprecipitation of MRN proteins with the truncated MRE11 protein (Figure 3.10, Figure 3.12A), supported by immunofluorescence microscopy (Figure 3.12B).

3.3.4 MRN complex formation

The MRN complex exists as a heterohexamer structure involving two NBS1, two RAD50 and two MRE11 protein molecules (Hopfner *et al*. 2001; van der Linden *et al*. 2009). Immunoprecipitation of endogenous proteins in the RT112 cell line with any of MRE11, RAD50 or NBS1 suggests that the truncated protein was interacting within the complex and binding to NBS1 and RAD50 (Figure 3.10). A limitation is that due to the dimer structure of the complex this did not fully address the question as to whether one truncated MRE11 protein was binding to a WT MRE11 protein and subsequently capable of interaction with NBS1 and RAD50 or two truncated MRE11 proteins could form a homodimer.

Specifically immunoprecipitating the HA-tagged truncated MRE11 protein implied that mostly homodimer complexes were being formed and subsequently interacting with NBS1 and RAD50 due to the low levels of WT MRE11 precipitated in the lysate (Figure 3.12A). In addition, the low levels of WT MRE11 present

suggests that heterodimer formation could occur. This suggests that the truncated MRE11 protein could be exerting a dominant negative effect on DSB repair through sequestration of NBS1 and RAD50 proteins. Consequently, this might prevent them from binding to WT MRE11 and so deplete levels of the fully functioning complex. The finding that truncated MRE11 can bind to NBS1 and RAD50 is consistent with previous studies that have shown that in patients with the syndromes ALTD1 and 2, where the C-terminus of MRE11 is lacking, the truncated form of MRE11 can be co-immunoprecipitated with NBS1 (Stewart *et al*. 1999; Theunissen *et al*. 2003). However, in ATLD 1 and 2 this occurs to a lesser extent than for WT MRE11, suggesting that some complex instability is caused by the truncated MRE11 protein (Stewart *et al*. 1999). In the study by Stewart *et al*. (1999), patients with ATLD do not express WT MRE11, whereas the experiments described in this thesis suggest competition between the two MRE11 proteins that has not previously been examined. Furthermore, expression of a truncated form of MRE11 could have a potential dominant negative effect on DSB repair. This has been observed in a C-terminally truncated CtIP variant that competitively disrupts DSB repair in a dominant negative fashion (Qvist *et al*. 2011).

Although by different means, a previously described *MRE11* mutant in colon cancer has been shown to disrupt MRE11 function in a dominant negative manner (Wen *et al*. 2008). This variant is thought able to still interact with chromatin. However, it exhibits reduced complex formation and nuclease function leading to increased sensitivity to DNA-damaging agents, such as thymidine and camptothecin, providing an interesting therapeutic target for patients with this phenotype (Rodriguez *et al*. 2008; Wen *et al*. 2008). It is

hypothesised that the nuclease activity would not be directly affected in patients with the truncated MRE11 variant described in this thesis, as these domains remain intact (Bressan *et al*. 1998). However, the efficiency of HR repair could be disrupted through a lack of CDK2 binding or missing ATM phosphorylation sites. CDK2 binds directly to C-terminal domain of MRE11, facilitating the phosphorylation of CtIP and its subsequent interaction with BRCA1. The 76 C-terminus amino acids are sufficient for interaction with CDK2 (Buis *et al*. 2012). However, these amino acids are not present in the MRE11 truncated variant described in this chapter, potentially leading to limited DNA end resection and disrupted HR. In contrast, it was recently identified that mutating two ATM phosphorylation sites at the C-terminus of MRE11, at positions S676A and S678A results in uncontrolled end resection by Exo1 (Kijas *et al*. 2015). This presents two different mechanisms by which HR could be disrupted in cells expressing a truncated MRE11 variant.

3.3.5 Recruitment of truncated MRE11 to IRIF

Confirmation that the MRN complex containing truncated MRE11 was present at the sites of DNA damage was demonstrated by co-localisation of the HA-tagged truncated MRE11 protein at IRIF with NBS1 and yH2AX (Figure 3.12B and Figure 3.13). This is in agreement with previous studies suggesting that NBS1 is integral for the localisation the MRE11/RAD50 protein complex at sites of DNA damage (Carney *et al*. 1998; Desai-mehta *et al*. 2001). However, these results differ from studies on the ATLD1 and 2 mutated MRE11 proteins, which showed that the truncated MRE11 protein is incapable of forming IRIF (Stewart *et al*. 1999;

Theunissen *et al*. 2003). This confirms that the truncated MRE11 protein described in this thesis is distinctly different from that seen in patients with the syndromes ATLD1 and 2, and so although MRE11 function in ALTD 1 and 2 is well characterised, there is a need to study the behaviour of the truncated MRE11 protein in the context of bladder cancer cells. This result again raises the possibility that truncated MRE11 is competing at the sites of DNA damage with WT MRE11, thus conferring a DSB repair defect in a dominant negative manner.

CHAPTER 4 Stability and cause of the truncated MRE11 variant

4.1 Introduction

After the detection and identification of a novel truncated MRE11 protein, the stability and cause of the variant were examined in order to determine the likelihood of any functional impact being exerted on DSB repair mechanisms. MRE11 is a highly conserved protein and functions in a complex with NBS1 and RAD50 to repair DSBs, predominantly through homologous recombination (HR). Each protein of the complex influences the stability of the others, as demonstrated in syndromes resulting from mutations in any one of the three proteins. These include Ataxia telangiectasia-like disorder (ATLD) and Nijmegen breakage syndrome (NBS), both of which are associated with high cancer susceptibility and high sensitivity to ionising radiation (Uchisaka *et al*. 2009; Hiel *et al*. 1996; Stewart *et al*. 1999). ATLD and NBS are caused by germline mutations in the genes encoding MRE11 and NBS1, respectively, leading to disruption of the complex (Stewart *et al*. 1999; Carney *et al*. 1998).

Protein stability has been shown to play a key role in genome stability and cancer development and the removal of and/or degradation of DNA damage response (DRR) proteins is an integral mechanism in the DSB repair process (Panier & Boulton 2014; Ramadan & Meerang 2011). Proteolytic digestion of key proteins in the DNA damage response is highly regulated and can trigger a cascade of cellular events influencing genome stability.

The ubiquitin proteasome pathway (UPP) is responsible for most of the degradation of intracellular proteins in the cell and control of protein turnover

(Ciechanover 2005). Several enzymes are responsible for generating ubiquitin (Ub) chains and linking these onto proteins, marking them for degradation (Ciechanover 2005). Once tagged, proteins are recognised and degraded by the 26S proteasome into smaller peptides (Ciechanover 2005). The proteasome allows for the removal of short-lived or abnormal proteins in eukaryotic cells. An imbalance in protein activity in the cell can be extremely detrimental; this may be due to accumulation of mutated proteins, protein over-activity or premature removal of key proteins. In cancer cells, normal homeostatic function is deregulated leading to hyperactivation of the proteasome, which can contribute to tumorigenesis (Leach *et al*. 1993). The DDR is tightly controlled throughout the cell cycle; one mechanism behind this is through the control of protein degradation. For example, the restriction of BRCA1 accumulation during G1 phase of the cell cycle via the RNF8 and RNF168 E3 ubiquitin ligases (Al-Hakim *et al*. 2010; Escribano-Diaz *et al*. 2013). Therefore, the proteasomal pathway was investigated as a potential cause of the MRE11 variant.

Caspases are a family of proteases that cleave proteins at recognition motifs specific for each caspase; these motifs will often contain aspartic acid residues (Poreba *et al*. 2013). Caspases are responsible for the cleavage of many proteins, involved in a wide range of cellular processes such as cell cycle regulation, DNA repair, inflammation and protein transcription and translation (Fischer *et al*. 2003).

Caspase function is critical for destruction of cellular constituents during apoptosis; however, there is evidence for non-apoptotic roles such as mediating immunity, cell cycle regulation, cell proliferation and migration (Yi & Yuan 2010).

These are key processes in malignant transformation. Caspase cleavage of Ataxia telangiectasia mutated protein (ATM) during apoptosis generates a kinase-inactive protein that is still able to bind to DNA but is unable to phosphorylate p53, causing ATM to act in a dominant-negative manner, blocking DNA repair and DNA damage signaling (Smith *et al*. 1999). Certain cancers, such as pancreatic, colon and breast carcinomas, have been shown to have high caspase activity which correlates with the aggressiveness and metastatic potential of the tumours (Vakkala *et al*. 1999; Yang *et al*. 2003).

In order to overcome this high level of caspase activity yet avoid cell death (a hallmark of cancer) (Good & Harrington 2013), cancer cells have also evolved to upregulate proteins known as "inhibitor of apoptosis proteins" (IAPs) such as survivin (Satoh *et al*. 2001). Survivin has been shown to be more highly expressed in common human malignancies including bladder cancer when compared with normal tissue (Weikert *et al*. 2005; Wang *et al*. 2014). Therefore caspase activity was also investigated as a potential cause of the MRE11 variant.

Histone deacetylase (HDAC) inhibitors prevent the deacetylation of histones, leading to chromatin relaxation, which in turn alters gene transcription (Wang *et al*. 2009). HDAC inhibitors can influence gene expression via several means. Firstly, by modifying transcription of the gene, through increased acetylation of promoter regions. Secondly, via post-translational modification of proteins, which could target the protein for degradation. Finally, via an indirect means by modification of an interactor protein, resulting in degradation of the target protein and reduced expression (Bolden *et al*. 2006; West & Johnstone 2014). Panobinostat, a pan HDAC inhibitor, has previously been shown to influence

expression of HR proteins in bladder cancer cell lines, including the MRN complex proteins (Groselj *et al*. 2013; Xie *et al*. 2013). Panobinostat reduces wild type (WT) MRE11 expression post-translationally by an as of yet unknown mechanism (personal communication Blaz Groselj). The effects of panobinostat on the truncated MRE11 protein are also unknown, so this was investigated.

4.2 Results

4.2.1 Stability of MRE11

Following the confirmation that the lower molecular weight band detected by western blot was a species of MRE11, likely with a C-terminus truncation, the stability of the protein was assessed, including turnover. The hypothesis was that if the protein was being rapidly removed from the cells, the truncation would be less likely to have a major influence on DNA repair mechanisms.

Cycloheximide chase experiments were performed to compare the stability of WT and truncated MRE11 proteins. After blocking protein synthesis with cycloheximide for up to 24 hours, protein expression of the MRN complex was determined by western blot analysis (Figure 4.1). Cell death prevented study over a longer time period. Experiments were conducted in two bladder cancer cell lines, RT112 and T24.

In both cell lines, RAD51 levels fell relatively rapidly after 4–8 hours, confirming the ability of cycloheximide to inhibit further translation of proteins.

In the RT112 cell line, WT MRE11 was relatively stable with no significant decrease in expression after 24 hours treatment with cycloheximide. Notably, the truncated MRE11 protein was less stable than the WT MRE11 protein, with a significant decrease in protein expression seen after 12 hours of cycloheximide treatment. There was an approximately 50 to 60% decrease in truncated MRE11 protein at 20 to 24 hours following the blockade (Figure 4.1A, B). Consistent with WT MRE11, expression of NBS1 and RAD50 was also stable following 24 hour cycloheximide treatment.

WT MRE11 was less stable in the T24 cell line than in RT112 cell line, with a

significant decrease in protein expression seen after 20–24 hours. This was not consistent with protein expression of NBS1 and RAD50, which remained stable after 24 hours treatment. In both cell lines, all three WT MRN complex proteins were significantly more stable than RAD51, with half-lives of at least 24 hours (Figure 4.1C and D).

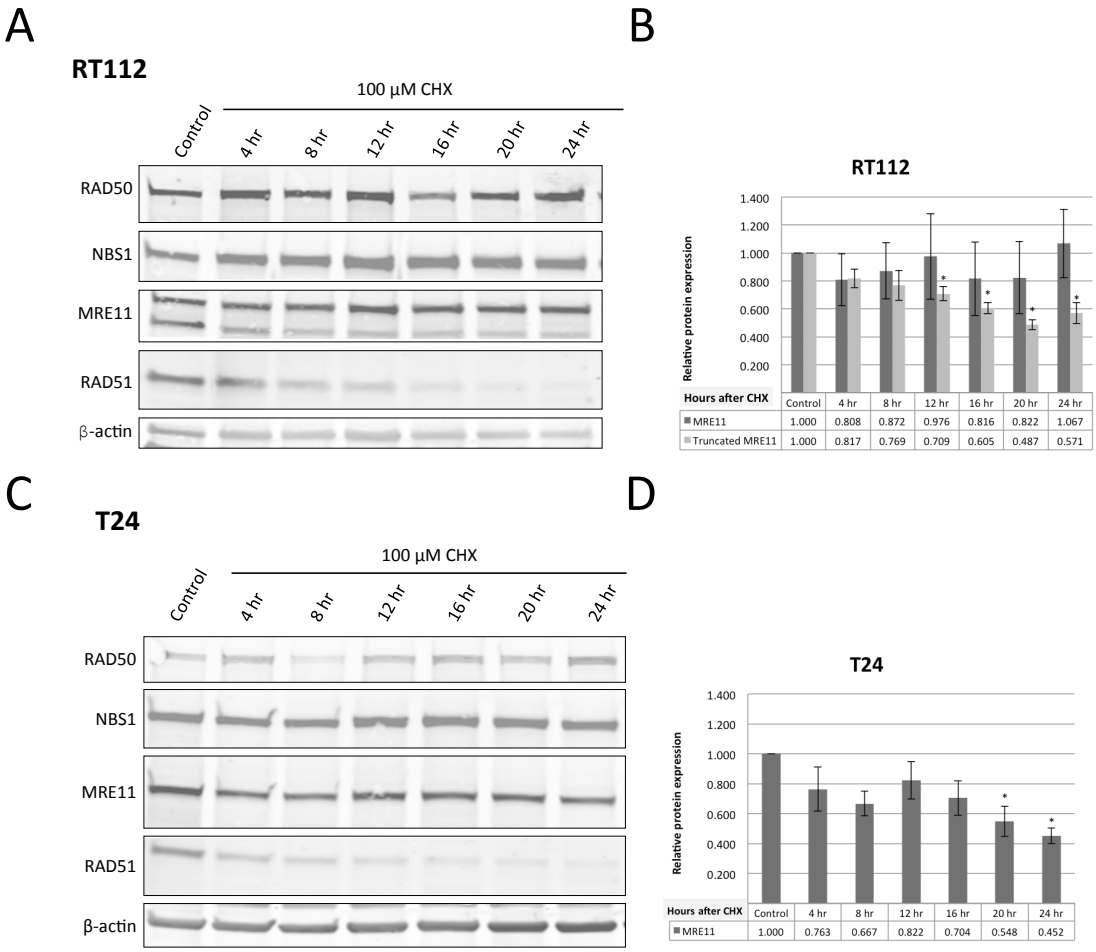

Figure 4.1 Stability of the MRN complex proteins.
Western blot analysis of the expression of the MRN complex proteins in A) RT112 and C) T24 bladder cancer cell lines after treatment with 100 µM cycloheximide (CHX) for times indicated. RAD51 was used as an indicator of CHX activity. β-actin was used as a loading control. Quantification of three independent experiments shown for B) RT112 and D) T24. The error bars represent mean and SEM of three independent experiments. Student's T-test over DMSO control; * p-value <0.05.

4.2.2 Proteasomal degradation of MRE11

Two bladder cancer cell lines with high basal levels of the truncation, RT112 and CALgem, were treated with the proteasome inhibitor MG-132 in order to assess whether the rapid turnover of the truncation was due to proteasomal degradation. Western blot analysis was then performed to evaluate MRE11 degradation over 6 hours post-treatment and to determine whether MRE11 was being cleaved by the proteasome, thereby generating a truncated variant (Figure 4.2).

In both cell lines, p21 expression increased at 4 to 6 hours post-treatment, confirming the ability of MG-132 to inhibit proteasomal degradation. In the RT112 cell line, WT MRE11 expression remained stable following 6 hours MG-132 treatment. In contrast, expression of the truncated MRE11 protein increased steadily from 1 to 6 hours post MG-132 treatment (Figure 4.2A, B).

In the CALgem cell line, WT MRE11 expression decreased slightly at 2 hours following MG-132 treatment. Expression continued to decrease over time and was 55% of the expression level in control treated cells 6 hours following MG-132 treatment. This coincided with increased expression of the truncated MRE11 protein, with expression increasing from 1 to 6 hours after MG-132 treatment.

Expression of NBS1 and RAD50 corresponded with the levels of WT MRE11 in RT112 and CALgem lines, remaining stable or exhibiting a slight decrease, respectively.

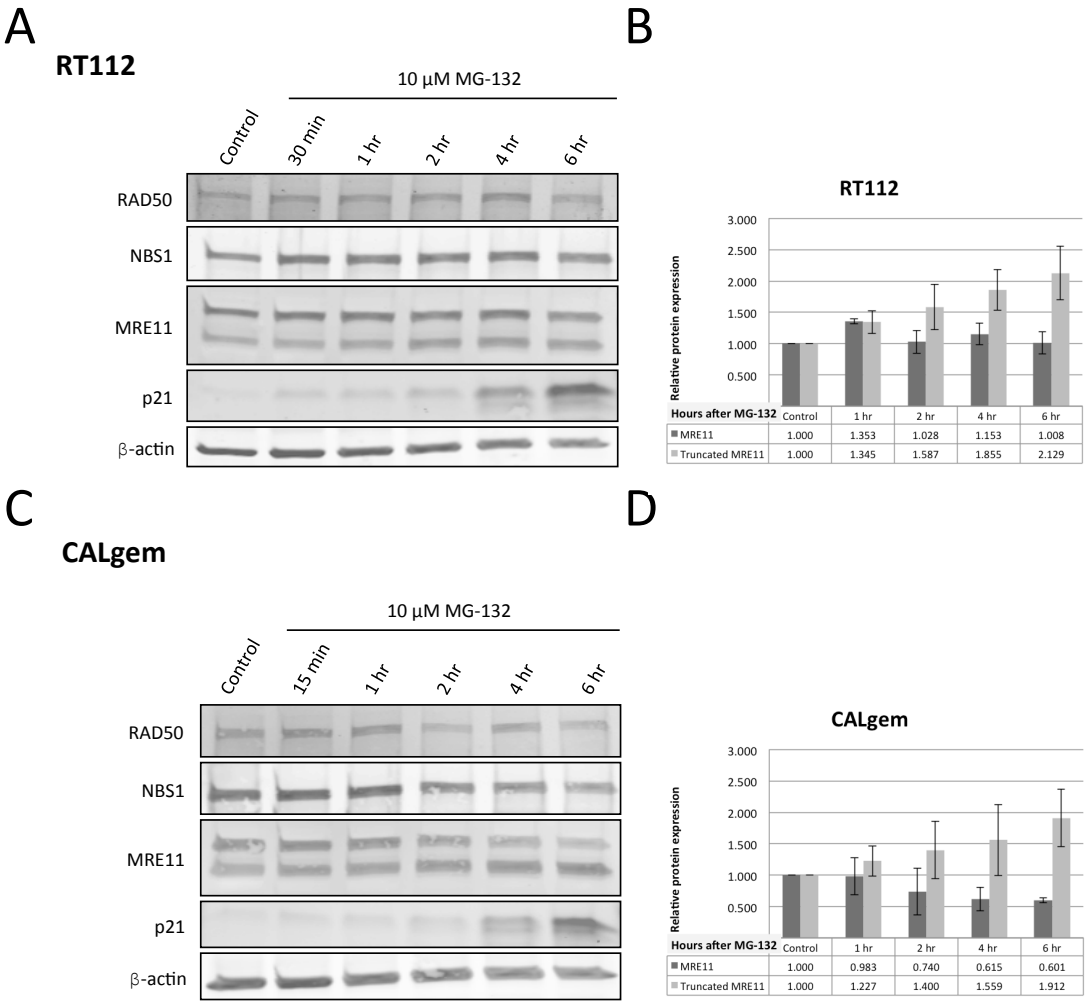

Figure 4.2 Proteasomal degradation of MRE11.

Time course of expression of the MRN complex proteins after treatment with 10 µM proteasome inhibitor MG-132 in the A) RT112 and C) CALgem bladder cancer cell lines for the times indicated. Expression of p21 was used as positive control of MG-132 proteasomal inhibition. β-actin was used as a loading control. Quantification of three independent experiments is shown for B) RT112 and D) CALgem cell lines. The error bars represent mean and SEM of three independent experiments.

4.2.3 The effect of inhibiting caspase function on the truncated MRE11 protein

Caspase activity was investigated in order to identify a possible cause of the MRE11 truncation. Z-VAD-FMK is a pan-caspase inhibitor that is capable of blocking caspase function by irreversibly binding to the catalytic site. The concentration required is cell type dependent.

Firstly, to establish the concentration of Z-VAD-FMK capable of blocking caspase function in the RT112 cell line, cells were treated with staurosporine for 6 hours to induce apoptosis and activate caspase function. Caspases were active after treatment with 2 μM staurosporine for 6 hours, as demonstrated by the appearance of a cleaved PARP fragment; PARP being a known target of caspase-3 (Tewari *et al*. 1995). The RT112 cell line was then pre-treated for 1 hour with increasing doses of Z-VAD-FMK ranging from 5–50 μM and subsequently treated with staurosporine for 6 hours. As seen by expression of cleaved PARP, pre-treatment with 5 μM Z-VAD was sufficient to partially block PARP cleavage. Higher doses of Z-VAD, i.e. 20 μM and 50 μM, completely abolished PARP cleavage after induction of apoptosis (Figure 4.3).

After establishing the Z-VAD-FMK concentration range suitable for caspase inhibition in the RT112 cell line, both RT112 and CALgem cell lines were treated with increasing doses of Z-VAD-FMK, ranging from 5–50 μM for 24 hours. Following treatment, expression of the MRN complex proteins was determined by western blot analysis (Figure 4.4).

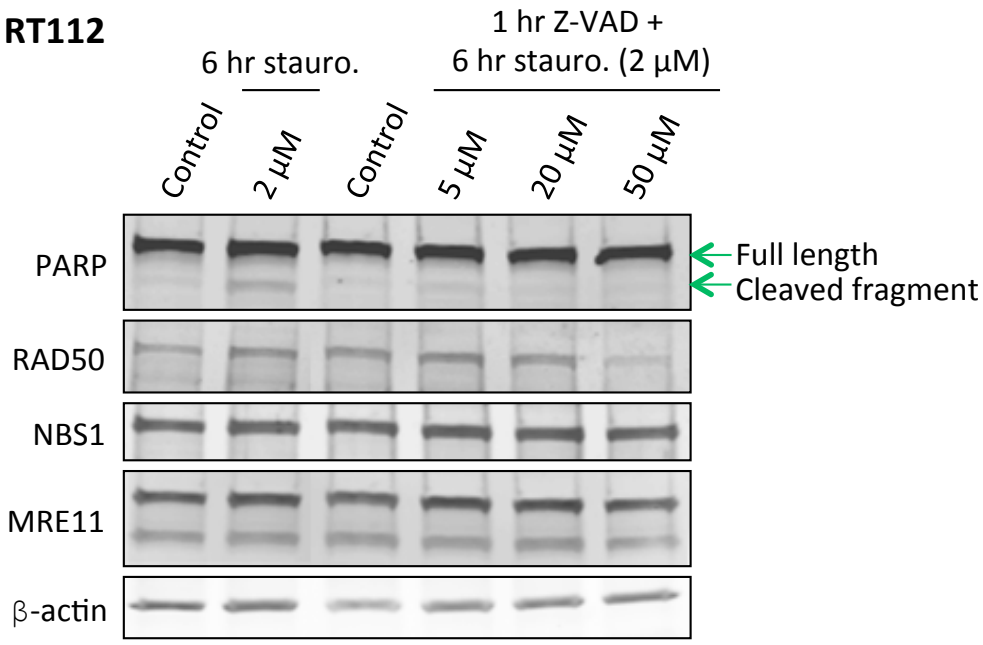

Figure 4.3 Establishing the concentration of Z-VAD capable of inhibiting caspase activity.

The expression of MRN complex proteins in the RT112 cell line after induction of apoptosis by staurosporine (2 µM), or following pre-incubation with caspase inhibitor Z-VAD-FMK at increasing doses indicated for 1 hour prior to 6 hour staurosporine treatment (2 µM). β-actin was used as a loading control.

In both cell lines, expression of WT MRE11 remained stable following Z-VAD-FMK treatment. In one replicate experiment in the RT112 cell line, MRE11 expression increased following Z-VAD-FMK treatment; however, this was not reproducible. Consistently, expression of the truncated MRE11 variant decreased in a dose-dependent manner. After treatment with 50 µM Z-VAD-FMK, expression of the truncated MRE11 protein fell significantly to approximately 45 and 30% of expression in control treated cells, in the RT112 and CALgem cell lines respectively (p-value= 0.026 and 0.046, respectively; Figure 4.4A-E). This indicated that caspase activity was responsible for causing the cleavage of WT MRE11 to generate the truncated MRE11 variant.

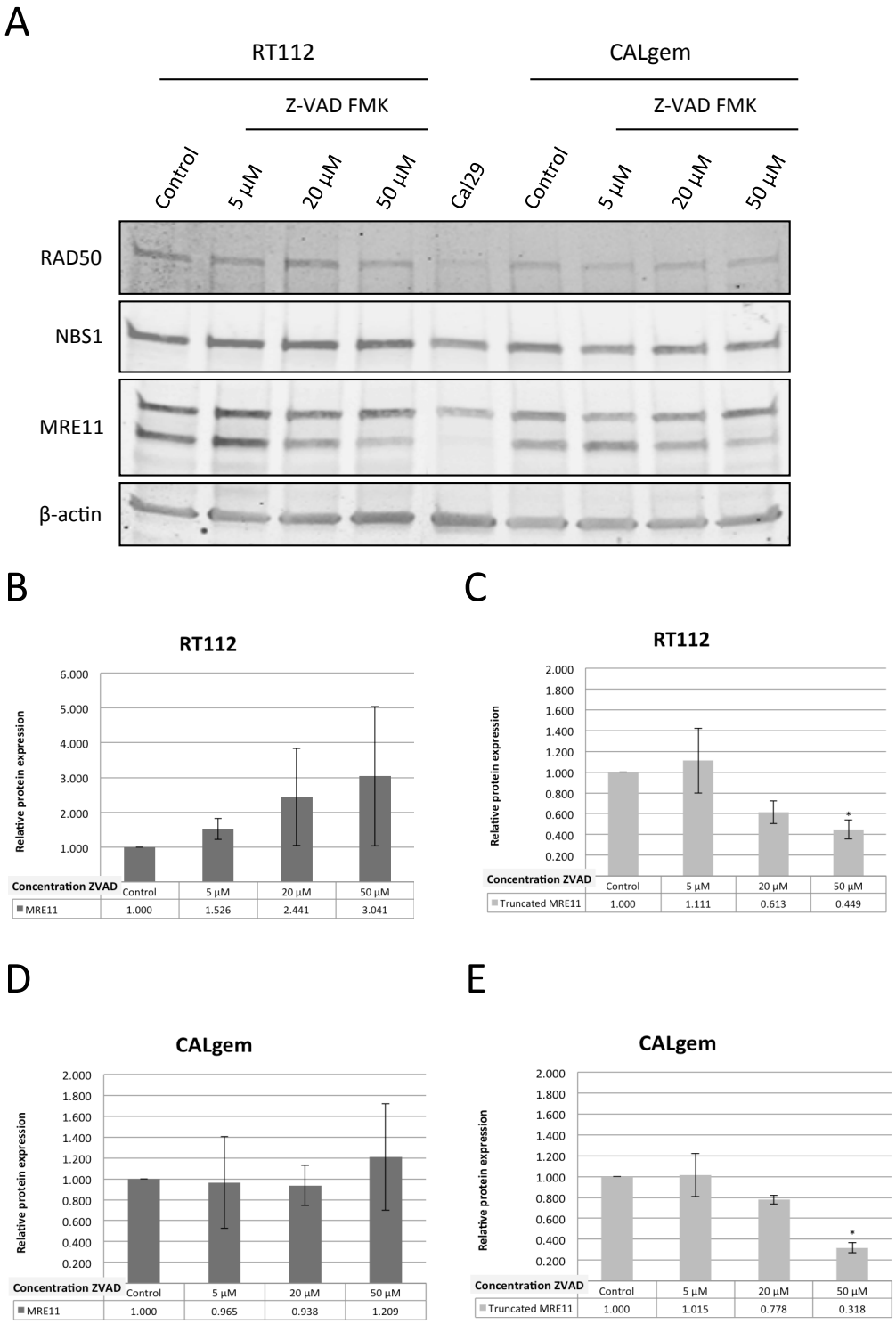

Figure 4.4 The effect of caspase inhibition on MRE11 expression.

A) Expression of the MRN complex proteins after 24 hr treatment with increasing indicated doses of Z-VAD FMK in the RT112 and CALgem bladder cancer cell lines. Quantification from three independent experiments of B) MRE11 and C) truncated MRE11 in RT112 and D) MRE11 and E) truncated MRE11 in CALgem cell lines. The error bars represent mean and SEM of three independent experiments. Student's T-test over DMSO control; * p-value <0.05.

4.2.4 Effect of induction of apoptosis on MRE11 expression

As caspase activity appeared to be responsible for MRE11 cleavage this was investigated further. Apoptosis is one of the main outcomes of caspase activity, therefore apoptosis was induced using staurosporine, after which expression of the MRN complex proteins was assessed by western blot analysis (Figure 4.5).

Two bladder cancer cell lines that express the truncated MRE11 protein under control conditions (RT112, CALgem) and two bladder cancer cell lines that do not (T24, CAL29) were treated with staurosporine at increasing doses for 6 hours. Incubation for longer times was not achievable due to cell death. The expression of a cleaved PARP fragment indicated that caspase function was being stimulated. In the two bladder cancer cell lines with the truncation present under control conditions, RT112 and CALgem, there was no increase in expression of the truncated MRE11 protein. Furthermore, there was no appearance of the truncated product after staurosporine treatment in the T24 and CAL29 cell lines (Figure 4.5). This suggests that stimulation of apoptotic caspase activity did not increase caspase cleavage of MRE11.

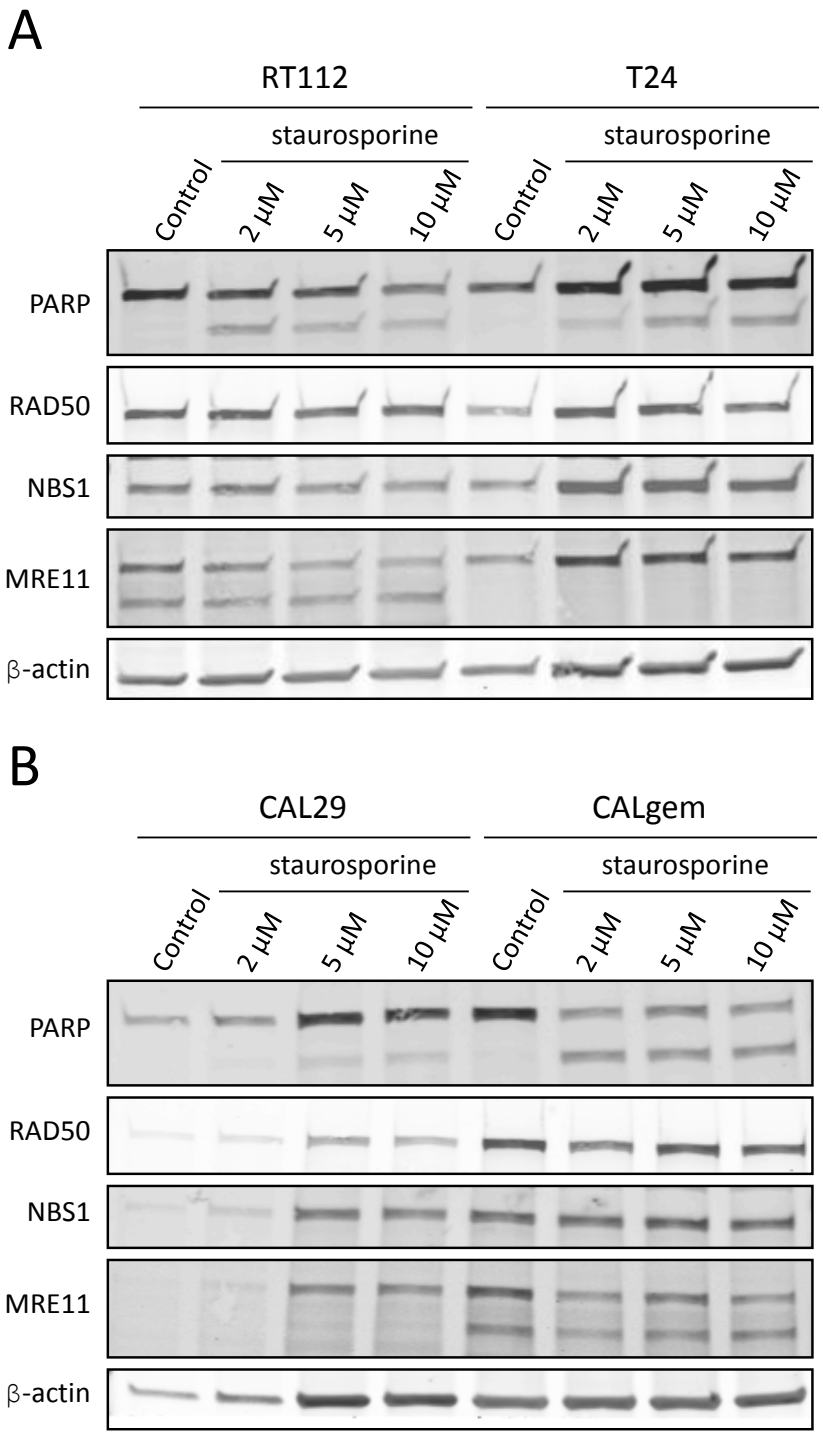

Figure 4.5 The effect of apoptotic stimulation on MRE11 expression.

A and B) Expression of the MRN complex proteins in the RT112, T24, CAL29 and CALgem bladder cancer cell lines after induction of apoptosis by 6 hr treatment with increasing doses of staurosporine. PARP cleavage indicated that apoptosis had been induced. β-actin was used as loading control. Representative blot for two independent experiments.

4.2.5 Effect of panobinostat on MRE11 expression

The HDAC inhibitor panobinostat has been shown to downregulate HR proteins in bladder cancer cell lines, including MRE11. It was hypothesised that this decrease in HR protein expression sensitises the bladder cancer cell lines to IR (Groselj *et al*. 2013). Therefore, the effect of panobinostat on the expression of truncated MRE11 was investigated. MRN expression was determined by western blot analysis in the T24 cell line treated with increasing doses of panobinostat for 24 hours (Figure 4.6).

Panobinostat acts to prevent the de-acetylation of proteins; therefore the increase in acetylation of histone H3 at lysine 14 (H3K14) following treatment with panobinostat was used as a positive control for drug action. As previously described, panobinostat reduced the expression of WT MRE11. Interestingly, although WT MRE11 expression was decreased, expression of the truncated MRE11 protein increased in the T24 cell line, in which the truncated MRE11 protein was barely detectable under control conditions. This occured in a dose-dependent manner after 24-hour incubation with panobinostat (Figure 4.6).

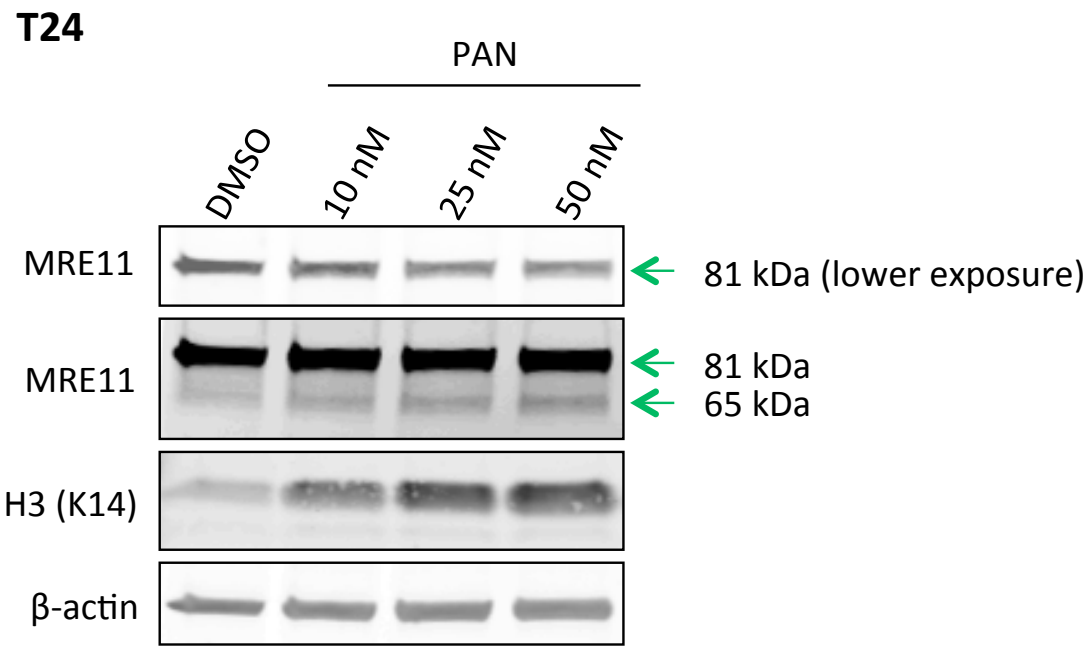

Figure 4.6 The effect of panobinostat on MRE11 expression.
Expression of MRE11 after 24 hour treatment with increasing doses of panobinostat (PAN) in the T24 cell line. Acetylation of H3 at the 14th lysine residue was used as positive control for panobinostat treatment. β-actin was used as a loading control.

4.2.6 Effect of panobinostat on MRE11 and caspase activity

To examine the effect of panobinostat on MRE11 further, the RT112 and T24 cell lines were treated with 50 nM panobinostat for 24 and 48 hours, after which the expression of HR proteins was determined by western blot analysis (Figure 4.7).

In both cell lines, the expression of WT MRE11 decreased following treatment with panobinostat. This occurred to a greater extent after 24 hours in the RT112 cell line, whereas in the T24 cell line there was a slight decrease at 24 hour but a more pronounced decrease following a 48 hour treatment. Corresponding to the decrease in WT MRE11, in both cell lines the detection of the truncated MRE11 protein increased after panobinostat treatment. Similar to the expression of WT MRE11, this occurred to a greater extent in the RT112 cell line after 24 hours, whereas in the T24 cell line expression of the truncated MRE11 protein had increased after 24 hours but expression was greater after 48 hours of treatment with panobinostat. Treatment with 50 µM Z-VAD-FMK for 1 hour prior to panobinostat treatment, with continuous treatment for 48 hours, abolished the increased detection of the truncated MRE11 protein. Furthermore, co-treatment with Z-VAD-FMK also overcame the downregulation of WT MRE11 and returned expression to that seen in control treated cells (Figure 4.7).

As a measure of panobinostat activity, the acetylation of H3 at lysine 18 was determined. Increased acetylation occurred after treatment with panobinostat for 24 and 48 hours in the T24 and RT112 cell lines, demonstrating that panobinostat was inhibiting the deacetylation of proteins. The acetylation of H3 (K18) was not inhibited with after co-treatment with Z-VAD-FMK in either cell line.

Treatment with Z-VAD-FMK decreased expression of truncated MRE11. Therefore, in order to investigate caspase activity after treatment with panobinostat, expression of PARP was examined. In the RT112 cell line, although there was no detectable cleaved PARP fragment, a decrease in full length PARP was observed following 48 hours panobinostat treatment, suggesting that panobinostat was activating caspase function. As hypothesised, expression of full length PARP returned to control levels after co-treatment with Z-VAD-FMK and panobinostat, demonstrating that Z-VAD-FMK was capable of inhibiting the caspase function which was activated by panobinostat. In the T24 cell line, a cleaved PARP fragment was observed after 24 hours treatment with panobinostat. The cleaved PARP fragment was no longer detected after 48 hours treatment. However, expression of full length PARP was decreased at this time point. Co-treatment of the T24 cell line with panobinostat and Z-VAD-FMK (48 hours), led to more full length PARP being detected compared with panobinostat treatment alone (48 hours). However, protein levels did not reach that seen in the control treated cells. This suggests that caspase activity was only partially inhibited by Z-VAD-FMK treatment in this cell line.

After treatment with panobinostat, expression of HR protein RAD51 was decreased in both cell lines; this reduction was not inhibited by co-treatment with Z-VAD-FMK.

To examine the stability of the MRN complex, expression of NBS1 and RAD50 was determined. In both cell lines, the expression of NBS1 and RAD50 was decreased after panobinostat treatment. As seen with WT MRE11 expression, co-treatment with Z-VAD-FMK appeared to partially rescue the decrease in NBS1 expression.

However, NBS1 expression did not recover to the level seen in control treated cells. The expression of RAD50 was not rescued by co-treatment with Z-VAD-FMK.

In the T24 cell line CtIP expression decreased after treatment with panobinostat, and no rescue was seen when co-treating with panobinostat and Z-VAD-FMK. CtIP expression was not detectable in the RT112 cell line under any of the conditions used.

This result suggests that panobinostat treatment influences the expression of the MRN complex proteins, as well as other HR proteins, such as CtIP and RAD51, via different mechanisms.

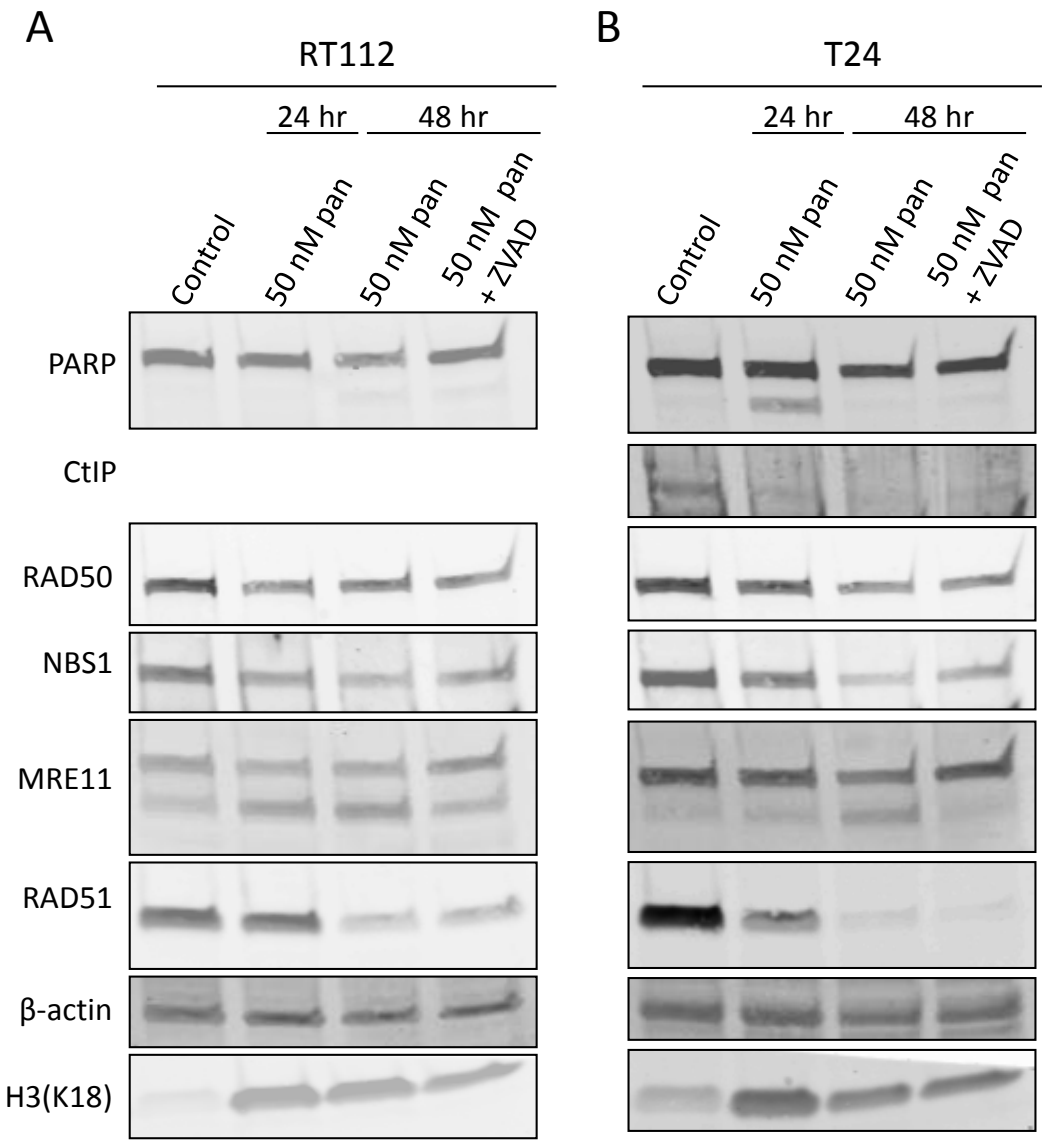

Figure 4.7 The effect of panobinostat on homologous repair (HR) protein expression.

Expression of HR related proteins after treatment with 50 nM panobinostat in the A) RT112 and B) T24 bladder cancer cell lines for 24 and 48 hours. Where indicated the RT112 and T24 cells were pre-treated with 50 µM Z-VAD-FMK for 1 hour, prior to 48 hr incubation with panobinostat. Acetylation of H3 at lysine 18 was used as positive control for panobinostat treatment. β-actin was used as a loading control. This is a representative blot from three independent experiments.

4.2.7 Modulation of caspase transcription by panobinostat

MRE11 cleavage is caspase dependent and since HDAC inhibitors are known to modulate transcription of many genes, transcription of caspase genes was therefore measured. Transcription of 10 *CASP* genes in the RT112 cell line under control conditions (DMSO) or after treatment with 50 nM panobinostat (24 hours, a concentration that induces the protein expression of truncated MRE11, Figure 4.7) was measured by quantitative polymerase chain reaction (qPCR). qPCR primers for *CASP5* were not optimal due to multiple peaks on the melt curve (appendix C). After treatment with panobinostat, none of the *CASP* genes tested showed a statistically significant upregulation of gene transcription (Figure 4.8). Transcription of *CASP14* was potentially upregulated; however, further investigation is required due to experimental variation (p-value= 0.14). Intriguingly, the opposite effect was observed in that transcription of *CASP6, CASP8* and *CASP10* were significantly downregulated after treatment with panobinostat (p-values <0.01). Downregulation of *CASP1*, *CASP2* and *CASP4* were also close to significance (p-values= 0.067, 0.097 and 0.08, respectively). This potentially rules out these caspases as causing truncation of MRE11. However, as caspases are also regulated by post-translational modifications, expression of active pro-caspase fragments needs to be addressed at the protein level.

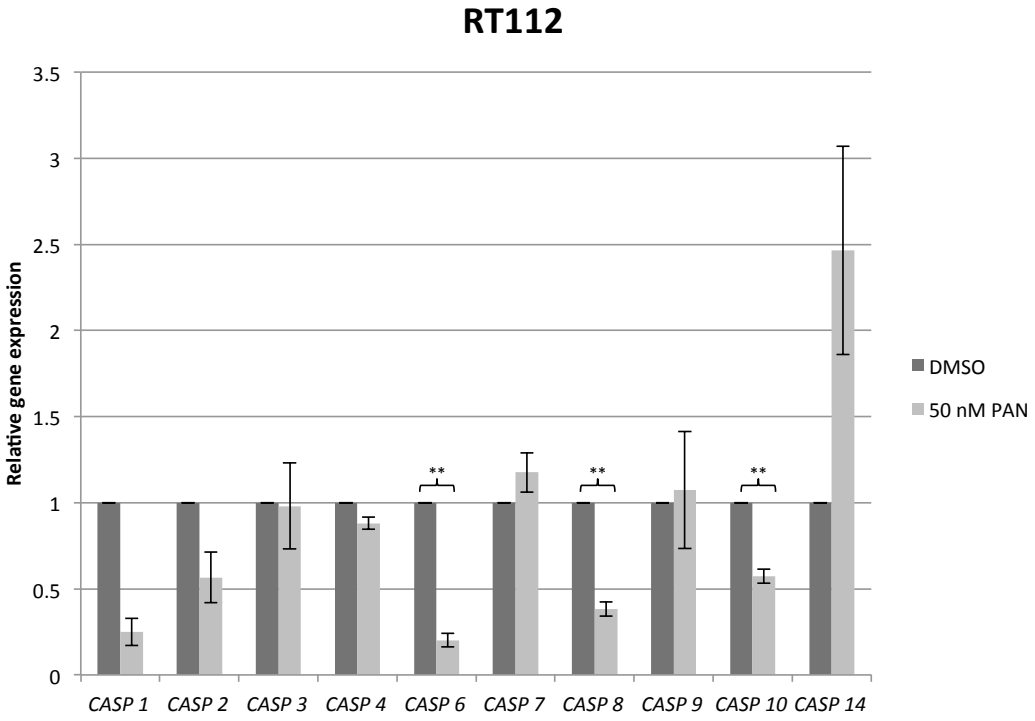

Figure 4.8 Transcription of *CASP* genes after panobinostat treatment in RT112 bladder cancer cell line.

mRNA expression levels were measured by qPCR for *CASP1, 2, 3, 4, 6, 7, 8, 9, 10 and 14* in RT112 cells. The expression levels for each condition were normalised against those of ATP and SHADA and the expression levels compared to the DMSO treated sample. The error bars represent mean and SEM of three independent experiments. Student's T test over DMSO control; * p-value <0.05, ** p-value <0.01.

4.2.8 Site-directed mutagenesis of caspase cleavage motif in MRE11

The results reported earlier indicate that the cause of the MRE11 cleavage was potentially due to caspase activity. Caspases have defined cleavage motifs and each individual caspase has a preference for certain sequences (Figure 4.9A). A potential caspase cleavage motif was identified in the C-terminus region of MRE11, close to the expected region of the truncation (determined by molecular weight of the product). The caspase motif sequence identified in MRE11 was DSDDS (Figure 4.9B). The first and fourth aspartic acid amino acids in the sequence are essential for caspase recognition. These aspartic acids were mutated using site-directed mutagenesis (SDM) into alanine residues to disrupt caspase recognition and cleavage. Sanger sequencing confirmed that mutation of the caspase cleavage site had occurred (Figure 4.9C).

In order to investigate whether the caspase mutant could still be cleaved, the experimental design would be to exploit panobinostat-dependent upregulation by overexpression of the mutant plasmid and subsequent treatment with panobinostat. By using the MRE11 plasmids described in Chapter 3.11, the caspase mutant protein would express HA and this would allow a distinction between the endogenous and mutant MRE11 proteins. Therefore, if HA was not detected at the level of truncated protein, it would indicate that that mutant protein had not undergone cleavage and that this was indeed the cleavage site of MRE11. Optimisation of HA detection was not achieved and, consequently, it could not be determined if transfected OR endogenous MRE11 was responsible for the truncated MRE11 product after panobinostat treatment. Therefore, it remains inconclusive whether this is the caspase cleavage site of MRE11.

A

Caspase	P_0	P_1	P_2	P_3	P_4 ↓	P_5
1, 4, 5, 14		W/Y	E	X	D	ϕ
8, 9, 10		I/L	E	X	D	ϕ
3, 7		D	E	X	D	ϕ
6		V	E	X	D	ϕ
2	V/L	D	E	X	D	ϕ

B

```
  1 MSTADALDDE NTFKILVATD IHLGFMEKDA VRGNDTFVTL DEILRLAQEN
 51 EVDFILLGGD LFHENKPSRK TLHTCLELLR KYCMGDRPVQ FEILSDQSVN
101 FGFSKFPWVN YQDGNLNISI PVFSIHGNHD DPTGADALCA LDILSCAGFV
151 NHFGRSMSVE KIDISPVLLQ KGSTKIALYG LGSIPDERLY RMFVNKKVTM
201 LRPKEDENSW FNLFVIHQNR SKHGSTNFIP EQFLDDFIDL VIWGHEHECK
251 IAPTKNEQQL FYISQPGSSV VTSLSPGEAV KKHVGLLRIK GRKMNMHKIP
301 LHTVRQFFME DIVLANHPDI FNPDNPKVTQ AIQSPCLEKI EEMLENAERE
351 RLGNSHQPEK PLVRLRVDYS GGFEPFSVLR FSQKFVDRVA NPKDIIHFFR
401 HREQKEKTGE EINFGKLITK PSEGTTLRVE DLVKQYFQTA EKNVQLSLLT
451 ERGMGEAVQE FVDKEEKDAI EELVKYQLEK TQRFLKERHI DALEDKIDEE
501 VRRFRETRQK NTNEEDDEVR EAMTRARALR SQSEESASAF SADDLMSIDL
551 AEQMANDSDD SLSAATNKGR GRGRGRRGGR GQNSASRGGS QRGRADTGLE
601 TSTRSRNSKT AVSASRNMSI IDAFKSTRQQ PSRNVTTKNY SEVIEVDESD
651 VEEDIFPTTS KTDQRWSSTS SSKIMSQSQV SKGVDFESSE DDDDDPFMNT
701 SSLRRNRR
```

C

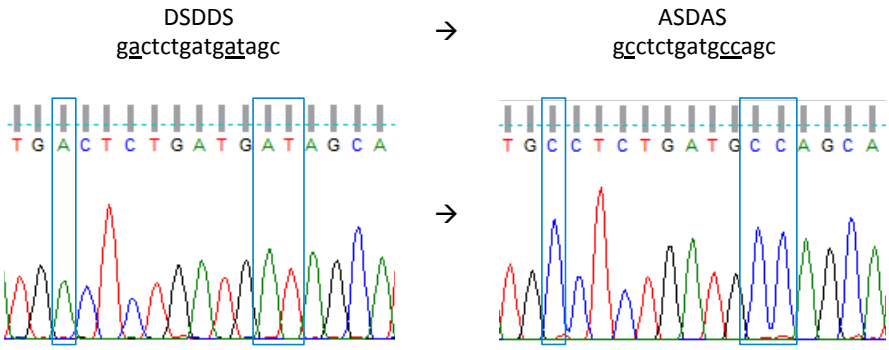

Figure 4.9 Site-directed mutagenesis of a potential caspase cleavage motif in MRE11.

A) Preferred cleavage motifs of caspases. All caspases show selectivity for Asp (D) in the P_4 position and a preference for Glu (E) in P_2. At P_5 there is a preference for uncharged residues such as; Gly (G), Ala (A), Thr (T), Ser (S), and Asn (N) (denoted by the symbol Φ). Different residues at the P_1 position distinguish between the caspase motifs and generate substrate specificity. Caspase-2 has an additional interaction at P_0 leading to enhanced catalytic activity. Blue arrow indicates the cleavage position. Adapted from Poreba *et al*. (2013) B) Peptide coverage of truncated MRE11. Blue box highlights the potential caspase cleavage motif with blue arrow indicating the site of cleavage. C) Sequencing traces demonstrating three nucleotides mutated within the caspase cleavage motif. Mutated nucleotides highlighted by blue boxes. Amino acid sequence DSDDS is mutated to ASDAS.

4.3 Discussion

4.3.1 MRE11 stability and degradation

The results of the cycloheximide chase experiment showed that the variant MRE11 protein was turned over more rapidly than the WT protein in the RT112 bladder cancer cell line. As WT MRE11 was more stable in this cell line compared with the T24 cell line, the decrease in truncated protein in RT112 might signify a decrease in overall protein levels. As treatment duration was limited due to cell death, it is possible that although overall MRE11 levels were decreasing, no effect was seen on WT MRE11.

Further experiments showed that the proteasomal pathway was degrading the truncated MRE11 protein, deduced by the accumulation of the protein following MG-132 treatment. This experiment also showed that WT MRE11 remained stable in the RT112 cell line and, in fact, decreased in CALgem cell line following MG-132 treatment. This suggests that full length MRE11 was not being truncated by the proteasome and therefore the truncated protein was not a step in the MRE11 degradation process. Further experiments with the lysosomal inhibitor chloroquine could be performed to investigate whether the lysosomal pathway is involved in the degradation of MRE11.

Although not achieved in this thesis, co-treatment with CHX and MG-132 would be expected to block protein synthesis and degradation but not the conversion of WT MRE11 into the truncation. This could provide further evidence that WT MRE11 was being converted into the truncated form. It is noteworthy that the turnover of truncated MRE11 was more rapid that WT. This could suggest that this form was not tolerated by cells or that it was more dispensable than WT

MRE11. It is also possible that this form is removed faster than WT due to a damaging impact on normal MRE11 function. This degradation of MRE11 has not previously been described; however, a precedent has been set in other diseases, such as neurodegeneration whereby disease-associated mutant proteins are more rapidly degraded (Araki *et al*. 2014).

4.3.2 MRE11 caspase and apoptotic response

After treating the RT112 and CALgem cell lines with the pan-caspase inhibitor Z-VAD-FMK, it became apparent that caspase activity was responsible for cleaving WT MRE11 into the C-terminus truncated form. Caspases are involved in cell death mediated by apoptosis, necroptosis and autophagy (Shalini *et al*. 2015). However, caspase function is not limited to cell death. Non-apoptotic roles of caspases include inflammation, proliferation, differentiation, neural development and aging (Shalini *et al*. 2015). Due to the role of caspases in the apoptotic response, it would be expected that inducing apoptosis using staurosporine would increase caspase activity and increase the amount of truncated MRE11 protein. This, however, was not the case. After staurosporine treatment there was no increase in the truncated form of MRE11 in a panel of four bladder cancer cell lines despite an increase in cleaved PARP fragments indicating caspase activation.

Previous studies have shown that tumour cell lines and cancer tissues have high basal levels of caspase-3 and caspase-8 activities compared with normal cell lines. This high level of activity occurs in the absence of apoptotic stimuli and does not correspond to increased cleaved PARP fragments (Yang *et al*. 2003). This is

perhaps due to high levels of IAPs also being present in tumour cells. The presence of these proteins could prevent the apoptotic response through interaction with caspases and blocking of the apoptotic pathway. This could also explain why active caspases are able to cause MRE11 to become truncated, yet the cells are not fated for apoptosis. In bladder cancer, high levels of survivin detected by immunohistochemistry have been demonstrated to correlate with tumour recurrences (Wang *et al*. 2014). There is also a correlation between survivin expression and poor clinical outcome and aggressive tumour phenotype in a number of malignancies, such as breast cancer (Tanaka *et al*. 2000), colorectal carcinoma (Williams *et al*. 2003), neuroblastoma (Kappler *et al*. 2003) and bladder cancer (Weikert *et al*. 2005).

It has been hypothesised that the apoptotic cascade is activated in malignant transformation after genetic and molecular alterations. However, the upregulation of IAPs in cancer cells inhibits apoptotic activity of caspases and blocks apoptosis leading to cancer cell survival (Yang *et al*. 2003). It is therefore possible for the high caspase activity of tumour cells to be responsible for cleaving MRE11 in a non-apoptotic setting. Another possibility might be that due to the limited exposure to staurosporine treatment (due to toxicity), the duration was sufficient to stimulate caspases to cleave PARP but insufficient for the caspases to cleave MRE11.

A limitation is that Z-VAD-FMK is a pan caspase inhibitor and by testing more specific caspase inhibitors a more conclusive answer may be achieved as to which caspase might be responsible for the cleavage of MRE11. This would also perhaps give an insight into the mechanism as different caspases have different roles.

From the lack of induction of truncated MRE11 expression after staurosporine treatment, it would be reasonable to focus on non-apoptotic caspase function. However, this needs to be studied further and the extra studies described earlier could determine the exact relationship between caspases, MRE11 and the truncated variant.

4.3.3 The effect of panobinostat on the MRN complex

Panobinostat is an HDAC inhibitor which is able to radiosensitise bladder cancer cell lines through down regulation of HR proteins (Groselj *et al*. 2013). In bladder cancer cell lines, this includes WT MRE11, although this differs from acute myeloid leukaemia (AML) in which MRE11 is not found to be downregulated after panobinostat treatment (Xie *et al*. 2013), suggesting that this response could be specific to bladder cancer. It was of interest to see that in two bladder cancer cell lines, RT112 and T24, expression of WT MRE11 was decreased but the truncated MRE11 variant increased after panobinostat treatment. This was counteracted by co-treatment with Z-VAD-FMK, suggesting that caspase activity was increased in response to panobinostat treatment, leading to the truncation of WT MRE11. The activation of caspases after panobinostat treatment was determined through reduced expression of full length PARP and the expression of cleaved PARP fragments and this was also abrogated when cells had undergone co-treatment with Z-VAD-FMK.

The reduced MRE11 expression after panobinostat treatment in the RT112 cell line has been shown to be post-translational, as mRNA transcription is not downregulated (Blaz Groselj, personal communication). Furthermore, the

expression of MRE11 in other bladder cancer cell lines has also been shown to be regulated at the protein level, as mRNA levels do not correlate with protein expression (Martin *et al*. 2014). However, this differs in the T24 cell line, with MRE11 mRNA levels decreasing after panobinostat treatment (Judith Nicholson, personal communication). It is therefore interesting that an increase in the MRE11 truncated protein was still detected despite reduced transcription, further providing evidence that the truncated variant is not due to an alternative transcript.

As previously described, RAD51 expression is reduced in both bladder and AML cell lines after panobinostat treatment (Groselj *et al*. 2013; Xie *et al*. 2013). Previous studies show this to be at the transcriptional level, suggesting a possible explanation why co-treatment with Z-VAD-FMK did not inhibit the decrease in expression of RAD51 in the current work. Overall, this demonstrates the broad range of panobinostat targets at both transcriptional and post-transcriptional levels, making it necessary to determine a more specific mechanism behind the downregulation of WT MRE11 and the increase in the truncated variant.

Acetylation marker H3 (K18) increased following panobinostat treatment; this was not inhibited by co-treatment with Z-VAD-FMK, despite WT MRE11 expression being restored. This is an important finding for future clinical biomarker development of panobinostat. Currently, acetylated lysine residues in the chromatin of the tumour biopsy (Ree *et al*. 2010), or from leucocytes collected from patients' blood are considered as key indicators of biological activity of HDAC inhibitors (Rigby *et al*. 2012). However, the acetylation of lysine residues on the chromatin, reported in this thesis, did not correspond to

expression of DDR proteins.

It is also intriguing that CtIP expression in the RT112 cell line was consistently low, or absent. It has been proposed that the C-terminus of MRE11 is required for maintaining the expression of CtIP (Buis *et al*. 2012) and so whether the presence of truncated MRE11 in the RT112 cell line is capable of influencing this, despite WT expression being present is an interesting hypothesis to examine further.

4.3.4 Caspase motif mutation

Further consideration was given to the possibility that caspase activity might be causing the cleavage of MRE11 due to the presence of a potential caspase cleavage motif (Poreba *et al*. 2013) within the anticipated truncation domain. The motif DDSDS was mutated to ASDAS using site-directed mutagenesis as the negative charge of the aspartic acid residue is needed for protein interaction. This was mutated to an alanine residue with no charge but a similar size, to disrupt protein interaction, yet leave the protein's confirmation unchanged. This has been shown to disrupt caspase cleavage in other proteins (Poreba *et al*. 2013). Due to time constraints, it remains inconclusive as to whether this is the site of caspase cleavage. However, optimisation of over-expression and HA-tagged protein detection can be achieved and an answer to this question can be fully addressed.

CHAPTER 5 MRE11 knockdown and functional impact of the MRE11 variant on DNA repair

5.1 Introduction

The MRN complex plays a key role in the multiple steps involved in DNA DSB detection, signalling and repair. The complex acts as a DNA damage sensor and recruiter to DSB sites, whereby the NBS1 protein recruits the ATM protein to the DSB sites. ATM then auto-phosphorylates at serine 1981 (Carson *et al*. 2003; Uziel *et al*. 2003; Falck *et al*. 2005; Bakkenist & Kastan 2003) and activated pATM goes on to phosphorylate multiple down-stream targets, including histone H2AX at the serine 139 position (known as γH2AX). The phosphorylation of γH2AX regulates DSB repair by recruitment of several repair factors, including additional MRN complex proteins, to the damage site. Upon repair of the damage, H2AX becomes dephosphorylated (Rupnik *et al*. 2010; Chowdhury *et al*. 2008).

The MRN complex has an important function in DSB end-stabilization and resection via the endo- and exonuclease activity of MRE11. The C-terminus of MRE11 facilitates the phosphorylation of CtIP, via CDK2 binding, which in turn enhances the nuclease activity of MRE11 (Sartori *et al*. 2007; Limbo *et al*. 2007; Buis *et al*. 2012). DNA end resection generates 3'-overhangs, which is a crucial step before the search for homologous sequence can be initiated (Moynahan & Jasin 2010). This step commits the cells to DSB repair using the HR pathway, as NHEJ is no longer feasible (Shibata *et al*. 2014). This process can also direct repair towards microhomology-mediated end-joining (MMEJ) if HR is abrogated (Mladenov *et al*. 2013). MMEJ is frequently used for repair by muscle-invasive

bladder tumours (Bentley *et al*. 2009).

Having established that the truncated MRE11 protein was present in the nucleus of cells, interacts with NBS1 and RAD50 and localises to IRIF, the next objective was to evaluate its effect on DNA repair. To achieve this aim, an MRE11 knockdown cell line, was generated to determine whether these cells displayed a defective repair phenotype and, if so, whether this could be rescued by expression of either WT or truncated MRE11 protein.

5.2 Results

5.2.1 Transient MRE11 knockdown

In order to deplete MRE11 in the RT112 cell line, a previously published siRNA oligonucleotide by Zhuang *et al*. was tested (Zhuang, 2009). The siRNA oligonucleotide sequence targets the 5'-untranslated region (5'UTR) of *MRE11* mRNA, a region not present in the MRE11 expression plasmids (Chapter 3, Figure 3.11). Such experimental design would therefore mean that these vectors would be resistant to MRE11 siRNA silencing in subsequent experiments. Forty-eight hours post-siRNA transfection, truncated and WT MRE11 expression were depleted by 40% and 60%, respectively, compared with cells transfected with a non-silencing control (NSC), as determined by western blot analysis (Figure 5.1). The MRE11 knockdown was still evident in cells 96 hours post-transfection, showing that the siRNA sequence used was effective at silencing both WT and truncated MRE11 expression.

A

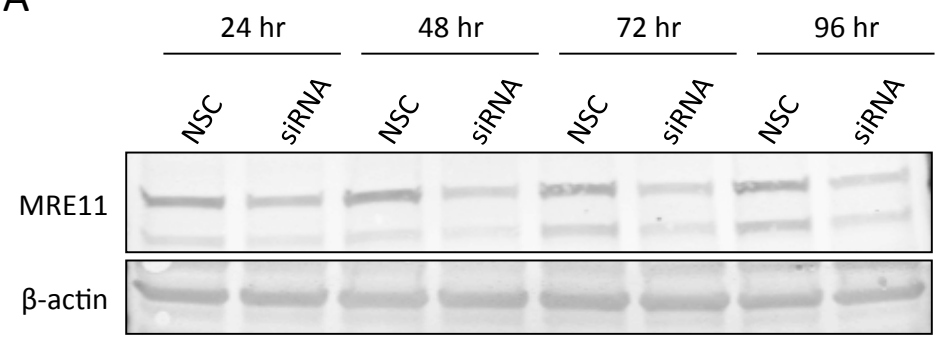

B

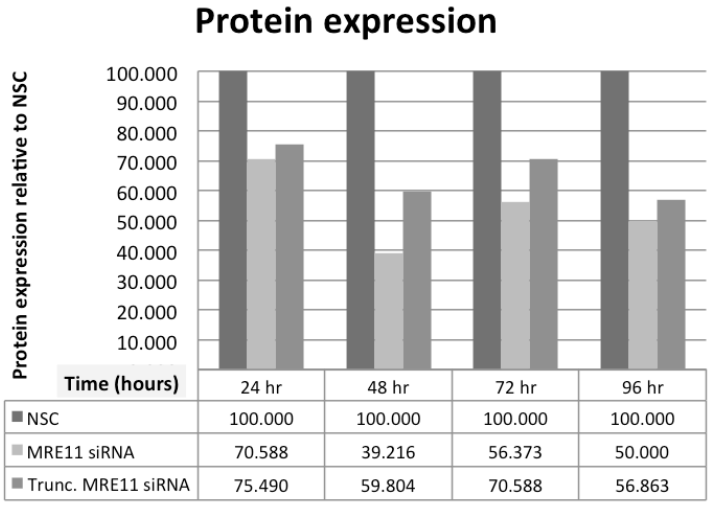

Time (hours)	24 hr	48 hr	72 hr	96 hr
NSC	100.000	100.000	100.000	100.000
MRE11 siRNA	70.588	39.216	56.373	50.000
Trunc. MRE11 siRNA	75.490	59.804	70.588	56.863

Figure 5.1 Transient knockdown of MRE11.

A) Western blot analysis of MRE11 expression in the RT112 cell line 24-96 hr post siRNA transfection. The non-silencing control (NSC) shows expression of MRE11 after transfection with a control siRNA. β-actin was used as loading control. B) Quantification of MRE11 expression. MRE11 WT or truncation expression was normalised to expression after treatment with the NSC.

5.2.2 Stable MRE11 knockdown

After optimisation of transient MRE11 knockdown and establishing the viability of these cells, a stable MRE11 knockdown cell line was generated. This was required in order to provide a useful resource for functional studies, such as clonogenic survival assays, in which homogeneous knockdown is required to generate optimal results.

Generation of stable MRE11 KD cells was achieved using the same siRNA sequence described in Figure 5.1 and as described in Materials and methods 2.15. Two complementary siRNA oligonucleotide templates were annealed to create a double stranded molecule. The oligonucleotides were designed containing a loop so that, once annealed, the resulting double-stranded molecule would form a hairpin structure. The hairpin was designed to have an enzyme restriction site at each end to allow for ligation into a p*Silencer* 2.1-U6 puro expression vector. After digestion of both the shMRE11 oligonucleotide and the p*Silencer* 2.1-U6 puro expression vector at these restriction sites, the two sequences were ligated. The ligated product was transformed into *E.coli* to replicate the plasmid. The plasmid DNA was then isolated from individual colonies using a Qiagen mini prep kit. Replicated plasmid DNA was screened from several colonies to confirm the insertion of the shMRE11 template. This was determined through restriction digest mapping at the sites of the ligation, and later by Sanger sequencing, to ensure the correct siRNA sequence was present (Appendix D).

A *pSilencer* vector with a puromycin selection cassette was used, so as not to hinder future experiments requiring the stable expression of the MRE11 expression plasmids (Chapter 3, Figure 3.11), as these contained a neomycin

selection cassette.

RT112 cells were seeded onto two 10 cm plates. One plate was transfected with the shMRE11 p*Silencer* plasmid and incubated for 24 hours to allow for expression of the plasmid. The second plate did not undergo transfection and served as a non-transfected control. For the selection of positively transfected cells, both plates were incubated with an established concentration of puromycin (1 μg/ml), resulting in rapid killing of non-transfected cells that were not expressing the shMRE11 vector. Once all of the non-transfected control cells were killed, it was assumed that only viable cells were expressing the shMRE11 plasmid. The cells were continuously incubated in selection medium until single transfected cells had formed colonies of approximately 50 cells. At this stage, individual clones were transferred into a 24-well plate and, once confluent, were subsequently transferred into larger culture dishes for both maintenance and protein lysate generation.

Knockdown (expression) of MRE11 after shMRE11 transfection was determined by western blot analysis when clones had reached 50–70% confluence. It was necessary to screen clones as soon as possible to reduce the possibility of them regaining the ability to express MRE11. Clones of interest, in particular those with the greatest MRE11 depletion, these were expanded and frozen stocks generated.

Figure 5.2A outlines an example of the individual screened clones. Several clones, namely 1C, 2A, 2C, 3A, 4A, had reduced expression of both WT and truncated MRE11 (Figure 5.2). Two clones (1A and 3B) had reduced, if not abolished, expression of the truncated MRE11 protein, whilst WT expression remained the

same as that in the control cells.

As seen in Figure 5.2A, expression of NBS1 and RAD50 were reduced in the MRE11 knockdown clones compared wtih the RT112 control. This highlights the dependency of MRN complex protein stability on MRE11 expression. Clones 1A and 3B show reduced expression of RAD50, despite WT MRE11 expression being comparable to the expression in control cells. This suggests that the truncated MRE11 protein added to overall MRE11 expression and could influence the expression of RAD50. NBS1 expression in these two clones was not influenced by expression of the truncated MRE11 protein and remained at the same level as in control cells. This suggests that the expression of NBS1 was less dependent on truncated MRE11 expression but was still influenced by a severe reduction in WT MRE11 expression (clones 1C and 4A but not 2A and 3A).

A

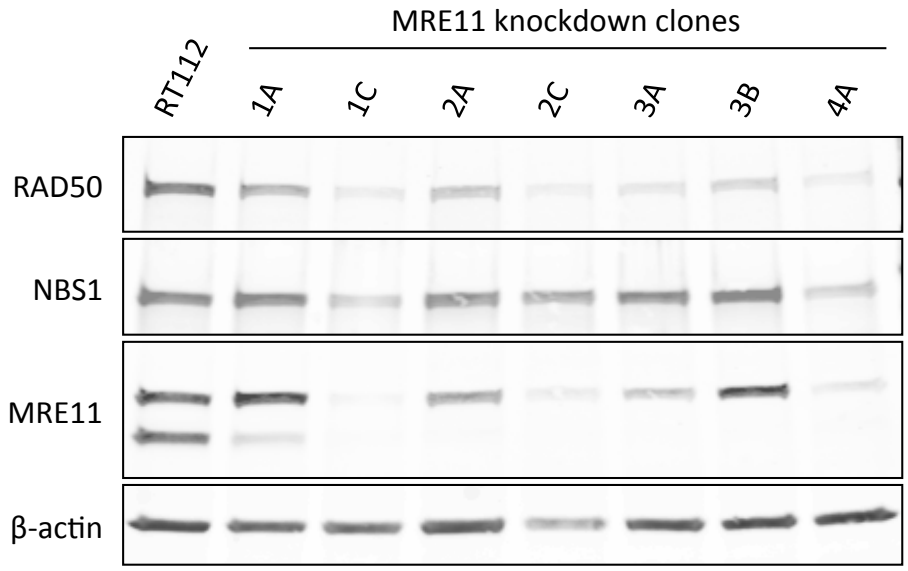

B

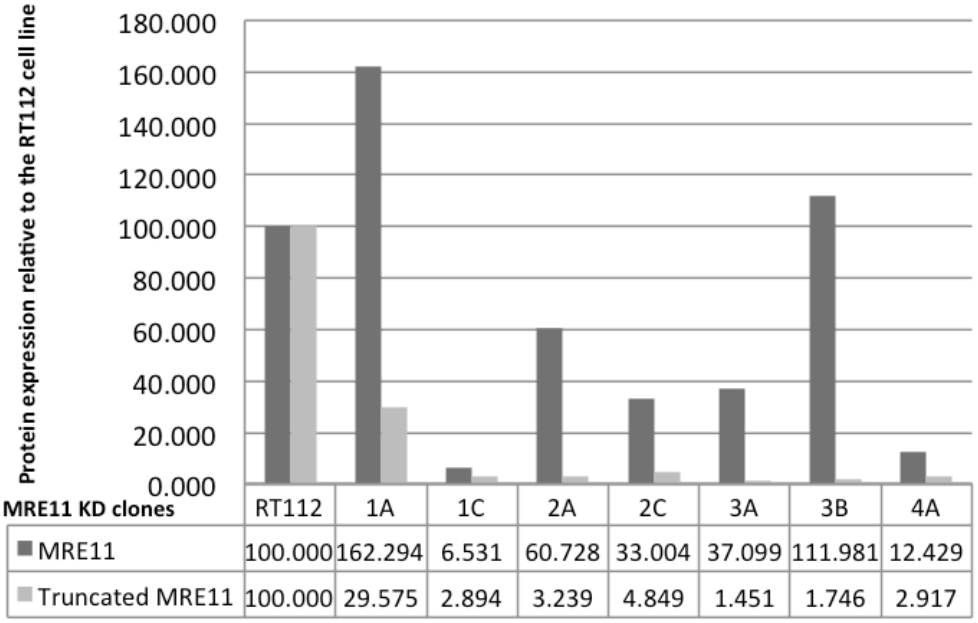

MRE11 KD clones	RT112	1A	1C	2A	2C	3A	3B	4A
MRE11	100.000	162.294	6.531	60.728	33.004	37.099	111.981	12.429
Truncated MRE11	100.000	29.575	2.894	3.239	4.849	1.451	1.746	2.917

Figure 5.2 Stable knockdown of MRE11.

A) Western blot analysis of expression of the MRN complex proteins in the MRE11 knockdown clones derived from the RT112 parental cell line. β-actin was used as a loading control. B) Quantification of MRE11 expression in knockdown clones, normalised to β-actin and further normalised to the RT112 cell line.

5.2.3 MRE11 knockdown radiosensitivity

Radiosensitivity of the MRE11 knockdown cell line compared with the parental RT112 cell line was determined by clonogenic survival assay. Cells were seeded at a low density (600 cells per 10 cm plate) to allow for the detection of individual cells capable of overcoming DNA damage caused by IR, as measured by colony formation. Cells were seeded in duplicate and exposed to IR, ranging from 2 Gy to 8 Gy. After a 2 week incubation for cell proliferation, the cells were fixed with methanol: acetic acid (3:1) and stained with Brilliant Blue R Concentrate (Materials and Methods 2.18). As a measure of proliferation, cells were counted that had undergone a minimum of five divisions and reached a colony size of at least 50 cells. Colonies below 50 cells were not counted, as, after exposure to IR, cells can replicate two to three times before the DNA damage becomes too great and they are no longer viable. Consequently, such colonies do not represent cells that have retained the ability to replicate (Franken *et al*. 2006). The MRE11 KD cell line was more sensitive to IR compared with the parental RT112 cell line, with a survival enhancement ratio at 10% kill (SER_{10}) of 1.33 (p-value= 0.006).

To confirm that this was due to MRE11 depletion and not expression of the p*Silencer* plasmid or incubation with puromycin, a scrambled control was also tested. This cell line had undergone transfection with the same p*Silencer* plasmid. However, the MRE11 sequence chosen was scrambled before ligation and therefore did not target MRE11. This cell line showed the same radiosensitivity as the parental RT112 cell line (SER_{10}= 1.04). The MRE11 knockdown cell line was more radiosensitive than the scrambled control, SER_{10}= 1.29 (p-value= 0.04). This

confirmed that the radiosensitivity was likely due to MRE11 depletion (Figure 5.3A).

Expression of the MRN complex proteins in the cell lines used for three replicate clonogenic survival assays was determined by western blot analysis (Figure 5.3B). The percentage knockdown of WT MRE11 in the clone used for the clonogenic experiments was on average 63%. However, expression of RAD50 and NBS1 was also depleted compared with the control cell lines. Therefore, MRE11 depletion cannot be considered exclusively responsible for the radiosensitisation in this cell line, but rather the destabilisation of the MRN complex proteins, which results from MRE11 depletion.

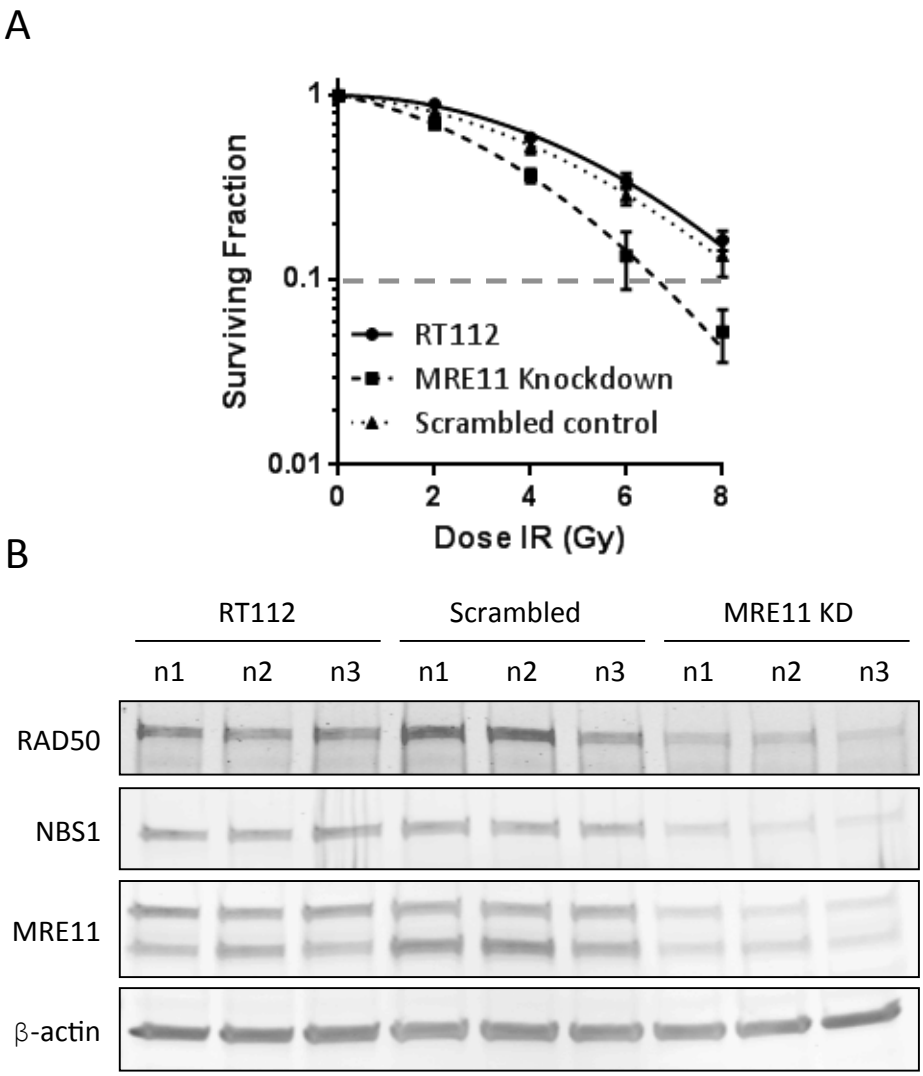

Figure 5.3 Sensitivity of the RT112-derived MRE11 knockdown cell line to ionising radiation.

A) Clonogenic survival curve of the RT112 cell line compared with the RT112 derived MRE11 knockdown cell line. A scrambled control cell line was used to confirm that increased sensitivity is due to MRE11 depletion. Error bars represent SEM of three replicate experiments. B) Western blot analysis for expression of MRN complex corresponding to expression in cells used for the clonogenic survival assays from three independent experiments. β-actin was used as a loading control.

5.2.4 Nuclease inhibitors of MRE11

The MRE11 knockdown cell line was more sensitive to IR. However, as MRE11 has multiple roles in the DSB response, a further explanation of the mechanism of sensitisation was sought. As the truncated MRE11 protein still encodes for the nuclease domain of MRE11, it was determined whether inhibiting the nuclease function of MRE11 was sufficient to result in radiosensitisation and also if this sensitised the cells to the same extent as depletion of MRE11. It had been hypothesised that inhibiting the endo- and exonuclease function of MRE11 would result in different repair pathway choice, determining cell fate after IR (Shibata *et al*. 2014) and so this was investigated in more detail.

Three different MRE11 inhibitors were used in combination with IR in a clonogenic survival assay in order to determine the effect of MRE11 nuclease inhibition on radiosensitivity. Mirin inhibits the exonuclease function of MRE11, as does the inhibitor PFM39 (Dupré *et al*. 2008). A specific endonuclease inhibitor, PFM01, was also examined (Shibata *et al*. 2014). The half-maximal inhibitory concentration (IC_{50}) of each inhibitor was determined (appendix E) and subsequently the sensitivity to IR in combination with the IC_{50} dose for each inhibitor. Incubation with neither mirin nor PFM01 caused an increase in sensitivity post exposure to 2–10 Gy IR (Figure 5.4B and C). The exonuclease inhibitor PFM39 caused an increase in radiosensitivity compared with the RT112 cell line treated with DMSO (Figure 5.4A) (SER_{10}= 1.21); however, this was not statistically significant (Two-way ANOVA over DMSO control p-value= 0.77). This suggests that the radiosensitivity when MRE11 was depleted was due to more than a lack of nuclease function provided by MRE11, and that depletion of the

protein was impacting on DNA repair via additional mechanisms. Therefore, although the truncated MRE11 protein has intact nuclease domains, the impact of the truncation on radiosensitivity was worthy of further investigation.

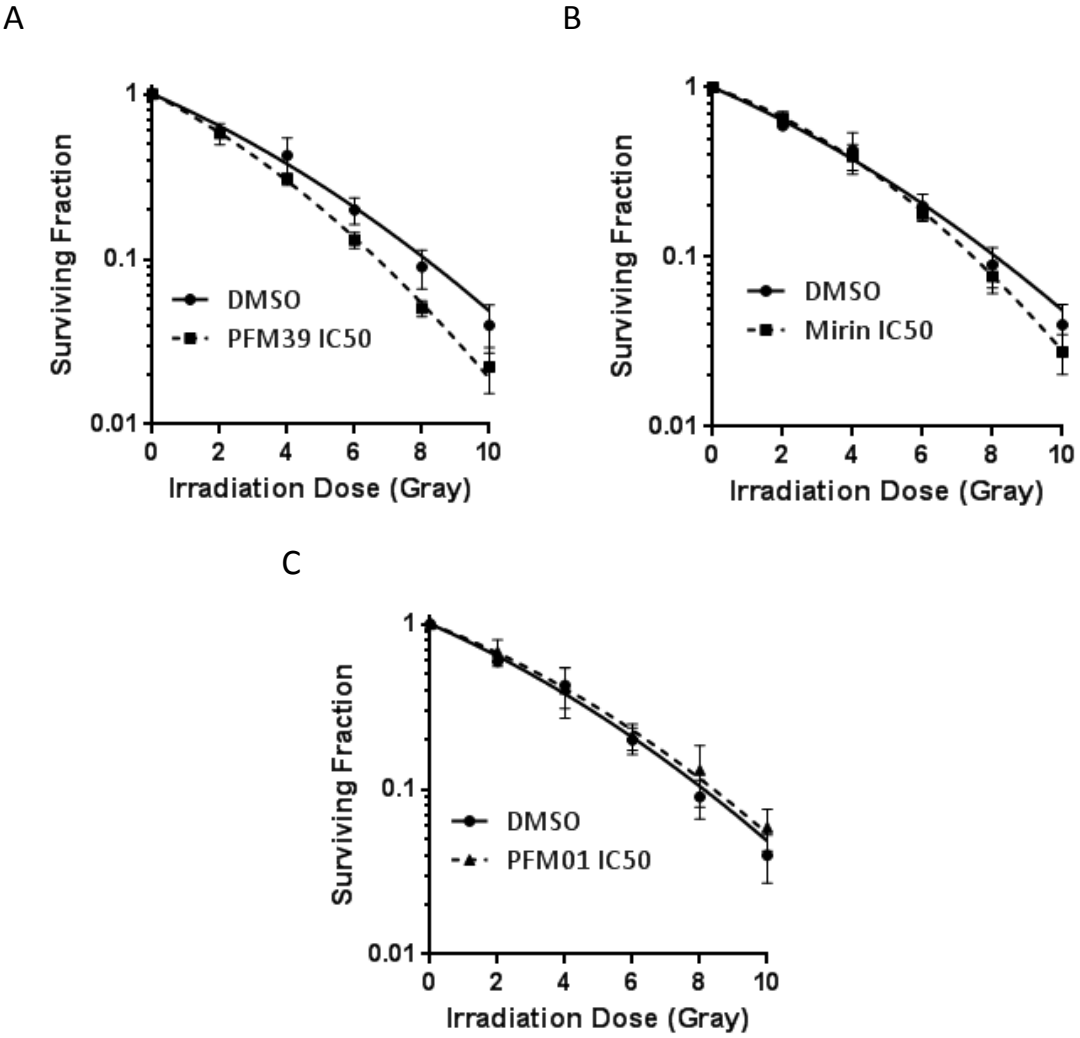

Figure 5.4 The effect of MRE11 nuclease inhibition on radiosensitivity.
Clonogenic survival curves of the RT112 cell line, DMSO treated or in combination with MRE11 nuclease inhibitors: A) PFM39, B) Mirin and C) PFM01 (Shibata *et al*. 2014). Error bars represent mean and SEM of three independent experiments.

5.2.5 Reduced pATM recruitment in the RT112-derived MRE11 knockdown cell line

The downstream signalling pathway was investigated next as it had been established that the radiosensitivity following MRE11 knockdown was not due to lack of nuclease activity alone. ATM is phosphorylated at serine 1981 after recruitment to DNA damage sites by the MRN complex (Bakkenist & Kastan 2003). RT112 and MRE11 knockdown cells were exposed to 5 Gy IR, and after 2 hours incubation at 37^{o}C, the number of pATM (s1981) foci counted using immunofluorescence (Figure 5.5). A 2 hour time point following IR was chosen because in the RT112 cell line this was the minimum time for distinct nuclear pATM foci to form (Figure 5.5A). The MRE11 knockdown cell line had significantly reduced pATM foci formation following 5 Gy IR compared with the RT112 control (Figure 5.5D). Slightly over 50% of cells in the MRE11 knockdown cell line had 11–20 pATM foci (p-value= 0.039), whereas in the RT112 cell line, approximately 50% of cells had more than 20 pATM foci (p-value= 0.056). The pATM foci in at least 100 nuclei were counted in three independent experiments. This suggests that the MRE11 knockdown cell line was more sensitive to IR not only due to reduced nuclease function of MRE11 but also due to reduced downstream signalling, potentially leading to delayed repair.

The next objective was to re-express either WT or truncated MRE11 in the knockdown cell line to establish whether this could rescue the knockdown phenotype and to investigate whether the truncated MRE11 protein could restore pATM recruitment.

A

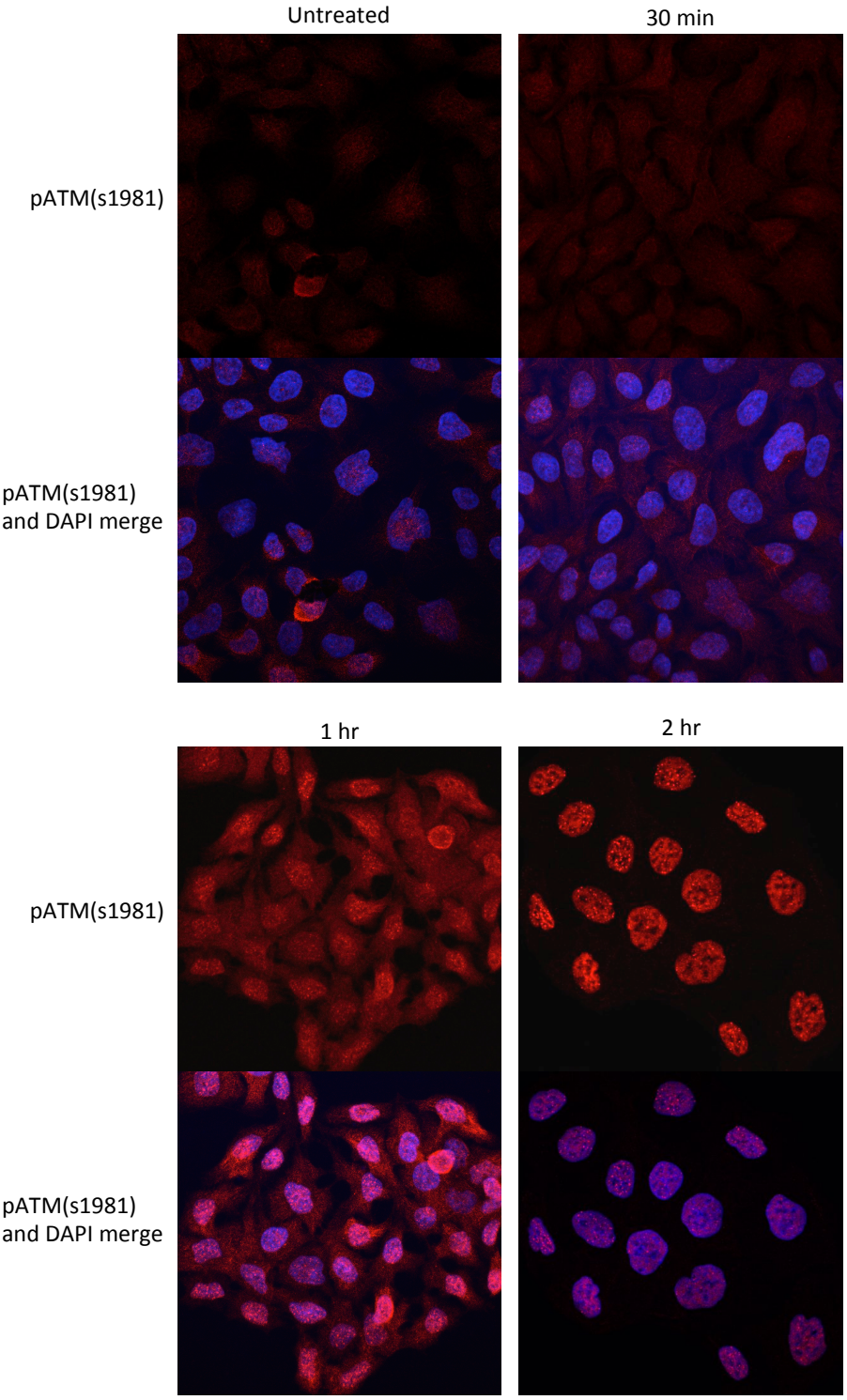
Untreated
30 min
pATM(s1981)
pATM(s1981)
and DAPI merge
1 hr
2 hr
pATM(s1981)
pATM(s1981)
and DAPI merge

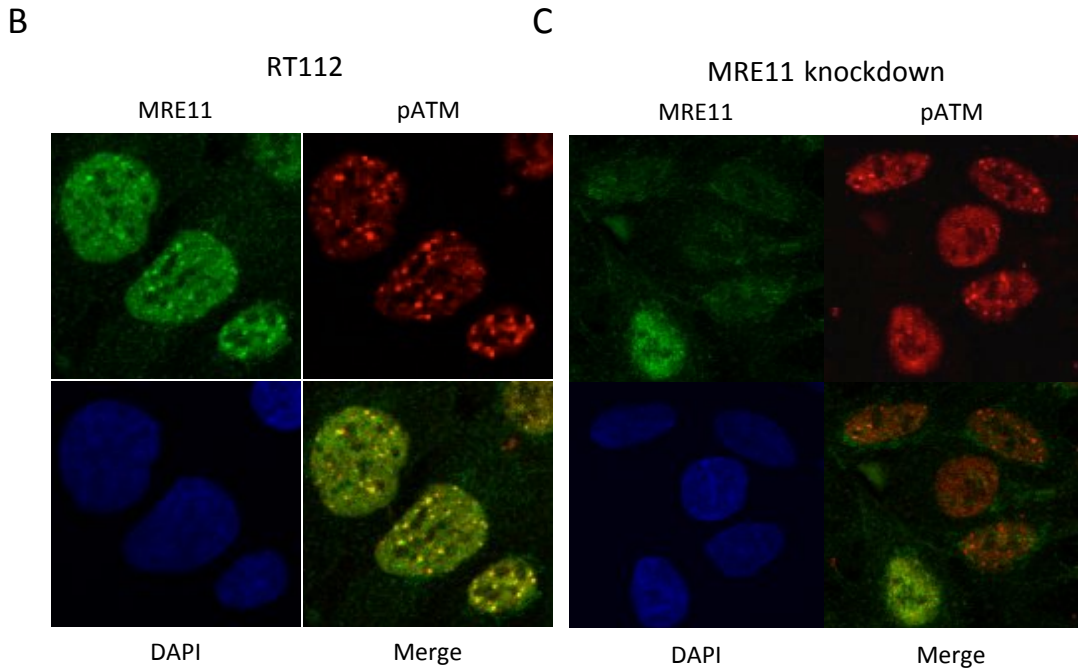

D

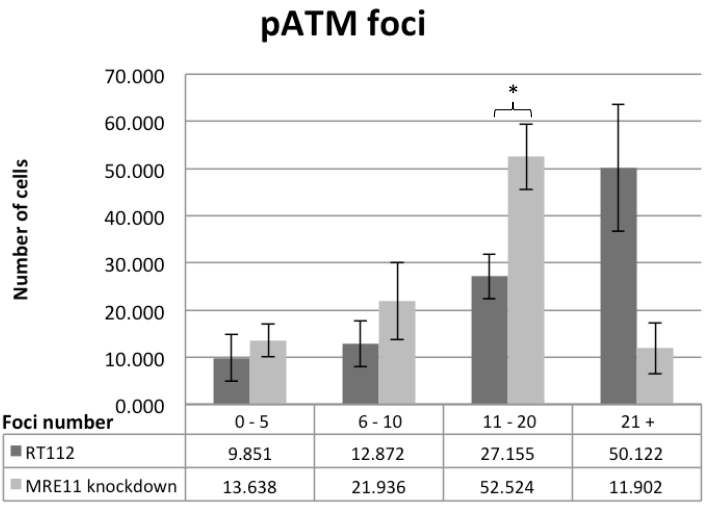

Figure 5.5 Reduced pATM signalling in the RT112-derived MRE11 knockdown cell line.

A) Immunofluorescence microscopy of the RT112 cell line over 2 hour time period following 5 Gy IR. Top panel is pATMs1981 signal, bottom panel is merged signal of pATMs1981 and DAPI. B) Immunofluorescence microscopy of the RT112 cell line 2 hours post 5 Gy IR. C) Immunofluorescence microscopy of the RT112-derived MRE11 knockdown cell line 2 hours post-5 Gy IR. Top left panel is MRE11 signal, top right is pATMs1981 signal, bottom left is DAPI nuclear stain and bottom right is the merged signal of MRE11 and pATM. D) Quantification of the number of pATM foci in the RT112 and MRE11 knockdown cell lines. Student's T-test over RT112 control, * p-value <0.05.

5.2.6 Re-expression of wild type or truncated MRE11 in the RT112 MRE11 knockdown cell line

In order to determine whether the C-terminus truncated MRE11 protein was associated with a DSB repair defect, stable re-expression of either WT or truncated MRE11 in the knockdown cell line was pursued. The aim was to determine if this rescued sensitivity to IR and reduced pATM recruitment (Figure 5.4 and 5.5). Expression plasmids described in Chapter 3, Figure 3.11 for both WT MRE11 and truncated MRE11 were linearised by restriction enzyme digest targeting a non-essential region of the plasmid. Linearised plasmids were transfected using both FuGENE and X-tremeGENE transfection reagents (Materials and Methods 2.10) into the RT112 MRE11 knockdown cell line. Cells with positive integration of the plasmids were selected for using neomycin. A non-transfected control plate was used to establish when only cells with integration of the plasmid were viable. When colonies had reached approximately 50 cells they were transferred to larger culture dishes (5 cm). When clones reached 50% confluence, MRE11 expression was determined by western blot analysis. A small proportion of each colony remained in culture to generate stocks for future experiments.

Western blot analysis of clones with re-expression of WT MRE11 are shown in Figure 5.6A. None of the clones screened re-expressed WT MRE11 to the levels seen in the control RT112 cell line. In fact, expression of MRE11 remained the same as that seen in the knockdown cell line. This suggests that expression of the MRE11 plasmid was not occurring in any of the clones. However, the plasmid had been integrated into the cells, as resistance to neomycin was observed. Figures

5.6B and C show western blot analysis of clones with truncated MRE11 re-expression. None of the clones screened showed expression of the truncated protein to the level of that in the control cell line. However, clone 6C (Figure 5.6C) did show expression of the truncated protein, but WT MRE11 expression had also returned to control levels, suggesting that the knockdown of MRE11 had been lost rather than the successful re-expression of the truncated MRE11 plasmid. Also, clone 4E (Figure 5.6C) appeared to have re-gained WT MRE11 expression. This could be due to the length of time the cells were in selection medium. Potentially, cells that have overcome MRE11 knockdown may have a growth advantage compared with knockdown cells and therefore are still resistant to antibiotic selection but contain no MRE11 depletion.

Approximately 50 clones were selected for each plasmid and of these, a minimum of 25 clones were analysed by western blot. The remaining clones were either not viable after selection or stored for screening. Figures 5.6A–C highlight that none of the clones selected had positive re-expression of WT or truncated MRE11. After this screening attempt it was judged that MRE11 re-expression had been unsuccessful and that it was necessary to take a different approach.

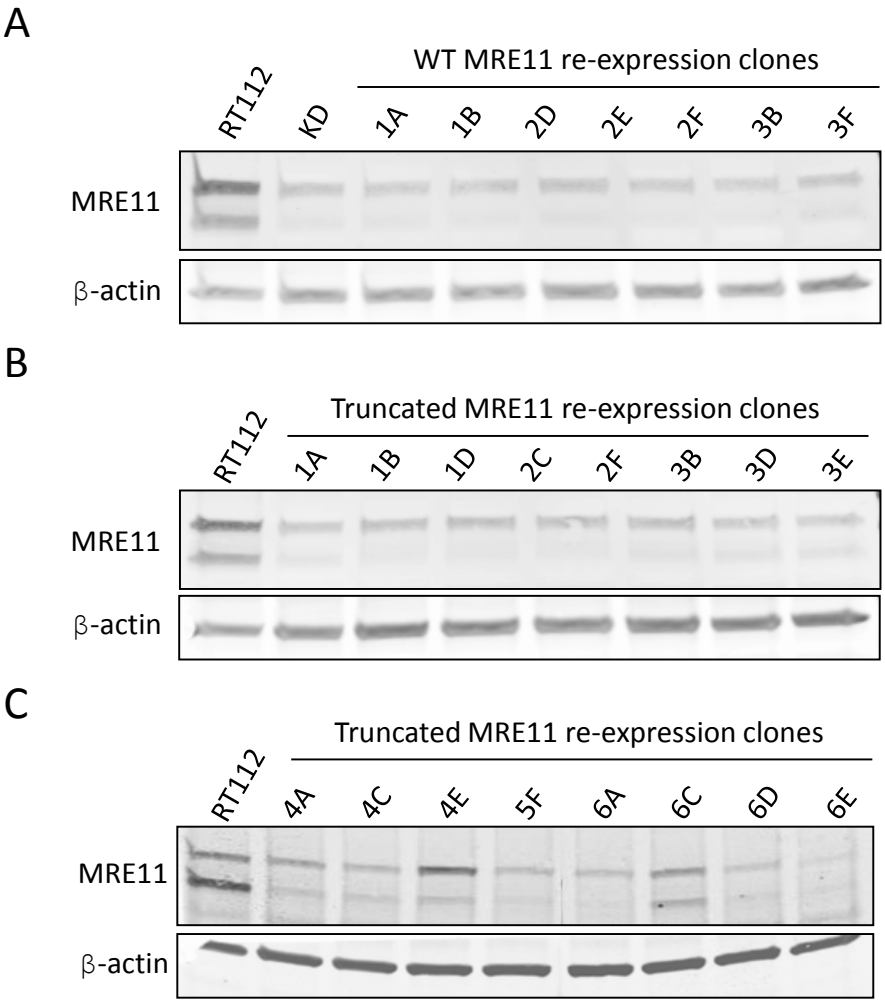

Figure 5.6 Western blot analysis of MRE11 re-expression.

Western blot analysis of MRE11 knockdown clones screened for re-expression of A) wild type MRE11 or B) and C) truncated MRE11, in the RT112 MRE11 knockdown cell line. β-actin was used as a loading control.

5.2.7 Optimisation of transient re-expression of wild type or truncated MRE11 in the RT112 MRE11 knockdown cell line

Stable re-expression of WT MRE11 or truncated MRE11 was not achieved in the RT112 MRE11 knockdown cell line and therefore an attempt was made to transiently re-express each protein in this cell line. Although this approach would not be suitable for clonogenic assays due to lack of homogeneity and poor transfection efficiency, experiments such as immunofluorescence could be performed, as individual cells expressing the protein of interest could be detected. Optimisation of the transient transfection of WT MRE11 in the RT112 MRE11 KD cell line is outlined in Figure 5.7. Three transfection reagents were tested, namely, FuGENE, X-tremeGENE and Lipofectamine. The plasmid concentration and plasmid to transfection reagent ratios were varied to optimise transfection efficiency. Western blot analysis indicated that X-tremeGENE transfection reagent at a ratio of 4:1 (reagent: plasmid) using 5 μg of plasmid gave optimal re-expression of WT MRE11 (Figure 5.7A).

The expression of WT MRE11 following FuGENE transfection was comparable to the control KD, thus indicative that little or no up-regulation of WT MRE11 was achieved with this transfection reagent. Lipofectamine resulted in substantial cell death due to the toxicity of the reagent; therefore, no cells were viable to analyse by western blot.

Transfection of WT MRE11 into the RT112 MRE11 knockdown cell line using X-tremeGENE transfection reagent returned expression levels to that seen in the RT112 cell line, as analysed by western blotting (Figure 5.7A). Despite this, the expression of NBS1 and RAD50 were not returned to the level seen in the RT112

control cell line. After analysing expression of the plasmids using immunofluorescence microscopy it appeared that, in fact, only a small proportion of cells had undergone positive transfection and were very strongly expressing MRE11 (Figure 5.7B). This offers a possible explanation as to why NBS1 and RAD50 expressions were not rescued. When analysing the cells in this way, the X-tremeGENE transfection reagent also appeared to be having a toxic effect on the cells, as nuclear debris was often present, judged by DAPI staining in areas that did not appear to be intact nuclei. The cells that showed expression of the MRE11 plasmids also had a different morphology to the parental cells. Therefore, despite several attempts at optimisation it was concluded that these cell were not representative of the real biological setting and this avenue was not pursued further.

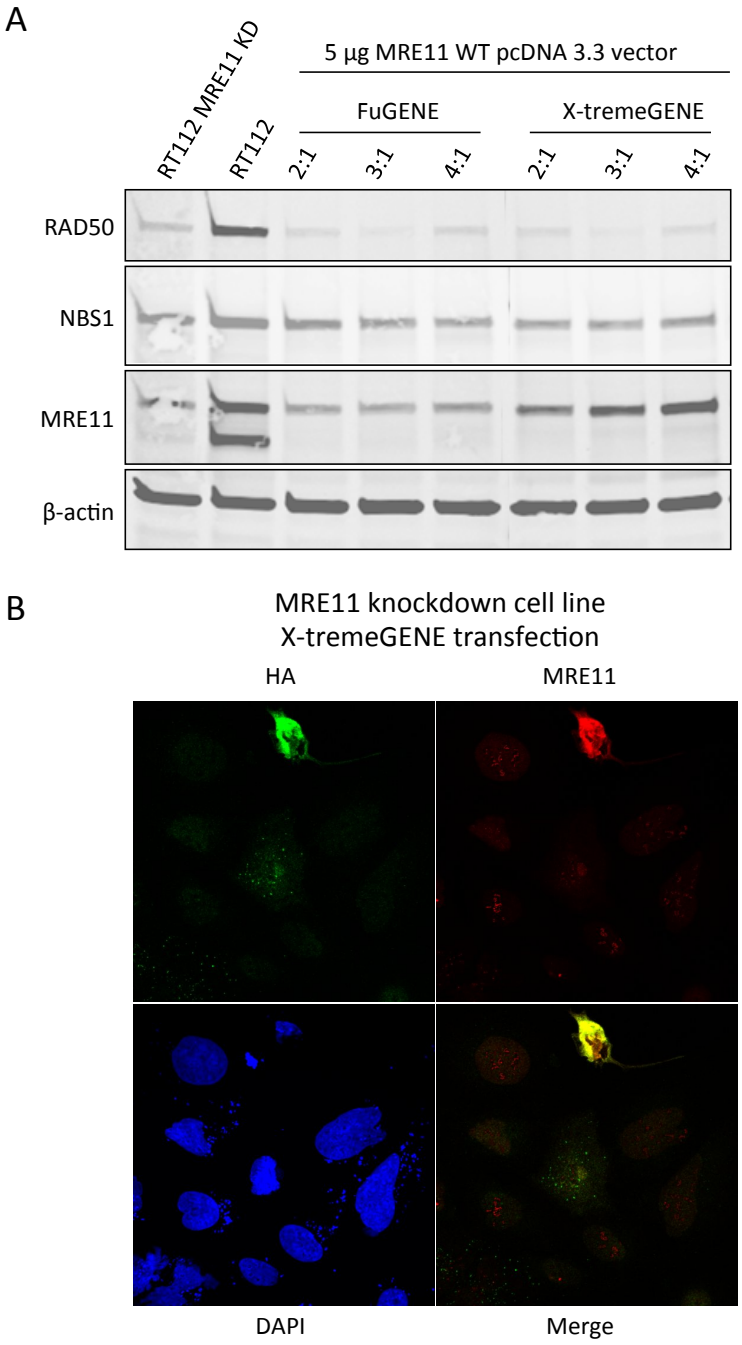

Figure 5.7 Transient expression of wild type (WT) MRE11 in the RT112-derived MRE11 knockdown cell line.

A) Western blot analysis showing expression of the MRN complex proteins after transfection with the WT MRE11 expression plasmid. Cells were transfected with 5 µg of HA-tagged WT MRE11 plasmid using FuGENE or X-tremeGENE transfection reagents at indicated ratios. β-actin was used as loading control. B) Immunofluorescence microscopy of RT112 MRE11 knockdown cell line after transfection with 5 µg of HA-tagged WT MRE11 plasmid using X-termeGENE transfection reagent at a 4:1 ratio. The top left panel shows the HA signal, the top right panel shows the MRE11 signal, the bottom left panel shows the DAPI signal and the bottom left panel is the merged signal from HA and MRE11.

5.2.8 Expression of truncated MRE11 in T24 bladder cancer cell line

The RT112 MRE11 knockdown cell line was no longer considered an appropriate experimental system for studying the re-expression of either WT or truncated MRE11 due to transfection issues experienced with these plasmids. Others researchers in the group were also experiencing difficulties with plasmid transfection protocols in this cell line. Therefore, the next approach was to use a different bladder cancer cell line, whilst continuing to optimise transfection conditions in the RT112 cell line. As the T24 cell line does not express the truncated MRE11 protein under basal conditions, but does express it following treatment with panobinostat (Chapter 4, Figures 4.6 and 4.7) it was reasoned that this was the best cell line to use. Transient transfection had already been shown to be effective (Chapter 3, Figures 3.12 and 3.13). However, in order to determine radiosensitivity, transient methods of transfection were not considered appropriate. Therefore, the aim was to generate two cell lines. Firstly, a T24 cell line with stable expression of the truncated MRE11 protein in the presence of endogenous WT MRE11. This would allow the investigation of whether the MRE11 truncated protein exhibits a dominant negative phenotype. Secondly, a T24 cell line with stable expression of the truncated MRE11 protein in a WT MRE11 knockdown background.

To generate a T24 cell line with stable expression of truncated MRE11, the truncated MRE11 expression plasmid was linearised and transfected into T24 cells using FuGENE transfection reagent (Materials and Methods 2.10). These cells underwent selection using neomycin. When colonies had reached approximately 50 cells they were transferred into larger dishes and grown until

there were enough cells to make a lysate for western blot analysis, whilst maintaining exponential growth. Western blot analysis of MRN expression in eight of the clones screened is shown in Figure 5.8A. Unfortunately, due to technical issues with the transfer, the expression of MRE11 was not clear in some of the clones. However, as can be seen by the detection of HA antibody signal at the expected size of the truncated MRE11, many of the clones had stable integration and expression of the truncated MRE11 protein to varying levels. These clones were expanded and frozen stocks generated. The most promising clone (A1), with the highest expression of truncated MRE11 was used in later experiments.

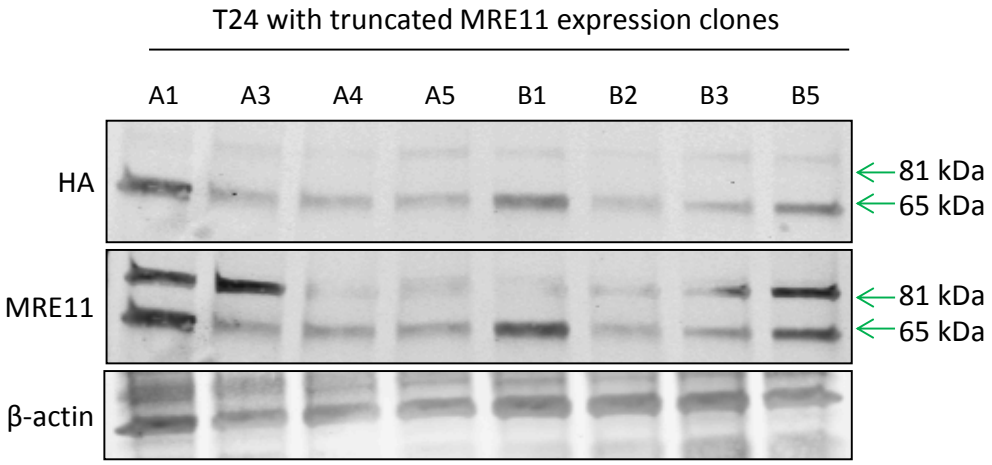

Figure 5.8 Stable expression of truncated MRE11 in the T24 cell line.
A) Western blot analysis of clones screened for HA and MRE11 expression in the T24 cell line after transfection with the truncated MRE11 expression plasmid. β-actin was used as loading control.

To generate a cell line with stable expression of the truncated MRE11 protein in the context of depleted WT MRE11 expression, clone A1 was selected and transfected with a shRNA plasmid targeting the 5'UTR of MRE11 to deplete endogenous WT MRE11 protein. Western blot analysis for the expression of MRE11 in clone A1 transfected with the MRE11 shRNA p*Silencer* plasmid is shown in Figure 5.9.

Several of the clones had successful knockdown of MRE11 but, unexpectedly, all of the clones screened had silenced expression of the truncated MRE11 protein. Additionally clones that had previously shown expression of the truncated MRE11 protein (Figure 5.8) were recovered from storage and re-tested for expression of the truncation. However, all of the clones had silenced expression of the plasmid and no longer showed expression of the truncated MRE11 protein, the reasons for which remain unclear.

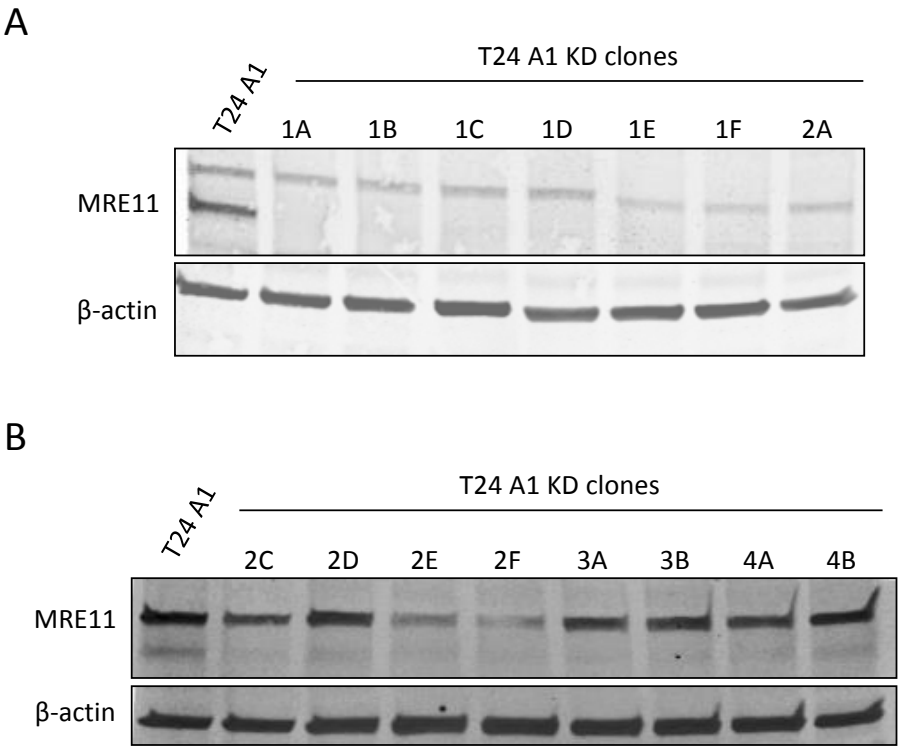

Figure 5.9 Expression of truncated MRE11 in the T24 cell line.

A and B) Western blot analysis of clones screened for MRE11 expression in the T24 cell line expressing truncated MRE11- clone A1 (Figure 5.8), after transfection with shRNA plasmid targeting MRE11. β-actin was used as a loading control.

Alongside the clones screened in Figure 5.8A and B, due to concerns about the longevity of truncated MRE11 expression in clone A1, WT T24 cells were co-transfected with both the shRNA plasmid targeting MRE11 and the linearised truncated MRE11 expression vector. These cells underwent a double selection using both puromycin and neomycin. Western blot analysis of clones that had undergone co-transfection to allow stable expression of the truncated MRE11 protein and depletion of endogenous WT is shown in Figure 5.10A–C. Many of the clones demonstrated MRE11 knockdown but none expressed the truncated MRE11 protein.

At this point, due to time constraints, it was concluded that transient expression of the MRE11 truncation in the T24 cell line was the best way forward. This might permit the establishment of the functional impact of the truncated protein on DNA repair, whilst simultaneously pursuing a different method of stable protein re-expression.

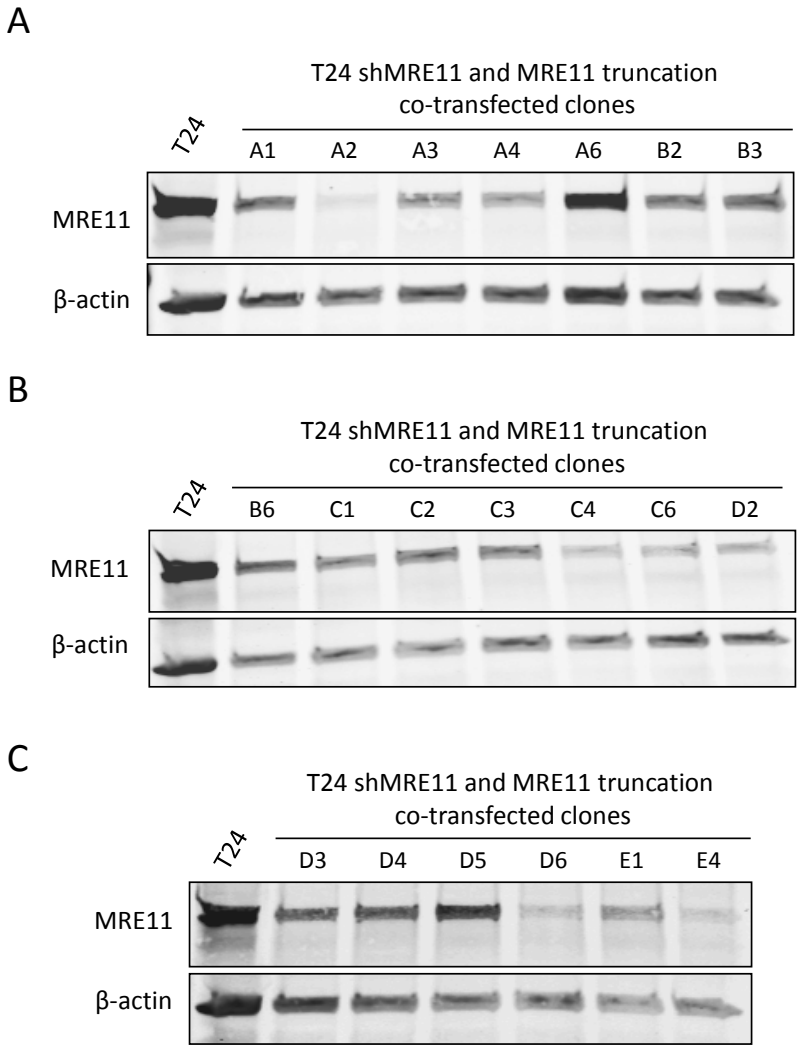

Figure 5.10 Expression of MRE11 in T24 cell line clones.

A-C) Western blot analysis of clones screened for MRE11 expression in the T24 cell line after co-transfection with shRNA plasmid targeting MRE11 and linearised truncated MRE11 expression plasmid. β-actin was used as a loading control.

5.2.9 yH2AX foci resolution

To establish whether expression of the truncated MRE11 protein leads to a defect in DNA damage repair, DNA repair kinetics were investigated in the T24 cell line compared with the T24 cell line with MRE11 knockdown and subsequent re-expression of WT or truncated MRE11. This was achieved through examining the presence of the well-established DNA damage marker yH2AX at multiple time points over a 24-hour period following exposure to 5 Gy IR. In order to examine only foci in cells with positive re-expression of either MRE11 protein, plasmids with an HA tag were utilised. This allowed for the detection of cells expressing HA, which could be selected for analysis. Figure 5.11A outlines an example of three positively transfected cells. At least 50 cells were counted for each condition. Unfortunately, due to time constraints this experiment was only conducted once and needs to be repeated to confirm results. As endogenous damage present can result in yH2AX foci, cells with 20 foci or more, containing a substantial amount of DNA damage, were considered likely to be caused by IR, and these cells were deemed to be 'yH2AX positive cells'. Under control conditions, the percentage of yH2AX positive cells in the T24 and MRE11 knockdown cell lines was ~8%. This suggests that knockdown of the MRE11 protein was not causing additional endogenous DNA damage. Furthermore, the transfected MRE11 knockdown cells contained 2–5% yH2AX positive cell under control conditions, which implies that the transfection method was not causing additional DNA damage.

A rapid induction of yH2AX signal was observed 30 minutes following irradiation, with 100% of cells counted positive for yH2AX (containing a minimum of 20 foci).

Hence MRE11 knockdown or re-expression of WT or truncated MRE11 was not influencing recruitment or phosphorylation of yH2AX. Three hours after 5 Gy IR, the percentage yH2AX positive cells had fallen to 60 and 66% in the T24 and MRE11 KD with full length re-expression, respectively. The percentage of yH2AX positive cells in the MRE11 KD and MRE11 KD with truncated MRE11 expression was 77% 3 hours post IR, potentially suggesting a slight delay in repair in cells depleted of MRE11 or cells expressing the truncated MRE11 protein. Six hours following irradiation, the percentage yH2AX positive cells had fallen to 50–55% in the T24 and MRE11 KD cells with either full length or truncated MRE11 expression. However, 84% of the MRE11 KD cells were still yH2AX positive. This suggests that there was a reduction of DNA damage repair efficiency in the MRE11 KD cell line. However, re-expression of WT MRE11 rescues this phenotype and expression of truncated MRE11 protein is also able to rescue this repair defect phenotype. After 24 hours the percentage yH2AX positive cells had returned to control levels in all cell lines, suggesting that there was no persistent DNA damage.

A

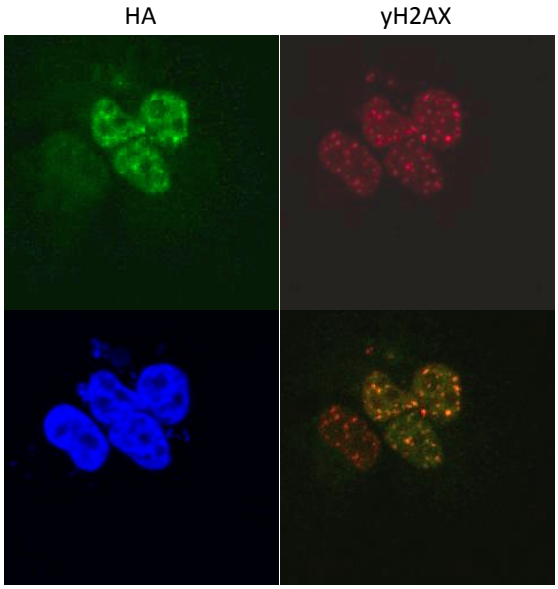

B

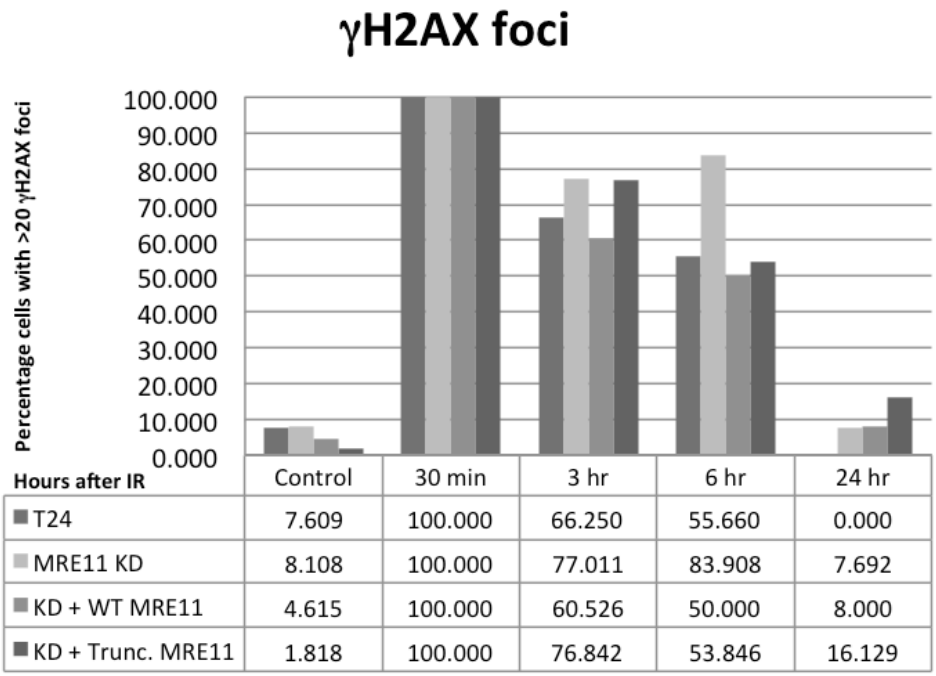

Hours after IR	Control	30 min	3 hr	6 hr	24 hr
T24	7.609	100.000	66.250	55.660	0.000
MRE11 KD	8.108	100.000	77.011	83.908	7.692
KD + WT MRE11	4.615	100.000	60.526	50.000	8.000
KD + Trunc. MRE11	1.818	100.000	76.842	53.846	16.129

Figure 5.11 DNA repair kinetics following ionising radiation.

A) An example of T24 MRE11 knockdown cells positive for HA expression. Top left panel shows HA signal. Top right shows yH2AX signal. Bottom left shows DAPI signal and bottom right shows HA and yH2AX merged signal. B) Quantification of foci number from four conditions tested; T24 control, T24 MRE11 knockdown, T24 MRE11 knockdown with wild type (WT) MRE11 re-expression and T24 MRE11 knockdown with truncated (Trunc.) MRE11 re-expression.

5.2.10 I-SceI homologous repair assay

As a global delay to DNA damage repair was not observed (Figure 5.11), we wanted to look more specifically at the effect on homologous recombination (HR). This was conducted using the *I-SceI* HR repair assay previously described by Seluanov *et al* (Seluanov *et al*. 2010). An HR plasmid construct, outlined in Figure 5.12A, was stably integrated into the T24 cell line (Dr Martin Kerr, CRUK/MRC Institute, Oxford). In the HR construct, the first GFP exon contains a 22 bp deletion, combined with the insertion of three restriction sites: *I-SceI/HindIII/I-SceI*. This deletion ensures that GFP cannot be reconstituted by NHEJ. The Δ22GFP exon is followed by a second GFP exon and a promoter-less (lacking ATG start codon) first exon of GFP. Induction of a DSB by transfection with an *I-SceI* expression plasmid will result in reconstitution of a functional GFP only after repair by gene conversion, as outlined in Figure 5.12A. Therefore the amount of HR repair can be measured and quantified by the number of GFP expressing cells, as identified by FACS analysis.

For this study the aim was to identify the level of HR repair in an MRE11 knockdown background and subsequently re-express either WT or truncated MRE11 and examine the impact on HR repair. This was achieved by stable depletion of MRE11 in the T24 cell line with stable expression of the MRE11 shRNA construct. The degree of MRE11 knockdown was determined by western blot analysis (Figure 5.12B). A knockdown of 60% compared with control MRE11 expression was achieved.

To perform the *I-SceI* assay, the MRE11 knockdown cell line was transfected with the *I-SceI* plasmid alone or co-transfected with *I-SceI* and WT MRE11 or truncated

HA-tagged MRE11 pcDNA 3.3 expression plasmids (Materials and Methods 2.17.2). Prior to *I-SceI* plasmid transfection, the cells were transfected with a DsRED plasmid. The expression of DsRED was used as a measure of transfection efficiency and subsequent GFP expression was normalised to this value. Figure 5.12C outlines an example of the GFP and DsRED detection by flow cytometry, GFP expressing cells were detected in the area highlighted in green and DsRED positive cells highlighted in orange. As the experiments were conducted in the MRE11 knockdown cell line, GFP expression was normalised to this level in order to measure HR efficiency. Results shown in Figure 5.12D represent four independent experiments.

As shown in Figure 5.12D re-expression of WT MRE11 increased the fraction of GFP expressing cells, suggesting that more HR is occurring after re-expression of WT MRE11 than in the MRE11 knockdown cell line. It also confirms that co-transfection of both *I-SceI* and an additional MRE11 plasmid does not reduce HR capability, or the efficacy of the assay. In contrast, expression of truncated MRE11 protein significantly reduced the fraction of GFP expressing cells compared with that in the MRE11 knockdown cell line and compared with cells in which WT MRE11 is re-expressed (p-value 0.020 and 0.023, respectively). This suggests that HR repair is less efficient when the truncated MRE11 protein is expressed, not only compared with cells expressing WT MRE11 but also compared to when MRE11 expression is depleted. Therefore, it appears that the truncated MRE11 protein is not able to function in HR repair and also hinders repair that would occur in its absence. Thus, the truncated MRE11 protein is potentially acting in a dominant negative manner.

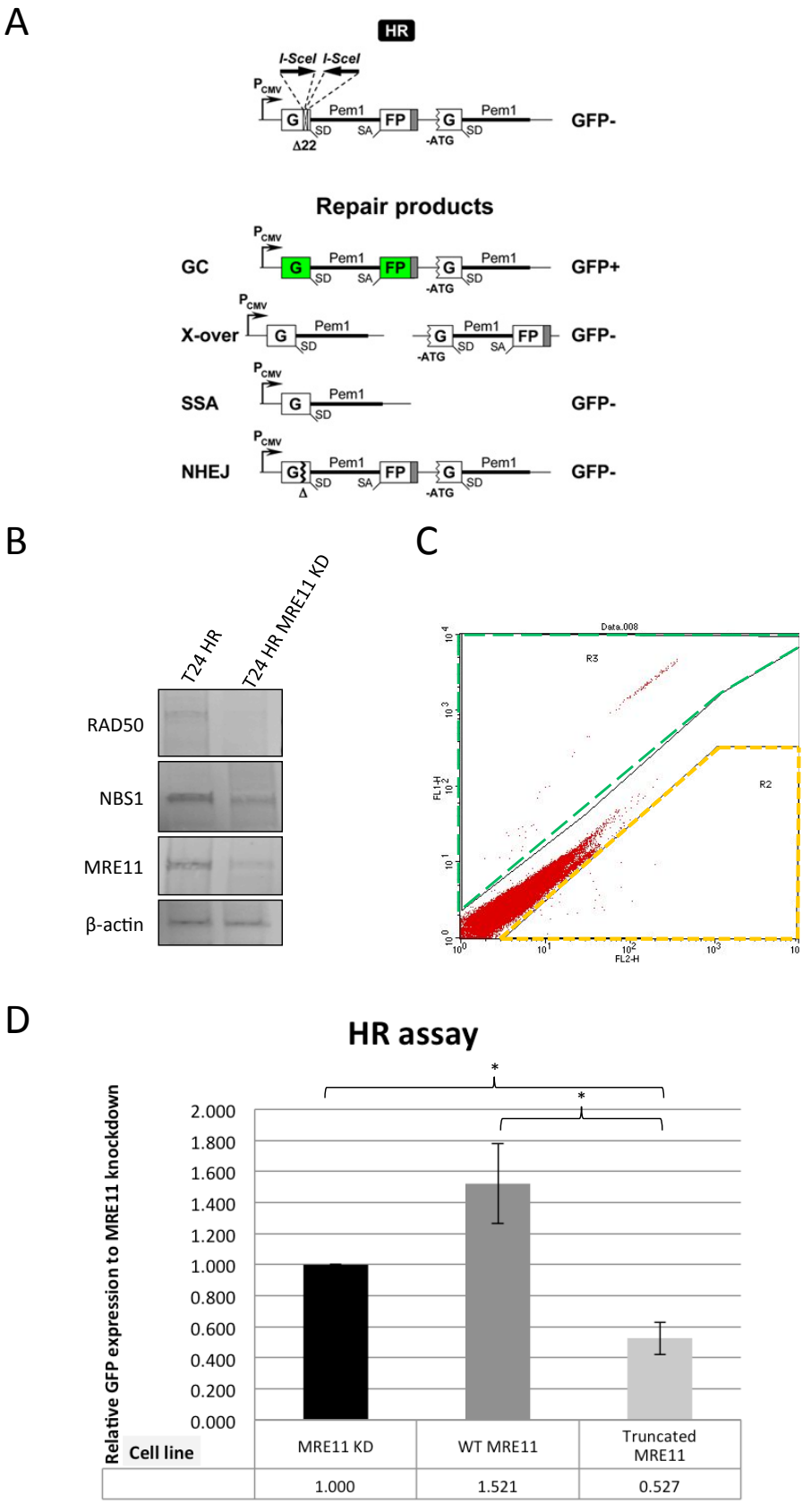

Figure 5.12 *I-SceI* HR repair assay.

A) The *I-SceI* HR construct and possible repair mechanisms after DSB induction by *I-SceI* digestion. Gene conversion (GC) after repair by homologous recombination (HR) is the only repair pathway that allows for GFP expression (indicated by green

colour). Products from the use of crossing over (X-over), single strand annealing (SSA) and non-homologous end joining (NHEJ) are shown. None of these result in GFP expression. Adapted from (Seluanov *et al*. 2010) B) Western blot analysis of MRE11 expression in the T24 *I-SceI* cell line. β-actin was used as loading control. C) An example of flow cytometry detection of GFP and DsRed positive cells. Red dots represent individual cells. Area containing GFP positive cells is highlighted in green, area containing DsRed positive cells is highlighted in orange D) GFP positive cells detected by FACS analysis, normalised to DsRed expression and further to GFP expression in the T24 *I*-SceI MRE11 knockdown cell line. Error bars represent mean and SEM of four independent experiments. Student's T-test over MRE11 knockdown cell line; *p-value <0.05.

5.3 Discussion

The experiments discussed in this chapter were designed to elucidate the functionality of the truncated MRE11 protein. Firstly, it was established that an MRE11 knockdown cell line exhibited sensitivity to IR and reduced pATM recruitment. Secondly, attempts were made to generate a cell line with stable re-expression of WT or truncated MRE11 to examine rescue of these phenotypes. At this stage several practical issues were encountered in terms of re-expression of the protein and different options were therefore investigated until optimisation of experimental procedure was achieved.

5.3.1 MRE11 knockdown

To generate an MRE11 knockdown bladder cancer cell line, an siRNA sequence previously described by Zhuang *et al*. (2009) targeted to the 5'UTR of MRE11 gave a sustainable knockdown of both WT and truncated MRE11 in the RT112 cell line. This sequence was then used to create stable MRE11 knockdown clones in the RT112 cell line. The 5'UTR sequence that was the target of the siRNA oligonucleotide was not transcribed in the expression plasmids generated for WT or truncated MRE11 described in Chapter 3, Figure 3.11. This was a deliberate choice made in order to allow for re-expression of either form of MRE11 in a knockdown background for functional studies. The stable knockdown of MRE11 proved successful, with clones depleted of the protein by as much as 85% compared with parental cell line expression. Complete knockdown of WT MRE11 to undetectable levels was not achieved and this may be due to the critical function of MRE11 in cells. This has been demonstrated previously by embryonic

lethality in an attempt to make a null MRE11 mutant in mice (Theunissen *et al*. 2003; Xiao & Weaver 1997) and is also the case for RAD50 and NBS1 null mutants (Luo *et al*. 1999; Tauchi *et al*. 2002). Our laboratory also attempted to generate an MRE11 knockout CRISPR cell line in collaboration with Haplogen (Vienna, Austria). However, this was unsuccessful, likely due to the critical role of MRE11 during replication, as previously described by Theunissen *et al.* 2003.

5.3.2 MRE11 knockdown radiosensitivity

In order to further assess the impact of the truncated MRE11 protein in bladder cancer cell lines, the radiosensitivity of the MRE11 knockdown cell line was determined by a clonogenic survival assay.

The MRE11 knockdown cell line showed an increased sensitivity to IR with an SER_{10} of 1.29 (p-value= 0.04) compared with a cell line with integration of an MRE11 scrambled shRNA. This was expected, as MRE11 plays a critical role in the DNA damage response (DDR) and MRE11 mutant and null cell lines have previously demonstrated increased sensitivity to IR (Stewart *et al*. 1999; Theunissen *et al*. 2003). It is possible that the radiosensitisation is not exclusively caused by the lack of MRE11 nuclease activity, as treatment with three MRE11 nuclease inhibitors did not radiosensitise cells to the same degree as for MRE11 knockdown in the RT112 cell line. This reflects the fact that the MRN complex has multiple roles in the DDR in terms of pATM recruitment and cell cycle response (Zha *et al*. 2009; Uziel *et al*. 2003; Kijas *et al*. 2015; Buis *et al*. 2012).

Although not statistically significant, there was an indication that treatment with a specific exonuclease inhibitor PFM39 radiosensitises the RT112 cell line (Figure

5.4) compared with the endonuclease inhibitor, supporting the hypothesis of Shibata *et al*. (2014), which states that inhibition of the endonuclease function of MRE11 would not result in a repair defect, as NHEJ remains functional. The lack of radiosensitivity with this inhibitor shown here supports this theory. Futhermore, the Shibata *et al* hypothesis suggests that inhibiting the exonuclease function of MRE11 still allows a nick in the DNA to be generated by the unperturbed endonucleolytic activity. This step commits the cells to HR but with the inhibition of MRE11 exonuclease function, HR cannot continue. Therefore, the cells are no longer capable of repair via NHEJ and the cells will not survive. The present data supports this, as enhanced radiosensitivity is caused after MRE11 exonuclease inhibition.

The MRE11 knockdown cell line showed reduced pATM foci 2 hours post-5 Gy IR, suggesting a lack recruitment of the protein and DNA signalling response caused by MRN depletion. Evaluation at this time point was performed, as distinct nuclear pATM foci were not detected at earlier time points. As MRE11 is known to be upstream of ATM this suggests a lack of recruitment rather than resolution of pATM foci in the MRE11 knockdown cell line (Carson *et al*. 2003).

It was then necessary to re-express either WT MRE11 or the truncation to establish cellular radiosensitivity, the hypothesis being that the truncation would generate a radiosensitive phenotype due to deficient HR. This was not achieved due to technical issues discussed below. Further work needs to be performed, therefore, to evaluate the effect of truncated MRE11 expression on radiosensitivity and pATM recruitment.

5.3.3 Re-expression of MRE11 in RT112

To determine radiosensitivity after re-expression of WT or truncated MRE11, an attempt was made to generate stable cell lines expressing either protein. The expression plasmids were linearised before transfection and, although this can result in lower DNA uptake compared with supercoiled DNA, it yields optimal integration of DNA into the host genome by avoiding plasmids opening at essential regions, such as the coding region of the gene or the antibiotic resistance cassette. Linearised plasmid DNA was transfected into the RT112 MRE11 knockdown cell line. As previously discussed, the shRNA plasmid would not affect re-expression due to the lack of 5'UTR in expression plasmids. Unfortunately, none of the clones screened had expression of WT or truncated MRE11, despite being resistant to neomycin. There could be several reasons for this, one being the cell line used. Transfection of various expression plasmids into the RT112 cell line has proved difficult for several members of the group. The viability and general health of cells prior to transfection is known to be an important source of variability from one transfection to another. It could be argued that a cell line depleted for MRE11 would not be in good health as MRE11 is critical for replication, possibly affecting transfection of the plasmids, despite these coding for the re-expression of MRE11. Another factor influencing the poor transfection and expression levels could be the size of the plasmid DNA, the MRE11 plasmid is over 7 Kb, with the *MRE11* gene being over 2 Kb, a relatively large product to be integrated.

As transient transfection is most efficient with supercoiled plasmid DNA, for these experiments the plasmid was not linearised prior to transfection. However,

after an attempt to optimise with four different transfection reagents, this also proved difficult. The most promising reagent for transfection shown using western blot analysis appeared to be X-tremeGENE, as this resulted in WT MRE11 expression returning to endogenous levels after transfection into the knockdown cell line. Although this appeared successful by western blot, when using immunofluorescence it became clear that when examining individual cells the re-expression of the plasmids was not suitable. This was due the intensity of over-expression of the plasmids in only very few cells and a large amount of cell death. It would therefore not be safe to deduce any meaningful results from these cells, as the conditions were vastly different to the genuine biological setting. Due to previous experience in the lab of working with the RT112 cell line for transfection of expression plasmids and the difficulties seen here with transient expression of the MRE11 plasmids, it was concluded that some intrinsic feature of this cell line was likely the reason behind this failure.

The next route taken was to attempt to generate stable expression of the truncated MRE11 protein in the T24 cell line. The rationale for this was that good transient transfection of the MRE11 plasmids was achieved in this cell line, analysed by western blot and immunofluorescence. The T24 cell line was also shown to express the truncated MRE11 protein after treatment with panobinostat (Chapter 4, Figures 4.6 and 7). Therefore, this would be relevant and a suitable method to address the effect of the MRE11 truncation on DNA repair pathways.

5.3.4 Re-expression of MRE11 in the T24 cell line

Transfection of the linearised truncated MRE11 expression plasmid was performed in the same way. Many of the screened clones had undergone successful integration of the plasmid and were expressing the truncated MRE11 protein. However, this expression was silenced after a few passages and although early passage stocks were frozen, the expression did not survive freeze thaw cycles. This could be due to the critical function of MRE11 in replication. This further suggests a negative impact of the truncation, as the cells are quick to silence expression. What can be concluded from these results is that expression of MRE11 is tightly controlled.

Due to time constraints, it was decided that attempts to achieve stable expression were not feasible; therefore a transient expression approach was taken. The next method that will be tested, beyond the scope of this thesis, is to generate a conditional re-expression system using a lentiviral vector. The benefit of this would be that expression could be induced, so it would not be present at the point of cell recovery and would hopefully be expressed for long enough to carry out functional studies, such as clonogenic survival assays.

5.3.5 γH2AX resolution after IR

The formation of a γH2AX signal normally occurs in the vicinity of DSBs and can be visualized by immunofluorescence as distinct nuclear foci. Changes in γH2AX foci number measured by confocal microscopy or the intensity of western blot signal are accepted methods of studying the dynamics of post-irradiation DNA DSB damage and repair mechanisms (Bonner *et al*. 2008). In the present study,

western blot analysis was not an acceptable method of examining cells expressing the truncated MRE11 protein, as uniform expression after transfection was not achieved. Therefore, confocal microscopy was used to identify the cells that had undergone positive transfection and were expressing the MRE11 proteins and subsequently to determine whether γH2AX foci resolution is affected by the absence of MRE11 or presence of the truncated MRE11 protein. The delay in γH2AX resolution in the MRE11 knockdown bladder cancer cells indicates impairment of DSB repair. The expression of either WT or truncated MRE11 proteins in the MRE11 knockdown cells was able to rescue the impairment in DNA repair. Therefore, it could be concluded that expression of the truncated MRE11 protein is not influencing overall DNA repair kinetics. The γH2AX foci assay used in this study has limitations, for example stalled replication forks and ssDNA will also be detected (Löbrich *et al*. 2010) and so the resolution of foci cannot be fully attributed to DSB repair.

This contrasts with recent results recently reported by Kijas *et al*. (2015) whereby it was demonstrated that mutation of two serine residues at the C-terminus of MRE11, that have been identified as ATM phosphorylation sites, results in unlimited resection by Exonuclease 1 (Exo1). These ATM phosphorylation sites are at residues 676 and 678 of MRE11, so would be absent in the truncated variant. The mutation of these sites confers a reduction in γH2AX resolution and an increased sensitivity to IR. This suggests that cells with the C-terminus truncated MRE11 protein would also have increased sensitivity to IR (Kijas *et al*. 2015). This data also leads to an intriguing possible explanation as to why MMEJ is more frequently utilised in MIBC (Bentley *et al*. 2009). It is possible that in cells

that are lacking the MRE11 C-terminus (and therefore also these critical phosphorylation sites) needed to regulated Exo1 resection, there is greater end resection subsequent repair via MMEJ.

The resolution of yH2AX foci is influenced by several DNA repair mechanisms. In order to evaluate the impact of the truncated MRE11 protein on HR using an *I-SceI* GFP reporter construct repair assay was performed.

5.3.6 I-SceI homologous repair assay

The MRE11 protein plays a significant role in homologous recombination repair and so this pathway was identified as the most likely to be effected by expression of an MRE11 variant. It was decided that an *I-SceI* construct repair assay would be most suitable to study HR due to the sensitivity of the assay, as single cells with GFP expression can be detected (Seluanov *et al*. 2010). Co-delivery of the *I-SceI* plasmid and MRE11 plasmids should also ensure that the cells detected in the assay are cells that are expressing the MRE11 proteins. This has been seen in several GFP positive cells that were also positive for HA-tagged MRE11 expression (appendix F). However, more robust analysis of co-transfection should be conducted to ensure the majority of GFP positive cells also show expression of the MRE11 protein of interest.

One limitation of the *I-SceI* assay is that the MRE11 knockdown cell line could not be directly compared with the WT T24 cell line. This was because in order to generate the knockdown, the cells underwent an extensive transformation. For example, upon screening of the knockdown clones some had silenced expression of the *I-SceI* HR construct. It was therefore concluded that the MRE11 knockdown

cell line would represent the control level of HR and the effect of re-expression of either WT or truncated MRE11 protein in this cell line would be examined.

Re-expression of WT MRE11 confirmed that the co-transfection of plasmids did not hinder *I-SceI* expression, as an increase in HR repair was observed. Previously it had been a concern that co-transfection would result in a reduction of *I-SceI* transfection, thus influencing the level of GFP detection. This was not the case as the fraction of GFP positive cells was greater in the cells with WT MRE11 re-expression compared with the MRE11 knockdown cell line. This implies that HR repair is more proficient when WT MRE11 is expressed, which was expected, due to the essential role of MRE11 in HR.

The most intriguing result was observed after expression of the truncated MRE11 protein. As measured by the decrease in GFP positive cells there was a significant reduction in HR repair, not only compared to when the WT protein was expressed but also compared to when MRE11 was depleted. This suggests that the truncated MRE11 protein hinders HR repair in comparison to WT MRE11 but also that expression of the truncated protein results in reduced HR compared to when MRE11 is depleted. Further work is needed to understand the exact reason for this. However, as the C-terminus of MRE11 is critical for CDK2 binding it could be hypothesised that the lack of CtIP recruitment and phosphorylation results in insufficient DNA end resection for homologous recombination to occur (Buis *et al*. 2012). Another possibility is that too much resection is occurring, due to the recently reported ATM phosphorylation sites at the C-terminus of MRE11 (Kijas *et al*. 2015), discussed above.

The truncation-expressing cells are more deficient at HR compared with MRE11

depleted cell. This could be due to truncated MRE11 being present at the DSB sites; blocking any residual functioning MRE11 remaining in the MRE11 depleted cell line, thus exerting a dominant negative phenotype. Furthermore, it is also possible that the positioning of truncated MRE11 at DSB sites could block additional repair factors such as Ku, resulting in disruption of other DNA repair pathways. However, the yH2AX foci resolution (Figure 5.11) suggests that overall repair is not affected, unlike in the study performed by Kijas *et al*. (2015).

Optimisation of additional *I-SceI* constructs to measure NHEJ and MMEJ is underway, allowing the influence of the truncated MRE11 protein on these pathways to be examined. Another limitation of the *I-SceI* assay is the complexity of the break, IR produces more complex lesions than those generated during the assay and a more thorough investigation into the truncated MRE11 protein's role in repair at such breaks should be pursued, to obtain more clinically relevant data (Lomax *et al*. 2013; Yajima *et al*. 2013).

The reduction of HR upon expression of truncated MRE11 compared with WT MRE11 suggests that these proteins could be competing for DSB sites. Similar dominant negative phenotypes of mutant DNA repair proteins have previously been described, such as CtIP (Qvist *et al*. 2011) and ATM (Smith *et al*. 1999). This leads to the exciting prospect of developing therapies to exploit the potential HR defect in patients who exhibit expression of the truncated MRE11 variant.

CHAPTER 6 General discussion and future plans

6.1 General discussion

The aim of this thesis was to gain a better understanding of the unexpected direct correlation previously seen between high MRE11 expression in bladder tumours, as measured by immunohistochemistry (IHC), and increased survival following radiotherapy (Choudhury *et al*. 2010; Laurberg *et al*. 2012). Research was conducted on tumour samples from bladder cancer patients and established bladder cancer cell lines. The principal findings were the detection and identification of an unreported MRE11 variant.

Further research reported in this thesis demonstrated that the MRE11 variant was a truncated protein, which lacked the C-terminal domain, a region critical for DNA and CDK2 binding, as well as two recently identified phosphorylation sites (Buis *et al*. 2012; Kijas *et al*. 2015; de Jager *et al*. 2001). This suggests several possibilities as to how the variant could disrupt the function of MRE11 in double strand break (DSB) repair. Firstly, through the inability to bind to CDK2, an interaction that Buis *et al.* showed to be critical for the phosphorylation status and therefore activity of CtIP (Buis *et al*. 2012). As CtIP enhances DNA end resection by MRE11 nuclease activity (Sartori *et al*. 2007), this could potentially lead to defective HR through a decrease in DNA end resection. Secondly, and in contrast to the previous hypothesis, Kijas *et al.* have recently reported two ATM phosphorylation sites at the C-terminus of MRE11 (Kijas *et al*. 2015). They also demonstrated that these phosphorylation sites are critical for asserting MRE11's control and restriction of Exo1 nuclease activity. Furthermore, Kijas *et al.*

reported that a protein with mutated C-terminus phosphorylation sites resulted in deficient HR due to excessive DNA end resection. This second hypothesis could have greater bearing for patients with bladder cancer as Bentley *et al.* have previously shown that microhomology-mediated end joining is more frequently utilised in DSB repair in muscle-invasive bladder tumours than conventional DNA repair pathways (Bentley *et al*. 2004). This could possibly be explained by uncontrolled DNA end resection, due the MRE11 variant described in this thesis lacking the C-terminus ATM phosphorylation sites.

Attempts were made to understand the mechanism by which the MRE11 truncation had occurred. It was concluded that the wild type MRE11 protein was cleaved post-translationally by caspases to produce a less stable truncated MRE11 protein, which was then removed from the cells via proteasomal degradation. Cleavage of the wild type MRE11 protein was enhanced by treatment with the pan-HDAC inhibitor panobinostat, which had previously been shown to have potential as a radiosensitising agent for the treatment of bladder cancer (Groselj *et al*. 2013). It has been hypothesised previously that panobinostat-induced radiosensitisation of bladder cancer cells occurs through the downregulation of HR proteins, such as MRE11 (Groselj *et al*. 2013). This thesis has provided further insight into the mechanism behind this, whereby panobinostat upregulates caspase activity, resulting in cleavage and degradation of MRE11.

It was determined that the truncated MRE11 protein was present in the nuclear fraction of the cells, was still capable of forming a complex with RAD50 and NBS1 and was localised at the sites of DSBs. However, in an MRE11 knockdown cell

line, there was even more deficient repair via HR after expression of the truncated MRE11 protein. This might indicate that there is potentially a dominant negative effect of truncated MRE11 over wild type MRE11.

The discovery of this novel MRE11 variant in bladder cancer cell lines as well as patient samples could have significant clinical implications. Patients who express the truncated MRE11 variant could potentially have a better response to radiotherapy due to deficient homologous repair in their tumours. MRE11 has already been identified as a potential biomarker for radiotherapy response in bladder cancer (Choudhury *et al*. 2010; Laurberg *et al*. 2012). However, the discovery of an MRE11 variant could lead to this protein (i.e. the variant) acting as a biomarker for treatment choice between radiotherapy and cystectomy. The presence of the variant would direct such decisions towards radiotherapy. There is a considerable need for such a biomarker in the treatment of MIBC, in order to improve clinical outcome and patient quality of life.

Several MRE11 variants have been identified previously (Stewart *et al*. 1999; Wen *et al*. 2008; Teo *et al*. 2014; Delia *et al*. 2004; Fukuda *et al*. 2001; Giannini *et al*. 2002), which have helped elucidate its role in DNA repair pathways, as well as the development of potential therapeutic strategies for patients carrying these mutations (Carson *et al*. 2003; Regal *et al*. 2013; Theunissen *et al*. 2003). Similar therapeutic strategies could prove beneficial for bladder cancer patients harbouring the truncated MRE11 variant in their tumour.

6.2 Future plans

Many new questions have arisen from the work conducted during this thesis, opening up several exciting avenues and hypotheses that could be further investigated. The use of the MRE11 variant as a biomarker depends upon showing that the paradoxical result seen between the correlation of patient response to radiotherapy and high MRE11 levels is due to indiscriminate detection of either MRE11 protein. Therefore, further research into differentiating between wild type and variant MRE11 detection is warranted. This is currently underway, using IHC to optimise an antibody that binds to the C-terminus of MRE11 and therefore does not detect the truncated protein. It would be of interest to re-analyse patient samples used in the study by Choudhury *et al.* in order to determine whether the levels of MRE11 reported were due to the wild type MRE11 or the truncated variant, or a combination of both. I would hypothesise that patients with low wild type MRE11/ high truncated MRE11 expression might have improved clinical outcome following radiotherapy compared with patients with high wild type MRE11/low truncated MRE11 expression. As there appears to be no relationship between the expression levels of the two MRE11 proteins, the outcome for patients whose tumours exhibit high expression of both proteins would be intriguing. If the MRE11 variant was acting in a dominant negative manner, it would be expected that these patients would have a better response to radiotherapy.

Another area of interest includes identifying the cleavage site of the truncation, the specific caspase(s) involved and whether panobinostat directly or indirectly increases caspase activity. This research is on-going in our research group. In

addition, research is warranted into the functionality of the truncated MRE11 protein. Although I have hypothesised that this variant could behave in a dominant negative manner, this needs to be investigated through expression of the variant and wild type MRE11 to varying degrees and examining the impact on HR and radiosensitivity. As the attempts to generate a cell line with stable expression of the truncated variant were unsuccessful, this would be a future aim to enable further functional investigation of the variant. Several attempts were made to achieve this and the next approach that would be taken is a conditional MRE11 depletion, to maintain health of the cells, as this influences transfection efficiency. This would be followed by a lentiviral transfection, as lipid transfections conducted in this work have demonstrated poor efficiency.

Also of interest would be the investigation into other cancer types, such as breast, due to similar reports of MRE11 expression correlating with radiotherapy response (Söderlund *et al*. 2007). The collection of further bladder tumour samples from patients and analysis of the truncation is on-going. Although too soon to report in this body of work, the assessment of cause-specific survival (CSS), for patients with expression of the truncated variant, as determined by western blot analysis, will be conducted to provide further insight into the clinical relevance of the truncated MRE11 variant.

References

Al-Hakim A, Escribano-Diaz C, Landry M-C, O'Donnell L, Panier S, Szilard RK, *et al*. The ubiquitous role of ubiquitin in the DNA damage response. DNA Repair. 2010;9(12):1229–40.

Apodaca G. The uroepithelium: Not just a passive barrier. Traffic. 2004;5(3):117–28.

Araki W, Minegishi S, Motoki K, Kume H, Hohjoh H, Araki YM, *et al*. Disease-associated mutations of TDP-43 promote turnover of the protein through the proteasomal pathway. Mol Neurobiol. 2014;1–10.

Arcangeli G, Strigari L, Arcangeli S. Radical cystectomy versus organ-sparing trimodality treatment in muscle-invasive bladder cancer: A systematic review of clinical trials. Crit Rev Oncol Hematol. 2015;1–10.

Babjuk M, Burger M, Zigeuner R, Shariat SF, Sylvester RJ, Kaasinen E, *et al*. EAU guidelines on non-muscle-invasive urothelial carcinoma of the bladder: update 2013. Eur Urol. 2013;64:639–53.

Bakkenist CJ, Kastan MB. DNA damage activates ATM through intermolecular autophosphorylation and dimer dissociation. Nature. 2003;421(6922):499–506.

Banin S, Moyal L, Shieh S, Taya Y, Anderson CW, Chessa L, *et al*. Enhanced phosphorylation of p53 by ATM in response to DNA damage. Science. 1998;281(5383):1674–7.

Bartek J, Lukas C, Lukas J. Checking on DNA damage in S phase. Nat Rev. 2004;5(10):792–804.

Bartkova J, Tommiska J, Oplustilova L, Aaltonen K, Tamminen A, Heikkinen T, *et al*. Aberrations of the MRE11-RAD50-NBS1 DNA damage sensor complex in human breast cancer: MRE11 as a candidate familial cancer-predisposing gene. Mol Oncol. 2008;2(4):296–316.

Bennett CB, Lewis A L, Baldwin KK, Resnick M A. Lethality induced by a single site-specific double-strand break in a dispensable yeast plasmid. Proc Natl Acad Sci U S A. 1993;90(12):5613–7.

Bentley J, Diggle CP, Harnden P, Knowles MA, Kiltie AE. DNA double strand break repair in human bladder cancer is error prone and involves microhomology-associated end-joining. Nucleic Acids Res. 2004;32(17):5249–59.

Bentley J, L'Hôte C, Platt F, Hurst CD, Lowery J, Taylor C, *et al*. Papillary and muscle invasive bladder tumors with distinct genomic stability profiles have different DNA repair fidelity and KU DNA-binding activities. Genes Chromosomes Cancer. 2009;48(4):310–21.

Bétermier M, Bertrand P, Lopez BS. Is non-homologous end-Joining really an inherently error-prone process? PLoS Genet. 2014;10(1):e1004086.

Beucher A, Birraux J, Tchouandong L, Barton O, Shibata A, Conrad S, *et al*. ATM and Artemis promote homologous recombination of radiation-induced DNA double-strand breaks in G2. EMBO J. 2009;28(21):3413–27.

Bohle A, Bock PR. Intravesical Bacillus Calmette-Guerin versus mitomycin C for superficial bladder cancer : a formal meta-analysis of comparative studies on recurrence and toxicity. J Urol. 2003;169:90–5.

Bolden JE, Peart MJ, Johnstone RW. Anticancer activities of histone deacetylase inhibitors. Nat Rev Drug Discov. 2006;5(9):769–84.

Bonner WM, Redon CE, Dickey JS, Nakamura AJ, Sedelnikova O A., Solier S, *et al*. γH2AX and cancer. Nat Rev Cancer. 2008;8(12):957–67.

Bostrom PJ, van Rhijn BWG, Fleshner N, Finelli A, Jewett M, Thoms J, *et al*. Staging and staging errors in bladder cancer. Eur Urol; 2010;9(1):2–9.

Brausi M, Collette L, Kurth K, Van Der Meijden AP, Oosterlinck W, Witjes JA, *et al*. Variability in the recurrence rate at first follow-up cystoscopy after TUR in stage Ta T1 transitional cell carcinoma of the bladder: A combined analysis of seven EORTC studies. Eur Urol. 2002;41(5):523–31.

Bressan DA, Olivares HA, Nelms BE, Petrini JH. Alteration of N-terminal phosphoesterase signature motifs inactivates Saccharomyces cerevisiae Mre11. Genetics. 1998;150(2):591–600.

British Uro-oncology Group. Multi-disciplinary Team (MDT) Guidance for Managing Bladder Cancer. 2013. http://www.baus.org.uk/_userfiles/pages/files/Publications/MDT%20Guidance%20For%20Managing%20Bladder%20Cancer%202013.pdf. Accessed 10 August 2015.

Brown T, Slack R, Rushton L, British Occupational Cancer Burden Study Group. Occupational cancer in Britain. Urinary tract cancers: bladder and kidney. Br J Cancer. 2012;107(Suppl 1):S76–84.

Buis J, Stoneham T, Spehalski E, Ferguson DO. Mre11 regulates CtIP-dependent double-strand break repair by interaction with CDK2. Nat Struct Mol Biol;19(2):246–52.

Buisson R, Dion-Côté A-M, Coulombe Y, Launay H, Cai H, Stasiak AZ, *et al*. Cooperation of breast cancer proteins PALB2 and piccolo BRCA2 in stimulating homologous recombination. Nat Struct Mol Biol; 2010;17(10):1247–54.

Burger M, Catto JWF, Dalbagni G, Grossman HB, Herr H, Karakiewicz P, *et al*. Epidemiology and risk factors of urothelial bladder cancer. Eur Urol. 2013;63(2):234–41.

Burma S, Chen BP, Murphy M, Kurimasa A, Chen DJ. ATM phosphorylates histone H2AX in response to DNA double-strand breaks. J Biol Chem. 2001;276(45):42462–7.

Cancer Research UK. http://www.cancerresearchuk.org/about-cancer/type/bladder-cancer. Accessed 10 August 2015.

Carney JP, Maser RS, Olivares H, Davis EM, Beau L, M. YIII, *et al*. The hMre11/hRad50 protein complex and Nijmegen breakage syndrome: linkage of double strand break repair to the cellular DNA damage response. Cell. 1998;93:477–86.

Carson CT, Schwartz R A, Stracker TH, Lilley CE, Lee D V, Weitzman MD. The Mre11 complex is required for ATM activation and the G2/M checkpoint. EMBO J. 2003;22(24):6610–20.

Chahal R, Sundaram SK, Iddenden R, Forman DF, Weston PMT, Harrison SCW. A study of the morbidity, mortality and long-term survival following radical

cystectomy and radical radiotherapy in the treatment of invasive bladder cancer in Yorkshire. Eur Urol. 2003;43(3):246–57.

Chan DW, Chen BP-C, Prithivirajsingh S, Kurimasa A, Story MD, Qin J, *et al*. Autophosphorylation of the DNA-dependent protein kinase catalytic subunit is required for rejoining of DNA double-strand breaks. Genes Dev. 2002;16(18):2333–8.

Chapman JR, Jackson SP. Phospho-dependent interactions between NBS1 and MDC1 mediate chromatin retention of the MRN complex at sites of DNA damage. EMBO Rep. 2008;9(8):795–801.

Chen L, Trujillo K, Ramos W, Sung P, Tomkinson AE. Promotion of Dnl4-Catalyzed DNA end-joining by the Rad50/Mre11/Xrs2 and Hdf1/Hdf2 complexes. Mol Cell. 2001;8(5):1105–15.

Choi W, Porten S, Kim S, Willis D, Plimack ER, Hoffman-Censits J, *et al*. Identification of distinct basal and luminal subtypes of muscle-invasive bladder cancer with different sensitivities to frontline chemotherapy. Cancer Cell. 2014;25(2):152–65.

Choudhury A, Nelson LD, Teo MTW, Chilka S, Bhattarai S, Johnston CF, *et al*. MRE11 expression is predictive of cause-specific survival following radical radiotherapy for muscle-invasive bladder cancer. Cancer Res. 2010;70(18):7017–26.

Choudhury A, Swindell R, Logue JP, Elliott PA, Livsey JE, Wise M, *et al*. Phase II study of conformal hypofractionated radiotherapy with concurrent gemcitabine in muscle-invasive bladder cancer. J Clin Oncol. 2011;29(6):733–8.

Chowdhury D, Xu X, Zhong X, Ahmed F, Zhong J, Liao J, *et al*. A PP4-Phosphatase complex dephosphorylates γ-H2AX generated during DNA replication. Mol Cell. 2008;31(1):33–46.

Ciechanover A. Proteolysis: from the lysosome to ubiquitin and the proteasome. Nat Rev Mol Cell Biol. 2005;6(1):79–87.

D'Amours D, Jackson SP. The Mre11 complex: at the crossroads of DNA repair and checkpoint signalling. Nat Rev Mol Cell Biol. 2002;3(5):317–27.

Dahm P, Gschwend JE. Malignant non-urothelial neoplasms of the urinary bladder: A Review. Eur Urol. 2003;44(6):672–81.

Damrauer JS, Hoadley KA, Chism DD, Fan C, Tiganelli CJ, Wobker SE, *et al*. Intrinsic subtypes of high-grade bladder cancer reflect the hallmarks of breast cancer biology. PNAS. 2014;111(8):3110–5.

Delia D, Paine M, Buscemi G, Savio C, Palmeri S, Lulli P, *et al*. MRE11 mutations and impaired ATM-dependent responses in an Italian family with ataxia-telangiectasia-like disorder. Hum Mol Genet. 2004;13(18):2155–63.

Dery U, Coulombe Y, Rodrigue A., Stasiak A., Richard S, Masson J-Y. A glycine-arginine domain in control of the human MRE11 DNA repair protein. Mol Cell Biol. 2008;28(9):3058–69.

Desai-mehta A, Cerosaletti KM, Concannon P. Distinct functional domains of Nibrin mediate Mre11 binding, focus formation, and nuclear localization. Mol Cell Biol. 2001;21(6):2184–91.

Donzelli M, Draetta GF. Regulating mammalian checkpoints through Cdc25 inactivation. EMBO Rep. 2003;4(7):671–7.

Dueva R, Iliakis G. Alternative pathways of non-homologous end joining (NHEJ) in genomic instability and cancer. Transl Cancer Res. 2013;2(3):163–77.

Dupré A, Boyer-Chatenet L, Sattler RM, Modi AP, Lee J-H, Nicolette ML, *et al*. A forward chemical genetic screen reveals an inhibitor of the Mre11-Rad50-Nbs1 complex. Nat Chem Biol. 2008;4(2):119–25.

Eble JN, Sauter G, Epstein JI, Sesterhenn IA (Eds.). World Health Organization Classification of Tumours Pathology and Genetics of Tumours of the Urinary System and Male Genital Organs. IARC Press: Lyon, France, 2004.

Escribano-Diaz C, Orthwein A, Fradet-Turcotte A, Xing M, Young JTF, Tkáč J, *et al*. A cell cycle-dependent regulatory circuit composed of 53BP1-RIF1 and BRCA1-CtIP controls DNA repair pathway choice. Mol Cell. 2013;49(5):872–83.

Fajkovic H, Halpern JA, Cha EK, Bahadori A, Chromecki TF, Karakiewicz PI, *et al*. Impact of gender on bladder cancer incidence, staging, and prognosis. World J Urol. 2011;29(4):457–63.

Falck J, Coates J, Jackson SP. Conserved modes of recruitment of ATM, ATR and DNA-PKcs to sites of DNA damage. Nature. 2005;434(7033):605–11.

Fischer U, Jänicke RU, Schulze-Osthoff K. Many cuts to ruin: a comprehensive update of caspase substrates. Cell Death Differ. 2003;10(1):76–100.

Fong PC, Boss DS, Yap TA, Tutt A, Wu P, Mergui-Roelvink M, *et al*. Inhibition of poly(ADP-Ribose) polymerase in tumors from *BRCA* mutation carriers. N Engl J Med. 2009;361(2):123–34.

Franken NAP, Rodermond HM, Stap J, Haveman J, van Bree C. Clonogenic assay of cells in vitro. Nat Protoc. 2006;1(5):2315–9.

Freedman ND, Silverman DT, Hollenbeck AR, Schatzkin A, Abnet CC. Association between smoking and risk of bladder cancer among men and women. JAMA. 2011;306(7):737–45.

Fukuda T, Sumiyoshi T, Takahashi M, Kataoka T, Asahara T, Inui H, *et al*. Alterations of the double-strand break repair gene MRE11 in cancer. Cancer Res. 2001;61(1):23–6.

Gallagher DJ, Milowsky MI. Bladder cancer. Curr Treat Options Oncol. 2009;10:205–15.

Garcia V, Phelps SEL, Gray S, Neale MJ. Bidirectional resection of DNA double-strand breaks by Mre11 and Exo1. Nature. 2011;479(7372):241–4.

Giannini G, Ristori E, Cerignoli F, Rinaldi C, Zani M, Viel A, *et al*. Human MRE11 is inactivated in mismatch repair-deficient cancers. EMBO Rep. 2002;3(3):248–54.

Goebell PJ, Knowles MA. Bladder cancer or bladder cancers? Genetically distinct malignant conditions of the urothelium. Urol Oncol. 2010;28(4):409–28.

Good JS, Harrington KJ. The hallmarks of cancer and the radiation oncologist: Updating the 5Rs of radiobiology. Clin Oncol. 2013;25(10):569–77.

Goodarzi AA, Noon AT, Deckbar D, Ziv Y, Shiloh Y, Löbrich M, *et al*. ATM signaling facilitates repair of DNA double-strand breaks associated with heterochromatin. Mol Cell. 2008;31(2):167–77.

Grabarz A, Guirouilh-Barbat J, Barascu A, Pennarun G, Genet D, Rass E, *et al*. A role for BLM in double-strand break repair pathway choice: prevention of CtIP/Mre11-mediated alternative nonhomologous end-Joining. Cell Rep. 2013;5(1):21–8.

Griffiths TRL. Current perspectives in bladder cancer management. Int J Clin Pract. 2013;67(5):435–48.

Groselj B, Kerr M, Kiltie AE. Radiosensitisation of bladder cancer cells by panobinostat is modulated by Ku80 expression. Radiother Oncol. 2013;108(3):429–33.

Groth P, Orta ML, Elvers I, Majumder MM, Lagerqvist A, Helleday T. Homologous recombination repairs secondary replication induced DNA double-strand breaks after ionizing radiation. Nucleic Acids Res. 2012;40(14):6585–94.

De Jager M, Dronkert ML, Modesti M, Beerens CE, Kanaar R, Van Gent DC. DNA-binding and strand-annealing activities of human Mre11: implications for its roles in DNA double-strand break repair pathways. Nucleic Acids Res. 2001;29(6):1317–25.

De Jager M, Van Noort J, Van Gent DC, Dekker C, Kanaar R, Wyman C. Human Rad50/Mre11 is a flexible complex that can tether DNA ends. Mol Cell. 2001;8(5):1129–35.

Gudjónsson S, Adell L, Merdasa F, Olsson R, Larsson B, Davidsson T, *et al*. Should all patients with non-muscle-invasive bladder cancer receive early intravesical chemotherapy after transurethral resection? The results of a prospective randomised multicentre study. Eur Urol. 2009;55(4):773–80.

Harper J V., Anderson JA, O'Neill P. Radiation induced DNA DSBs: Contribution from stalled replication forks? DNA Repair. 2010;9(8):907–13.

Hautmann RE, Abol-Enein H, Hafez K, Haro I, Mansson W, Mills RD, *et al*. Urinary Diversion. Urology. 2007;69(1):17–49.

Hiel JA, Weemaes CM, van den Heuvel LP, van Engelen BG, Gabreëls FJ, Smeets DF, *et al*. Nijmegen breakage syndrome. J Med Genet. 1996;33(2):153–6.

Hohl M, Kwon Y, Galván SM, Xue X, Tous C, Aguilera A, *et al*. The Rad50 coiled-coil domain is indispensable for Mre11 complex functions. Nat Struct Mol Biol. 2011;18(10):1124–31.

Hopfner K-P, Craig L, Moncalian G, Zinkel R A, Usui T, Owen B A L, *et al*. The Rad50 zinc-hook is a structure joining Mre11 complexes in DNA recombination and repair. Nature. 2002;418(6897):562–6.

Hopfner KP, Karcher A, Craig L, Woo TT, Carney JP, Tainer JA. Structural biochemistry and interaction architecture of the DNA double-strand break repair Mre11 nuclease and Rad50-ATPase. Cell. 2001;105(4):473–85.

Hoskin PJ, Rojas AM, Bentzen SM, Saunders MI. Radiotherapy with concurrent carbogen and nicotinamide in bladder carcinoma. J Clin Oncol. 2010;28(33):4912–8.

Huddart RA, Hall E, Lewis R, Birtle A. Life and death of SPARE (selective bladder preservation against radical excision): Reflections on why the spare trial closed. BJU Int. 2010;106(6):753–5.

International Union Against Cancer (UICC). TNM Classification of Malignant Tumours, 7th edition. Wiley Press: New York, 2009, pp. 262–5.

Jackson SP, Bartek J. The DNA-damage response in human biology and disease. Nature. 2009;461(7267):1071–8.

James ND, Hussain SA, Hall E, Jenkins P, Tremlett J, Rawlings C, *et al*. Radiotherapy with or without chemotherapy in muscle-invasive bladder cancer. N Engl J Med. 2012;366(16):1477–88.

Wouters BG, Begg AC. Irradiation-induced damage and the DNA damage response. In: Basic Clinical Radiobiology, 4th edition. Joiner M, van der Kogel A (Eds.). Hodder Arnold: UK, 2009, pp 11–26.

Kappler M, Kotzsch M, Bartel F, Fussel S, Lautenschluger C, Wurl P, *et al*. Elevated expression level of survivin protein in soft-tissue sarcomas. Clin Cancer Res. 2003;9:1098–104.

Kass EM, Jasin M. Collaboration and competition between DNA double-strand break repair pathways. FEBS Lett. 2010;584(17):3703–8.

Kerr M, Scott HE, Groselj B, Stratford MRL, Karaszi K, Sharma NL, *et al*. Deoxycytidine kinase expression underpins response to gemcitabine in bladder cancer. Clin Cancer Res. 2014;20(21):5435–45.

Khosravi R, Maya R, Gottlieb T, Oren M, Shiloh Y, Shkedy D. Rapid ATM-dependent phosphorylation of MDM2 precedes p53 accumulation in response to DNA damage. PNAS. 1999;96(26):14973–7.

Kijas AW, Lim YC, Bolderson E, Cerosaletti K, Gatei M, Jakob B, *et al*. ATM-dependent phosphorylation of MRE11 controls extent of resection during homology directed repair by signalling through Exonuclease 1. Nucleic Acids Res. 2015;1(3):1–16.

Kiriluk KJ, Prasad SM, Patel AR, Steinberg GD, Smith ND. Bladder cancer risk from occupational and environmental exposures. Urol Oncol. 2012;30(2):199–211.

Knowles M A, Hurst CD. Molecular biology of bladder cancer : new insights into pathogenesis and clinical diversity. Nat Rev. 2015;15(1):25–41.

Konety BR, Allareddy V, Herr H. Complications after radical cystectomy: Analysis of population-based data. Urology. 2006;68(1):58–64.

Kotwal S, Choudhury A, Johnston C, Paul AB, Whelan P, Kiltie AE. Similar treatment outcomes for radical cystectomy and radical radiotherapy in invasive bladder cancer treated at a United Kingdom specialist treatment center. Int J Radiat Oncol Biol Phys. 2008;70(2):456–63.

Labbé K, McIntire CR, Doiron K, Leblanc PM, Saleh M. Cellular inhibitors of apoptosis proteins cIAP1 and cIAP2 are required for efficient caspase-1 activation by the inflammasome. Immunity. 2011;35(6):897–907.

Lamarche BJ, Orazio NI, Weitzman MD. The MRN complex in double-strand break repair and telomere maintenance. FEBS Lett. 2010;584(17):3682–95.

Laurberg JR, Brems-Eskildsen AS, Nordentoft I, Fristrup N, Schepeler T, Ulhøi BP, *et al*. Expression of TIP60 (tat-interactive protein) and MRE11 (meiotic recombination 11 homolog) predict treatment-specific outcome of localised invasive bladder cancer. BJU Int. 2012;110(11):1228–36.

Leach FS, Tokino T, Meltzer P, Burrell M, Oliner JD, Smith S, *et al*. p53 Mutation and MDM2 amplification in human soft tissue sarcomas. Cancer Res. 1993;2231–4.

Lee J-H, Paull TT. Direct activation of the ATM protein kinase by the Mre11/Rad50/Nbs1 complex. Science. 2004;304:93–6.

Levy-Lahad E, Friedman E. Cancer risks among BRCA1 and BRCA2 mutation carriers. Br J Cancer. 2007;96(1):11–5.

Lieber MR. The Mechanism of double-strand DNA break repair by the nonhomologous DNA end-Joining pathway. Annu Rev Biochem. 2010;79(1):181–211.

Limbo O, Chahwan C, Yamada Y, de Bruin RAM, Wittenberg C, Russell P. Ctp1 is a cell-cycle-regulated protein that functions with Mre11 complex to control double-strand break repair by homologous recombination. Mol Cell. 2007;28(1):134–46.

Livak KJ, Schmittgen TD. Analysis of relative gene expression data using real-time quantitative PCR and the 2(-Delta Delta C(T)) method. Methods. 2001;25(4):402–8.

Löbrich M, Shibata A, Beucher A, Fisher A, Ensminger M, Goodarzi AA, *et al*. γH2AX foci analysis for monitoring DNA double-strand break repair: Strengths, limitations and optimization. Cell Cycle. 2010;9(4):662–9.

Lomax ME, Folkes LK, O'Neill P. Biological consequences of radiation-induced DNA damage: Relevance to radiotherapy. Clin Oncol. 2013;25(10):578–85.

Lou Z, Minter-Dykhouse K, Franco S, Gostissa M, Rivera MA, Celeste A, *et al*. MDC1 maintains genomic stability by participating in the amplification of ATM-dependent DNA damage signals. Mol Cell. 2006;21(2):187–200.

Luo G, Yao MS, Bender CF, Mills M, Bladl AR, Bradley A, *et al*. Disruption of mRad50 causes embryonic stem cell lethality, abnormal embryonic development, and sensitivity to ionizing radiation. PNAS. 1999;96(13):7376–81.

Mak RH, Hunt D, Shipley WU, Efstathiou JA, Tester WJ, Hagan MP, *et al*. Long-term outcomes in patients with muscle-invasive bladder cancer after selective

bladder-preserving combined-modality therapy: A pooled analysis of radiation therapy oncology group protocols 8802, 8903, 9506, 9706, 9906, and 0233. J Clin Oncol. 2014;32(34):3801–9.

Malmström PU, Sylvester RJ, Crawford DE, Friedrich M, Krege S, Rintala E, *et al*. An individual patient data meta-analysis of the long-term outcome of randomised studies comparing intravesical mitomycin C versus bacillus Calmette-Guérin for non-muscle-invasive bladder cancer. Eur Urol. 2009;56(2):247–56.

Mariappan P, Zachou A, Grigor KM. Detrusor muscle in the first, apparently complete transurethral resection of bladder tumour specimen is a surrogate marker of resection quality, predicts risk of early recurrence, and is dependent on operator experience. Eur Urol. 2010;57(5):843–9.

Martin RM, Kerr M, Teo MTW, Jevons SJ, Koritzinsky M, Wouters BG, *et al*. Post-transcriptional regulation of MRE11 expression in muscle-invasive bladder tumours. Oncotarget. 2014;5(4):993–1003.

Matsuoka S, Huang M, Elledge SJ. Linkage of ATM to cell cycle regulation by the Chk2 protein kinase. Science. 1998;282:1893–7.

Mazzucchelli R, Cheng L, Lopez-Beltran A, Scarpelli M, Montironi R. Classification and grading of noninvasive and invasive neoplasms of the urothelium. Anal Quant Cytol Histol. 2012;34(3):111–9.

McGrath M, Michaud DS, De Vivo I. Hormonal and reproductive factors and the risk of bladder cancer in women. Am J Epidemiol. 2006;163(3):236–44.

McVey M, Lee SE. MMEJ repair of double-strand breaks (director's cut): deleted sequences and alternative endings. Trends Genet. 2008;24(11):529–38.

Mladenov E, Magin S, Soni A, Iliakis G. DNA double-strand break repair as determinant of cellular radiosensitivity to killing and target in radiation therapy. Front Oncol. 2013;3:1–18.

Morgan WF, Sowa MB. Effects of ionizing radiation in nonirradiated cells. PNAS. 2005;102(40):14127–8.

Morrison CD, Liu P, Woloszynska-Read A, Zhang J, Luo W, Qin M, *et al*. Whole-genome sequencing identifies genomic heterogeneity at a nucleotide and chromosomal level in bladder cancer. PNAS. 2014;111(6):672–81.

Mostafid H, Brausi M. Measuring and improving the quality of transurethral resection for bladder tumour (TURBT). BJU Int. 2012;109(11):1579–82.

Moynahan ME, Jasin M. Mitotic homologous recombination maintains genomic stability and suppresses tumorigenesis. Nat Rev Mol Cell Biol. 2010;11(3):196–207.

Nicholson S. Chemotherapy for bladder cancer in patients with impaired renal function. Nat Rev Urol;9(1):52–7.

Nieuwenhuijzen JA, de Vries RR, Bex A, van der Poel HG, Meinhardt W, Antonini N, *et al*. Urinary diversions after cystectomy: The association of clinical factors, complications and functional results of four different diversions. Eur Urol. 2008;53(4):834–44.

Office for National Statistics. Statistical Bulletin Cancer Survival in England: Patients Diagnosed 2007 – 2011 and Followed up to 2012. Office for National Statistics. 2014.

Pal T, Permuth-Wey J, Betts JA, Krischer JP, Fiorica J, Arango H, *et al*. BRCA1 and BRCA2 mutations account for a large proportion of ovarian carcinoma cases. Cancer. 2005;104(12):2807–16.

Panier S, Boulton SJ. Double-strand break repair: 53BP1 comes into focus. Nat Rev. 2014;15(1):7–18.

Pappin DJC, Creasy DM, Cottrell JS. Probability-based protein identification by searching sequence databases using mass spectrometry data. Electrophoresis. 1999;3551–67.

Parrish AB, Freel CD, Kornbluth S. Cellular mechanisms controlling caspase activation and function. Cold Spring Harb Perspect Biol. 2013;1–24.

Paull TT, Gellert M. The 3’ to 5' exonuclease activity of Mre11 facilitates repair of DNA double-strand breaks. Mol Cell. 1998;1(7):969–79.

Ploeg M, Aben KKH, Kiemeney LA. The present and future burden of urinary bladder cancer in the world. World J Urol. 2009;27(3):289–93.

Ploussard G, Daneshmand S, Efstathiou JA, Herr HW, James ND, Rödel CM, *et al*. Critical analysis of bladder sparing with trimodal therapy in muscle-invasive bladder cancer: A systematic review. Eur Urol. 2014;66(1):120–37.

Poreba M, Strózyk A, Salvesen GS, Drag M. Caspase substrates and inhibitors. Cold Spring Harb Perspect Biol. 2013;5(8):1–20.

Qvist P, Huertas P, Jimeno S, Nyegaard M, Hassan MJ, Jackson SP, *et al*. CtIP mutations cause Seckel and Jawad Syndromes. PLoS Genet. 2011;7(10):e1002310.

Ramadan K, Meerang M. Degradation-linked ubiquitin signal and proteasome are integral components of DNA double strand break repair: New perspectives for anti-cancer therapy. FEBS Lett. 2011;585(18):2868–75.

Ree AH, Dueland S, Folkvord S, Hole KH, Seierstad T, Johansen M, *et al*. Vorinostat, a histone deacetylase inhibitor, combined with pelvic palliative radiotherapy for gastrointestinal carcinoma: the Pelvic Radiation and Vorinostat (PRAVO) phase 1 study. Lancet Oncol. 2010;11(5):459–64.

Regal JA, Festerling TA, Buis JM, Ferguson DO. Disease-associated MRE11 mutants impact ATM/ATR DNA damage signaling by distinct mechanisms. Hum Mol Genet. 2013;1–14.

Rigby L, Muscat A, Ashley D, Algar E. Methods for the analysis of histone H3 and H4 acetylation in blood. Epigenetics. 2012;2(8):875–82.

Rodriguez R, Hansen LT, Phear G, Scorah J, Spang-Thomsen M, Cox A, *et al*. Thymidine selectively enhances growth suppressive effects of camptothecin/irinotecan in MSI+ cells and tumors containing a mutation of MRE11. Clin Cancer Res. 2008;14(17):5476–83.

Rosenberg JE, Carroll PR, Small EJ. Update on chemotherapy for advanced bladder cancer. J Urol. 2005;174(1):14–20.

Rupnik A, Lowndes NF, Grenon M. MRN and the race to the break. Chromosoma. 2010;119(2):115–35.

Sartori AA, Lukas C, Coates J, Mistrik M, Fu S, Bartek J, *et al*. Human CtIP promotes DNA end resection. Nature. 2007;450:509–14.

Satoh K, Kaneko K, Hirota M, Masamune a, Satoh a, Shimosegawa T. Expression of survivin is correlated with cancer cell apoptosis and is involved in the development of human pancreatic duct cell tumors. Cancer. 2001;92(2):271–8.

Schaue D, McBride WH. Opportunities and challenges of radiotherapy for treating cancer. Nat Rev Clin Oncol. 2015;12(9):527–40.

Seluanov A, Mao Z, Gorbunova V. Analysis of DNA double-strand break (DSB) repair in mammalian cells. J Vis Exp. 2010:1–6.

Shalini S, Dorstyn L, Dawar S, Kumar S. Old, new and emerging functions of caspases. Cell Death Differ. 2015;22(4):526–39.

Shao Z, Davis AJ, Fattah KR, So S, Sun J, Lee K-J, *et al*. Persistently bound Ku at DNA ends attenuates DNA end resection and homologous recombination. DNA Repair, 2012;11(3):310–6.

Shelley MD, Wilt TJ, Court J, Coles B, Kynaston H, Mason MD. Intravesical bacillus Calmette-Guerin is superior to mitomycin C in reducing tumour recurrence in high-risk superficial bladder cancer: a meta-analysis of randomized trials. BJU Int. 2004;93:485–90.

Shibata A, Moiani D, Arvai AS, Perry J, Harding SM, Genois M-M, *et al*. DNA Double-Strand Break Repair Pathway Choice Is Directed by Distinct MRE11 Nuclease Activities. Mol Cell. 2014;53:1–12.

Shrivastav M, De Haro LP, Nickoloff J A. Regulation of DNA double-strand break repair pathway choice. Cell Res. 2008;18(1):134–47.

Sievert KD, Amend B, Nagele U, Schilling D, Bedke J, Horstmann M, *et al*. Economic aspects of bladder cancer: What are the benefits and costs? World J Urol. 2009;27(3):295–300.

Sjödahl G, Lauss M, Lövgren K, Chebil G, Gudjonsson S, Veerla S, *et al*. A molecular taxonomy for urothelial carcinoma. Clin Cancer Res. 2012;18(12):3377–86.

Smith GC, d'Adda di Fagagna F, Lakin ND, Jackson SP. Cleavage and inactivation of ATM during apoptosis. Mol Cell Biol. 1999;19(9):6076–84.

Söderlund K, Stål O, Skoog L, Rutqvist LE, Nordenskjöld B, Askmalm MS. Intact Mre11/Rad50/Nbs1 Complex Predicts Good Response to Radiotherapy in Early Breast Cancer. Int J Radiat Oncol Biol Phys. 2007;68(1):50–8.

Sørensen CS, Syljuåsen RG, Falck J, Schroeder T, Rönnstrand L, Khanna KK, *et al*. Chk1 regulates the S phase checkpoint by coupling the physiological turnover and ionizing radiation-induced accelerated proteolysis of Cdc25A. Cancer Cell. 2003;3(3):247–58.

Stewart GS, Maser RS, Stankovic T, Bressan DA, Kaplan MI, Jaspers NG, *et al*. The DNA double-strand break repair gene hMRE11 is mutated in individuals with an ataxia-telangiectasia-like disorder. Cell. 1999;99(6):577–87.

Sullivan KD, Gallant-Behm CL, Henry RE, Fraikin JL, Espinosa JM. The p53 circuit board. Biochim Biophys Acta. 2012;1825(2):229–44.

Surova O, Zhivotovsky B. Various modes of cell death induced by DNA damage. Oncogene. 2013;32(33):3789–97.

Swenberg JA, Lu K, Moeller BC, Gao L, Upton PB, Nakamura J, *et al*. Endogenous versus exogenous DNA adducts: Their role in carcinogenesis, epidemiology, and risk assessment. Toxicol Sci. 2011;120:130–45.

Sylvester RJ, Van Der Meijden APM, Oosterlinck W, Witjes JA, Bouffioux C, Denis L, *et al*. Predicting recurrence and progression in individual patients with stage Ta T1 bladder cancer using EORTC risk tables: A combined analysis of 2596 patients from seven EORTC trials. Eur Urol. 2006;49(3):466–75.

Sylvester RJ, Willem O, van der Meijden APM. A single immediate postoperative instillation of chemotherapy decreases the risk of recurrence in patients with stage Ta T1 bladder cancer: a meta-analysis of published results of randomized clinical trials. J Urol. 2004;171(6):2186–90.

Tanaka K, Iwamoto S, Gon G, Nohara T, Iwamoto M, Tanigawa N. Expression of survivin and its relationship to loss of apoptosis in breast carcinoma. Clin Cancer Res. 2000;6:127–34.

Tauchi H, Kobayashi J, Morishima K, Gent DC van, Shiraishi T, Verkaik NS, *et al*. Nbs1 is essential for DNA repair by homologous recombination in higher vertebrate cells. Nature. 2002;420:93–8.

Teo MTW, Dyrskjøt L, Nsengimana J, Buchwald C, Snowden H, Morgan J, *et al*. Next-generation sequencing identifies germline MRE11A variants as markers of radiotherapy outcomes in muscle-invasive bladder cancer. Ann Oncol. 25(4):877–83.

Tewari M, Quan LT, O'Rourke K, Desnoyers S, Zeng Z, Beidler DR, *et al*. Yama/CPP32 beta, a mammalian homolog of CED-3, is a CrmA-inhibitable protease that cleaves the death substrate poly(ADP-ribose) polymerase. Cell. 1995;81(5):801–9.

The Cancer Genome Atlas Research Network. Comprehensive molecular characterization of urothelial bladder carcinoma. Nature. 2014;507:315–22.

Theunissen JF, Kaplan MI, Hunt PA, Williams BR, Ferguson DO, Alt FW, *et al*. Checkpoint failure and chromosomal instability without lymphomagenesis in Mre11 ATLD1/ ATLD1 Mice. Mol Cell. 2003;12:1511–23.

Truong LN, Li Y, Shi LZ, Hwang PY, He J, Wang H, *et al*. Microhomology-mediated end joining and homologous recombination share the initial end resection step to repair DNA double-strand breaks in mammalian cells. PNAS. 2013;110:7720–5.

Tutt A, Robson M, Garber JE, Domchek SM, Audeh MW, Weitzel JN, *et al*. Oral poly(ADP-ribose) polymerase inhibitor olaparib in patients with BRCA1 or BRCA2 mutations and recurrent ovarian cancer: A proof-of-concept trial. Lancet. 2010;376:245–51.

Uchisaka N, Takahashi N, Sato M, Kikuchi A, Mochizuki S, Imai K, *et al*. Two brothers with Ataxia-Telangiectasia-like disorder with lung adenocarcinoma. J Pediatr. 2009;155(3):435–8.

Usui T, Ohta T, Oshiumi H, Tomizawa J, Ogawa H, Ogawa T. Complex formation and functional versatility of Mre11 of budding yeast in recombination. Cell. 1998;95(5):705–16.

Uziel T, Lerenthal Y, Moyal L, Andegeko Y, Mittelman L, Shiloh Y. Requirement of the MRN complex for ATM activation by DNA damage. EMBO J. 2003;22(20):5612–21.

Vakkala M, Pääkkö P, Soini Y. Expression of caspases 3, 6 and 8 is increased in parallel with apoptosis and histological aggressiveness of the breast lesion. Br J Cancer. 1999;81(4):592–9.

Van der Linden E, Sanchez H, Kinoshita E, Kanaar R, Wyman C. RAD50 and NBS1 form a stable complex functional in DNA binding and tethering. Nucleic Acids Res. 2009;37(5):1580–8.

Waltes R, Kalb R, Gatei M, Kijas AW, Stumm M, Sobeck A, *et al*. Human RAD50 deficiency in a Nijmegen Breakage Syndrome-like Disorder. Am J Hum Genet. 2009;84(5):605–16.

Wang H, Shi LZ, Wong CCL, Han X, Hwang PY-H, Truong LN, *et al*. The interaction of CtIP and Nbs1 connects CDK and ATM to regulate HR-mediated double-strand break repair. PLoS Genet. 2013;9(2):e1003277.

Wang J, Zhang X, Wei P, Zhang J, Niu Y, Kang N, *et al*. Livin, Survivin and Caspase 3 as early recurrence markers in non-muscle-invasive bladder cancer. World J Urol. 2014;32(6):1477–84.

Wang Z, Zang C, Cui K, Schones DE, Barski A, Peng W, *et al*. Genome-wide mapping of HATs and HDACs reveals distinct functions in active and inactive genes. Cell. 2009;138(5):1019–31.

Weikert S, Christoph F, Schrader M, Krause H, Miller K, Müller M. Quantitative analysis of survivin mRNA expression in urine and tumor tissue of bladder cancer patients and its potential relevance for disease detection and prognosis. Int J Cancer. 2005;116(1):100–4.

Wen Q, Scorah J, Phear G, Rodgers G, Rodgers S, Mark M. A mutant allele of MRE11 found in mismatch repair-deficient tumor cells suppresses the cellular response to DNA replication fork stress in a dominant negative manner. Mol Biol Cell. 2008;19(1):308–17.

West AC, Johnstone RW. New and emerging HDAC inhibitors for cancer treatment. J Clin Invest. 2014;124(1):30–9.

Williams GJ, Lees-Miller SP, Tainer JA. Mre11-Rad50-Nbs1 conformations and the control of sensing, signaling, and effector responses at DNA double-strand breaks. DNA Repair. 2010;9(12):1299–306.

Williams NS, Gaynor RB, Scoggin S, Verma U, Gokaslan T, Simmang C, *et al*. Identification and validation of genes involved in the pathogenesis of colorectal cancer using cDNA microarrays and RNA interference. Clin Cancer Res. 2003;9:931–46.

Williams RS, Dodson GE, Limbo O, Yamada Y, Williams JS, Guenther G, *et al*. Nbs1 flexibly tethers Ctp1 and Mre11-Rad50 to coordinate DNA double-strand break processing and repair. Cell. 2009;139(1):87–99.

Williams RS, Williams JS, Tainer JA. Mre11-Rad50-Nbs1 is a keystone complex connecting DNA repair machinery, double-strand break signaling, and the chromatin template. Biochem Cell Biol. 2007;85(4):509–20.

Witjes JA, Compérat E, Cowan NC, De Santis M, Gakis G, Lebret T, *et al*. EAU guidelines on muscle-invasive and metastatic bladder cancer: Summary of the 2013 guidelines. Eur Urol. 2014;65(4):778–92.

Wu L, Luo K, Lou Z, Chen J. MDC1 regulates intra-S-phase checkpoint by targeting NBS1 to DNA double-strand breaks. PNAS. 2008;105(32):11200–5.

Xiao Y, Weaver DT. Conditional gene targeted deletion by Cre recombinase demonstrates the requirement for the double-strand break repair Mre11 protein in murine embryonic stem cells. Nucleic Acids Res. 1997;25(15):2985–91.

Xiao Z, Chen Z, Gunasekera AH, Sowin TJ, Rosenberg SH, Fesik S, *et al*. Chk1 mediates S and G2 arrests through Cdc25A degradation in response to DNA-damaging agents. J Biol Chem. 2003;278(24):21767–73.

Xie C, Drenberg C, Edwards H, Caldwell JT, Chen W, Inaba H, *et al*. Panobinostat enhances cytarabine and daunorubicin sensitivities in AML cells through suppressing the expression of BRCA1, CHK1, and Rad51. PLoS One. 2013;8(11).

Yajima H, Fujisawa H, Nakajima NI, Hirakawa H, Jeggo PA, Okayasu R, *et al*. The complexity of DNA double strand breaks is a critical factor enhancing end-resection. DNA Repair. 2013;12(11):936–46.

Yang L, Cao Z, Yan H, Wood WC. Coexistence of high levels of apoptotic signaling and inhibitor of apoptosis proteins in human tumor cells: Implication for cancer specific therapy. Cancer Res. 2003;63:6815–24.

Yi C, Yuan J. The Jekyll and Hyde functions of caspases. Dev Cell. 2010;16(1):21–34.

Yu X, Chen J. DNA damage-induced cell cycle checkpoint control requires CtIP , a phosphorylation-dependent binding partner of BRCA1 C-terminal domains. Mol Cell Biol. 2004;24:9478–86.

Yuan J, Chen J. N terminus of CtIP is critical for homologous recombination-mediated double-strand break repair. J Biol Chem. 2009;284(46):31746–52.

Zha S, Boboila C, Alt FW. Mre11: roles in DNA repair beyond homologous recombination. Nat Struct Mol Biology. 2009;16(8):798–800.

Zheng Y-L, Amr S, Saleh DA, Dash C, Ezzat S, Mikhail NN, *et al*. Urinary bladder cancer risk factors in egypt: A multicenter case-control study. Cancer Epidemiol Biomarkers Prev. 2012;21(3):537–46.

Zhu J, Petersen S, Tessarollo L, Nussenzweig A. Targeted disruption of the Nijmegen breakage syndrome gene NBS1 leads to early embryonic lethality in mice. Curr Biol. 2001;11(2):105–9.

Zhuang J, Jiang G, Willers H, Xia F. Exonuclease function of human Mre11 promotes deletional nonhomologous end joining. J Biol Chem. 2009;284(44):30565–73.

Zuiverloon TCM, Beukers W, Van Der Keur K a., Nieuweboer AJM, Reinert T, Dyrskjot L, *et al*. Combinations of urinary biomarkers for surveillance of patients with incident nonmuscle invasive bladder cancer: The European FP7 UROMOL project. J Urol. 2013;189(5):1945–51.

APPENDICES A-G

Appendix A: Mass spectrometry analysis of MRE11

Ai: MASCOT peptide sequence of wild type MRE11 after tryptic digest.

Aii: MASCOT peptide sequence of wild type MRE11 after tryptic digest "top hits".

Aiii: MASCOT peptide sequence of wild type MRE11 after elastase digest.

Aiiii: MASCOT peptide sequence of wild type MRE11 after elastase digest "top hits".

Av: MASCOT peptide sequence of MRE11 variant after tryptic digest.

Avi: MASCOT peptide sequence of MRE11 variant after tryptic digest "top hits".

Avii: MASCOT peptide sequence of MRE11 variant after elastase digest.

Aviii: MASCOT peptide sequence of MRE11 variant after elastase digest "top hits".

Appendix B: MRN complex expression in the CAL29 cell line after 48 hr treatment with gemcitabine.

Appendix C: Melting temperature profiles for *CASP* primers.

Appendix D: Restriction enzyme digest of plasmid DNA from shRNA MRE11 plasmid clones.

Appendix E: Cytotoxicity curves of the MRE11 inhibitors in the RT112 cell line.

Appendix F: Co-transfection of the *I-SceI* and HA-tagged MRE11 plasmids used during the HR assay.

Appendix G: Published papers.

Appendices A-G

Appendix Ai. MASCOT analysis of wild type MRE11 after tryptic digest.

MASCOT Search Results

Protein View: P49959

RecName: Full=Double-strand break repair protein MRE11A; AltName: Full=Meiotic recombination 11 homolog 1; Short=MRE11 homolog 1; AltName: Full=Meiotic recombination 11 homolog A; Short=MRE11 homolog A;

Database:	UniProt_SwissProt
Score:	777
Nominal mass (M_r):	80885
Calculated pI:	5.61
Taxonomy:	Homo sapiens

Sequence similarity is available as an NCBI BLAST search of P49959 against nr.

Search parameters

MS data file:	E:\mgf_Orbi\OTE0297_SarahJevons_Tryp_2.mgf
Enzyme:	Trypsin: cuts C-term side of KR unless next residue is P.
Fixed modifications:	Carbamidomethyl (C)
Variable modifications:	Deamidated (N), Deamidated (Q), Oxidation (M)

Protein sequence coverage: 42%

Matched peptides shown in ***bold red***.

```
   1 MSTADALDDE NTFKILVATD IHLGFMEKDA VRGNDTFVTL DEILRLAQEN
  51 EVDFILLGGD LFHENKPSRK TLHTCLELLR KYCMGDRPVQ FEILSDQSVN
 101 FGFSKFPWVN YQDGNLNISI PVFSIHGNHD DPTGADALCA LDILSCAGFV
 151 NHFGRSMSVE KIDISPVLLQ KGSTKIALYG LGSIPDERLY RMFVNKKVTM
 201 LRPKEDENSW FNLFVIHQNR SKHGSTNFIP EQFLDDFIDL VIWGHEHECK
 251 IAPTKNEQQL FYISQPGSSV VTSLSPGEAV KKHVGLLRIK GRKMNMHKIP
 301 LHTVRQFFME DIVLANHPDI FNPDNPKVTQ AIQSFCLEKI EEMLENAERE
 351 RLGNSHQPEK PLVRLRVDYS GGFEPFSVLR FSQKFVDRVA NPKDIIHFFR
 401 HREQKEKTGE EINFGKLITK PSEGTTLRVE DLVKQYFQTA EKNVQLSLLT
 451 ERGMGEAVQE FVDKEEKDAI EELVKYQLEK TQRFLKERHI DALEDKIDEE
 501 VRRFRETRQK NTNEEDDEVR EAMTRARALR SQSEESASAF SADDLMSIDL
 551 AEQMANDSDD SISAATNKGR GRGRGRRGGR GQNSASRGGS QRGRADTGLE
 601 TSTRSRNSKT AVSASRNMSI IDAFKSTRQQ PSRNVTTKNY SEVIEVDESD
 651 VEEDIFPTTS KTDQRWSSTS SSKIMSQSQV SKGVDFESSE DDDDDPFMNT
 701 SSLRRNRR
```

Unformatted sequence string: 708 residues (for pasting into other applications).

Query	Start – End	Observed	Mr(expt)	Mr(calc)	ppm	M	Score	Expect	Rank	U	Peptide
8159	29 – 45	967.5041	1932.9937	1932.9905	1.68	1	22	0.043	1	U	K.DAVRGNDTFVTLDEILR.L
5517	33 – 45	747.3777	1492.7408	1492.7409	-0.078	0	31	0.0013	1	U	R.GNDTFVTLDEILR.L + Deamidated (N)
7394	156 – 171	894.0020	1785.9894	1785.9910	-0.92	1	38	0.00042	1	U	R.SMSVEKIDISPVLLQK.G
7521	156 – 171	901.9984	1801.9822	1801.9859	-2.09	1	24	0.026	1	U	R.SMSVEKIDISPVLLQK.G + Oxidation (M)
7522	156 – 171	601.6690	1801.9852	1801.9859	-0.40	1	33	0.0079	1	U	R.SMSVEKIDISPVLLQK.G + Oxidation (M)
7536	156 – 171	902.5032	1802.9918	1801.9859	558	1	54	1.3e-05	1	U	R.SMSVEKIDISPVLLQK.G + Oxidation (M)
2346	162 – 171	563.3474	1124.6801	1124.6805	-0.31	0	40	0.00034	1	U	K.IDISPVLLQK.G
4700	176 – 188	702.3799	1402.7453	1402.7456	-0.19	0	79	5.8e-08	1	U	K.IALYGLGSIPDER.L
8634	205 – 220	683.6594	2047.9563	2047.9388	8.53	0	22	0.21	1	U	K.EDENSWFNLFVIHQNR.S + Deamidated (N)
10836	251 – 281	1092.5757	3274.7052	3274.7085	-1.00	1	58	3.3e-06	1	U	K.IAPTKNEQQLFYISQPGSSVVTSLSPGEAVK.K
10839	251 – 281	1092.9113	3275.7119	3274.7085	306	1	40	0.00017	1	U	K.IAPTKNEQQLFYISQPGSSVVTSLSPGEAVK.K
10840	251 – 281	819.9362	3275.7158	3275.6925	7.10	1	24	0.064	1	U	K.IAPTKNEQQLFYISQPGSSVVTSLSPGEAVK.K + Deamidated (Q)
10841	251 – 281	820.1858	3276.7141	3275.6925	312	1	25	0.0066	1	U	K.IAPTKNEQQLFYISQPGSSVVTSLSPGEAVK.K + Deamidated (Q)
10094	256 – 281	922.8069	2765.3990	2764.3919	364	0	24	0.0066	1	U	K.NEQQLFYISQPGSSVVTSLSPGEAVK.K
10191	256 – 282	965.1686	2892.4839	2892.4869	-1.03	1	32	0.00092	1	U	K.NEQQLFYISQPGSSVVTSLSPGEAVKK.H
10192	256 – 282	965.5042	2893.4908	2893.4709	6.88	1	57	4.7e-05	1	U	K.NEQQLFYISQPGSSVVTSLSPGEAVKK.H + Deamidated (Q)
10193	256 – 282	965.8392	2894.4957	2893.4709	354	1	25	0.0047	1	U	K.NEQQLFYISQPGSSVVTSLSPGEAVKK.H + Deamidated (Q)
159	283 – 288	347.7215	693.4284	693.4286	-0.21	0	22	0.023	1	U	K.HVGLLR.I
678	299 – 305	418.2607	834.5069	834.5076	-0.83	0	27	0.007	1	U	K.IPLHTVR.Q
9946	306 – 327	868.0879	2601.2418	2601.2210	8.03	0	26	0.0089	1	U	R.QFFMEDIVLANHPDIFNPDNPK.V + Deamidated (N)
9963	306 – 327	873.7526	2618.2359	2617.2159	390	0	31	0.032	1	U	R.QFFMEDIVLANHPDIFNPDNPK.V + Deamidated (Q); Oxidation (M)
4873	328 – 339	712.3661	1422.7177	1422.7177	0.036	0	42	0.00079	1	U	K.VTQAIQSFCLEK.I
5316	352 – 364	492.2755	1473.8045	1473.8052	-0.45	0	35	0.00048	1	U	R.LGNSHQFEKPLVR.L
5317	352 – 364	492.2755	1473.8047	1473.8052	-0.33	0	36	0.00078	1	U	R.LGNSHQFEKPLVR.L
5319	352 – 364	737.9099	1473.8051	1473.8052	-0.028	0	30	0.0074	1	U	R.LGNSHQFEKPLVR.L
5331	352 – 364	492.6000	1474.7782	1474.7892	-7.48	0	29	0.0035	1	U	R.LGNSHQFEKPLVR.L + Deamidated (N)
5332	352 – 364	492.6038	1474.7895	1474.7892	0.17	0	25	0.0049	1	U	R.LGNSHQFEKPLVR.L + Deamidated (N)
7740	365 – 380	614.6562	1840.9469	1840.9472	-0.15	1	39	0.0013	1	U	R.LRVDYSGGFEPFSVLR.F
7741	365 – 380	921.4819	1840.9492	1840.9472	1.09	1	28	0.0023	1	U	R.LRVDYSGGFEPFSVLR.F
7747	365 – 380	614.9909	1841.9509	1840.9472	545	1	23	0.034	1	U	R.LRVDYSGGFEPFSVLR.F
6160	367 – 380	786.8886	1571.7625	1571.7620	0.33	0	36	0.00041	1	U	R.VDYSGGFEPFSVLR.F
1698	381 – 388	513.7723	1025.5300	1025.5294	0.56	1	32	0.0052	1	U	R.FSQKFVDR.V
3430	406 – 416	626.3140	1250.6134	1250.6143	-0.70	1	55	1.1e-05	1	U	K.EKTGEEINFGK.L
1474	408 – 416	498.2375	994.4605	994.4607	-0.24	0	24	0.017	1	U	K.TGEEINFGK.L + Deamidated (N)
9054	435 – 452	723.3829	2167.1270	2167.1273	-0.15	1	25	0.0079	1	U	K.QYFQTAEKNVQLSLLTER.G
2746	443 – 452	586.8349	1171.6552	1171.6561	-0.70	0	22	0.024	1	U	K.NVQLSLLTER.G
2747	443 – 452	586.8351	1171.6557	1171.6561	-0.28	0	53	0.00012	1	U	K.NVQLSLLTER.G
3909	465 – 475	651.8380	1301.6615	1301.6714	-7.64	1	24	0.12	2	U	K.EEKDAIEELVK.Y
3512	593 – 604	632.3171	1262.6196	1262.6215	-1.49	1	22	0.0084	1	U	R.GRADTGLETSTR.S
3513	593 – 604	421.8810	1262.6212	1262.6215	-0.22	1	26	0.035	1	U	R.GRADTGLETSTR.S
1846	595 – 604	525.7565	1049.4985	1049.4989	-0.39	0	47	0.00059	1	U	R.ADTGLETSTR.S
1759	617 – 625	519.7679	1037.5213	1037.5215	-0.20	0	27	0.05	1	U	R.NMSIIDAFK.S
9987	639 – 661	882.4066	2644.1978	2644.1916	2.37	0	27	0.0032	1	U	K.NYSEVIEVDESDVEEDIFPTTSK.T
9989	639 – 661	882.7414	2645.2024	2644.1916	382	0	25	0.0042	1	U	K.NYSEVIEVDESDVEEDIFPTTSK.T
9988	639 – 661	882.7347	2645.1822	2645.1756	2.51	0	21	0.2	1	U	K.NYSEVIEVDESDVEEDIFPTTSK.T + Deamidated (N)
10419	639 – 665	1049.4852	3145.4339	3145.4099	7.62	1	27	0.055	1	U	K.NYSEVIEVDESDVEEDIFPTTSKTDQR.W + Deamidated (Q)
10420	639 – 665	1049.8204	3146.4395	3145.4099	327	1	22	0.018	1	U	K.NYSEVIEVDESDVEEDIFPTTSKTDQR.W + Deamidated (Q)
1549	674 – 682	504.2630	1006.5114	1006.5117	-0.33	0	28	0.041	1	U	K.IMSQSQVSK.G
9748	683 – 704	827.0004	2477.9795	2477.9653	5.72	0	25	0.0077	1	U	K.GVDFESSEDDDDDPFMNTSSLR.R + Deamidated (N)
9977	683 – 705	878.7021	2633.0844	2633.0824	0.78	1	46	8.3e-05	1	U	K.GVDFESSEDDDDDPFMNTSSLRR.N
9982	683 – 705	879.3703	2635.0891	2634.0664	388	1	54	8.6e-06	1	U	K.GVDFESSEDDDDDPFMNTSSLRR.N + Deamidated (N)
9996	683 – 705	884.0331	2649.0776	2649.0773	0.11	1	40	0.00019	1	U	K.GVDFESSEDDDDDPFMNTSSLRR.N + Oxidation (M)
9997	683 – 705	884.3679	2650.0817	2650.0613	7.71	1	44	0.00024	1	U	K.GVDFESSEDDDDDPFMNTSSLRR.N + Deamidated (N); Oxidation (M)

Appendix Aii. MASCOT analysis of wild type MRE11 after tryptic digest "top hits".

MASCOT Search Results

User : bmk
E-mail :
Search title : RK OTE0297_SarahJevons_Tryp_2.mgf
MS data file : E:\mgf_Orbi\OTE0297_SarahJevons_Tryp_2.mgf
Database : UniProt_SwissProt 20131208 (541,762 sequences; 192,577,305 residues)
Taxonomy : Homo sapiens (human) (20,353 sequences)
Timestamp : 19 Sep 2014 at 15:07:00 GMT

Not what you expected? Try the select summary.

Search parameters

Score distribution

Legend

Protein Family Summary

Significance threshold p< 0.05 Max. number of families AUTO
Ions score or expect cut-off 0 Dendrograms cut at 0
Show Percolator scores
Preferred taxonomy All entries

Decoy search summary (reversed protein sequences)

Protein families 1–10 (out of 296)

10 per page 1 2 3 4 5 6 ... 30 Next

1		Q9UHB6	1584	RecName: Full=LIM domain and actin-binding protein 1; AltName: Full=Epithelial protein lost in neoplasm;
2		Q15149	1366	RecName: Full=Plectin; Short=PCN; Short=PLTN; AltName: Full=Hemidesmosomal protein 1; Short=HD1; AltName: Full=Plectin-1;
3	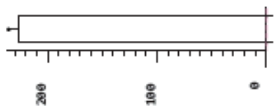	1 P14923 2 P35222	1195 464	RecName: Full=Junction plakoglobin; AltName: Full=Catenin gamma; AltName: Full=Desmoplakin III; AltName: Full=Desmoplakin-... RecName: Full=Catenin beta-1; AltName: Full=Beta-catenin;
4		Q16891	910	RecName: Full=Mitochondrial inner membrane protein; AltName: Full=Cell proliferation-inducing gene 4/52 protein; AltName: Full=...
5	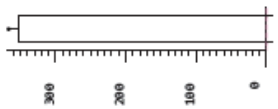	1 O43707 2 P12814	869 784	RecName: Full=Alpha-actinin-4; AltName: Full=F-actin cross-linking protein; AltName: Full=Non-muscle alpha-actinin 4; RecName: Full=Alpha-actinin-1; AltName: Full=Alpha-actinin cytoskeletal isoform; AltName: Full=F-actin cross-linking protein; AltN...

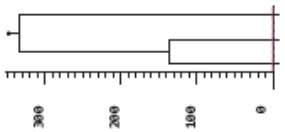

6	1 P35579	814	RecName: Full=Myosin-9; AltName: Full=Cellular myosin heavy chain, type A; AltName: Full=Myosin heavy chain 9; AltName: Full...
	2 Q7Z406	526	RecName: Full=Myosin-14; AltName: Full=Myosin heavy chain 14; AltName: Full=Myosin heavy chain, non-muscle IIc; AltName: F...
	3 P35580	226	RecName: Full=Myosin-10; AltName: Full=Cellular myosin heavy chain, type B; AltName: Full=Myosin heavy chain 10; AltName: F...
7	P49959	805	RecName: Full=Double-strand break repair protein MRE11A; AltName: Full=Meiotic recombination 11 homolog 1; Short=MRE11 ho...

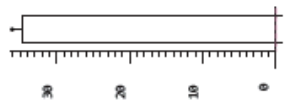

8	1 Q01082	773	RecName: Full=Spectrin beta chain, non-erythrocytic 1; AltName: Full=Beta-II spectrin; AltName: Full=Fodrin beta chain; AltName...
	2 O15020	61	RecName: Full=Spectrin beta chain, non-erythrocytic 2; AltName: Full=Beta-III spectrin; AltName: Full=Spinocerebellar ataxia 5 pr...

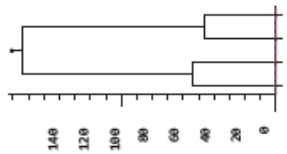

9	1 P08238	749	RecName: Full=Heat shock protein HSP 90-beta; Short=HSP 90; AltName: Full=Heat shock 84 kDa; Short=HSP 84; Short=HSP84;
	4 P14625	153	RecName: Full=Endoplasmin; AltName: Full=94 kDa glucose-regulated protein; Short=GRP-94; AltName: Full=Heat shock protein ...
	2 P07900	577	RecName: Full=Heat shock protein HSP 90-alpha; AltName: Full=Heat shock 86 kDa; Short=HSP 86; Short=HSP86; AltName: Full...
	3 Q12931	160	RecName: Full=Heat shock protein 75 kDa, mitochondrial; Short=HSP 75; AltName: Full=TNFR-associated protein 1; AltName: Full...
10	O60716	671	RecName: Full=Catenin delta-1; AltName: Full=Cadherin-associated Src substrate; Short=CAS; AltName: Full=p120 catenin; Short...

Appendix Aiii. MASCOT analysis of wild type MRE11 after elastase digest.

MASCOT Search Results

Protein View: P49959

RecName: Full=Double-strand break repair protein MRE11A; AltName: Full=Meiotic recombination 11 homolog 1; Short=MRE11 homolog 1; AltName: Full=Meiotic recombination 11 homolog A; Short=MRE11 homolog A;

Database:	UniProt_SwissProt
Score:	108
Nominal mass (M_r):	80885
Calculated pI:	5.61
Taxonomy:	Homo sapiens

Sequence similarity is available as an NCBI BLAST search of P49959 against nr.

Search parameters

MS data file:	E:\mgf_Orbi\OTE0297_SarahJevons_Elas_2.mgf
Enzyme:	No enzyme cleavage specificity.
Fixed modifications:	Carbamidomethyl (C)
Variable modifications:	Deamidated (N), Deamidated (Q), Oxidation (M)

Protein sequence coverage: 31%

Matched peptides shown in ***bold red***.

```
   1 MSTADALDDE NTFKILVATD IHLGFMEKDA VRGNDTFVTL DEILRLAQEN
  51 EVDFILLGGD LFHENKPSRK TLHTCLELLR KYCMGDRPVQ FEILSDQSVN
 101 FGFSKFPWVN YQDGNLNISI PVFSIHGNHD DPTGADALCA LDILSCAGFV
 151 NHFGRSMSVE KIDISPVLLQ KGSTKIALYG LGSIPDERLY RMFVNKKVTM
 201 LRPKEDENSW FNLFVIHQNR SKHGSTNFIP EQFLDDFIDL VIWGHEHECK
 251 IAPTKNEQQL FYISQPGSSV VTSLSPGEAV KKHVGLLRIK GRKMNMHKIP
 301 LHTVRQFFME DIVLANHPDI FNPDNPKVTQ AIQSFCLEKI EEMLENAERE
 351 RLGNSHQPEK PLVRLRVDYS GGFEPFSVLR FSQKFVDRVA NPKDIIHFFR
 401 HREQKEKTGE EINFGKLITK PSEGTTLRVE DLVKQYFQTA EKNVQLSLLT
 451 ERGMGEAVQE FVDKEEKDAI EELVKYQLEK TQRFLKERHI DALEDKIDEE
 501 VRRFRETRQK NTNEEDDEVR EAMTRARALR SQSEESASAF SADDLMSIDL
 551 AEQMANDSDD SISAATNKGR GRGRGRRGGR GQNSASRGGS QRGRADTGLE
 601 TSTRSRNSKT AVSASRNMSI IDAFKSTRQQ PSRNVTTKNY SEVIEVDESD
 651 VEEDIFPTTS KTDQRWSSTS SSKIMSQSQV SKGVDFESSE DDDDDPFMNT
 701 SSLRRNRR
```

Unformatted sequence string: 708 residues (for pasting into other applications).

Sort peptides by ◉ Residue Number ○ Increasing Mass ○ Decreasing Mass

Query	Start – End	Observed	Mr(expt)	Mr(calc)	ppm	M	Score	Expect	Rank	U	Peptide
3826	5 – 14	584.2617	1166.5088	1166.5091	-0.32	0	35	0.56	1	U	A.DALDDENTFK.I
4835	5 – 15	640.8046	1279.5947	1279.5932	1.17	0	34	0.26	1	U	A.DALDDENTFKI.L
247	19 – 24	328.1740	654.3335	654.3337	-0.34	0	20	0.76	1	U	A.TDIHLG.F
1487	25 – 31	428.1993	854.3841	854.3844	-0.39	0	21	0.52	1	U	G.FMEKDAV.R + Oxidation (M)
6406	33 – 45	746.8858	1491.7571	1491.7569	0.085	0	31	0.12	1	U	R.GNDTFVTLDEILR.L
793	40 – 45	379.7240	757.4334	757.4334	0.0079	0	33	0.6	1	U	T.LDEILR.L
1572	40 – 46	436.2659	870.5172	870.5174	-0.29	0	41	0.044	1	U	T.LDEILRL.A
2018	40 – 47	471.7843	941.5541	941.5545	-0.47	0	24	1.1	2	U	T.LDEILRLA.Q
2417	48 – 55	497.2295	992.4444	992.4451	-0.72	0	21	1.4	5	U	A.QENEVDFI.L
4105	58 – 68	400.8594	1199.5564	1199.5571	-0.59	0	28	0.27	1	U	L.GGDLFHENKPS.R
3103	60 – 68	543.7644	1085.5143	1085.5142	0.088	0	20	0.37	1	U	G.DLFHENKPS.R
3810	90 – 99	583.2901	1164.5656	1164.5663	-0.53	0	21	0.085	1	U	V.QFEILSDQSV.N
4419	123 – 133	620.2732	1238.5318	1238.5316	0.16	0	34	0.049	1	U	V.FSIHGNHDDPT.G
5551	123 – 135	684.3019	1366.5893	1366.5902	-0.64	0	32	0.036	1	U	V.FSIHGNHDDPTGA.D
5802	177 – 189	702.3798	1402.7450	1402.7456	-0.45	0	21	0.19	1	U	I.ALYGLGSIPDERL.Y
4252	178 – 188	610.3195	1218.6244	1218.6244	-0.058	0	48	0.012	1	U	A.LYGLGSIPDER.L
4260	178 – 188	610.8205	1219.6264	1218.6244	822	0	31	0.032	1	U	A.LYGLGSIPDER.L
3060	238 – 246	541.2856	1080.5566	1080.5604	-3.50	0	27	1.1	2	U	F.IDLVIWGHE.H
3960	261 – 271	592.3036	1182.5926	1182.5921	0.44	0	22	0.11	1	U	L.FYISQPGSSVV.T
4868	261 – 272	642.8270	1283.6394	1283.6398	-0.32	0	28	0.032	1	U	L.FYISQPGSSVVT.S
1484	295 – 301	426.7415	851.4685	851.4687	-0.28	0	22	0.91	1	U	M.NMHKIPL.H
3965	305 – 313	592.7921	1183.5697	1183.5696	0.081	0	26	1.5	2	U	V.RQFFMEDIV.L
7027	316 – 329	804.3941	1606.7737	1606.7740	-0.20	0	41	0.0018	1	U	A.NHPDIFNPDNPKVT.Q
4253	352 – 362	407.2189	1218.6349	1218.6357	-0.64	0	33	0.15	1	U	R.LGNSHQPEKPL.V
2257	416 – 424	486.7895	971.5644	971.5651	-0.78	0	21	0.98	1	U	G.KLITKPSEG.T
3901	448 – 458	588.3082	1174.6018	1174.6016	0.16	0	48	0.0032	1	U	S.LLTERGMGEAV.Q
1817	475 – 481	455.2554	908.4963	908.4967	-0.43	0	26	1.4	2	U	V.KYQLEKT.Q
6619	489 – 501	763.8762	1525.7379	1524.7307	661	0	22	0.059	1	U	R.HIDALEDKIDEEV.R
4894	494 – 503	430.2214	1287.6425	1287.6419	0.48	0	25	0.46	1	U	L.EDKIDEEVRR.F
7739	508 – 522	611.6171	1831.8294	1831.8296	-0.13	0	25	0.12	1	U	T.RQKNTNEEDDEVREA.M
7303	509 – 522	838.8709	1675.7273	1675.7285	-0.73	0	43	0.00064	1	U	R.QKNTNEEDDEVREA.M
7304	509 – 522	559.5836	1675.7290	1675.7285	0.31	0	26	0.068	1	U	R.QKNTNEEDDEVREA.M
5909	511 – 522	710.7947	1419.5749	1419.5750	-0.028	0	51	0.0031	1	U	K.NTNEEDDEVREA.M
1493	594 – 601	431.7174	861.4202	861.4192	1.16	0	27	0.45	1	U	G.RADTGLET.S

Appendix Aiii. MASCOT analysis of wild type MRE11 after elastase digest "top hits".

MASCOT Search Results

User : bmk
E-mail :
Search title : RK OTE0297_SarahJevons_Tryp_4.mgf
MS data file : E:\mgf_Orbi\OTE0297_SarahJevons_Tryp_4.mgf
Database : UniProt_SwissProt 20131208 (541,762 sequences; 192,577,305 residues)
Taxonomy : Homo sapiens (human) (20,353 sequences)
Timestamp : 19 Sep 2014 at 15:03:04 GMT

Not what you expected? Try the select summary.

▸ Search parameters
▸ Score distribution
▸ Legend

Protein Family Summary

Significance threshold p< 0.05 Max. number of families AUTO
Ions score or expect cut-off 0 Dendrograms cut at 0
Show Percolator scores ☐
Preferred taxonomy All entries

▸ Decoy search summary (reversed protein sequences)

Protein families 1–10 (out of 269)

10 per page 1 2 3 4 5 6 ... 27 Next

▸1	P10515	2371	RecName: Full=Dihydrolipoyllysine-residue acetyltransferase component of pyruvate dehydrogenase complex, mitochondrial; EC=2...
▸2	P49959	1839	RecName: Full=Double-strand break repair protein MRE11A; AltName: Full=Meiotic recombination 11 homolog 1; Short=MRE11 ho...
▸3	1 P11142	1722	RecName: Full=Heat shock cognate 71 kDa protein; AltName: Full=Heat shock 70 kDa protein 8;
	4 P11021	267	RecName: Full=78 kDa glucose-regulated protein; Short=GRP-78; AltName: Full=Endoplasmic reticulum lumenal Ca(2+)-binding p...
	2 P08107	819	RecName: Full=Heat shock 70 kDa protein 1A/1B; AltName: Full=Heat shock 70 kDa protein 1/2; Short=HSP70-1/HSP70-2; Short...
	3 P17066	459	RecName: Full=Heat shock 70 kDa protein 6; AltName: Full=Heat shock 70 kDa protein B';
▸4	P38646	1191	RecName: Full=Stress-70 protein, mitochondrial; AltName: Full=75 kDa glucose-regulated protein; Short=GRP-75; AltName: Full=...
▸5	1 P02545	1169	RecName: Full=Prelamin-A/C; Contains: RecName: Full=Lamin-A/C; AltName: Full=70 kDa lamin; AltName: Full=Renal carcinoma ...
	4 Q03252	275	RecName: Full=Lamin-B2; Flags: Precursor;
	3 P08729	285	RecName: Full=Keratin, type II cytoskeletal 7; AltName: Full=Cytokeratin-7; Short=CK-7; AltName: Full=Keratin-7; Short=K7; Alt...
	5 P05787	143	RecName: Full=Keratin, type II cytoskeletal 8; AltName: Full=Cytokeratin-8; Short=CK-8; AltName: Full=Keratin-8; Short=K8; Alt...
	2 P20700	379	RecName: Full=Lamin-B1; Flags: Precursor;

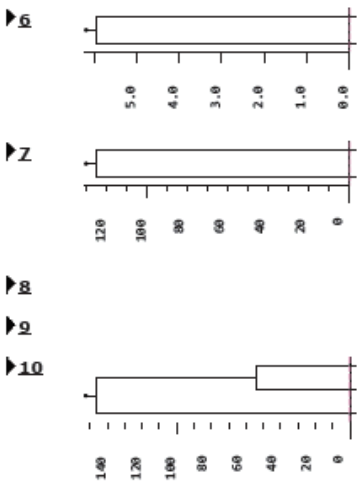

6	1	P60709	942 RecName: Full=Actin, cytoplasmic 1; AltName: Full=Beta-actin; Contains: RecName: Full=Actin, cytoplasmic 1, N-terminally proces...
	2	P68032	664 RecName: Full=Actin, alpha cardiac muscle 1; AltName: Full=Alpha-cardiac actin; Flags: Precursor;
7	1	O43707	875 RecName: Full=Alpha-actinin-4; AltName: Full=F-actin cross-linking protein; AltName: Full=Non-muscle alpha-actinin 4;
	2	P12814	365 RecName: Full=Alpha-actinin-1; AltName: Full=Alpha-actinin cytoskeletal isoform; AltName: Full=F-actin cross-linking protein; AltN...
8		Q8N4N3	875 RecName: Full=Kelch-like protein 36;
9		O00515	721 RecName: Full=Ladinin-1; Short=Lad-1; AltName: Full=Linear IgA disease antigen; Short=LADA;
10	1	P35579	718 RecName: Full=Myosin-9; AltName: Full=Cellular myosin heavy chain, type A; AltName: Full=Myosin heavy chain 9; AltName: Full...
	3	P35580	84 RecName: Full=Myosin-10; AltName: Full=Cellular myosin heavy chain, type B; AltName: Full=Myosin heavy chain 10; AltName: F...
	2	Q7Z406	271 RecName: Full=Myosin-14; AltName: Full=Myosin heavy chain 14; AltName: Full=Myosin heavy chain, non-muscle IIc; AltName: F...

Appendix Av. MASCOT analysis of MRE11 variant after trypic digest

MASCOT Search Results

Protein View: P49959

RecName: Full=Double-strand break repair protein MRE11A; AltName: Full=Meiotic recombination 11 homolog 1; Short=MRE11 homolog 1; AltName: Full=Meiotic recombination 11 homolog A; Short=MRE11 homolog A;

Database:	UniProt_SwissProt
Score:	1785
Nominal mass (M_r):	80885
Calculated pI:	5.61
Taxonomy:	Homo sapiens

Sequence similarity is available as an NCBI BLAST search of P49959 against nr.

Search parameters

MS data file:	E:\mgf_Orbi\OTE0297_SarahJevons_Tryp_4.mgf
Enzyme:	Trypsin: cuts C-term side of KR unless next residue is P.
Fixed modifications:	Carbamidomethyl (C)
Variable modifications:	Deamidated (N), Deamidated (Q), Oxidation (M)

Protein sequence coverage: 49%

Matched peptides shown in ***bold red***.

```
  1 MSTADALDDE NTFKILVATD IHLGFMEKDA VRGNDTFVTL DEILRLAQEN
 51 EVDFILLGGD LFHENKPSRK TLHTCLELLR KYCMGDRPVQ FEILSDQSVN
101 FGFSKFPWVN YQDGNLNISI PVFSIHGNHD DPTGADALCA LDILSCAGFV
151 NHFGRSMSVE KIDISPVLLQ KGSTKIALYG LGSIPDERLY RMFVNKKVTM
201 LRPKEDENSW FNLFVIHQNR SKHGSTNFIP EQFLDDFIDL VIWGHEHECK
251 IAPTKNEQQL FYISQPGSSV VTSLSPGEAV KKHVGLLRIK GRKMNMHKIP
301 LHTVRQFFME DIVLANHPDI FNPDNPKVTQ AIQSFCLEKI EEMLENAERE
351 RLGNSHQPEK PLVRLRVDYS GGFEPFSVLR FSQKFVDRVA NPKDIIHFFR
401 HREQKEKTGE EINFGKLITK PSEGTTLRVE DLVKQYFQTA EKNVQLSLLT
451 ERGMGEAVQE FVDKEEKDAI EELVKYQLEK TQRFLKERHI DALEDKIDEE
501 VRRFRETRQK NTNEEDDEVR EAMTRARALR SQSEESASAF SADDLMSIDL
551 AEQMANDSDD SISAATNKGR GRGRGRRGGR GQNSASRGGS QRGRADTGLE
601 TSTRSRNSKT AVSASRNMSI IDAFKSTRQQ PSRNVTTKNY SEVIEVDESD
651 VEEDIFPTTS KTDQRWSSTS SSKIMSQSQV SKGVDFESSE DDDDDPFMNT
701 SSLRRNRR
```

Unformatted sequence string: 708 residues (for pasting into other applications).

Sort peptides by ◉ Residue Number ○ Increasing Mass ○ Decreasing Mass

Show predicted peptides also

Query	Start – End	Observed	Mr(expt)	Mr(calc)	ppm	M	Score	Expect	Rank	U	Peptide
9509	29 – 45	967.5017	1932.9889	1932.9905	-0.85	1	36	0.00059	1	U	K.DAVRGNDTFVTLDEILR.L
9513	29 – 45	645.6649	1933.9729	1933.9745	-0.82	1	24	0.017	1	U	K.DAVRGNDTFVTLDEILR.L + Deamidated (N)
9517	29 – 45	645.6711	1933.9916	1933.9745	8.83	1	23	0.013	1	U	K.DAVRGNDTFVTLDEILR.L + Deamidated (N)
6315	33 – 45	746.8845	1491.7544	1491.7569	-1.72	0	31	0.002	1	U	R.GNDTFVTLDEILR.L
6317	33 – 45	746.8856	1491.7566	1491.7569	-0.24	0	64	2.2e-06	1	U	R.GNDTFVTLDEILR.L
6335	33 – 45	747.3825	1492.7505	1491.7569	666	0	45	0.00016	1	U	R.GNDTFVTLDEILR.L
6336	33 – 45	747.3869	1492.7593	1491.7569	672	0	36	0.0013	1	U	R.GNDTFVTLDEILR.L
6338	33 – 45	498.5947	1492.7622	1491.7569	674	0	21	0.047	1	U	R.GNDTFVTLDEILR.L
6333	33 – 45	747.3782	1492.7419	1492.7409	0.66	0	71	5e-07	1	U	R.GNDTFVTLDEILR.L + Deamidated (N)
11719	46 – 69	914.7974	2741.3703	2741.3660	1.54	0	21	0.047	1	U	R.LAQENEVDFILLGGDLFHENKPSR.K + Deamidated (N)
11720	46 – 69	686.3530	2741.3828	2741.3660	6.10	0	21	0.11	1	U	R.LAQENEVDFILLGGDLFHENKPSR.K + Deamidated (N)
11725	46 – 69	915.1348	2742.3825	2741.3660	371	0	30	0.002	1	U	R.LAQENEVDFILLGGDLFHENKPSR.K + Deamidated (N)
3857	71 – 80	419.2325	1254.6756	1254.6754	0.15	0	21	0.092	1	U	K.TLHTCLELLR.K
8699	156 – 171	894.0021	1785.9897	1785.9910	-0.72	1	45	0.00013	1	U	R.SMSVEKIDISPVLLQK.G
8700	156 – 171	596.3375	1785.9907	1785.9910	-0.14	1	45	0.0003	1	U	R.SMSVEKIDISPVLLQK.G
8701	156 – 171	894.0040	1785.9934	1785.9910	1.34	1	23	0.0071	1	U	R.SMSVEKIDISPVLLQK.G
8721	156 – 171	894.5027	1786.9909	1785.9910	560	1	23	0.051	1	U	R.SMSVEKIDISPVLLQK.G
8841	156 – 171	601.6689	1801.9850	1801.9859	-0.50	1	27	0.03	1	U	R.SMSVEKIDISPVLLQK.G + Oxidation (M)
8842	156 – 171	601.6689	1801.9850	1801.9859	-0.50	1	45	0.00048	1	U	R.SMSVEKIDISPVLLQK.G + Oxidation (M)
8843	156 – 171	601.6691	1801.9856	1801.9859	-0.20	1	54	5.6e-05	1	U	R.SMSVEKIDISPVLLQK.G + Oxidation (M)
8845	156 – 171	902.0009	1801.9873	1801.9859	0.76	1	34	0.0028	1	U	R.SMSVEKIDISPVLLQK.G + Oxidation (M)
8846	156 – 171	902.0027	1801.9909	1801.9859	2.79	1	49	3.9e-05	1	U	R.SMSVEKIDISPVLLQK.G + Oxidation (M)
8853	156 – 171	902.5013	1802.9881	1801.9859	556	1	54	1.7e-05	1	U	R.SMSVEKIDISPVLLQK.G + Oxidation (M)
8854	156 – 171	902.5018	1802.9891	1801.9859	557	1	26	0.0045	1	U	R.SMSVEKIDISPVLLQK.G + Oxidation (M)
6391	162 – 175	749.9459	1497.8772	1497.8766	0.36	1	25	0.015	1	U	K.IDISPVLLQKGSTK.I
8651	172 – 188	888.9787	1775.9428	1775.9417	0.62	1	70	2.8e-07	1	U	K.GSTKIALYGLGSIPDER.L
8657	172 – 188	889.4803	1776.9460	1775.9417	565	1	44	7.4e-05	1	U	K.GSTKIALYGLGSIPDER.L
5361	176 – 188	702.3797	1402.7448	1402.7456	-0.54	0	43	0.00035	1	U	K.IALYGLGSIPDER.L
5362	176 – 188	702.3802	1402.7458	1402.7456	0.16	0	46	8.3e-05	1	U	K.IALYGLGSIPDER.L
5363	176 – 188	702.3804	1402.7463	1402.7456	0.50	0	67	5.6e-07	1	U	K.IALYGLGSIPDER.L
5365	176 – 188	702.3817	1402.7489	1402.7456	2.33	0	22	0.009	1	U	K.IALYGLGSIPDER.L
5374	176 – 188	702.8814	1403.7483	1402.7456	715	0	25	0.021	1	U	K.IALYGLGSIPDER.L
9010	176 – 191	612.6718	1834.9936	1834.9941	-0.26	1	49	4e-05	1	U	K.IALYGLGSIPDERLYR.M
10024	205 – 220	1024.4849	2046.9552	2046.9548	0.20	0	23	0.0077	1	U	K.EDENSWFNLFVIHQNR.S
10025	205 – 220	683.3259	2046.9558	2046.9548	0.49	0	45	0.00068	1	U	K.EDENSWFNLFVIHQNR.S
10030	205 – 220	683.6585	2047.9537	2047.9388	7.28	0	29	0.0031	1	U	K.EDENSWFNLFVIHQNR.S + Deamidated (N)
12759	251 – 281	1092.5765	3274.7078	3274.7085	-0.22	1	57	6.2e-06	1	U	K.IAPTKNEQQLFYISQPGSSVVTSLSPGEAVK.K
12760	251 – 281	819.6846	3274.7094	3274.7085	0.28	1	37	0.00034	1	U	K.IAPTKNEQQLFYISQPGSSVVTSLSPGEAVK.K
12761	251 – 281	1092.9070	3275.6991	3275.6925	2.01	1	51	0.00013	1	U	K.IAPTKNEQQLFYISQPGSSVVTSLSPGEAVK.K + Deamidated (Q)
11743	256 – 281	922.4721	2764.3945	2764.3919	0.92	0	47	3.6e-05	1	U	K.NEQQLFYISQPGSSVVTSLSPGEAVK.K
11746	256 – 281	922.8092	2765.4058	2764.3919	367	0	23	0.021	1	U	K.NEQQLFYISQPGSSVVTSLSPGEAVK.K
11948	256 – 282	965.1699	2892.4879	2892.4869	0.36	1	64	1.5e-06	1	U	K.NEQQLFYISQPGSSVVTSLSPGEAVKK.H
11949	256 – 282	965.5046	2893.4921	2893.4709	7.32	1	42	0.0012	1	U	K.NEQQLFYISQPGSSVVTSLSPGEAVKK.H + Deamidated (Q)
11951	256 – 282	965.8389	2894.4950	2893.4709	354	1	42	0.00075	1	U	K.NEQQLFYISQPGSSVVTSLSPGEAVKK.H + Deamidated (Q)
673	282 – 288	411.7690	821.5235	821.5235	-0.012	1	23	0.0051	1	U	K.KHVGLLR.I
167	283 – 288	347.7214	693.4283	693.4286	-0.48	0	24	0.014	1	U	K.HVGLLR.I
170	283 – 288	347.7215	693.4285	693.4286	-0.13	0	22	0.023	1	U	K.HVGLLR.I
746	299 – 305	418.2605	834.5064	834.5076	-1.42	0	32	0.0024	1	U	K.IPLHTVR.Q
747	299 – 305	418.2610	834.5075	834.5076	-0.10	0	22	0.0087	1	U	K.IPLHTVR.Q
11567	306 – 327	867.7529	2600.2368	2600.2370	-0.067	0	48	0.00015	1	U	R.QFTMEDIVLANHPDIFNPDNPK.V
11571	306 – 327	868.0862	2601.2367	2601.2210	6.06	0	47	0.00067	1	U	R.QFTMEDIVLANHPDIFNPDNPK.V + Deamidated (N)
11573	306 – 327	868.4226	2602.2460	2601.2210	394	0	40	0.00043	1	U	R.QFTMEDIVLANHPDIFNPDNPK.V + Deamidated (N)
11596	306 – 327	873.4192	2617.2357	2617.2159	7.59	0	43	0.002	1	U	R.QFTMEDIVLANHPDIFNPDNPK.V + Deamidated (N); Oxidation (M)
5567	328 – 339	712.3658	1422.7171	1422.7177	-0.39	0	28	0.004	1	U	K.VTQAIQSFCLEK.I
5571	328 – 339	712.8663	1423.7180	1422.7177	703	0	27	0.0092	1	U	K.VTQAIQSFCLEK.I
3624	340 – 349	617.2924	1232.5703	1232.5706	-0.29	0	38	0.0027	1	U	K.IEEMLENAER.E

3806	340 – 349	625.7919	1249.5693	1248.5656	804	0	31	0.007	1	U	K.IEEMLENAER.E + Oxidation (M)
6615	340 – 351	506.9119	1517.7138	1517.7143	-0.38	1	33	0.009	1	U	K.IEEMLENAERER.L
6091	352 – 364	737.9037	1473.7928	1473.8052	-8.39	0	20	0.08	1	U	R.LGNSHQPEKPLVR.L
6093	352 – 364	492.2749	1473.8030	1473.8052	-1.51	0	30	0.0016	1	U	R.LGNSHQPEKPLVR.L
6098	352 – 364	492.2755	1473.8048	1473.8052	-0.26	0	36	0.00067	1	U	R.LGNSHQPEKPLVR.L
6100	352 – 364	737.9099	1473.8051	1473.8052	-0.028	0	33	0.0011	1	U	R.LGNSHQPEKPLVR.L
6101	352 – 364	492.2757	1473.8052	1473.8052	-0.016	0	40	0.00026	1	U	R.LGNSHQPEKPLVR.L
6102	352 – 364	492.2757	1473.8052	1473.8052	-0.016	0	52	2.8e-05	1	U	R.LGNSHQPEKPLVR.L
6104	352 – 364	737.9100	1473.8054	1473.8052	0.14	0	21	0.012	1	U	R.LGNSHQPEKPLVR.L
6115	352 – 364	738.4017	1474.7889	1474.7892	-0.19	0	25	0.0046	1	U	R.LGNSHQPEKPLVR.L + Deamidated (N)
6116	352 – 364	492.6038	1474.7895	1474.7892	0.23	0	56	2.9e-05	1	U	R.LGNSHQPEKPLVR.L + Deamidated (N)
6119	352 – 364	492.6057	1474.7951	1474.7892	4.02	0	50	0.00028	1	U	R.LGNSHQPEKPLVR.L + Deamidated (Q)
6120	352 – 364	492.6067	1474.7983	1474.7892	6.19	0	33	0.011	1	U	R.LGNSHQPEKPLVR.L + Deamidated (Q)
9087	365 – 380	614.6558	1840.9455	1840.9472	-0.94	1	31	0.011	1	U	R.LRVDYSGGFEPFSVLR.F
9091	365 – 380	614.6562	1840.9469	1840.9472	-0.15	1	40	0.00058	1	U	R.LRVDYSGGFEPFSVLR.F
9093	365 – 380	921.4830	1840.9515	1840.9472	2.35	1	24	0.0052	1	U	R.LRVDYSGGFEPFSVLR.F
9098	365 – 380	614.9907	1841.9502	1840.9472	545	1	31	0.0058	1	U	R.LRVDYSGGFEPFSVLR.F
7222	367 – 380	786.8890	1571.7634	1571.7620	0.88	0	43	0.0001	1	U	R.VDYSGGFEPFSVLR.F
1832	381 – 388	513.7718	1025.5290	1025.5294	-0.40	1	23	0.013	1	U	R.FSQKFVDR.V
1833	381 – 388	342.8505	1025.5297	1025.5294	0.31	1	27	0.005	1	U	R.FSQKFVDR.V
1934	385 – 393	349.1977	1044.5713	1044.5716	-0.27	1	29	0.044	1	U	K.FVDRVANPK.D
5895	389 – 400	486.2733	1455.7980	1455.7987	-0.43	1	23	0.011	1	U	R.VANPKDIIHFFR.H
5905	389 – 400	486.2736	1455.7990	1455.7987	0.26	1	32	0.0015	1	U	R.VANPKDIIHFFR.H
5906	389 – 400	486.2737	1455.7991	1455.7987	0.32	1	30	0.0046	1	U	R.VANPKDIIHFFR.H
5911	389 – 400	486.2740	1455.8002	1455.7987	1.07	1	26	0.0051	1	U	R.VANPKDIIHFFR.H
1279	394 – 400	474.2585	946.5024	946.5025	-0.14	0	20	0.32	2	U	K.DIIHFFR.H
1594	408 – 416	497.7452	993.4759	993.4767	-0.85	0	57	5.3e-05	1	U	K.TGEEINFGK.L
1595	408 – 416	497.7456	993.4767	993.4767	0.0050	0	56	5.1e-05	1	U	K.TGEEINFGK.L
1596	408 – 416	497.7457	993.4768	993.4767	0.13	0	39	0.0013	1	U	K.TGEEINFGK.L
1607	408 – 416	498.2368	994.4591	994.4607	-1.59	0	25	0.022	1	U	K.TGEEINFGK.L + Deamidated (N)
1608	408 – 416	498.2375	994.4605	994.4607	-0.18	0	45	0.00017	1	U	K.TGEEINFGK.L + Deamidated (N)
4526	417 – 428	658.3829	1314.7512	1314.7507	0.38	0	30	0.0015	1	U	K.LITKPSEGTTLR.V
4527	417 – 428	439.2577	1314.7512	1314.7507	0.41	0	28	0.0067	1	U	K.LITKPSEGTTLR.V
9796	417 – 434	667.0522	1998.1347	1998.1361	-0.68	1	28	0.0025	1	U	K.LITKPSEGTTLRVEDLVK.Q
1742	435 – 442	507.7481	1013.4817	1013.4818	-0.071	0	25	0.0047	1	U	K.QYFQTAEK.N
10492	435 – 452	723.3828	2167.1266	2167.1273	-0.32	1	27	0.0031	1	U	K.QYFQTAEKNVQLSLLTER.G
10493	435 – 452	1084.5708	2167.1271	2167.1273	-0.12	1	68	4.5e-07	1	U	K.QYFQTAEKNVQLSLLTER.G
10494	435 – 452	723.3831	2167.1273	2167.1273	0.018	1	50	7.9e-05	1	U	K.QYFQTAEKNVQLSLLTER.G
10495	435 – 452	723.3832	2167.1277	2167.1273	0.19	1	42	0.0016	1	U	K.QYFQTAEKNVQLSLLTER.G
10496	435 – 452	723.7155	2168.1245	2168.1113	6.10	1	40	0.0025	1	U	K.QYFQTAEKNVQLSLLTER.G + Deamidated (Q)
10497	435 – 452	723.7175	2168.1306	2168.1113	8.88	1	28	0.035	1	U	K.QYFQTAEKNVQLSLLTER.G + Deamidated (N)
3012	443 – 452	586.8353	1171.6561	1171.6561	0.030	0	25	0.026	1	U	K.NVQLSLLTER.G
3013	443 – 452	586.8354	1171.6562	1171.6561	0.13	0	59	3.5e-05	1	U	K.NVQLSLLTER.G
3015	443 – 452	586.8356	1171.6567	1171.6561	0.55	0	37	0.0043	1	U	K.NVQLSLLTER.G
1124	468 – 475	458.7530	915.4914	915.4913	0.16	0	28	0.054	1	U	K.DAIEELVK.Y
153	484 – 488	346.7080	691.4015	691.4017	-0.24	1	20	0.11	1	U	R.FLKER.H
155	484 – 488	346.7081	691.4016	691.4017	-0.061	1	21	0.1	1	U	R.FLKER.H
8065	489 – 502	561.2847	1680.8322	1680.8318	0.20	1	23	0.028	1	U	R.HIDALEDKIDEEVR.R
8879	511 – 525	603.5963	1807.7671	1807.7642	1.59	1	26	0.0038	1	U	K.NTNEEDDEVREAMTR.A
8973	511 – 525	608.9273	1823.7601	1823.7592	0.51	1	22	0.0093	1	U	K.NTNEEDDEVREAMTR.A + Oxidation (M)
3948	593 – 604	421.8810	1262.6213	1262.6215	-0.15	1	21	0.11	1	U	R.GRADTGLETSTR.S
1991	595 – 604	525.7565	1049.4984	1049.4989	-0.50	0	54	0.00014	1	U	R.ADTGLETSTR.S
1993	595 – 604	525.7600	1049.5054	1049.4989	6.22	0	28	0.031	1	U	R.ADTGLETSTR.S
2037	617 – 625	527.7654	1053.5163	1053.5165	-0.13	0	26	0.017	1	U	R.NMSIIDAFK.S + Oxidation (M)

Appendix Avi. MASCOT analysis of MRE11 variant after tryptic digest "top hits".

MASCOT Search Results

User : bmk
E-mail :
Search title : RK OTE0297_SarahJevons_Elas_2.mgf
MS data file : E:\mgf_Orbi\OTE0297_SarahJevons_Elas_2.mgf
Database : UniProt_SwissProt 20131208 (541,762 sequences; 192,577,305 residues)
Taxonomy : Homo sapiens (human) (20,353 sequences)
Timestamp : 22 Sep 2014 at 11:54:20 GMT

Not what you expected? Try the select summary.

▸ Search parameters
▸ Score distribution
▸ Legend

Protein Family Summary

Significance threshold p< 0.05 Max. number of families AUTO
Ions score or expect cut-off 0 Dendrograms cut at 0
Show Percolator scores ☐
Preferred taxonomy All entries

▸ Decoy search summary (random protein sequences)

Protein families 1–10 (out of 82)

10 per page 1 2 3 4 5 6 ... 9 Next

▸1			Q9UHB6	254 RecName: Full=LIM domain and actin-binding protein 1; AltName: Full=Epithelial protein lost in neoplasm;
▸2		1 2	O43707 P12814	217 RecName: Full=Alpha-actinin-4; AltName: Full=F-actin cross-linking protein; AltName: Full=Non-muscle alpha-actinin 4; 121 RecName: Full=Alpha-actinin-1; AltName: Full=Alpha-actinin cytoskeletal isoform; AltName: Full=F-actin cross-linking protein; AltN...
▸3			P40199	208 RecName: Full=Carcinoembryonic antigen-related cell adhesion molecule 6; AltName: Full=Non-specific crossreacting antigen; AltN...
▸4			O75369	118 RecName: Full=Filamin-B; Short=FLN-B; AltName: Full=ABP-278; AltName: Full=ABP-280 homolog; AltName: Full=Actin-binding-li...
▸5			P49959	108 RecName: Full=Double-strand break repair protein MRE11A; AltName: Full=Meiotic recombination 11 homolog 1; Short=MRE11 ho...
▸6			P10515	106 RecName: Full=Dihydrolipoyllysine-residue acetyltransferase component of pyruvate dehydrogenase complex, mitochondrial; EC=2...
▸7	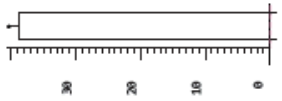	1 2	P14923 P35222	98 RecName: Full=Junction plakoglobin; AltName: Full=Catenin gamma; AltName: Full=Desmoplakin III; AltName: Full=Desmoplakin-... 84 RecName: Full=Catenin beta-1; AltName: Full=Beta-catenin;

▶8		P29966	90	RecName: Full=Myristoylated alanine-rich C-kinase substrate; Short=MARCKS; AltName: Full=Protein kinase C substrate, 80 kDa p...
▶9	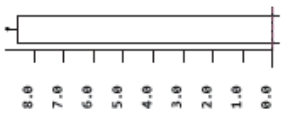	1 P08238	86	RecName: Full=Heat shock protein HSP 90-beta; Short=HSP 90; AltName: Full=Heat shock 84 kDa; Short=HSP 84; Short=HSP84;
		2 P07900	69	RecName: Full=Heat shock protein HSP 90-alpha; AltName: Full=Heat shock 86 kDa; Short=HSP 86; Short=HSP86; AltName: Full...
▶10		Q13813	76	RecName: Full=Spectrin alpha chain, non-erythrocytic 1; AltName: Full=Alpha-II spectrin; AltName: Full=Fodrin alpha chain; AltNa...

Appendix Avii. MASCOT analysis of MRE11 variant after elastase digest.

MASCOT Search Results

Protein View: P49959

RecName: Full=Double-strand break repair protein MRE11A; AltName: Full=Meiotic recombination 11 homolog 1; Short=MRE11 homolog 1; AltName: Full=Meiotic recombination 11 homolog A; Short=MRE11 homolog A;

Database:	UniProt_SwissProt
Score:	502
Nominal mass (M_r):	80885
Calculated pI:	5.61
Taxonomy:	Homo sapiens

Sequence similarity is available as an NCBI BLAST search of P49959 against nr.

Search parameters

MS data file:	E:\mgf_Orbi\OTE0297_SarahJevons_Elas_4.mgf
Enzyme:	No enzyme cleavage specificity.
Fixed modifications:	Carbamidomethyl (C)
Variable modifications:	Deamidated (N), Deamidated (Q), Oxidation (M)

Protein sequence coverage: 54%

Matched peptides shown in ***bold red***.

```
  1 MSTADALDDE NTFKILVATD IHLGFMEKDA VRGNDTFVTL DEILRLAQEN
 51 EVDFILLGGD LFHENKPSRK TLHTCLELLR KYCMGDRPVQ FEILSDQSVN
101 FGFSKFPWVN YQDGNLNISI PVFSIHGNHD DPTGADALCA LDILSCAGFV
151 NHFGRSMSVE KIDISPVLLQ KGSTKIALYG LGSIPDERLY RMFVNKKVTM
201 LRPKEDENSW FNLFVIHQNR SKHGSTNFIP EQFLDDFIDL VIWGHEHECK
251 IAPTKNEQQL FYISQPGSSV VTSLSPGEAV KKHVGLLRIK GRKMNMHKIP
301 LHTVRQFFME DIVLANHPDI FNPDNPKVTQ AIQSFCLEKI EEMLENAERE
351 RLGNSHQPEK PLVRLRVDYS GGFEPFSVLR FSQKFVDRVA NPKDIIHFFR
401 HREQKEKTGE EINFGKLITK PSEGTTLRVE DLVKQYFQTA EKNVQLSLLT
451 ERGMGEAVQE FVDKEEKDAI EELVKYQLEK TQRFLKERHI DALEDKIDEE
501 VRRFRETRQK NTNEEDDEVR EAMTRARALR SQSEESASAF SADDLMSIDL
551 AEQMANDSDD SISAATNKGR GRGRGRRGGR GQNSASRGGS QRGRADTGLE
601 TSTRSRNSKT AVSASRNMSI IDAFKSTRQQ PSRNVTTKNY SEVIEVDESD
651 VEEDIFPTTS KTDQRWSSTS SSKIMSQSQV SKGVDFESSE DDDDDPFMNT
701 SSLRRNRR
```

Unformatted sequence string: 708 residues (for pasting into other applications).

Sort peptides by ◉ Residue Number ○ Increasing Mass ○ Decreasing Mass

8402	5 – 16	697.3452	1392.6759	1392.6773	-0.99	0	35	0.73	1	U	A.DALDDENTFKIL.V
3467	25 – 32	498.2522	994.4898	994.4906	-0.75	0	40	0.081	1	U	G.FMEKDAVR.G
3468	25 – 32	332.5040	994.4902	994.4906	-0.42	0	38	0.063	1	U	G.FMEKDAVR.G
3653	25 – 32	337.8357	1010.4853	1010.4855	-0.16	0	21	0.9	1	U	G.FMEKDAVR.G + Oxidation (M)
10702	29 – 43	833.4097	1664.8049	1663.8053	601	0	21	1.3	2	U	K.DAVRGNDTFVTLDEI.L
3803	32 – 40	511.7672	1021.5199	1021.5193	0.65	0	24	0.74	1	U	V.RGNDTFVTL.D
8288	32 – 43	690.3433	1378.6721	1378.6729	-0.56	0	39	0.25	1	U	V.RGNDTFVTLDEI.L
8300	32 – 43	690.8358	1379.6570	1379.6569	0.058	0	27	0.95	1	U	V.RGNDTFVTLDEI.L + Deamidated (N)
9451	32 – 44	746.8851	1491.7556	1491.7569	-0.90	0	46	0.066	1	U	V.RGNDTFVTLDEIL.R
9452	32 – 44	746.8854	1491.7562	1491.7569	-0.49	0	53	0.021	1	U	V.RGNDTFVTLDEIL.R
9450	33 – 45	746.8848	1491.7550	1491.7569	-1.31	0	40	0.0048	1	U	R.GNDTFVTLDEILR.L
9467	33 – 45	747.3905	1492.7665	1491.7569	677	0	48	0.0035	1	U	R.GNDTFVTLDEILR.L
8811	34 – 45	718.3739	1434.7332	1434.7355	-1.54	0	54	0.00046	1	U	G.NDTFVTLDEILR.L
8818	34 – 45	718.8760	1435.7375	1434.7355	698	0	48	0.00081	1	U	G.NDTFVTLDEILR.L
2192	40 – 46	436.2658	870.5171	870.5174	-0.43	0	52	0.0053	1	U	T.LDEILRL.A
12470	46 – 69	686.6026	2742.3813	2741.3660	370	0	22	0.51	1	U	R.LAQENEVDFILLGGDLFHENKPSR.K + Deamidated (N)
4243	47 – 55	532.7483	1063.4820	1063.4822	-0.15	0	29	0.95	1	U	L.AQENEVDFI.L
3428	48 – 55	497.2299	992.4453	992.4451	0.20	0	24	3.1	3	U	A.QENEVDFI.L
8707	56 – 68	713.8695	1425.7245	1425.7252	-0.53	0	67	0.00055	1	U	I.LLGGDLFHENKPS.R
7447	57 – 68	657.3272	1312.6399	1312.6412	-0.99	0	32	0.036	1	U	L.LGGDLFHENKPS.R
7448	57 – 68	657.3280	1312.6415	1312.6412	0.22	0	27	0.071	1	U	L.LGGDLFHENKPS.R
5931	58 – 68	400.8591	1199.5554	1199.5571	-1.43	0	31	0.41	1	U	L.GGDLFHENKPS.R
5932	58 – 68	600.7852	1199.5558	1199.5571	-1.12	0	37	0.45	1	U	L.GGDLFHENKPS.R
4442	60 – 68	543.7645	1085.5144	1085.5142	0.20	0	22	1.4	5	U	G.DLFHENKPS.R
237	76 – 80	322.2103	642.4061	642.4064	-0.52	0	21	0.91	1	U	C.LELLR.K
4907	81 – 89	563.2620	1124.5094	1124.5107	-1.16	0	21	0.3	1	U	R.KYCMGDRPV.Q
4908	81 – 89	563.2656	1124.5167	1124.5107	5.35	0	22	0.16	1	U	R.KYCMGDRPV.Q
5449	90 – 99	583.2901	1164.5656	1164.5663	-0.53	0	51	0.00093	1	U	V.QFEILSDQSV.N
4457	95 – 104	544.2380	1086.4615	1086.4618	-0.28	0	26	0.23	1	U	L.SDQSVNFGFS.K
2580	103 – 109	455.7450	909.4754	909.4749	0.61	0	22	0.33	1	U	G.FSKFPWV.N
1370	105 – 110	395.7159	789.4171	789.4174	-0.26	0	31	0.11	1	U	S.KFPWVN.Y
4084	110 – 118	525.7463	1049.4780	1049.4778	0.22	0	36	0.051	1	U	V.NYQDGNLNI.S
6423	123 – 133	620.2732	1238.5318	1238.5316	0.16	0	25	0.07	1	U	V.FSIHGNHDDPT.G
8132	123 – 135	684.3021	1366.5896	1366.5902	-0.47	0	55	0.00036	1	U	V.FSIHGNHDDPTGA.D
8142	123 – 135	684.7949	1367.5752	1367.5742	0.70	0	23	0.11	1	U	V.FSIHGNHDDPTGA.D + Deamidated (N)
8150	123 – 135	685.2975	1368.5805	1367.5742	736	0	25	0.076	1	U	V.FSIHGNHDDPTGA.D + Deamidated (N)
10709	123 – 138	833.8784	1665.7423	1665.7383	2.38	0	21	0.9	1	U	V.FSIHGNHDDPTGADAL.C
10713	123 – 138	834.3782	1666.7419	1665.7383	602	0	30	0.032	1	U	V.FSIHGNHDDPTGADAL.C
11194	156 – 171	596.3376	1785.9909	1785.9910	-0.039	0	26	0.074	1	U	R.SMSVEKIDISPVLLQK.G
652	157 – 162	353.6935	705.3725	705.3731	-0.80	0	21	0.85	3	U	S.MSVEKI.D
2455	160 – 167	450.7553	899.4961	899.4964	-0.28	0	27	1.3	2	U	V.EKIDISPV.L
7132	177 – 188	645.8381	1289.6616	1289.6615	0.040	0	33	0.16	1	U	I.ALYGLGSIPDER.L
8498	177 – 189	702.3752	1402.7359	1402.7456	-6.89	0	44	0.026	1	U	I.ALYGLGSIPDERL.Y
8500	177 – 189	702.3804	1402.7462	1402.7456	0.42	0	21	0.24	1	U	I.ALYGLGSIPDERL.Y
8509	177 – 189	702.8818	1403.7490	1402.7456	715	0	34	0.025	1	U	I.ALYGLGSIPDERL.Y
6138	178 – 188	610.3190	1218.6234	1218.6244	-0.86	0	66	0.00083	1	U	A.LYGLGSIPDER.L
7673	178 – 189	666.8613	1331.7081	1331.7085	-0.29	0	57	0.0008	1	U	A.LYGLGSIPDERL.Y
9502	178 – 190	748.3933	1494.7721	1494.7718	0.17	0	28	0.046	1	U	A.LYGLGSIPDERLY.R
10625	178 – 191	551.2979	1650.8719	1650.8729	-0.61	0	26	0.21	1	U	A.LYGLGSIPDERLYR.M
4682	179 – 188	553.7767	1105.5389	1105.5404	-1.32	0	46	0.0049	1	U	L.YGLGSIPDER.L
6139	179 – 189	610.3197	1218.6249	1218.6244	0.34	0	42	0.0041	1	U	L.YGLGSIPDERL.Y
1604	261 – 267	406.2029	810.3912	810.3912	0.0062	0	24	0.46	1	U	L.FYISQPG.S
5685	261 – 271	592.3001	1182.5857	1182.5921	-5.44	0	29	0.063	1	U	L.FYISQPGSSVV.T
7064	261 – 272	642.8270	1283.6394	1283.6398	-0.32	0	42	0.0037	1	U	L.FYISQPGSSVVT.S
2042	295 – 301	426.7417	851.4688	851.4687	0.15	0	21	1.5	3	U	M.NMHKIPL.H
2047	295 – 301	427.2336	852.4525	852.4527	-0.21	0	29	1.8	10	U	M.NMHKIPL.H + Deamidated (N)
493	299 – 304	340.2103	678.4060	678.4065	-0.71	0	21	0.73	1	U	K.IPLHTV.R

5694	305 – 313	592.7925	1183.5705	1183.5696	0.80	0	28	0.34	2	U	V.RQFFMEDIV.L
5935	305 – 313	600.7891	1199.5637	1199.5645	-0.67	0	26	1.3	2	U	V.RQFFMEDIV.L + Oxidation (M)
11212	314 – 329	597.9719	1790.8939	1790.8951	-0.67	0	21	0.85	1	U	V.LANHPDIFNPDNPKVT.Q
6982	316 – 326	640.2891	1278.5637	1278.5629	0.61	0	28	0.57	1	U	A.NHPDIFNPDNP.K
8540	316 – 327	704.3336	1406.6526	1406.6579	-3.77	0	30	0.018	1	U	A.NHPDIFNPDNPK.V
10409	316 – 329	804.3945	1606.7745	1606.7740	0.33	0	42	0.0013	1	U	A.NHPDIFNPDNPKVT.Q
10424	316 – 329	804.8883	1607.7621	1607.7580	2.54	0	21	0.36	1	U	A.NHPDIFNPDNPKVT.Q + Deamidated (N)
3827	333 – 340	512.7604	1023.5063	1023.5059	0.41	0	28	0.098	1	U	I.QSFCLEKI.E
8519	341 – 351	469.2182	1404.6327	1404.6303	1.71	0	23	0.3	1	U	I.EEMLENAERER.L
4688	352 – 361	553.7830	1105.5514	1105.5516	-0.22	0	22	0.25	1	U	R.LGNSHQPEKP.L
6140	352 – 362	610.3231	1218.6317	1218.6357	-3.26	0	23	0.23	2	U	R.LGNSHQPEKPL.V
6141	352 – 362	407.2190	1218.6352	1218.6357	-0.34	0	31	0.12	1	U	R.LGNSHQPEKPL.V
6151	352 – 362	610.8180	1219.6214	1219.6197	1.44	0	27	0.12	1	U	R.LGNSHQPEKPL.V + Deamidated (N)
7507	352 – 363	659.8589	1317.7033	1317.7041	-0.56	0	28	0.023	1	U	R.LGNSHQPEKPLV.R
7508	352 – 363	440.2421	1317.7045	1317.7041	0.28	0	21	1.3	2	U	R.LGNSHQPEKPLV.R
11495	365 – 380	614.9896	1841.9469	1840.9472	543	0	23	0.57	1	U	R.LRVDYSGGFEPFSVLR.F
1201	390 – 396	385.7238	769.4330	769.4334	-0.47	0	22	0.59	1	U	V.ANPKDII.H
537	413 – 418	346.2105	690.4065	690.4064	0.029	0	26	0.15	1	U	I.NFGKLI.T
1327	416 – 422	393.7578	785.5010	785.5011	-0.071	0	23	0.76	1	U	G.KLITKPS.E
2915	417 – 425	473.2659	944.5172	944.5179	-0.64	0	28	0.19	1	U	K.LITKPSEGT.T
6315	423 – 433	616.3300	1230.6454	1230.6456	-0.18	0	32	0.59	1	U	S.EGTTLRVEDLV.K
5576	425 – 434	587.3447	1172.6748	1172.6765	-1.45	0	21	1.5	5	U	G.TTLRVEDLVK.Q
3340	428 – 435	493.7849	985.5552	985.5556	-0.43	0	30	0.6	1	U	L.RVEDLVKQ.Y
2346	434 – 440	443.2268	884.4391	884.4392	-0.098	0	32	0.44	1	U	V.KQYFQTA.E
5565	443 – 452	586.8361	1171.6577	1171.6561	1.39	0	21	1.3	2	U	K.NVQLSLLTER.G
5591	448 – 458	588.3087	1174.6028	1174.6016	0.99	0	54	0.00048	1	U	S.LLTERGMGEAV.Q
10211	448 – 461	790.8950	1579.7754	1578.7712	636	0	21	0.27	1	U	S.LLTERGMGEAVQEF.V
2934	450 – 458	475.2242	948.4338	948.4335	0.30	0	28	0.57	1	U	L.TERGMGEAV.Q
7957	450 – 461	677.3087	1352.6029	1352.6031	-0.13	0	54	0.012	1	U	L.TERGMGEAVQEF.V
9700	462 – 474	759.3900	1516.7654	1515.7668	659	0	23	1.2	2	U	F.VDKEEKDAIEELV.K
2564	475 – 481	455.2555	908.4964	908.4967	-0.30	0	35	0.33	1	U	V.KYQLEKT.Q
3241	482 – 488	326.1943	975.5611	975.5614	-0.29	0	21	0.77	1	U	T.QRFLKER.H
4133	489 – 497	527.2824	1052.5503	1052.5502	0.064	0	22	0.36	1	U	R.HIDALEDKI.D
9784	489 – 501	763.3749	1524.7353	1524.7307	3.01	0	23	0.31	1	U	R.HIDALEDKIDEEV.R
9791	489 – 501	763.8747	1525.7348	1524.7307	659	0	39	0.01	1	U	R.HIDALEDKIDEEV.R
10286	491 – 503	529.9373	1586.7899	1586.7900	-0.024	0	39	0.01	1	U	I.DALEDKIDEEVRR.F
7096	494 – 503	430.2214	1287.6425	1287.6419	0.48	0	21	0.97	1	U	L.EDKIDEEVRR.F
11443	508 – 522	611.6133	1831.8180	1831.8296	-6.33	0	29	0.12	1	U	T.RQKNTNEEDDEVREA.M
11444	508 – 522	611.6166	1831.8281	1831.8296	-0.83	0	27	0.1	1	U	T.RQKNTNEEDDEVREA.M
11445	508 – 522	611.6167	1831.8283	1831.8296	-0.73	0	21	0.12	1	U	T.RQKNTNEEDDEVREA.M
11446	508 – 522	458.9646	1831.8293	1831.8296	-0.17	0	22	1.1	4	U	T.RQKNTNEEDDEVREA.M
11448	508 – 522	611.9475	1832.8207	1832.8136	3.87	0	45	0.0066	1	U	T.RQKNTNEEDDEVREA.M + Deamidated (N)
10746	509 – 522	838.8710	1675.7274	1675.7285	-0.66	0	76	9.6e-07	1	U	R.QKNTNEEDDEVREA.M
12016	509 – 525	688.9803	2063.9192	2063.9178	0.70	0	31	0.032	1	U	R.QKNTNEEDDEVREAMTR.A
12020	509 – 525	689.3127	2064.9164	2064.9018	7.08	0	29	0.28	1	U	R.QKNTNEEDDEVREAMTR.A + Deamidated (N)
8670	511 – 522	710.7953	1419.5760	1419.5750	0.75	0	40	0.002	1	U	K.NTNEEDDEVREA.M
8676	511 – 522	711.2960	1420.5775	1419.5750	706	0	44	0.0013	1	U	K.NTNEEDDEVREA.M
8675	511 – 522	711.2918	1420.5691	1420.5590	7.10	0	27	0.17	1	U	K.NTNEEDDEVREA.M + Deamidated (N)
5978	513 – 522	603.2499	1204.4852	1204.4844	0.70	0	34	0.033	1	U	T.NEEDDEVREA.M
5326	538 – 548	578.7631	1155.5117	1155.5118	-0.074	0	39	0.089	2	U	A.SAFSADDLMSI.D
5555	538 – 548	586.7599	1171.5053	1171.5067	-1.15	0	34	0.02	1	U	A.SAFSADDLMSI.D + Oxidation (M)
4283	539 – 548	535.2469	1068.4793	1068.4798	-0.38	0	48	0.033	1	U	S.AFSADDLMSI.D
4420	539 – 548	543.2448	1084.4751	1084.4747	0.37	0	58	0.0016	1	U	S.AFSADDLMSI.D + Oxidation (M)
11089	549 – 565	876.8600	1751.7054	1751.7156	-5.77	0	45	0.0032	1	U	I.DLAEQMANDSDDSISAA.T
11090	549 – 565	876.8600	1751.7054	1751.7156	-5.77	0	40	0.005	1	U	I.DLAEQMANDSDDSISAA.T
11091	549 – 565	876.8644	1751.7143	1751.7156	-0.70	0	42	0.0015	1	U	I.DLAEQMANDSDDSISAA.T

Appendix Aviii. MASCOT analysis of MRE11 variant after elastase digest "top hits".

MASCOT Search Results

User : bmk
E-mail :
Search title : RK OTE0297_SarahJevons_Elas_4.mgf
MS data file : E:\mgf_Orbi\OTE0297_SarahJevons_Elas_4.mgf
Database : UniProt_SwissProt 20131208 (541,762 sequences; 192,577,305 residues)
Taxonomy : Homo sapiens (human) (20,353 sequences)
Timestamp : 22 Sep 2014 at 12:09:29 GMT

Not what you expected? Try the select summary.

- Search parameters
- Score distribution
- Legend

Protein Family Summary

Significance threshold p< 0.05 Max. number of families AUTO
Ions score or expect cut-off 0 Dendrograms cut at 0
Show Percolator scores
Preferred taxonomy All entries

- Decoy search summary (random protein sequences)

Protein families 1–10 (out of 95)

10 per page 1 2 3 4 5 6 ... 10 Next

1		P10515	1310	RecName: Full=Dihydrolipoyllysine-residue acetyltransferase component of pyruvate dehydrogenase complex, mitochondrial; EC=2...
2		P49959	502	RecName: Full=Double-strand break repair protein MRE11A; AltName: Full=Meiotic recombination 11 homolog 1; Short=MRE11 ho...
3		P60709	367	RecName: Full=Actin, cytoplasmic 1; AltName: Full=Beta-actin; Contains: RecName: Full=Actin, cytoplasmic 1, N-terminally proces...
4	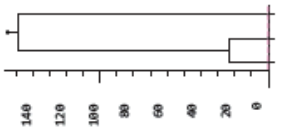	1 P38646	291	RecName: Full=Stress-70 protein, mitochondrial; AltName: Full=75 kDa glucose-regulated protein; Short=GRP-75; AltName: Full=...
		2 P11142	260	RecName: Full=Heat shock cognate 71 kDa protein; AltName: Full=Heat shock 70 kDa protein 8;
		3 P08107	139	RecName: Full=Heat shock 70 kDa protein 1A/1B; AltName: Full=Heat shock 70 kDa protein 1/2; Short=HSP70-1/HSP70-2; Short...
5	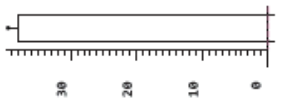	1 O43707	208	RecName: Full=Alpha-actinin-4; AltName: Full=F-actin cross-linking protein; AltName: Full=Non-muscle alpha-actinin 4;
		2 P12814	105	RecName: Full=Alpha-actinin-1; AltName: Full=Alpha-actinin cytoskeletal isoform; AltName: Full=F-actin cross-linking protein; AltN...

6	P13797	201	RecName: Full=Plastin-3; AltName: Full=T-plastin;
7	O00515	178	RecName: Full=Ladinin-1; Short=Lad-1; AltName: Full=Linear IgA disease antigen; Short=LADA;
8	P40199	177	RecName: Full=Carcinoembryonic antigen-related cell adhesion molecule 6; AltName: Full=Non-specific crossreacting antigen; AltN...
9	P04843	156	RecName: Full=Dolichyl-diphosphooligosaccharide--protein glycosyltransferase subunit 1; EC=2.4.99.18; AltName: Full=Dolichyl-di...
10	1 P02545	131	RecName: Full=Prelamin-A/C; Contains: RecName: Full=Lamin-A/C; AltName: Full=70 kDa lamin; AltName: Full=Renal carcinoma ...
	3 Q03252	55	RecName: Full=Lamin-B2; Flags: Precursor;
	2 P20700	61	RecName: Full=Lamin-B1; Flags: Precursor;

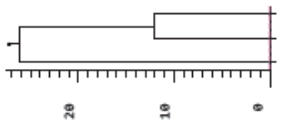

Appendix B. Western blot analysis of CAL29 cell line treated with increasing concentrations of gemcitabine for 48 hours. γH2AX is positive control for drug action. β-actin was used as a loading control.

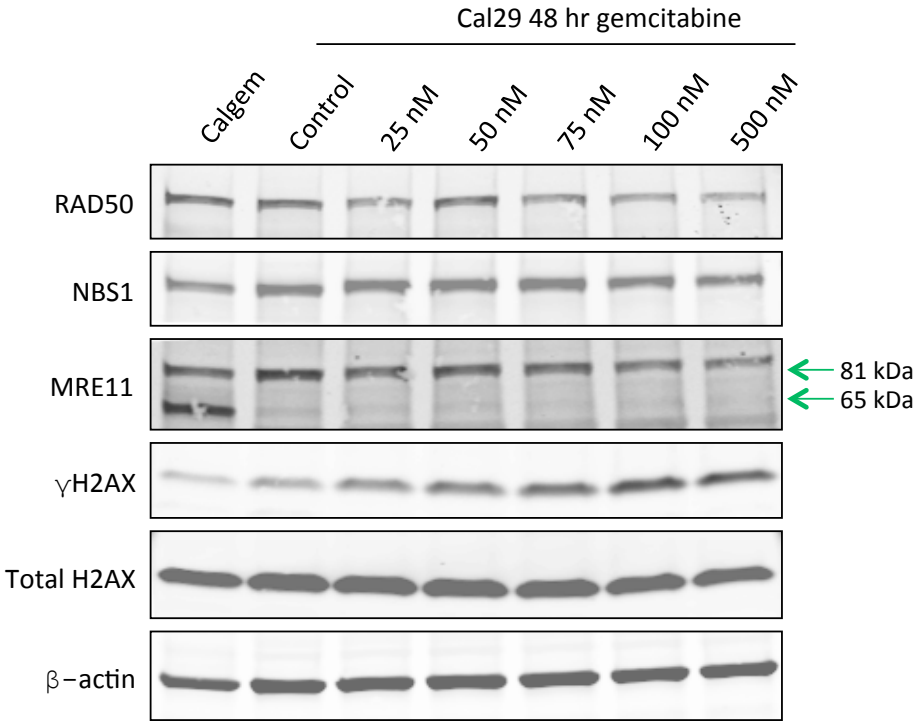

Appendix C. Melting temperature profiles for *CASP* primers

CASP1

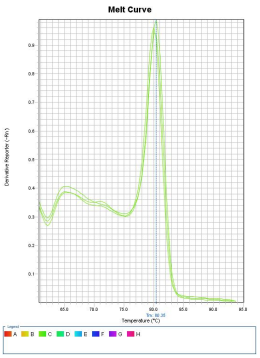

CASP2

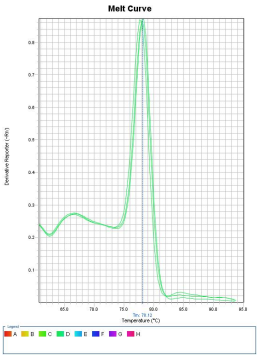

CASP3

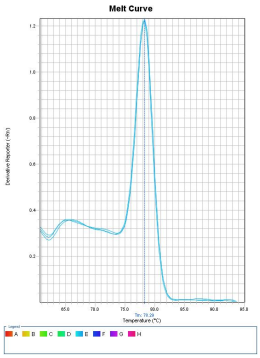

CASP4

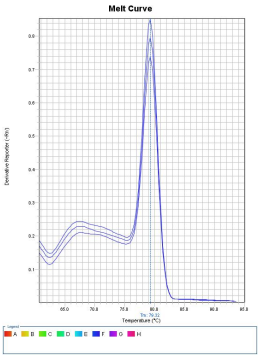

CASP5

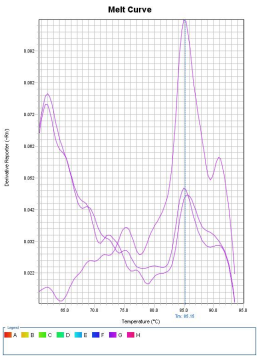

CASP6

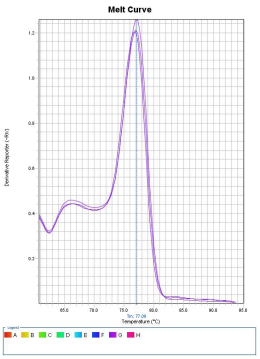

CASP7

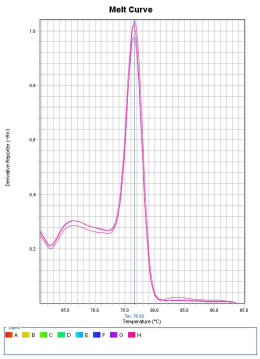

CASP8

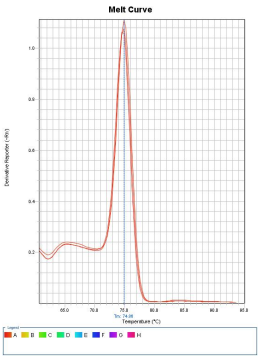

CASP9

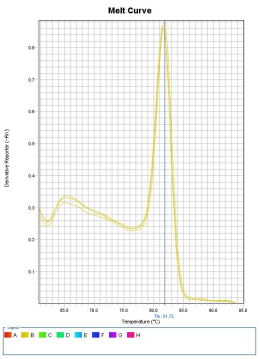

CASP10

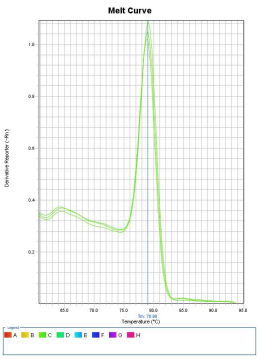

CASP14

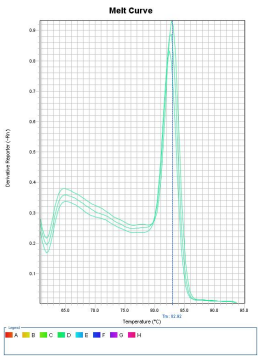

CASP qPCR amplification plot

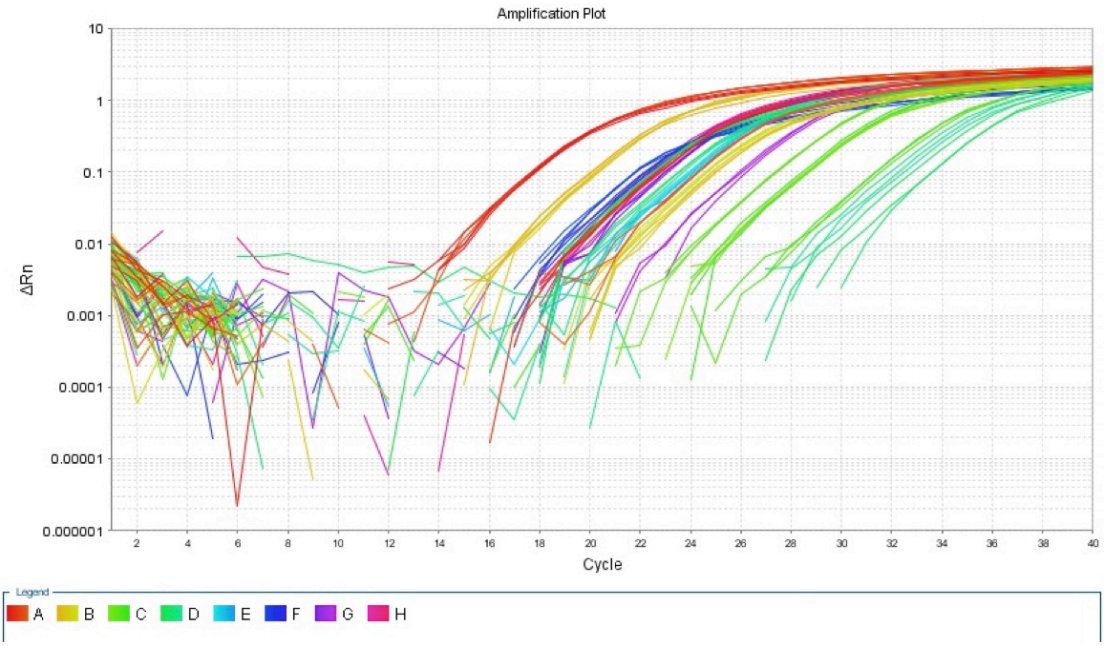

Appendix D. Restriction enzyme digest of plasmid DNA from eight individual shRNA MRE11 plasmid clones to confirm 65 base pair insert. Plasmid DNA was not digested (uncut) or digested with *BamHI* (cut).

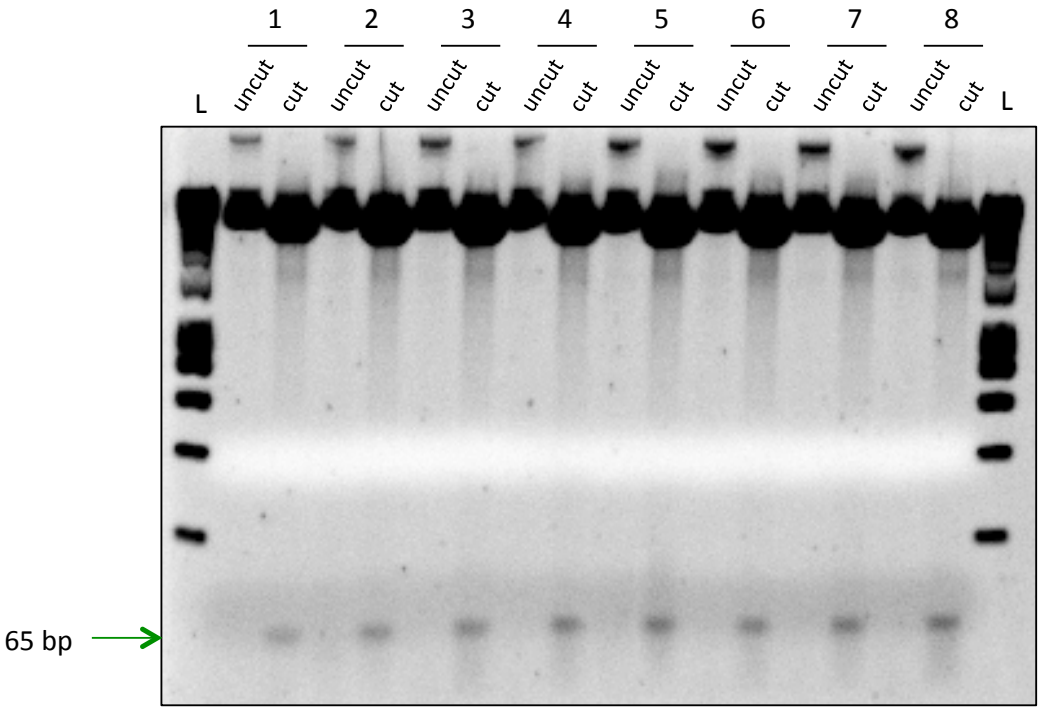

Appendix E. Evaluation of the cytotoxity of MRE11 inhibitors in the RT112 cell line. IC_{10} and IC_{50} dose for each inhibitor are indicated.

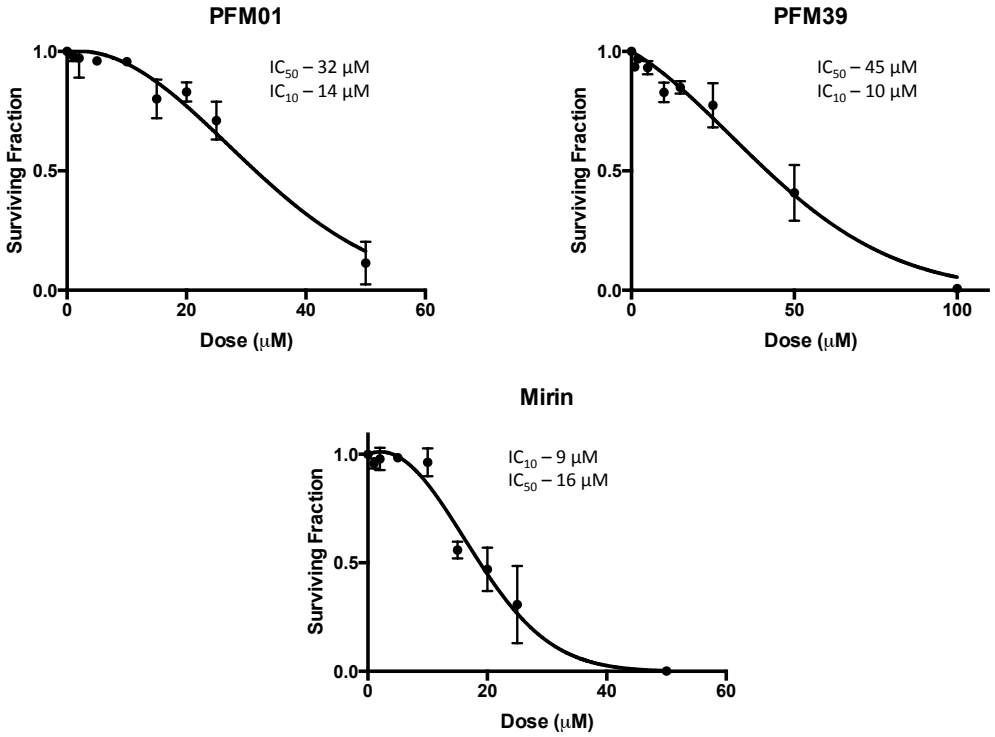

Appendix F. Example of co-transfected T24 MRE11 knockdown cell for *I-SceI* assay. T24 MRE11 knockdown cells co-transfected with *I-SceI* (generating GFP signal after repair via homologous recombination) and pcDNA3.3 truncated MRE11 plasmid with an HA-tag. GFP signal is indicated in the top left panel, HA signal in the top right panel, DAPI in the bottom left panel and the merged signal from GFP and HA in the bottom right panel.

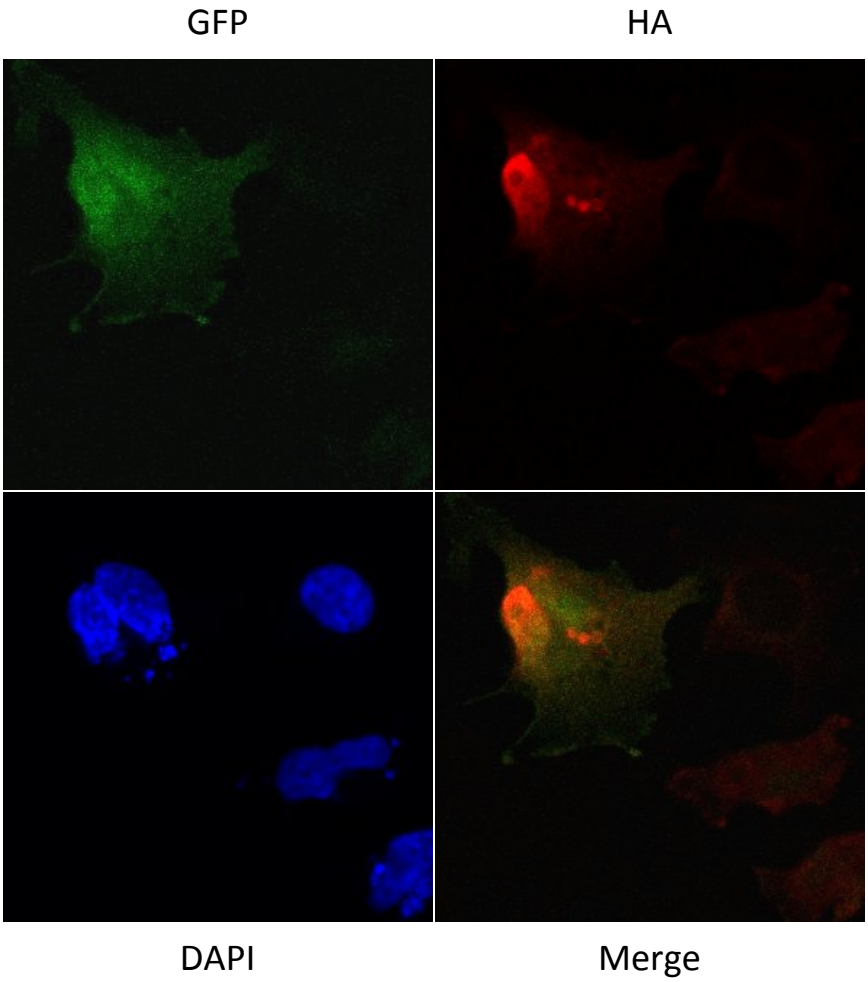

Appendix G. Published papers

1. Martin, R. M., Kerr, M., Teo, M. T. W., Jevons, S. J., Koritzinsky, M., Wouters, B. G.,Kiltie, A. E. (2014). Post-transcriptional regulation of MRE11 expression in muscle-invasive bladder tumours. Oncotarget, 5(4), 993–1003.

2. Jevons, S. J., Green, A., Lunter, G., Kartsonaki, C., Buck, D., Piazza, P., & Kiltie, A. E. (2015). High-throughput DNA Sequencing Identifies Novel CtIP (RBBP8) Variants in Muscle-invasive Bladder Cancer Patients. Bladder Cancer, 1(1), 31–44.